University of Alberta

BioMEMS and Nanoscience for Genetic Analysis

by

Agnello Ranjit Prakash 

A thesis submitted to the Faculty of Graduate Studies and Research in partial fulfillment of the requirements for the degree of

Master of Science

Department of *Electrical and Computer Engineering*

Edmonton, Alberta, Canada

Fall 2004

Your file Votre référence
ISBN: 0-612-95834-5
Our file Notre référence
ISBN: 0-612-95834-5

Table of Contents

List of Figures

List of Abbreviations

μTAS	Micro total analysis systems
μTk	microfluidic tool kit
A/D	Analog to digital converter
Au	Gold
BioMEMS	Biomedical micro electro mechanical systems
BM	Bone marrow
BSA	Bovine Serum Albumin
CCD	Charge-coupled device
CDCE	Constant denaturing capillary electrophoresis
CDNA	Complimentary Deoxyribonucleic acid
CE	Capillary electrophoresis
CHP	Chip holder plate
CNS	Central nervous system
Cr	Chrome
D/A	Digital to analog converter
DC	Direct current
DEP	Dielectrophoresis
DIB	Digital input binary number
DNA	Deoxyribonucleic acid
DNTP	Deoxiribonucleose triphosphates
DOP	Expected process variable
DPV	Observed process value
EPROM	Erasable programmable read only memory
EtBr	Ethidium bromide
FISH	Fluorescent in-suit hybridization
GUI	Graphical user interface
HAS	Hyaluronan Synthase

HV	High voltage
IC	Integrated circuit
I2C	Inter-Integrated Circuit
IPA	Isopropanol
IPN	Interpenetrating polymer network
IR	Infrared
lab-on-a-chip	Laboratory on a chip
LCP	Lower copper plate
LIF	Laser induced fluorescence
LNA	Locked nucleic acids
MAb	Monoclonal antibody
MEMS	Micro electro mechanical systems
MM	Multiple myeloma
MPC	2-methacryloyloxyethyl phosphorylcholine
NTS	nucleus of tractus solitarus
P	Proportional
P/I/D	Proportional/Integral/Derivative
PCR	Polymerase chain reaction
PDMS	Polydimethysiloxane
PD-PI	Proportional Derivative- Proportional Integral
PE	Polyethylene
PEG	Polyethylene glycol
PI_2	Proportional Integral controller module 2
PIC	Peripheral interface controller
PMMA	Polymethylmethacrylate
PMT	Photomultiplier tube
Pt	Platinum
PWM	Pulse width modulation
RT-PCR	Reverse transcriptase polymerase chain reaction
RFI	Relative fluorescence intensity

RIE	Reactive Ion Etch
RNA	Ribonucleic acid
RTD	Resistive temperature device
Si	Silicon
SL	Sample loading
SMU	Source measuring unit
SNP	Single-nucleotide polymorphism
SSCP	Single-stranded conformal polymorphosis
SUL	Sample unloading
SW	Square wave heater
TBE	Tris- Boric acid-EDTA
TCR	Temperature coefficient of resistance
TGCE	Temperature gradient capillary electrophoresis
UV	Ultra violet

List of Notations

Notation	Description
ν	Migration velocity of a molecule in CE
ζ	Damping ratio
λ	Thermal conductivity of a material
ρ	Thermal density of a material
μ_I	Fragment mobility in CE
ΔT	Temperature difference between a hot region and a cold region for thermal diffusion to occur
ΔL	Distance between separated fragments
A	Membrane surface area
Au	Gold
C	Concentration of water in the PDMS
c	Specific heat capacity of a material
Cr	Chrome
D	Diffusion coefficient of a particle in CE
d	Diffusion length – the distance to which a water molecule will travel
D	Diffusion coefficient of water in PDMS
D	diffusion coefficient in a medium
d'	Membrane thickness across which the diffusion occurs
D_T	Diffusion coefficient of heat
$D_{Thermal}$	Thermal diffusion coefficient (thermophoresis) of DNA
$D(t_k)$	Derivative controller output at t_k
D_o	Pre-exponential factor of diffusion coefficient
dt	Time derivative
d_T	Dead time in the system
D_T	thermal diffusivity coefficient of DNA
E	Applied electric field in CE
e	Error signal (setpoint-feedback)

E'	Efficiency factor in PCR
$e(t_k)$	Error signal at t_k
E_D	Activation energy of water in PDMS
F	Factor of influence on the PCR product
F	Flux of water in PDMS
f	Feedback signal from the system
$f(t_k)$	Feedback signal at t_k
H	Sampling interval
I	Input signal to the thermal system (setpoint)
I	Current flowing through the resistor
$I(t_k)$	Integral controller output at t_k
$I(t_k)$	Input signal to the system at t_k
$I_{SMU\text{-}meter}$	Current sourced by the Kiethley Source Measuring Unit
K_D	Derivative gain of the derivative controller
K_i	Integral gain of the integral controller
K_p	Proportional gain for the proportional controller
L	Thickness for thermal diffusion to occur
l	Distance to which a DNA will travel
n	Number of thermal cycles
N	Number of theoretical plates for resolution measurements
o	Output signal from the system
$o(t_k)$	Output signal from the system at t_k
P	Permeability coefficient
$P(t_k)$	Proportional controller output at t_k
P_g	Process gain
Pt	Platinum
P_{in}	Input power given to the Peltier
pv	Process variable
$pv(t_k)$	Process variable at t_k
q	Charge of the fragment in CE

Q_c	Amount of heat absorbed from the cold side
R	Gas constant
R	Resistance of the metal at a elevated temperature
R_{meter}	Resistance of the resistor measured by an external ohmmeter
R_o	Initial resistance of the resistor
R_p	Permeance resistance of a material
R_T	Thermal resistance of a heat exchanger
sp	Setpoint
t	Time duration over which the diffusion occurs
T	Temperature in Kelvin/ Celsius
Ti	Titanium
T_{amb}	Temperature of the surrounding (ambient)
T_C	Time constant of the system
T_D	Differential time for the differential controller
t_d	Thermal time delay
T_{hot}	Temperature of the hot side
Ti	Integral time for the integral controller
t_k	Sampling at the instance k
T_{meter}	Temperature measured by an external thermocouple
T_o	Initial temperature of the resistor
u	Controller output signal
u_{PD}	PD controller output
u_{PI}	PI controller output
V	Applied voltage in CE
V	Voltage across the resistor
$V_{ext\text{-}meter}$	Voltage measured across the resistor by an external voltmeter
V_{out}	Output voltage of the temperature sensor
$V_{SMU\text{-}meter}$	Voltage measured by the Kiethley Source Measuring Unit
Δp	Pressure difference across the membrane

Chapter – 1

Introduction to MEMS and Genetic Analysis

1.1 Introduction

This introductory chapter provides an overview on the potential of a relatively new field of engineering – biomedical microelectromechanical systems (bioMEMS). BioMEMS is expected to impact the way clinical testing is performed for molecular diagnosis using DNA and cells. In the future, these devices are hoped to enable molecular diagnosis in an easily accessible, simple, cost-efficient and portable manner.

The requirement for the success of any technology is an application with high demand. The applications themselves act as 'technology drivers' to provide adequate economic sustenance for on-going research in the field. Advances in technologies such as micromachining, microelectromechanical system (MEMS), microsystems and more recently, nanotechnology, have opened avenues for fabricating miniaturized devices for a myriad of applications in clinical testing. Clinical applications of molecular technologies to elucidate, diagnose and monitor human diseases are referred to as medical diagnostics. The term genetic analysis is used for applications of molecular diagnostic technology in genomics, the study of all of the genes in an organism – their sequences, structure, regulations, interaction, and products. Miniaturized fabrications of devices that support medical or genetic diagnosis are referred to by a variety of terms such as micro total analysis systems (μTAS), lab-on-a-chip technology, integrated microfluidics, biomedical MEMS (bioMEMS)[1, 2] These systems offer several advantages compared to

conventional medical tools. They include[3, 4]: (1) smaller size with features even in the nanometer meter scale and hence lower costs due to batch fabrication (2) the ability to integrate many sequential processing steps in a unified device (3) superior functionality (e.g. resolution, sensitivity).

Though the semiconductor industry has used the MEMS technology in the past few decades, it was the groundbreaking work of Manz *et al.*.[5] in 1990 that established the field of bioMEMS as one with a high potential for circumventing the primary bottle-necks in the clinical field – i.e. the cost and accessibility of medical diagnostics. However, most of the activities in the bioMEMS area in the 90's were in academia and were focused on exploring the feasibility of the field for real-time medical application. Over the decade, the success with these devices has propelled research in bioMEMS[2]. More recently, as we encounter new medical challenges, commercializing bioMEMS devices for real-time applications is becoming increasingly important[6-11]. For example, bioMEMS devices are now commercially available from companies like Cepheid (USA), MicroCHIPS (USA), Motorola (USA), Micralyne (Canada), and others.

Considering the fact that bioMEMS based devices were extensively tested with DNA only in the mid-nineties by Manz[12] and others, the progress of this field has been rapid and has enormous potential for propagating vigorous interdisciplinary research work. In this age, genetic testing has become indispensable in medicine (e.g. genetic diagnostics in humans[13]), biology, forensic diagnostics, environmental studies (e.g. detection of pathogens in foods, agriculture and farming), terrorist biochemical warfare weapon detection and many other fields of science and engineering[2, 4, 14-18].

With work such as the Human Genome Project (HMG)[19], disease detection in humans (based on genetic information) is becoming increasingly reliable. The HMG has also provides a means for early detection of deadly diseases (e.g. cancer[20]) and offers an opportunity for target specific drug discovery[21]. An early and accurate diagnosis enables patients to receive the maximum benefit from medication for symptoms.

Humans have approximately 100,000 genes[1] that could potentially be tested for hereditary defects or propensity for diseases, although only about 30, 000 to 40, 000

genes are well characterized. As per reports in the late 90's, about 400 diseases are diagnosed by genetic testing, and this number is increasing. The Human Genome Project[19] has greatly heightened the importance of molecular diagnostics on various aspects of health care in the 21st century. It is believed that a specific relationships can be drawn between genetic information obtained from a human sample and a person's risk of a given disease and response to a particular treatment. Potentially, this implies that new ways of conducting clinical tests, and more rational approaches to conducting therapy are possible, which might greatly improve health care. Figure 1-1[22] is an example schematic of molecular diagnostics in relation to other fields of research.

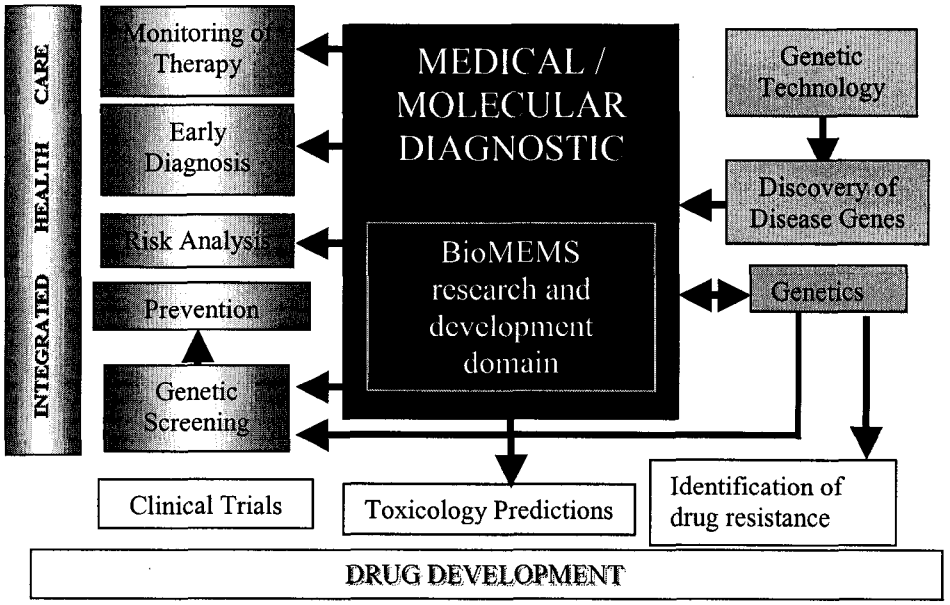

Figure 1-1. Application of molecular diagnostics and BioMEMS to related fields

Performing genetic analysis in microfluidics devices (also called microchips or biochips) presents new and interesting challenges[10]. The extraction of genetic information involves a series of biochemical manipulations of the sample requiring mixing of reagents, thermal cycling, fluorescent labelling of the sample, fragmentation analysis, all in miniaturized devices with micron scale features and sub-microliter

volumes[1, 2, 4]. Undoubtedly, such a broad base application of bioMEMS may prove to be the ultimate technology driver of all time. This is evident by the widespread use of terms such as "lab-on-a-chip", and is anticipated to be the industrial revolution of modern times.

The design and fabrication of biochips, study of the change in physical phenomena at such a small scale, functional integration with minimal real estate of the device, minimizing user intervention and macroscopic tools support, are some of the engineering challenges that require careful attention before the widespread prototype testing of bioMEMS devices in clinical laboratories is seen.

1.2 Genetics

In this section, the landmarks in biotechnology are first summarized followed by a brief discussion of the basic principles and terminology in molecular biology that are necessary for an engineering understanding of this interdisciplinary work.

The following table (compiled from Demidov[22]) summarizes the historical evolution of molecular diagnosis[19] with relevance to one of the central genetic testing components in this research – the polymerase chain reaction (PCR) genetic amplification technique.

Table 1-1. A list of landmark achievements in molecular diagnostics

Year	Landmark (reference)
1860	Friedrich Miescher identified acid and basic protein components in cell nuclei which were mistakenly believed to carry the genetic material
1920	The expression "Genome" used in German for the haploid chromosome set, which, together with the pertinent protoplasm, specifies the material foundations of the species
1944	DNA shown to carry genetic code in pneumococci (Avery 1944)
1953	Identification of the double-stranded structure of the DNA (Watson and Crick 1953) 1950s Discovery of the enzyme DNA polymerase (Kornberg 1959)
1956	Separation of proteins with a combination of paper and starch gel two-dimensional electrophoresis (Smithies and Poulik 1956)

1969	Discovery of in-situ hybridization for gene location by labeled RNA probes (Gall & Pardue 1969)
1970	Discovery of restriction enzymes that cut DNA at the site of specific sequences (Arber 1978)
1970	Discovery of reverse transcriptase. Copying of RNA into DNA (Baltimore *et al.*. 1970)
1975	Southern blot test (Southern 1975)
1975	Monoclonal antibody (MAb) technology (Köhler & Milstein 1975)
1980s	DNA probes: segments of DNA labelled with radioactive markers
1985	**Discovery of the polymerase chain reaction (PCR)** (Mullis *et al.*. 1986)
1986	Development of fluorescent in-situ hybridization (FISH) technique (Pinkel *et al.* 1986)
1990	First publication on in-suit polymerase chain reaction (Haase *et al.* 1990)
1991	Ligase chain reaction (Barany 1991)
1991	Synthesis of DNA on a silicon chip – birth of the biochip (Fodor *et al.* 1991)
1991	Merging of biology, cytogenetics and molecular cytogenetics (Lichter *et al.* 1991)
1992	Branched DNA technology used to quantify HIV levels (Urdea *et al.* 1993)
1998	Discovery of Locked Nucleic Acids (LNA), a novel class of DNA analogues, with potential applications in molecular diagnostics (Kumar *et al.* 1998)
2000	Sequencing of the human genome completed. About 30, 000 to 40, 000 genes identified.

The timeline clearly shows that the early 90's drew more attention to genetic diagnostic research after the discovery of PCR. PCR is a highly versatile laboratory genetic analysis tool capable of replicating a single strand of DNA to many millions by an enzymatic reaction. Application of PCR for DNA amplification ranges from forensic studies, the diagnosis and treatment of cancer, environmental studies, to detecting

pathogenic organisms used as biological warfare agents[4, 14]. A more detailed overview of the PCR genetic amplification technique is presented in Chapter 2.

Basic Introduction to Genetics

A fundamental understanding of genetics is essential in applying engineering principles for the development of integrated devices. In this section, fundamental concepts and microbiology terminology are reviewed that provide a basic understanding of the task at hand. Specific reference is made to PCR and relevant assays that are of interest to current and future work based on this research project.

Genetic information in humans is stored in chromosomes within each cell. Each human chromosome is a long, linear double-stranded deoxyribonucleic acid (DNA) molecule ranging in size from 50 to 250 million base pairs.

The units of each DNA strand are called nucleotides[1]. Each nucleotide consists of a base (B), a sugar linkage (S), and a phosphate bridge (P); this is depicted in Figure 1-2. The sugar linkage gives the nucleotide directionality with two distinct ends labelled 5' and 3'. Only four nucleotide bases are normally found in DNA: adenine (A), guanine (G), cytosine (C), and thymine (T). The information content of the nuclear DNA is embodied in the sequential arrangement of nucleotides. Nucleotides can only be linked in a specific direction forming single strands of DNA, as shown in Figure 1-2, and the individual bases in the DNA are hydrophobic. DNAs are either single stranded or double stranded. Single stranded DNA tends to attach (or hybridize) to another strand of complementary base pairs (i.e. A binds to T, G binds to C), forming a double strand as shown in Figure 1-2c.

To extract the genetic information of a human, the DNA has to be first extracted from the cell nucleus and purified. Although many methods are available in such an extraction process, one of the chemical extraction methods is described below. Breaking the cell membrane by chemical exposure to a solution is often the first step in the extraction process. This is followed by purification using centrifugation (or many other methods) for removal of unwanted cell material, proteins, and enzymes. Once the DNA is obtained, genetic information stored in the DNA that is useful in understanding a disease,

hereditary defects, can be extracted and interpreted using a myriad of genetic analysis tools of which PCR forms the foundational building block[23].

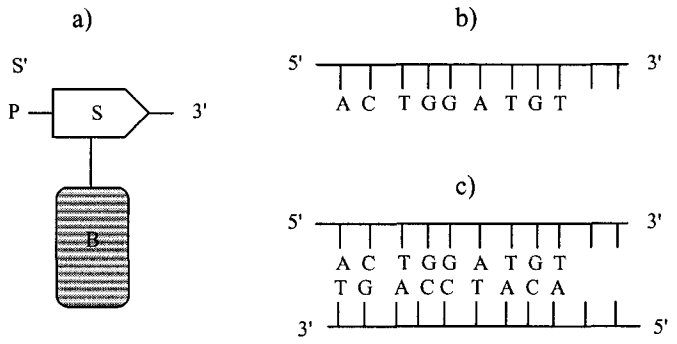

Figure 1-2. a) DNA nucleotide. b) single-stranded DNA chain, and c) double-stranded DNA with complementary base-pairs. The two strands are joined by hydrogen bonds

The core of this research focuses on performing PCR genetic amplification with DNA and subsequent analysis in bioMEMS devices. This is hoped to serve as a means to performing genetic testing and subsequent analysis in an inexpensive, portable and increasingly simple manner for point-of-care treatment. A description of the bioMEMS device and experimental demonstration of PCR can be found in this thesis.

1.3 Overview of this Thesis

This chapter introduced a relatively new field of engineering – bioMEMS. This was followed by an overview on the landmarks in the field of genetics and a brief discussion on molecular diagnosis was provided to familiarize the reader with terminologies.

Chapter 2 and 3 provide an introduction to the two central genetic analysis tools used in this work, the polymerase chain reaction (PCR) and capillary electrophoresis (CE). PCR forms the core tool around which a vast majority of the engineering work of

this thesis revolves. Chapter 2 also reviews the literature work on the demonstrations of PCR performed in bioMEMS devices.

In Chapter 4, the microfabrication of bioMEMS devices (i.e. biochips) in which the genetic analysis experimentation performed in this work is described. Here two chip designs are fabricated using glass and a relatively new material called polydimethlysiloxane (PDMS) and glass. The first design is that of a PDMS-glass PCR chip and the second is that of an integrated PDMS-glass PCR-CE chip with patterned thin film heaters. The microfabrication methods described here involve a first-of-a-kind enhanced soft-lithography technique.

Chapter 5 discusses another important engineering component to enable demonstrating PCR in biochips, i.e. the thermal instrumentation and control required to perform the thermal cycling required for PCR genetic amplification. Thermoelectric elements (Peltiers), custom-built electronics, and a novel in-house controller was designed and implemented in the form of a 'digital split non-linear PD-PI feedback controller' with dual mode performance for parallel processing to control two Peltiers.

The construction and macro-to-micro integration of microfluidic pump and valves in the form of the diaphragm pump and pinch-off valves is presented in Chapter 6.

Chapter 7 forms another critical component of this thesis. The relatively new microfabrication material PDMS is seldom used in heated microfluidic applications (e.g. PCR). Apparently this is because of the rather high liquid/vapor permeability properties of the PDMS. Highly permeable materials are problematic in microfluidics as they can result in the rapid loss of fluid sample, especially during the thermal cycling required for PCR. An investigation into the loss phenomena revealed that the loss was primarily due to the vapor loss from the chip to the atmosphere. By implanting a low permeable material (in the form of a polyethylene) in the PDMS, this loss was reduced to a manageable level. Minimizing the vapor loss enabled the performance of the PCR with low copy number samples (i.e. with human DNA samples), which otherwise did not seem possible.

The successful demonstration of PCR and CE in biochips led to an attempt to integrate these methods in a unified chip. This work is presented in Chapter 8, which first reviews the literature on this topic and then presents the potential integration of thin film heaters onto the chip to facilitate PCR thermal cycling without the requirement of Peltiers.

Finally, Chapter 9 presents a new microfluidic chip design with integrated on-chip platinum thin film heaters. The chips were designed and fabricated with capabilities of performing CE, thermophoresis for DNA concentration, and heated separation CE for mutation detection.

1.4 Recognitions

The researches presented in this thesis provides preliminary demonstrations in this relatively new field of bioMEMS. Due to the interdisciplinary nature of this work, i.e. one that involves work in engineering and life-sciences, the contributions of engineers as well as molecular biologists have been significant. This thesis focuses heavily on the engineering aspects of the projects. A year of work on the core research presented herein has resulted in recognition in the form of publication and conference presentations/papers.

- Blood, Volume 102, Nov 2003 – ' Microsystems and cancer: Improved detection of disease related genes in myeloma patients using microfluidics platforms', S. Admia, P. Pilarski, R. Prakash, J. Lauzon, L. Pilarski, C. Backhouse.

- Sensors and Actuators B- chemical, *submitted* July 2004, 'Small Volume PCR Genetic Amplification in PDMS Biochips with Integrated Fluid Control and Vapor Barrier', R. Prakash, S. Adamia, V. Sieben, P. Pilarski, L. Pilarski, C. Backhouse.

- Bio, Micro, and Nanosystems, July 2003, American Society for Microbiology, New York, USA – 'Microfluidics Platform for Genetic Analysis', S. Adamia, T. Footz, R. Prakash, P. Pilarski, L Pilarski, C. Backhouse.

- 45th Annual Meeting of American Society of Hematology, December 2003, San Diego, USA – 'Disease Detection Using Microfluidics Platforms', S. Admia, P. Pilarski, R. Prakash, J. Lauzon, L. Pilarski, C. Backhouse.

- International Conference on MEMS, Nano and Smart Systems (ICMENS), Banff, July 03, Micro & Nanotechnology Commercialization Ed. Foundation, Canada – 'Microvalving in Genetic Analysis System', P. Pilarski, R. Prakash, S. Adamia, L. Pilarski, C. Backhouse.

- Second Annual Nanomedicine Workshop, Feb 2004, Toronto, Canada – 'Enhanced Detection of Disease Related Genes Using Microfluidics Platforms', S. Admia, P. Pilarski, R. Prakash, J. Lauzon, L. Pilarski, C. Backhouse.

1.5 References

[1] C. H. Mastrangelo, M. A. Burns, D. T. Burke, *Microfabricated devices for genetic diagnostics,* Proceedings of the IEEE, 1998, *86*, 1769.

[2] E. Verpoorte, N. F. De Rooij, *Microfluidics meets MEMS,* Proceedings of the Ieee, 2003, *91*, 930.

[3] B. Ziaie, A. Baldi, M. Lei, Y. D. Gu, R. A. Siegel, *Hard and soft micromachining for BioMEMS: review of techniques and examples of applications in microfluidics and drug delivery,* Advanced Drug Delivery Reviews, 2004, *56*, 145.

[4] D. Erickson, D. Li, *Integrated microfluidic devices,* Analytica Chimica Acta, 2004, *507*, 11.

[5] A. Manz, N. Graber, H. M. Widmer, *Miniaturized Total Chemical-Analysis Systems - a Novel Concept for Chemical Sensing,* Sensors and Actuators B-Chemical, 1990, *1*, 244.

[6] R. S. Shawgo, A. C. R. Grayson, Y. W. Li, M. J. Cima, *BioMEMS for drug delivery,* Current Opinion in Solid State & Materials Science, 2002, *6*, 329.

[7] J. N. Yang, Y. J. Liu, C. B. Rauch, R. L. Stevens, R. H. Liu, R. Lenigk, P. Grodzinski, *High sensitivity PCR assay in plastic micro reactors,* Lab on a Chip, 2002, *2*, 179.

[8] C. F. Chou, R. Changrani, P. Roberts, D. Sadler, J. Burdon, F. Zenhausern, S. Lin, A. Mulholland, N. Swami, R. Terbrueggen, *A miniaturized cyclic PCR device - modeling and experiments,* Microelectronic Engineering, 2002, *61-2*, 921.

[9] Y. J. Liu, C. B. Rauch, R. L. Stevens, R. Lenigk, J. N. Yang, D. B. Rhine, P. Grodzinski, *DNA amplification and hybridization assays in integrated plastic monolithic devices,* Analytical Chemistry, 2002, *74*, 3063.

[10] P. Grodzinski, J. Yang, R. H. Liu, M. D. Ward, *A modular microfluidic system for cell pre-concentration and genetic sample preparation,* Biomedical Microdevices, 2003, *5*, 303.

[11] R. H. Liu, J. Bonanno, J. Yang, R. Lenigk, P. Grodzinski, *Single-use, thermally actuated paraffin valves for microfluidic applications,* Sensors and Actuators B: Chemical, 2004, *98*, 328.

[12] A. Manz, D. J. Harrison, E. Verpoorte, H. M. Widmer, *Planar Chips Technology for Miniaturization of Separation Systems - a Developing Perspective in Chemical Monitoring,* Advances in Chromatography, 1993, *33*, 1.

[13] J. Reiss, *The Polymerase Chain-Reaction and Its Potential Role in Clinical Diagnostics and Research,* Journal of Internal Medicine, 1991, *230*, 391.

[14] J. Wang, *Microchip devices for detecting terrorist weapons,* Analytica Chimica Acta, 2004, *507*, 3.

[15] J. Khandurina, A. Guttman, *Bioanalysis in microfluidic devices,* Journal of Chromatography A, 2002, *943*, 159.

[16] S. K. Sia, G. M. Whitesides, *Microfluidic devices fabricated in poly(dimethylsiloxane) for biological studies,* Electrophoresis, 2003, *24*, 3563.

[17] P. R. Selvaganapathy, E. T. Carlen, C. H. Mastrangelo, *Recent progress in microfluidic devices for nucleic acid and antibody assays,* Proceedings of the Ieee, 2003, *91*, 954.

[18] A. C. R. Grayson, R. S. Shawgo, A. M. Johnson, N. T. Flynn, Y. W. Li, M. J. Cima, R. Langer, *A BioMEMS review: MEMS technology for physiologically integrated devices,* Proceedings of the Ieee, 2004, *92*, 6.

[19] J. D. Watson, *The Human Genome Program - Past, Present and Future,* Biotechnology Education, 1991, *2*, 3.

[20] A. J. Szczepek, K. Seeberger, J. Wizniak, M. J. Mant, A. R. Belch, L. M. Pilarski, *A high frequency of circulating B cells share clonotypic Ig heavy-chain VDJ rearrangements with autologous bone marrow plasma cells in multiple myeloma, as measured by single-cell and in situ reverse transcriptase polymerase chain reaction,* Blood, 1998, *92*, 2844.

[21] L. M. Pilarski, A. J. Szczepek, A. R. Belch, *Deficient drug transporter function of bone marrow-localized and leukemic plasma cells in multiple myeloma,* Blood, 1997, *90*, 3751.

[22] V. V. Demidov, *DNA diagnostics in the fifty-year retrospect,* Expert Review of Molecular Diagnostics, 2003, *3*, 121.

[23] L. J. Kricka, P. Wilding, *Microchip PCR,* Analytical and Bioanalytical Chemistry, 2003, *377*, 820.

Chapter – 2

The Polymerase Chain Reaction

This chapter initially provides an overview on the biochemical working principle of the polymerase chain reaction (PCR) for genetic amplification. This is followed by a brief discussion on the popular mechanisms for fluorescently staining DNA to facilitate further bioassays of the amplified DNA. Finally, a literature review on the history of PCR performed in biochips is presented.

2.1 Genetic Analysis

In genetic diagnostic applications, a means of detecting the presence of a genetic mutation is required to provide information on the disease state of the subject. To detect a mutation, the processes involved are: an amplification of the DNA by PCR followed by the detection of the amplified-labelled fragment by capillary electrophoresis (CE). In the following section, the working principle of PCR is reviewed followed by a description of popular methods for tagging the DNA molecules so as to enable analysis of the amplified DNA using the CE technique. Finally, a literature summary on the topic of PCR performed in bioMEMS devices is presented.

2.2 Genetic Amplification by Polymerase Chain Reaction (PCR)

DNA is often present in samples at concentrations that are too low for performing genetic analysis and hence an amplification technique is required to replicate the DNA (usually from within a specific gene(s) of interest) to perform various forms of genetic

diagnostics. The most popular amplification method is PCR that was first devised by Kary Mullis in 1985 and since then has revolutionized molecular genetics. PCR mimics the natural amplification process (i.e. cell mitosis[1]) that regularly occurs within living cells in mammals. The mechanism of PCR is briefly discussed below[2-5].

The DNA replication starts with a process of first denaturing a double stranded DNA at about 94 °C. This denaturation results in the separation of the DNA strands to form two individual strands. This is followed by lowering the temperature to an annealing temperature (typically between 45-65 °C) to cause the binding of the primers to a specific location in the DNA. A wide variety of primers can be designed to bind to a specific location in the DNA. Two sets of primers are used – one that starts binding from the 5' end and the other from the 3' end of the DNA as shown in the insert in Figure 2-1. These primers are often fluorescently labeled and hence when they bind to the DNA, the DNA is also marked with the fluorophore. In the final step, the temperature is increased from the annealing temperature to the extension temperature (72 °C). At the extension temperature, the thermostable magnesium ion-dependent polymerase derived from a microorganism *Thermophilus aquaticus* (*Taq* polymerase) synthesizes the complementary DNA strands. The complementary strands are assembled by the *Taq* polymerase using the dNTP's in the reaction mixture. The end of this extension completes one PCR cycle that results in the replication of a double-stranded of DNA to two double-stranded DNA. Typically, this process of denaturing, annealing and extension is repeated 30 to 40 times. In this three-step PCR, the dwell time at the denaturation temperature of the first temperature cycle only is typically extended up to 5 min to cause complete separation of all the (template) double-stranded DNA. Similarly, the dwell time at the extension temperature at the final cycle is extended by several minutes to ensure complete replication of all the amplified DNA.

Figure 2-1 schematically represents the PCR process. As shown in the insert, one double-stranded DNA is first denatured, then the (forward and reverse) primers bind to the DNA at a specific location, and finally the Taq polymerase along with the dNTP's assemble the complementary DNA strand, thus forming two double stranded DNA.

Theoretically (and ideally), since the target DNA is doubled after every cycle, in the absence of reagent exhaustion, the yield of PCR experiment should scale as 2^n, where n is the number of cycles. That is, if a PCR experiment was started with a single template copy of a double-stranded DNA, at the end of 35 thermal cycles there should be ~34 million (2^{35}) copies of the template DNA. However, this kind of efficiency is almost never achieved in practice[2]. The factor (F) by which the copies increase after n cycles is roughly given by[2]

$$F = \left(1 + E'(n)\right)^n \qquad (1.1)$$

where E' is an efficiency factor which is a function of n. For $n < 20$, E' is typically 1, but for $n > 20$, the efficiency drops drastically[6]. This efficiency drop is dependent on a number of factors such as the performance of the heat-stable enzyme (i.e. the *Taq*), presence of inhibitors, and (if the PCR is performed in biochips,) enzyme and DNA adsorption at the walls of the chamber[7].

For example, a 10% drop in the reaction efficiency for n=30 might typically result in a 80% fall in the yield. Hence the PCR is a very sensitive genetic amplification technique and small variations in any of the experimental parameters may result in a manifold decrease in the final product (i.e. the final DNA concentration). The success of a PCR experiment depends on the correct composition of components (proportions of Taq, DNA templates and dNTPs)[2], accurate temperature control (at each of the denaturation, annealing and extension temperatures)[2, 7], the nature of the reactor walls (increased surface-to-volume ratio causes increased adsorption of reagents)[2, 6, 7], the presence of inhibitors that might be in contact with the mixture (e.g. metals, some plastics and Si are strong inhibitors) [7-9], and the presence of contaminants (e.g. incompatible bio-reagents)[10]. In this research, many of these impediments are addressed and new challenges in the form of incompatible material properties that were used to fabricate the bioMEMS device are studied.

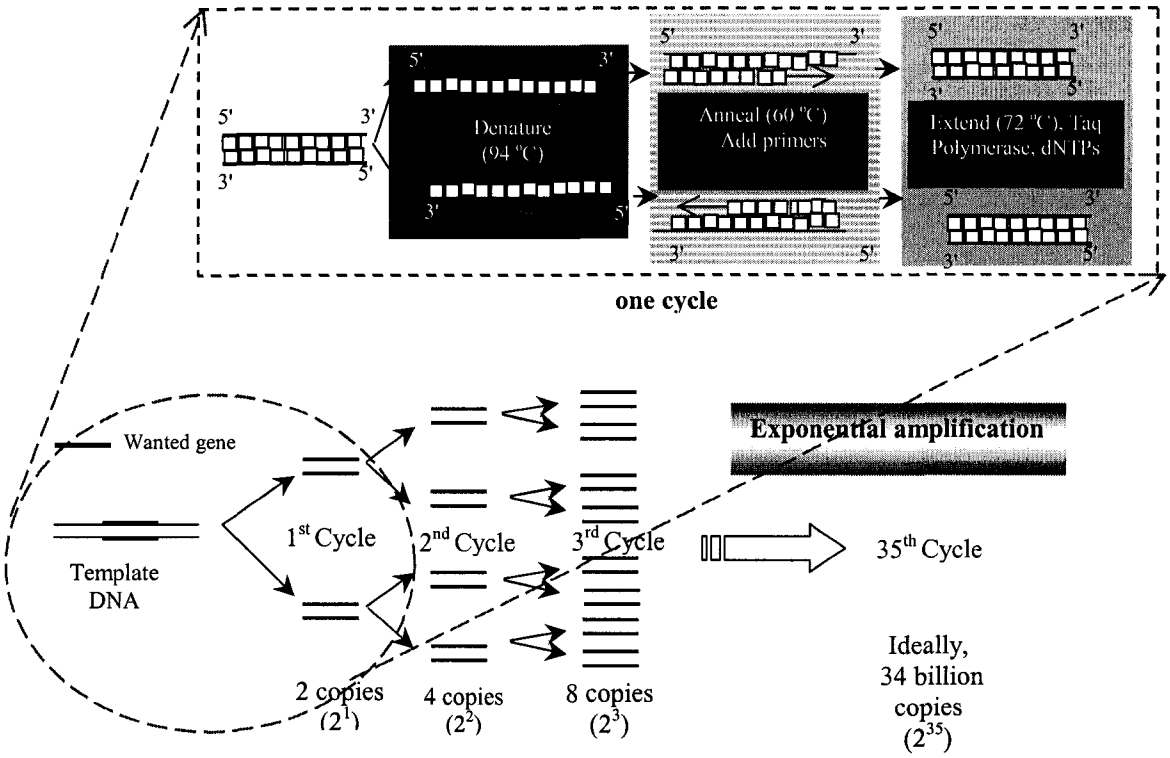

Figure 2-1. Representation of the mechanism and the multiplication factor of the PCR genetic amplification process

2.2.1 Fluorescence Staining of DNA Molecules

The most mature DNA detection schemes have involved optical methods. The DNA itself is not visible in these detection schemes, but rather a fluorescent label molecule (or dye) that is attached to the DNA. This process of staining the DNA with a fluorescent molecule is known as labelling[2].

Early labelling methods used radioactive ^{32}P incorporated in the DNA fragments. Modern labelling methods often use fluorophore dyes that emit light only when bound to a DNA under external excitation. Fluorescence detection is highly sensitive, permitting the detection of individual molecules[11]. Hence these dyes are almost universally used for the detection of DNA fragments.

Intercalating dyes such as ethidium bromide (EtBr) strongly fluoresce when excited by ultraviolet (UV) light only if bonded to a double stranded DNA. A double

stranded DNA molecule can accommodate many dye molecules since one dye molecule can be placed per several base pairs. Our laboratory has recently demonstrated[12] a method for performing this intercalating technique in a microfluidic chip as part of sensing mutations in PCR products.

Often in PCR applications, fluorescently labeled primers are used. These primers tag the DNA with the dye molecule during the replication process[4] thereby eliminating the additional step of fluorescent labeling after the PCR is completed. Hence the entire population of replicated DNA is fluorescently labeled and immediately suited for fluorescence based detection methods[13] (as described in Chapter 3).

The emission signal must be separated from the excitation using filters and dichroic mirrors[14]. Alternatively, light emission by the dye can be chemically activated[15], but these methods are not as popular. The emitted light can be observed on a photomultiplier tube[14, 16], a charge-coupled device (CCD) camera[17] or other similar sensor-transducer device.

2.3 Application of PCR

The application of PCR forms the basic building block of many clinical diagnostics at the molecular level[3]. It has been used for the study of embryogenesis[18], hepatitis C virus from blood samples of patient[19], male-infertility[20], water-borne bacterial disease called Helicobacter pylori[21], malaria detection[6], routinely in forensic studies.

Mutation (defined as an alteration of the nucleotide base sequence creating a change in the sequence of base pairs on a DNA molecule) detection by genetic amplification and subsequent analysis is perhaps the earliest[22] and one of the most widely used applications of the PCR. Numerous research groups including our laboratory have extensively used the PCR technique to amplify sequences of point-mutations for the detection and characterization of diseases such as hereditary X-linked anemia (gene: G514A)[23], breast cancer (gene: BRCA1) [24], hereditary haemochromatosis (genes:

C282Y, H63D and S65C)[25], the deficiency of phenylalanine hydroxylase (genes: phenylketonuria and hyperphenylalaninaemia) [26], stem cell research[27], detecting the infectious west-nile virus[28], the detection and monitoring of drug resistance mutation among HIV infected patients[29-32], and numerous other diseases.

Clearly PCR is a very versatile laboratory process that is now an integral part of many clinical application at the molecular level[2, 3, 5, 7, 33, 34]. It is also believed that in the future, new and unanticipated applications will emerge based on this form of amplification technique[5].

Multiple myeloma (MM) is an incurable cancer disease of the human immune system. It is characterized by the presence of monoclonal immunoglobullin in the blood, lytic bone lesions and often a large number of monoclonal plasma cells in the bone marrow (BM)[35, 36]. Studies have shown that in MM cancer patients, the white blood cells include a large population of the malignant clone (i.e. the cancer cells) that relate to the degree to which the patient is affected by this disease. The malignant cell is characterized by a unique genetic sequence that can be readily detected using PCR amplification and CE detection. With the obtained genetic information it is possible to uniquely identify any cell that is part of a population of the malignant clone. On average the survival time of a patient diagnosed with MM is about 3 to 4 years, but death as early as one month after diagnosis is not uncommon[35-39].

L.M. Pilarski and co-workers at the Cross Cancer Institute (Edmonton, Canada) have extensively researched the diagnosis, treatment and monitoring of the malignant cells in MM patients[35, 36, 38-40]. One need that exists in this realm is the need to provide cost-efficient and readily accessible healthcare for cancer patients during the course of the disease to enable suitable treatment. By frequently monitoring the malignant clone during the course of the treatment, it is possible to provide therapy (whether aggressive or mild), tailored to the patient's disease. Unfortunately, the limitations of the current clinical system do not permit low-cost molecular monitoring of patient treatment. The costs and complexity in conventional clinical processing limits monitoring the malignant clone.

The efforts in the research project undertaken as part of this thesis rest in the development of a prototype genetic analysis tool that may ultimately improve healthcare, particularly in the diagnosis and treatment of cancer[35]. At the current level of this project, prototype devices including PCR and CE performed in bioMEMS devices have been tested for their abilities for this application. In this thesis it will be demonstrated that the prototype bioMEMS devices were capable of the successful amplification and detection of messenger RNA encoding the Hyaluronan Synthase (HAS) family of proteins from the RNA of malignant circulating B cells obtained with the informed consent of myeloma and Waldenstrom's macroglobulinemia patients[39]. It appears that the HAS variant is characteristic of these diseases[40].

2.4 History of bioMEMS PCR

The feasibility of performing PCR in microfabricated devices (i.e. biochips) was first presented by Northrup and coworkers[41]. Since then a whole new research opportunity has been opened for biotech engineers to explore performing the PCR genetic amplification process in biochips to facilitate the goal of someday demonstrating a lab-on-a-chip device that incorporates this critical genetic analysis building block.

There have been three distinct approaches for performing PCR in biochips: (1) Flow PCR – a space-domain approach in which the sample is transported along temperature zones[42-50] (2) Stationary PCR – a time domain approach in which the sample is enclosed in chambers and the biochip (or the chamber alone) is thermally cycled[9, 51-62] and (3) Array PCR – a multivessel approach in which an array of wells in a chip are fabricated and such devices are often made compatible with commercial thermocyclers[23, 63, 64]. In Figure 2-2, the flow, stationary and array PCR chip designs are schematically represented.

In the following section, some recent work on PCR performed in microfabricated devices is presented.

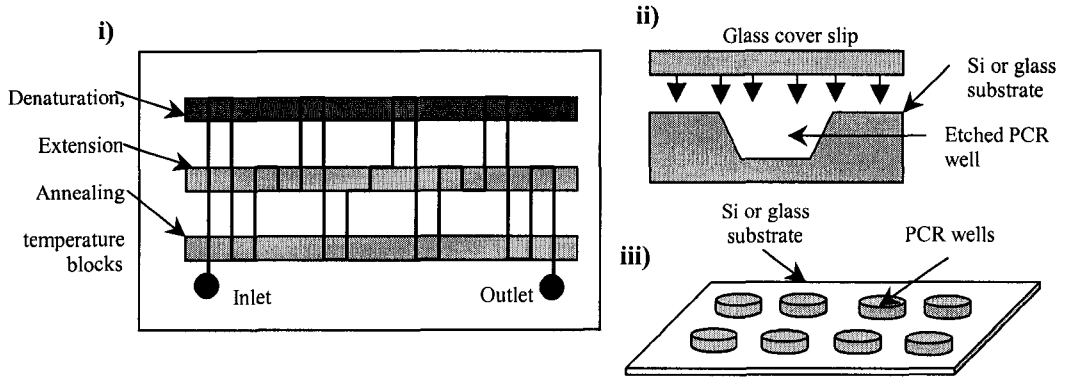

Figure 2-2: Schematic examples of i) Flow, ii) Stationary, and iii) Array PCR chip designs.

2.4.1 Stationary PCR - Time Domain Approach

Among the early demonstrations of stationary PCR, Daniel *et al.* [51] fabricated Si substrate chips with integrated platinum heaters. An anisotropic etch on the Si substrate to form air pockets around the PCR chamber prevented horizontal heat conduction losses from the chamber and created good thermal isolation of the chamber. This was shown to be an effective technique for thermally isolating the PCR chamber from the remainder of the chip structure – the frame of the chip remained a little above room temperature (20 °C) even when the temperature inside the PCR chamber was as high as 80 °C. The combination of platinum (Pt) film heaters and thermal isolation resulted in thermal ramp rates as high as 90 °C/sec.

In a progressive development of the above concept, Yoon *et al.* [53] used grooves instead of air pockets and experimentally studied the groove depth variation (1 mm width) as a function of the horizontal heat conduction from the PCR chamber. The temperature in the PCR chamber varied up to 40 °C as the groove depth was increased from 0 to 280 μm. However, the thermal ramp rates in this groove design chips were much lower (~ 35 °C) as compared to the earlier air pockets [51] design.

It is possible that this slow ramp rate was due to the added thermal mass in the form of an upper glass cover slip used to seal the PCR chamber. Another possibility is based on the design of the chip, as explained below. The upper glass substrate, a poor conductor, seals the groves leaving air trapped in them with a finite thermal mass. This

could potentially lead to a condition where thermal cycling will cause accumulation of heat in these grooves and cooling rates could reduce as the cycle number increase. It is possible that to circumvent these problems, a cooling fan was employed to provide forced cooling during the cooling stage of the PCR thermal cycle. However, with the air chamber design by Daniel *et al.* (as explained earlier) with unsealed air pockets [51] (open to ambient), the air draft probably led to faster cooling rates (up to 60 °C/s) even without cooling fans.

Bu *et al.* [49] have further investigated the use of air pockets based on the initial work of Daniel *et al.* [49], and suggested the grooves to be an effective means for providing thermal isolation of PCR chambers while using minimal real estate on the chip. Clearly, from these studies we see that thermal isolation design in chips can enhance the thermal response especially if Si substrates are used, due to the good thermal conductivity of the Si material (150 W/mK) [65].

A pulse width modulation (PWM) heating effect on nitride layered oxidized silicon-glass chips with embedded platinum films has been proposed as another means to enhance the on-chip heating process[55]. A hand-held PWM thermal cycling unit capable of ramp rates of up to 15 °C/sec and small volume (2 μl) PCR were the features of this demonstration.

A serpentine channel with 50 μl volume that forms the PCR chamber has been developed and demonstrated in Si-pyrex structures[66]. Two open ports on the surface were drilled to enable pressure driven flow for loading and unloading of the hepatitis C sample. A similar serpentine channel approach (with total volume of 40 μl) was also used in polycarbonate (plastic) chips fabricated using the injection moulding technique [58]. In both cases, thermoelectric devices provided forced heating and cooling for PCR thermal cycling.

In a first of its kind for PCR applications, Landers and coworkers[57, 67] showed non-contact IR thermal cycling for PCR applications in commercial polyimide chips. It is claimed that the reduction of thermal mass in the form of the heating device and the heat

transfer delay from heat source to the chip will lead to rates of as much as 10 °C/sec. However, this ramp rate is much lower than those attained by other groups using thin film integrated heaters[51, 53-55]. This could possibly be due to the high optical transmission [57] of the IR light by the polyimide chip, which has resulted in an experimental setup in which a mirror arrangement was used to reflect the light back to the chip. Although a novel non-contact heating mechanism was presented in their work, the complexity in the experimental set-up and the expense of IR sources makes it an unattractive approach for cost efficient experimental devices.

Casting of a optically clear epoxy (Epotek, Epoxy Tech., USA) to fabricate biochips was recently demonstrated by Mastrangelo and coworkers[61]. The fabrication process involved patterning a silica substrate by standard photolithography and then casting the epoxy on this substrate. The epoxy cast was then sealed onto another flat cast of epoxy substrate to form enclosed fluid circuits. PCR chips and CE chips were fabricated using this epoxy casting technique that also included a nozzle diffuser pump with an expandable wax. The PCR genetic amplification was demonstrated with 1.5 µl of sample and a wax material called Chill-out™ wax was used to seal the PCR chamber and prevent evaporation during the PCR thermal cycling.

More recently, El-Ali *et al.*[68] demonstrated PCR (with 20 µl volume) performed in glass substrates with patterned thin film heaters. The feature of their work was the patterning of channels and wells in SU-8 (a negative photoresist) and demonstration of a technique to prevent inhibition of the PCR by the SU-8 material. This inhibition prevention was achieved by surface coating the SU-8 with a silanizing agent (dichlorodimethylsilane) [68].

Finite element analysis and thermal experimental results in Si and glass structures with high thermal ramping rates [69] in portable device [70] have also been presented in the work of Poser *et al.* [69] and Pal *et al.* [70]. However, no DNA samples were used for genetic testing and hence the demonstrations do not offer a means of fully analyzing the performance of the system. In fact, feedback temperature was obtained from a thermocouple inserted into the PCR chamber[70], while metals are known to inhibit PCR

reaction[8, 52, 67]. Taylor *et al.* [8] have done extensive studies on PCR compatibility using x-ray photoelectron spectroscopy and found metals, specifically chromium, to strongly inhibit the PCR genetic amplification.

2.4.2 Array PCR - Multi-Vessel Approach

PCR performed in conventional tubes in commercial thermocyclers offers the advantage of multiple tests in a single run by accommodating many Eppendorf tubes in the device, but with the disadvantage of low ramp rates (as low as 0.9 °C/s [57]) and high PCR sample volumes (~ 25 μl). On the other hand, multiple PCR chambers in chips offer similar advantages with the added feature of much lower volumes. The early demonstration of such a device was that by Chaudhari *et al.* [52] in which an 18 element array of 2 μl chambers in Si-pyrex chip was fabricated where thermoelectric elements were used to provide forced heating and cooling for PCR thermal cycling. Later, a similar chip design with 20 μl volume was fabricated to suit a PCB substrate with thin film heaters[47, 65]. Multi-array PCR chips compatible with standard commercial thermocyclers have also been fabricated and demonstrated[23, 64]. Nagai *et al.* [71] have also shown array PCR in Si chips with volumes ranging up to 32 μl.

2.4.3 Flow PCR - Space Domain Approach

In the space domain approach this is eliminated by circulating the sample across temperature boundaries, and hence PCR amplification can be achieved in rapid time but usually with larger sample volumes [18] (as compared to the time domain approach).

Similar to the time domain PCR, demonstrations of flow PCR to date have either involved thin film heaters[46-48, 50, 72] or conventional heating blocks[42, 43]. A common approach to control the flow of sample through the capillary tube in such systems has been realized by using pressured driven flow.

The other mechanisms in space domain PCR is the rotary flow[44, 45] and bidirectional flow[49] approach. In these modified space domain approaches, there exists an opportunity to reduce the size of the chip since the sample is circulated in a circular or

bidirectional manner between heated regions. Actuated pressure driven flow using commercial peristaltic pumps has been employed in such systems[44, 48]. Liu *et al.* [44] in their rotary flow mechanism used PDMS and glass to structure the chip and demonstrated PCR in a 12 nl channel; (although the actual sample loading volume was ~2 μl.) Laser induced fluorescence detection systems have also been integrated to such systems for PCR product quantification/analysis [45].

Using peristaltic pumps, bi-directional flow is also realizable for the space domain approach[49]. This work presents a detailed mechanical model of the system with finite element analysis study and integrated optical cables for PCR product quantification. However, no DNA PCR genetic amplification was performed to verify the functionality of the device.

There are complexities involved with the space domain approach. First, in the case of continuous flow in capillary tubes, an accurate sample flow rate is required since this, along with the length of the capillary tube, determines the dwell times at each temperature, which is a critical aspect in the success of the genetic amplification. The possibility of a DNA sample adhering to the walls with no chance of recovery exists in such capillary tube systems. Second, in the case of rotary or bidirectional flow mechanism, a very complex valving and pumping mechanism seems necessary which hinders portability and possible integration of other bioassays in the same device[49]. Third, the chip requires large real estate due to the lengthy capillary, thus hindering compact chip structures. Finally, cross-contamination[10] is a concern from one sample to the next in these devices if the same chip is reused. As a consequence of the above, in general, the interest in flow or space domain PCR has been unenthusiastic.

2.5 Conclusion

This chapter provided an introduction to genetic amplification using PCR. This was followed by an overview on the wide variety of applications of the PCR. PCR has emerged as a critical step in clinical diagnosis in the molecular level. Finally this chapter also presented a literature review on the work on microfabrication for PCR applications.

The research project undertaken as part of this thesis further explores the stationary PCR approach using a relatively new material called PDMS as presented in Chapter 7.

2.6 References

[1] E. M. Levine, *Cell cycling through development,* Development, 2004, *131*, 2241.

[2] C. H. Mastrangelo, M. A. Burns, D. T. Burke, *Microfabricated devices for genetic diagnostics,* Proceedings of the IEEE, 1998, *86*, 1769.

[3] J. Reiss, *The Polymerase Chain-Reaction and Its Potential Role in Clinical Diagnostics and Research,* Journal of Internal Medicine, 1991, *230*, 391.

[4] K. Hayashi, M. Orita, Y. Suzuki, T. Sekiya, *Use of Labeled Primers in Polymerase Chain-Reaction (Lp-Pcr) for a Rapid Detection of the Product,* Nucleic Acids Research, 1989, *17*, 3605.

[5] S. C. Hamilton, J. W. Farchaus, M. C. Davis, *DNA polymerases as engines for biotechnology,* Biotechniques, 2001, *31*, 370.

[6] P. Gascoyne, J. Satayavivad, M. Ruchirawat, *Microfluidic approaches to malaria detection,* Acta Tropica, 2004, *89*, 357.

[7] L. J. Kricka, P. Wilding, *Microchip PCR,* Analytical and Bioanalytical Chemistry, 2003, *377*, 820.

[8] T. B. Taylor, S. E. Harvey, M. Albin, L. Lebak, Y. Ning, I. Mowat, T. Schuerlein, E. Principe, *Process Control for Optimal PCR Performance in Glass Microstructures,* Biomedical Microdevices, 1998, *1*, 65.

[9] I. Erill, S. Campoy, N. Erill, J. Barbe, J. Aguilo, *Biochemical analysis and optimization of inhibition and adsorption phenomena in glass-silicon PCR-chips,* Sensors and Actuators B-Chemical, 2003, *96*, 685.

[10] J. B. Findlay, S. M. Atwood, L. Bergmeyer, J. Chemelli, K. Christy, T. Cummins, W. Donish, T. Ekeze, J. Falvo, D. Patterson, J. Puskas, J. Quenin, J. Shah, D. Sharkey, J. W. H. Sutherland, R. Sutton, H. Warren, J. Wellman, *Automated Closed-Vessel System for in-Vitro Diagnostics Based on Polymerase Chain-Reaction,* Clinical Chemistry, 1993, *39*, 1927.

[11] M. Eigen, R. Rigler, *Sorting Single Molecules - Application to Diagnostics and Evolutionary Biotechnology,* Proceedings of the National Academy of Sciences of the United States of America, 1994, *91*, 5740.

[12] G. Vahedi, C. Kaler, C. J. Backhouse, *An integrated method for mutation detection using on-chip sample preparation, single-stranded conformation polymorphism, and heterduplex analysis,* Electrophoresis, 2004, *25*, 2346.

[13] L. Chen, J. C. Ren, *High-throughput DNA analysis by microchip electrophoresis,* Combinatorial Chemistry & High Throughput Screening, 2004, *7*, 29.

[14] C. J. Backhouse, H. J. Crabtree, D. M. Glerum, *Frontal analysis on a microchip,* Analyst, 2002, *127*, 1169.

[15] M. E. Casperson, R. W. Coughlin, E. M. Davis, *Detecting DNA Bands in Electrophoresis Gels with Chemiluminescence,* Trac-Trends in Analytical Chemistry, 1991, *10*, 133.

[16] H. J. Crabtree, E. C. S. Cheong, D. A. Tilroe, C. J. Backhouse, *Microchip injection and separation anomalies due to pressure effects,* Analytical Chemistry, 2001, *73*, 4079.

[17] M. R. Harris, *Nonradioactive Techniques for the Labeling of Nucleic-Acids,* Biotechnology Advances, 1991, *9*, 185.

[18] H. W. Zou, M. X. Sun, H. Y. Yang, *Single-embryo RT-PCR: Application for gene expression dynamics and some technical aspects,* Acta Botanica Sinica, 2004, *46*, 578.

[19] K. W. Lai, K. C. Young, P. N. Cheng, S. H. Chen, T. T. Chang, *Interspousal transmission of hepatitis C virus: Application of comparing the variability of HVR1 nucleotide region,* Hepato-Gastroenterology, 2004, *51*, 791.

[20] S. Lee, H. S. Joo, S. H. Lee, J. E. Park, J. M. Kim, J. H. Hwang, K. S. Cho, S. Y. Hwang, *Application of DNA chip techniques for Yq microdeletion analysis in infertile males,* Experimental and Molecular Medicine, 2004, *36*, 179.

[21] S. Fujimura, S. Kato, T. Kawamura, *Helicobacter pylori in Japanese river water and its prevalence in Japanese children,* Letters in Applied Microbiology, 2004, *38*, 517.

[22] M. Orita, Y. Suzuki, T. Sekiya, K. Hayashi, *Rapid and Sensitive Detection of Point Mutations and DNA Polymorphisms Using the Polymerase Chain-Reaction,* Genomics, 1989, *5*, 874.

[23] X. M. Yu, D. C. Zhang, T. Li, L. Hao, X. H. Li, *3-D microarrays biochip for DNA amplification in polydimethylsiloxane (PDMS) elastomer,* Sensors and Actuators a-Physical, 2003, *108*, 103.

[24] T. Footz, M. J. Somerville, R. Tomaszewski, K. A. Sprysak, C. J. Backhouse, *Heteroduplex-based genotyping with microchip electrophoresis and dHPLC,* Genetic Testing, 2003, *7*, 283.

[25] T. Footz, M. J. Somerville, R. Tomaszewski, B. Elyas, C. J. Backhouse, *Integration of combined heteroduplex/restriction fragment length polymorphism analysis on an electrophoresis microchip for the detection of hereditary haemochromatosis,* Analyst, 2004, *129*, 25.

[26] J. J. Johnston, U. Lichter-Konecki, E. Wilson, B. R. Cobb, B. M. Evans, R. E. Schnur, L. J. C. Wong, *Discordant PKU phenotype in one family due to disparate genotypes and a novel mutation,* Journal of Inherited Metabolic Disease, 2004, *27*, 157.

[27] H. Clayton, I. Titley, M. D. Vivanco, *Growth and differentiation of progenitor/stem cells derived from the human mammary gland,* Experimental Cell Research, 2004, *297*, 444.

[28] S. J. Arnold, S. R. Osvath, R. A. Hall, N. J. C. King, L. M. Sedger, *Regulation of antigen processing and presentation molecules in West Nile virus-infected human skin fibroblasts,* Virology, 2004, *324*, 286.

[29] M. J. Kozal, K. Kroodsma, M. A. Winters, R. W. Shafer, B. Efron, D. A. Katzenstein, T. C. Merigan, *Didanosine Resistance in Hiv-Infected Patients Switched from Zidovudine to Didanosine Monotherapy,* Annals of Internal Medicine, 1994, *121*, 263.

[30] M. Gomez-Cano, A. Rubio, T. Puig, M. Perez-Olmeda, L. Ruiz, V. Soriano, J. A. Pineda, L. Zamora, N. Xaus, E. Clotet, M. Leal, *Prevalence of genotypic resistance to nucleoside analogues in antiretroviral-naive and antiretroviral-experienced HIV-infected patients in Spain,* Aids, 1998, *12*, 1015.

[31] J. D. Jiang, Y. Wang, Z. Z. Wang, X. H. Chen, Z. M. Guo, H. L. Pan, G. J. Bekesi, A. X. Wang, H. S. Chen, *Low frequency of the ccr5 Delta 32 HIV-resistance allele in mainland China: Identification of the first case of ccr5 Delta 32 mutation in the Chinese population,* Scandinavian Journal of Infectious Diseases, 1999, *31*, 345.

[32] Q. X. Meng, T. Su, J. P. O'Neil, V. E. Walker, *Molecular analysis of mutations at the HPRT and TK loci of human lymphoblastoid cells after combined treatments with 3 '-azido-3 '-deoxythymidine and 2 ',3 '-dideoxyinosine,* Environmental and Molecular Mutagenesis, 2002, *39*, 282.

[33] T. L. Hawkins, J. C. Detter, P. M. Richardson, *Whole genome amplification - applications and advances,* Current Opinion in Biotechnology, 2002, *13*, 65.

[34] P. R. Selvaganapathy, E. T. Carlen, C. H. Mastrangelo, *Recent progress in microfluidic devices for nucleic acid and antibody assays,* Proceedings of the Ieee, 2003, *91*, 954.

[35] S. Adamia, P. M. Pilarski, R. Prakash, J. Lauzon, C. J. Backhouse, L. M. Pilarski, *Microsystems and cancer: Improved detection of disease related genes in myeloma patients using microfluidics platforms,* Blood, 2003, *102*, 682A.

[36] C. J. Backhouse, T. Footz, S. Adamia , L. M. Pilarski, in *International Conference on MEMS, Nano and Smart Systems (ICMENS),*, 2003.

[37] L. M. Pilarski, A. J. Szczepek, A. R. Belch, *Deficient drug transporter function of bone marrow-localized and leukemic plasma cells in multiple myeloma,* Blood, 1997, *90*, 3751.

[38] A. J. Szczepek, K. Seeberger, J. Wizniak, M. J. Mant, A. R. Belch, L. M. Pilarski, *A high frequency of circulating B cells share clonotypic Ig heavy-chain VDJ rearrangements with autologous bone marrow plasma cells in multiple myeloma, as measured by single-cell and in situ reverse transcriptase polymerase chain reaction,* Blood, 1998, *92*, 2844.

[39] S. Adamia , M. Crainie , J. Kriangkum , M. Mant , A. Belch , L. Pilarski, *Abnormal expression of hyaluronan synthases in patients with Waldenstrom's macroglobulimenia,* Seminars in Oncology, 2003, 165.

[40] S. Adamia, T. Reiman, M. Crainie, A. R. Belch, L. M. Pilarski, *Aberrant splicing of hyaluronan synthase 1 (HAS1) gene in multiple myeloma (MM): HAS1 and novel HAS1 splice variants in MM B cells have an adverse impact on patient survival,* Blood, 2003, *102*, 371B.

[41] M. A. Northrup, B. Benett, D. Hadley, P. Landre, S. Lehew, J. Richards, P. Stratton, *A miniature analytical instrument for nucleic acids based on micromachined silicon reaction chambers,* Analytical Chemistry, 1998, *70*, 918.

[42] P. J. Obeid, T. K. Christopoulos, H. J. Crabtree, C. J. Backhouse, *Microfabricated device for DNA and RNA amplification by continuous-flow polymerase chain reaction and reverse transcription-polymerase chain reaction with cycle number selection,* Analytical Chemistry, 2003, *75*, 288.

[43] P. J. Obeid, T. K. Christopoulos, *Continuous-flow DNA and RNA amplification chip combined with laser-induced fluorescence detection,* Analytica Chimica Acta, 2003, *494*, 1.

[44] J. Liu, M. Enzelberger, S. Quake, *A nanoliter rotary device for polymerase chain reaction,* Electrophoresis, 2002, *23*, 1531.

[45] M. Curcio, J. Roeraade, *Continuous segmented-flow polymerase chain reaction for high-throughput miniaturized DNA amplification,* Analytical Chemistry, 2003, *75*, 1.

[46] K. Sun, A. Yamaguchi, Y. Ishida, S. Matsuo, H. Misawa, *A heater-integrated transparent microchannel chip for continuous-flow PCR,* Sensors and Actuators B-Chemical, 2002, *84*, 283.

[47] I. Schneega[ss], J. M. Kohler, *Flow-through polymerase chain reactions in chip thermocyclers,* Reviews in Molecular Biotechnology, 2001, *82*, 101.

[48] C. F. Chou, R. Changrani, P. Roberts, D. Sadler, J. Burdon, F. Zenhausern, S. Lin, A. Mulholland, N. Swami, R. Terbrueggen, *A miniaturized cyclic PCR device - modeling and experiments,* Microelectronic Engineering, 2002, *61-2*, 921.

[49] M. Q. Bu, M. Tracy, G. Ensell, J. S. Wilkinson, A. G. R. Evans, *Design and theoretical evaluation of a novel microfluidic device to be used for PCR,* Journal of Micromechanics and Microengineering, 2003, *13*, S125.

[50] T. Fukuba, T. Yamamoto, T. Naganuma, T. Fujii, *Microfabricated flow-through device for DNA amplification - towards in situ gene analysis,* Chemical Engineering Journal, 2004, *101*, 151.

[51] J. H. Daniel, S. Iqbal, R. B. Millington, D. F. Moore, C. R. Lowe, D. L. Leslie, M. A. Lee, M. J. Pearce, *Silicon microchambers for DNA amplification,* Sensors and Actuators a-Physical, 1998, *71*, 81.

[52] A. M. Chaudhari, T. M. Woudenberg, M. Albin, K. E. Goodson, *Transient liquid crystal thermometry of microfabricated PCR vessel arrays,* Journal of Microelectromechanical Systems, 1998, *7*, 345.

[53] D. S. Yoon, Y. S. Lee, Y. Lee, H. J. Cho, S. W. Sung, K. W. Oh, J. Cha, G. Lim, *Precise temperature control and rapid thermal cycling in a micromachined DNA polymerase chain reaction chip,* Journal of Micromechanics and Microengineering, 2002, *12*, 813.

[54] Y. C. Lin, M. Y. Huang, K. C. Young, T. T. Chang, C. Y. Wu, *A rapid micro-polymerase chain reaction system for hepatitis C virus amplification,* Sensors and Actuators B-Chemical, 2000, *71*, 2.

[55] Z. Zhao, Z. Cui, D. Cui, S. Xia, *Monolithically integrated PCR biochip for DNA amplification,* Sensors and Actuators A: Physical, 2003, *108*, 162.

[56] B. C. Giordano, E. R. Copeland, J. P. Landers, *Towards dynamic coating of glass microchip chambers for amplifying DNA via the polymerase chain reaction,* Electrophoresis, 2001, *22*, 334.

[57] B. C. Giordano, J. Ferrance, S. Swedberg, A. F. R. Huhmer, J. P. Landers, *Polymerase chain reaction in polymeric microchips: DNA amplification in less than 240 seconds,* Analytical Biochemistry, 2001, *291*, 124.

[58] J. N. Yang, Y. J. Liu, C. B. Rauch, R. L. Stevens, R. H. Liu, R. Lenigk, P. Grodzinski, *High sensitivity PCR assay in plastic micro reactors,* Lab on a Chip, 2002, *2*, 179.

[59] Y. S. Shin, K. Cho, S. H. Lim, S. Chung, S. J. Park, C. Chung, D. C. Han, J. K. Chang, *PDMS-based micro PCR chip with parylene coating,* Journal of Micromechanics and Microengineering, 2003, *13*, 768.

[60] J. W. Hong, T. Fujii, M. Seki, T. Yamamoto, I. Endo, *Integration of gene amplification and capillary gel electrophoresis on a polydimethylsiloxane-glass hybrid microchip,* Electrophoresis, 2001, *22*, 328.

[61] P. Sethu, C. H. Mastrangelo, *Cast epoxy-based microfluidic systems and their application in biotechnology,* Sensors and Actuators B: Chemical, 2004, *98*, 337.

[62] A. R. Prakash, S. Adamia, V. Sieben, P. Pilarski, L. M. Pilarski, C. J. Backhouse, *Small Volume PCR in PDMS Biochips with Integrated Fluid Control and Vapour Barrier,* Sensors and Actuators B-Chemical, 2004, *submitted on July 30, 2004.*

[63] S. Shandrick, Z. Ronai, A. Guttman, *Rapid microwell polymerase chain reaction with subsequent ultrathin-layer gel electrophoresis of DNA,* Electrophoresis, 2002, *23*, 591.

[64] J. Liu, C. Hansen, S. R. Quake, *Solving the "world-to-chip" interface problem with a microfluidic matrix,* Analytical Chemistry, 2003, *75*, 4718.

[65] Q. B. Zou, Y. B. Miao, Y. Chen, U. Sridhar, C. S. Chong, T. C. Chai, Y. Tie, C. H. L. Teh, T. M. Lim, C. Heng, *Micro-assembled multi-chamber thermal cycler for low-cost reaction chip thermal multiplexing,* Sensors and Actuators a-Physical, 2002, *102*, 114.

[66] S. Y. Wu, Q. Lin, Y. Yuen, Y. C. Tai, *MEMS flow sensors for nano-fluidic applications,* Sensors and Actuators a-Physical, 2001, *89*, 152.

[67] A. F. R. Huhmer, J. P. Landers, *Noncontact infrared-mediated thermocycling for effective polymerase chain reaction amplification of DNA in nanoliter volumes,* Analytical Chemistry, 2000, *72*, 5507.

[68] J. El-Ali, I. R. Perch-Nielsen, C. R. Poulsen, D. D. Bang, P. Telleman, A. Wolff, *Simulation and experimental validation of a SU-8 based PCR thermocycler chip with integrated heaters and temperature sensor,* Sensors and Actuators a-Physical, 2004, *110*, 3.

[69] S. Poser, T. Schulz, U. Dillner, V. Baier, J. M. Kohler, D. Schimkat, G. Mayer, A. Siebert, *Chip elements for fast thermocycling,* Sensors and Actuators A: Physical, 1997, *62*, 672.

[70] D. Pal, V. Venkataraman, *A portable battery-operated chip thermocycler based on induction heating,* Sensors and Actuators a-Physical, 2002, *102*, 151.

[71] H. Nagai, Y. Murakami, Y. Morita, K. Yokoyama, E. Tamiya, *Development of a microchamber array for picoliter PCR,* Analytical Chemistry, 2001, *73*, 1043.

[72] D. J. Sadler, R. Changrani, P. Roberts, C.-F. Chou, F. Zenhausern, *Thermal management of BioMEMS: temperature control for ceramic-based PCR and DNA detection devices,* Components and Packaging Technologies, IEEE Transactions on [see also Components, Packaging and Manufacturing Technology, Part A: Packaging Technologies, IEEE Transactions on], 2003, *26*, 309.

Chapter – 3

Capillary Electrophoresis

3.1 Introduction

Capillary electrophoresis (CE)[1, 2] is a popular PCR product analysis method. DNA fragments of different sizes are separated by the application of a high voltage and often fluorescently labeled DNA is detected by a laser induced fluorescence (LIF) detection[1] scheme. This CE process is usually performed following PCR for the analysis of the amplified DNA. The following section provides an overview of the working principle of CE. Then, an instrument and a biochip that were used in this work for performing the CE analysis are presented.

3.2 Electrophoresis Separation and Fluorescence Detection

Electrophoresis is a technique used for separating DNA fragments of different sizes from a mixture[3, 4] and is 'the differential movement or migration of ions by attraction or repulsion in an electric field'[5]. The migration of particles is determined to a large extent by their size and charge.

A DNA fragment in a solution is negatively charged (at a pH of ~7 or above)[4] and hence will migrate under the influence of an applied electric field. The mobility of the fragments depends on their size and the solution properties (e.g. pH, conductivity). The migration velocity v (m/sec) of a fragment under the presence of an applied electric field E (V/m) is represented as[5]

$$v = \mu_i \cdot N_i \cdot E \qquad (3.1)$$

where μ (m^2/Vsec) is the fragment mobility and N is the fragment size. The fragment mobility μ due to electrophoresis (also known as the electrophoretic mobility) is expressed as[5] in Eq 3.2 and is valid in general

$$\mu = \left(\frac{q}{6\pi\eta r} \right) \tag{3.2}$$

where q is the charge on the fragment, η is the solution viscosity and r is the fragment radius. Therefore, if a mixture of DNA fragments is introduced in a solution (mobile phase) along a column of fluid medium, the fragments are separated into bands composed of different sizes of DNA as they migrate from the electrode at the start of the column to the other electrode at the end of the column, as shown in Figure 3-1. The distance between the separated fragments is given by, $\Delta L = \Delta\mu\, E\, t$, where t is the migration time. The fragment position along the column and the band pattern are indicative of the fragment size and the number of fragments present in the mixture.

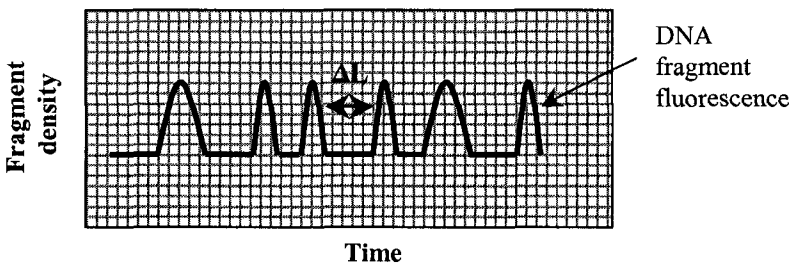

Figure 3-1. Representation of the DNA separation under the influence of an electrical field and detection by fluorescence at the end of the column.

The solution or the mobile phase used in this electrophoresis separation is usually a viscous polymer gel (sieving medium) and this is necessary[5] because DNA has uniform charge to mass ratio and in the absence of a gel medium the fragment mobility is independent of the size. The velocities of the DNA fragments in the gel medium is given by Eq. 3.1 under low field conditions, or under higher field conditions the mobility is roughly proportional to the logarithm of the fragment size. The choice of the sieving medium will depend on the range of the fragment sizes to be separated. Gels such as agarose are commonly used for separating large DNA fragments (> 3 kbp), while a denser polymer like polyacrylamide is used for shorter fragments[5]. Both double and

single-stranded DNA fragments can be separated with gels although the separation resolution of single-stranded fragments is higher than that of double stranded DNA. The number of theoretical plates N measures the resolution of the separation, which is equal to the square of the number of distinguishable bands that fit within the length of the gel. When the bandwidth is determined by diffusional spreading with diffusion coefficient D, then

$$N = \left(\frac{\mu \cdot V}{2D}\right) \tag{3.3}$$

where V is the applied voltage. Evidently, higher resolution requires high voltage. Voltages of many thousand volts[6] may be required for DNA fragment separation in a gel-filled column (typically up to 100 cm long).

DNA fragment separation in biochips with capillaries as small as 10-300 μm diameter and several centimeters long greatly benefit from low reagent consumption (few microliters) and faster separation (a few minutes) as compared to large reagent consumption (tens of microliters) and many hours required for conventional instruments to perform the same task. In addition the integration of laser optical systems to enable tracking of the fluorescently stained DNA fragment is easily possible. The CE technique is extensively used for the analysis of PCR product, DNA sequencing, mutation detection[7, 8].

3.3 Capillary Electrophoresis System

This section is aimed at providing a description of the instrument and the biochip design used to perform CE analysis of DNA. This is followed by a brief outline of the protocol followed to perform CE in what is referred to as an 'injection-separation'[1, 6] step.

3.3.1 Microfluidic Tool Kit (μTk)

A microfluidic tool kit (μTk) [1, 6] (Micralyne, AB, Canada) capable of performing the DNA fragment analysis by CE was used in the experimental analysis of the PCR product. The instrumentation of the system is briefly described below with a block diagram of the system shown in Figure 3-2. The uTk is comprised of two main units – the

high voltage (HV) supply coupled with a laser-induced fluorescence (LIF) detection system.

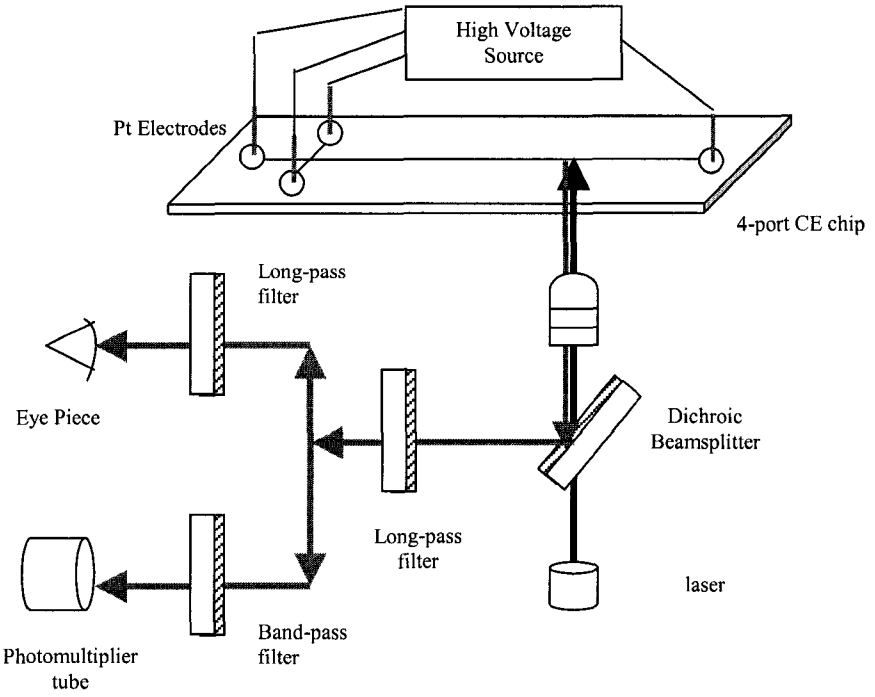

Figure 3-2: Block diagram of the Microfluidic tool kit for performing the capillary electrophoresis DNA analysis

The HV electronics is composed of two HV boards, each of which has two 6000 V power supplies capable of 80 μA. The output of the HV unit is connected to four platinum electrodes in a height-adjustable grid above the chip. Depending on the fluorophore used to label the DNA, a red laser (excitation wavelength of 635 nm and detection wavelength of 670 nm) or green laser (excitation wavelength of 532 nm and detection wavelength of 578 nm) system may be required. The μTk system has provision for easily interchanging the laser system. Note that the choice of this laser system is specific to the excitation and emission light of the fluorophore that is used to fluorescently label the DNA (i.e. the amplified PCR product). The confocal excitation system in the μTk makes use of a 40x, 0.55 NA lens to focus the beam from a solid-state laser onto the separation channel on the chip to excite the fluorophore. The emitted fluorescence from the fluorescently labeled DNA is collected with the same objective, and deflected with a dichroic mirror towards either an eyepiece or a photomultiplier tube

(PMT), depending on which is rotated into the optical path. The PMT optical path has a 10 nm band pass filter. The signal from the PMT is collected on an optics circuit board (16 bit resolution at 200 Hz).

The μTk is connected to a computer through a serial port and a LabView executable file supplied by the manufacturer controls the HV, laser and PMT modules. The entire hardware setup is enclosed in an aluminum casing that is grounded and the system is designed with safety interlock features for the HV, PMT and laser.

3.3.2 Capillary Electrophoresis Chip

The CE chip used with the μTk is a 'simple cross' chip[1, 6, 9] depicted in Figure 3-3. Although such chips were fabricated in-house with PDMS and glass materials, the DNA fragment analysis using this system (presented in Chapter 7) was performed on a glass-on-glass chip (Micralyne, Edmonton, Canada). The chip design features two crossed channels and the ends of the channels are connected to 4 open reservoirs (referred to as the sample, sample waste, buffer, and buffer waste wells), each of which has a volume of about 4 μl. Others types of CE chip designs include the 'T'[3], double 'T'[10].

To perform the CE analysis, first the channels in the chip are loaded with a sieving medium (also known as a gel) (GeneScan polymer, Applied Biosystems, CA, USA), using a pressure driven flow by means of a syringe from the buffer waste well. Although the GeneScan polymer was used for most analysis experiments, a polyacrylimide gel (POP6, Applied Biosystems, USA) is also commonly used if single stranded DNA is to be analyzed. When POP6 is used, the PCR product with double stranded DNAs is first mixed with a template suppression reagent (TSR, Applied Biosystems, USA) in a proportion of about 1:3 and then the mixture is heated to 95 °C for 3 min and finally quenched in an ice-water bath to provide single stranded DNAs.

During the gel loading process from the buffer waste well, by visual inspection, care was taken to prevent the gel from entering the three open wells (i.e. the sample in which the DNA sample is loaded, sample waste well which will contain the DNA that has migrated due to electrophoresis and the buffer wells). The chip was inspected under a microscope to observe for any discontinuities (in the form of air gaps) in the gel filled channel; if a discontinuity did exist, the channels are again refilled with the gel. Air gap

discontinuities are known to affect the conductivity in the gel medium (and consequently the DNA separation process) and hence should be avoided[1, 6].

Once the channel was properly filled with the gel, the buffer, buffer waste and sample waste wells are filled with 3 μl of 1x running buffer (prepared in-house with Tris 8.8 mM, Boric acid 8.9 mM, EDTA 2 mM) (TBE), while the sample well is filled with 3 μl of a combined mixture of 0.1 x TBE (i.e. 10 times dilution of the 1x TBE) and the PCR sample.The chip is then placed on a chip holder plate in the μTk directly below the high-voltage electrodes, as shown earlier in Figure 3-2. The movable arm in the μTk is then lowered such that the electrodes are seated inside the four wells in the chip. Then the laser is focused on the separation channel at a distance of 76 mm from the intersection, after which the photomultiplier tube is engaged.

Finally the DNA fragment analysis is performed by a two-step high voltage technique called 'injection and separation'. The injection-separation process is schematically depicted in Figure 3-3(i-iii). In the injection step, 0.4 kV is applied between the sample and sample waste wells for 60 sec. This causes the PCR product sample diluted in 0.1x TBE to be moved from the sample well along the injection channel towards the sample waste well. Now the high voltage between the sample and sample waste wells are disconnected and this is followed by a separation step. In the separation step, 6 kV is applied between the buffer and buffer waste wells for about 180 sec. (The time for which this 6 kV voltage is applied in the separation step is dependent on the base pair fragments to be separated[5] and for our experimental analysis a time of 180 sec was well above the maximum time required for the heaviest fragment to be separated and travel across the detection spot in the separation channel.) During the separation step, the negatively charged DNA fragments along with the primer caught at the intersection of the channels move towards the positive potential (buffer waste) and the separation of DNA fragments occurs. As explained earlier, the mobility of the fragments is dependent on the molecular weight, with lower molecular weight DNA fragments (i.e. fewer base pair DNA or smaller fragments) traveling faster along the channel than the higher molecular weight fragments (i.e. larger base pair DNA or larger fragments). As the fluorescently labeled DNA fragments arrive at the detection spot (76 mm from the channel

intersection) the laser source excites the fragment and the emitted fluorescence light is transduced into an electrical signal by the photomultipler tube and is recorded graphically as a x-y plot (time verses relative fluorescence intensity). This method is referred to as laser induced fluorescence (LIF) detection. Typically in this CE chip based separation, the PCR product in the channel intersection (of about 240 pl) is the volume required for performing the CE analysis. Usually a PCR product volume of 0.3 µl is loaded in the sample well and this provides sufficient DNA for many injection-separation runs. Typically three injection-separation runs are performed with a single load of reagents.

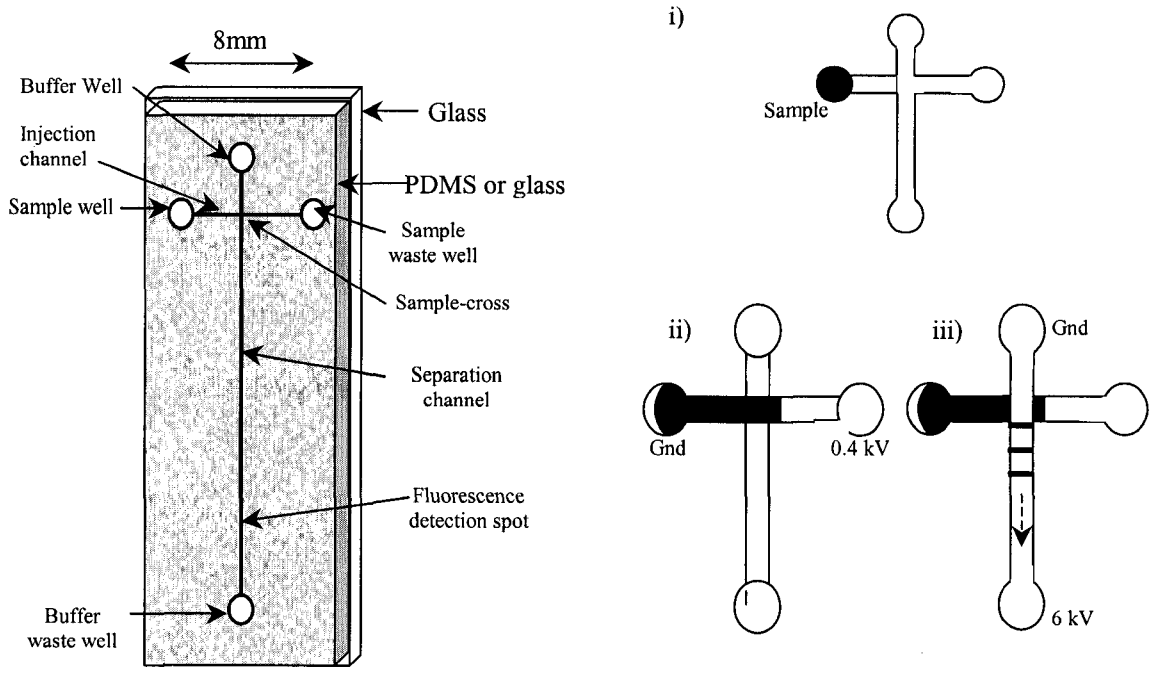

Figure 3-3. (Left) Schematic of a 'four port sample cross CE chip'. (Right). i) Sample (PCR product) loaded in the sample well in the chip. ii) the injection step causes the sample to move towards the channel intersection. iii) the separation step causes the different base pairs of the DNA to be separated and move towards the buffer waste well.

Thus the graphical x-y plot will have fluorescence peaks from all the fluorescence constituents – the size standard fragments (a commercially purchased set of fluorescently labeled DNA fragments of known size), the DNA fragments from the PCR product, and the primers. Since the size standard and primers have predefined fragment size (as specified by the supplier), any other fluorescence peak (e.g. the PCR amplified DNA fragment(s)) can be sized by comparison.

Issues such as contamination, stray electrical noise[1], can also result in peaks in the x-y plot but we have not encountered such incidences since care was taken in the form of standardized protocols. For example, a contamination check in which a chip without the PCR product or the size standard is run on the CE system to check for contamination peaks; cleaning of the electrodes is performed prior to lowering them to the chip to prevent PCR product from the previous run contaminating the current run.

3.4 Summary

In this chapter a popular PCR product analysis scheme was presented – capillary electrophoresis (CE). This CE analysis performed in microfluidic chips was described as being more advantageous in terms of reagent consumption and time of analysis; this implies overall reduced costs for such medical diagnostics. A description of the μTk, the instrument used in this work for the CE analysis, was outlined followed by a description of a sample-cross CE chip that uses an injection-separation technique for analyzing the PCR product.

The μTk system along with the CE analysis protocol described in this chapter were used for analyzing the amplified DNA retrieved from the PCR experiments performed in the biochips presented in Chapter 7.

3.5 References

[1] C. J. Backhouse, H. J. Crabtree, D. M. Glerum, *Frontal analysis on a microchip,* Analyst, 2002, *127*, 1169.

[2] C. J. Backhouse, A. Gajdal, L. M. Pilarski, H. J. Crabtree, *Improved resolution with microchip-based enhanced field inversion electrophoresis,* Electrophoresis, 2003, *24*, 1777.

[3] D. J. Harrison, A. Manz, Z. H. Fan, H. Ludi, H. M. Widmer, *Capillary Electrophoresis and Sample Injection Systems Integrated on a Planar Glass Chip,* Analytical Chemistry, 1992, *64*, 1926.

[4] A. Manz, D. J. Harrison, E. Verpoorte, H. M. Widmer, *Planar Chips Technology for Miniaturization of Separation Systems - a Developing Perspective in Chemical Monitoring,* Advances in Chromatography, 1993, *33*, 1.

[5] C. H. Mastrangelo, M. A. Burns, D. T. Burke, *Microfabricated devices for genetic diagnostics,* Proceedings of the IEEE, 1998, *86*, 1769.

[6] H. J. Crabtree, E. C. S. Cheong, D. A. Tilroe, C. J. Backhouse, *Microchip injection and separation anomalies due to pressure effects,* Analytical Chemistry, 2001, *73*, 4079.

[7] T. Footz, M. J. Somerville, R. Tomaszewski, K. A. Sprysak, C. J. Backhouse, *Heteroduplex-based genotyping with microchip electrophoresis and dHPLC,* Genetic Testing, 2003, *7*, 283.

[8] T. Footz, M. J. Somerville, R. Tomaszewski, B. Elyas, C. J. Backhouse, *Integration of combined heteroduplex/restriction fragment length polymorphism analysis on an electrophoresis microchip for the detection of hereditary haemochromatosis,* Analyst, 2004, *129*, 25.

[9] T. Footz, S. Wunsam, S. Kulak, H. J. Crabtree, D. M. Glerum, C. J. Backhouse, *Sample purification on a microfluidic device,* Electrophoresis, 2001, *22*, 3868.

[10] N. Chiem, D. J. Harrison, *Microchip-based capillary electrophoresis for immunoassays: Analysis of monoclonal antibodies and theophylline,* Analytical Chemistry, 1997, *69*, 373.

Chapter – 4

Microfabrication of Biochips

The microfabrication of bioMEMS devices enables rapid prototyping of biochips and facilitates performing clinical testing in an inexpensive and an easily accessible manner. This chapter presents microfabrication techniques to fabricate PDMS-glass hybrid biochips. Two types of application-specific chips were fabricated for the evolving PCR application – the first a PDMS-glass PCR chip and the second a PDMS-glass integrated PCE-CE chip with thin-film heaters. The PDMS processing for either of the chips presented here is a first-of-a-kind technique in which a novel low water/vapor permeable material in the form of a polyethylene is implanted in the PDMS. This implant was necessary to enable small volume PCR in PDMS structures.

4.1 Introduction

In recent years, extensive research and laboratory facilities to support bioMEMS device fabrication have been developed both in universities and in industry. The University of Alberta, Edmonton, Canada, houses one such extensive facility (with equipment worth over $30 million) and this has facilitated the prototype fabrication of the bioMEMS devices presented in this research.

Until recently, bioMEMS device processing of biochips had been limited to silicon (Si), glass (and rarely) ceramics with processing techniques that had been adopted from the semiconductor industry. However, microfabrication processes with these materials is time-consuming and expensive. For instance, in Si material biochips, a nitride[1] or oxide[2] is typically used as a coating layer on the Si by an expensive, time consuming process using vapor deposition is required to prevent PCR inhibition; the

formation of reaction chambers requires prolonged etching of surfaces[1-6]. The rapid growth of bioMEMS has prompted extensive research to explore alternatives to Si and glass that will facilitate the rapid prototyping of devices.

Low fabrication cost is a major attraction in choosing polymers for microfluidics processes. Another attractive property of polymers is that they can exist in either hard (glassy) state[7, 8] or soft (rubbery) state[9], a choice that is not offered by either Si or glass structures[10].

In recent years, polymers like polycarbonate[8], polyamide[7, 11], polymethylmethacrylate (PMMA), polydimethysiloxane (PDMS), and even epoxies[12] have been researched as potential materials for bioMEMS device fabrication[13]. Of these polymers, PDMS has drawn increased attention due to a 'replica molding fabrication technique' (called soft-lithography[14]) that facilitates the cost-efficient batch production of PDMS devices. The soft-lithography replica molding of PDMS devices is revolutionizing microfluidic applications as it facilitates rapid prototyping with feature sizes as small as 2 nm[15]. It is believed[14] that in the coming years PDMS will be the most widely used polymer in bioMEMS processing and can be expected to change the trends in the microfabrication industry[14].

Some of the attractive properties of using PDMS in bioMEMS can be summarized below.

(a) *Biochemical compatibility and safety:* for example, it is not known to strongly inhibit genetic analysis processes (e.g. PCR amplification)[9, 14]. Alternatively, modification of its structure or surface for target specific applications is possible[14] as described below. For example, to control properties like wetting (hydrophilicity), adhesion, friction, and biosensing, to name a few, either physical or chemically induced modification may be required and such a property modification can be (relatively) easily performed by physical or chemical methods[14, 16] (e.g. cross linking[13], chemical grafting[17-23]).

(b) *Fabrication fidelity:* very cost effective compared to traditional microfabrication materials like glass and Si (< $50/lb of PMDS polymer).

(c) V*ersatile mechanical* properties such as adjustable stiffness and surface adhesion energy by altering the proportion of the polymer mixture.

(d) O*ptical transparency* in both the visible and UV spectrum, which is desired in many DNA analysis techniques either for visual monitoring of fluid flow or for functional integration with DNA detection systems (e.g. CE[24, 25]).

The application of PDMS in microfluidics has been enormous. Some of these applications that are closely relate to bioprocesses relevant to this research have been summarized in the following table (Table 4-I).

Table 4-I. A summary of the applications of PDMS in microfluidics

Application	Reference
Biochemical assays	[26-28]
Cell sorting and counting	[29, 30]
Capillary electrophoresis	[13, 31, 32]
Cell culture	[33, 34]
Control of fluid flow (valves and pumps)	[35-40]
Liquid chromatography	[41]
Mass spectroscopy	[42, 43]
Dielectrophoresis	[44]
Optical components	[45]
Patterning surfaces	[46, 47]

Evidently, PDMS has become a very widely used material in modern bioMEMS devices. However, none of the above applications have involved genetic testing with elevated temperature (e.g. PCR). Vaporization of fluids due to heat causes a vapor pressure build-up within enclosed chambers and in a material like PDMS, the vapor is not retained within the chamber due to the porosity[48] of the PDMS. This results in the loss of fluid samples. Until recently, this form of fluid sample loss in PDMS had been an issue that has not been explicitly addressed in the literature. Addressing this problem forms a substantial part of the work in this thesis and is described in Chapter 7 (and in Prakash *et al.*[49]).

The soft polymer of PDMS is composed of a mixture of two chemical components that gives this silicone rubber some of the unique properties outlined earlier. The chemical composition is described below.

PDMS composition

The PDMS elastomer (Sylgard 184, Dow Corning, USA) is composed of two parts, a pre-polymer (part A) and a cross linker (part B, curing agent) [33]. The pre-polymer, defined as a polymer in its uncured form, is mainly an oligomer terminated with a vinyl group. The cross-linker is composed of a Pt catalyst and the PDMS oligomer with active hydrogen[50] (SiH) molecules. When the PDMS is prepared with the pre-polymer and cross-linker, not all the oligomers strands are incorporated into the cross-linked network upon curing the PDMS[51]. Therefore the cured PDMS contains uncross-linked, low molecular weight oligomers that are present in the bulk structure of the PDMS. A PDMS chemical structure has repeating O-Si$(CH_3)_2$ groups (as shown in Figure 4-1 [18]) with Si-O bonds at a distance of approximately 0.165 nm[18].

This form of Si chemical bond is unique to PDMS and this chemical structure is responsible for the high thermal stability of PDMS. (It is believed by Kim *et al.*[52] that PDMS can be heated to 200 °C for a year and will still remain unchanged in its physical and chemical properties. The PDMS chemical structure is also resistant to acids[52, 53].)

With these many attractive properties, PDMS was a compelling choice as a material to fabricate the biochips used in this work.

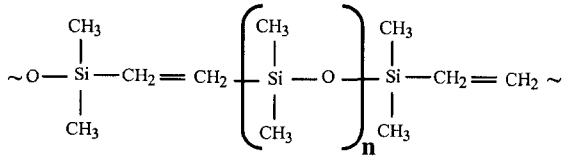

Figure 4-1. Chemical structure of the PDMS

In the following sections, two biochip designs and fabrication techniques are described to produce PDMS-glass hybrid biochip structures. The first is that of a PCR biochip microfabricated with microfluidic channel, well and chamber in the PDMS that was then sealed to a lower (unpatterned) glass substrate. The second design is that of an

integrated PCR-CE biochip, which incorporates much the same PDMS processing as the PCR chip but with the lower glass substrate also processed to incorporate resistive thin-film heaters. The resistive thin film heaters were composed of a gold (Au) layer (with chrome (Cr) as the adhesion layer). Optical lithography and wet etching techniques were used to process the Au-Cr metals. The resistive heater was integrated onto the chip to facilitate on-chip heating for the PCR thermal cycling.

The soft-lithography PDMS processing described here is a first-of-a-kind enhanced technique, in that an implant material in the form of a polyethylene (PE) layer was embedded in the PDMS. This was necessary, particularly to enable performance of small volume PCR in such devices as discussed in Chapter 7.

4.2 Chip Designs

The targeted application of both the biochip designs was to primarily enable performing the PCR. The first chip design was that of a PDMS-glass PCR biochip and the second was an evolution of the earlier design aimed at functionally integrating the CE to PCR, again, in a PDMS-glass PCR-CE biochip. These designs are described in the following sub-sections.

4.2.1 PCR Biochip Design

The PCR biochip design is shown in Figure 4-2. Two open wells on the extreme ends of the chip serve as fluid reservoirs. An enclosed PCR chamber is located at the center of the chip and microfluidic channels (10 mm x 50 μm x 20 μm) from either sides of the PCR chamber connect the two reservoirs to the chamber.

The capacity of the reservoirs was approximately 4 μl. The volume of the enclosed PCR chamber was designed to be ~ 1.75 μl. The overall dimensions of the chip are: length = 22 mm, width = 11 mm, glass substrate height (thickness) = 1.1 mm, and PDMS height (thickness) ≈ 1.7 mm. Thermal cycling for PCR is performed using external heating/cooling devices as described in Chapter 5.

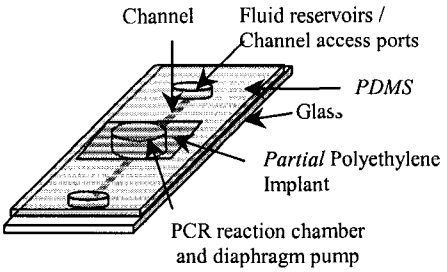

Figure 4-2. Model of the PDMS-glass hybrid biochip

4.2.2 PCR-CE Chip Design

The design of the earlier PCR biochip was such that upon completion of PCR, the PCR product would be moved to one of the reservoirs using the pumping technique that are external actuator based as described in Chapter 6. The fluid would then be manually retrieved and loaded into the sample well of the 4-port CE chip used to perform the PCR product analysis (as described in Chapter 3). In a functionally integrated chip design, it would be ideal if the PCR chamber was combined with the CE channels. In addition, the integration of Au thin film heaters to this chip design is also discussed below. The PCR-CE chip was designed with all of the above functionalities. A performance evaluation of these PCR-CE fabricated chips can be found in Chapter 8 and an operational overview is presented below.

In the integrated PCR-CE chip design, as shown in Figure 4-3, the enclosed PCR chamber was placed along the channel connecting the 'sample well' to the 'sample waste well'. The volumes of the open wells were about 4 μl and that of the PCR chamber was about 1.75 μl. The microfluidic channel in the chip had dimensions of 50 μm x 20 μm. The thickness of the Cr and the Au metals is 20 nm and 200 nm, respectively. The overall dimensions of the chip were: length = 95 mm, width = 30 mm, and thickness (PDMS+glass) ≈2.8 mm.

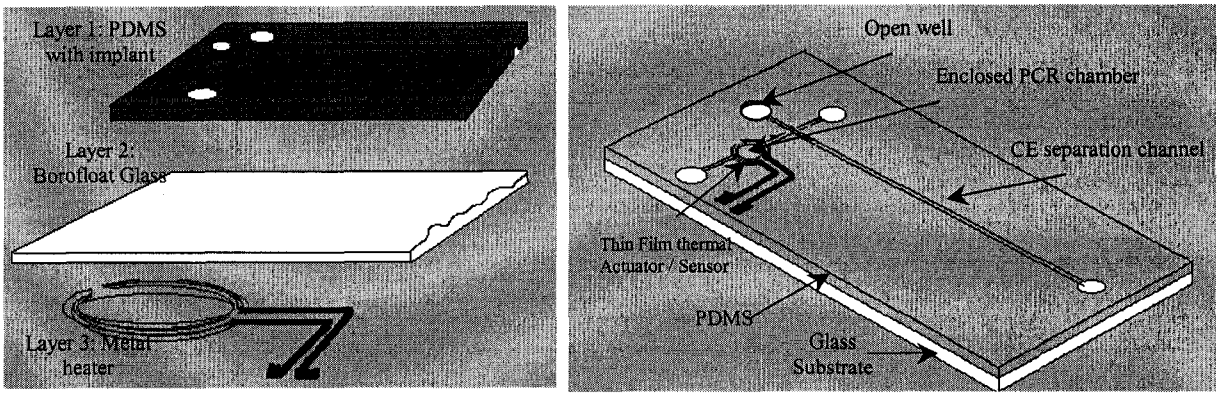

Figure 4-3. The multi-layer chip structure.Left: Layer 1 is the PDMS layer with channels, enclosed and open wells, and mositure barrier implant. Layer 2 is the lower glass substrate of the chip. Layer 3 is the thin film heater (Cr-Au) layer. Right: The PCR-CE chip layout

The functional operation of the chip was designed to be as follows: first, load the PCR sample with a micropipette into the sample well. Second, move the PCR sample from the sample well into the PCR chamber. Third, seal the channels connecting the PCR chamber and perform the PCR genetic amplification thermal cycling using the Au thin film heaters. Fourth, upon completion of the genetic amplification process, pump the PCR product from the PCR chamber into the sample well (using the pumping method described later in Chapter 6, section 6.3). Fifth, load the gel (or sieving medium, polymer) in all the channels in the chip starting from the buffer waste well by means of a syringe driven pressure flow (as described earlier in Chapter 3). Finally, perform the CE injection-separation in the same manner described earlier in Chapter 3, section 3.3.2.

4.3 Biochip Fabrication

There are primarily three major processing steps involved in the fabrication of these PDMS-glass hybrid biochips – the master mold preparation, PDMS molding with vapor barrier implant, and the PDMS-glass bonding process. In addition, in the case of the PCR-CE chips with an integrated heater, the glass is also processed to form metal heaters prior to bonding to the PDMS. The following subsections describe these processes followed by a brief discussion on the requirement and optimization of the PDMS bonding protocol.

4.3.1 PDMS Master for PCR and PCR-CE Chips

Chip designs were drawn in L-Edit v8.0, (MEMS Pro, MEMS CAP, CA, USA) and then transferred to a chromium mask wafer using a pattern generator, (DWL 200, Heidelberg Instruments, CA, USA). A 4"x4" borofloat glass substrate, (Silicon Valley Microelectronics, CA, USA), is cleaned in a fresh Pirahna (1:3 by volume of hydrogen peroxide and sulphuric acid, T > 80 °C) and then sputtered with a layer of chromium to a thickness of 200 nm (chamber pressure in argon gas: 7 mTorr and power: 300 Watts) in a sputtering system, (KJLC-CMS-18HV, Kurt J Lesker, Clariton, USA). The metalised glass substrate is then spin-coated, (5110-CD, Solitec Spinner, CA, USA), with 10 ml of SRJ5740 ultra-thick positive photoresist, (Shipley Microelectronics, MA, USA), at a spin speed of 200 rpm for 10 seconds and a spread speed of 1500 rpm for 15 seconds and then soft-baked in an oven at 115°C for 60 minutes. The substrate is then stored overnight in a light-tight box with a beaker of water (10 ml) before further processing. We have found that overnight humidified storage quickens the developing time after UV exposure. UV exposure (30 seconds, 356 nm, intensity of 19.2 mW/cm^2) on the spin-coated substrate is performed through the chrome mask using a mask aligner system, (ABM Inc., CA, USA). The substrate is then developed with Developer 354, (Shipley Microelectronics, MA, USA), for about 45 minutes (- end time determined by visible inspection), which dissolves the unexposed region of the photoresist. The substrate now serves as the master mould for PDMS replica moulding[51]. The features of the photoresist are inspected on an optical profilometer, (model # 99-33-50083, Zygo Corp., CT, USA). With a single coating of this photoresist a channel height of about 18 μm was attained. Figure 4-4 shows an optical profilometer measurement of the photoresist that shows the height of the photoresist-patterned channel.

To increase the height of the photoresist features, the process of spin coating and soft baking can be repeated several times before UV exposure.

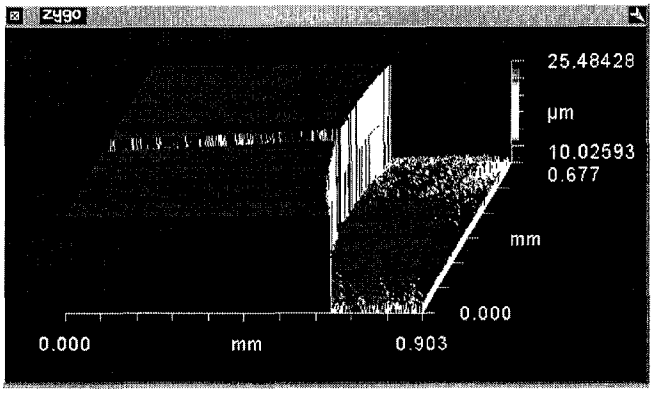

Figure 4-4 Optical profilometer of the SRJ 5740 photoresist on a metalized glass substrate

4.3.2 PDMS Molding with Vapor Barrier Implant

With photoresist patterning as performed earlier or glass/Si substrate etching[46], it is fairly challenging to attain features with very high aspect-ratio (i.e. high height). However, a high height design is desirable for the PCR chambers as it reduces the 'surface spread area' of the fluid within the chamber and provides an optimized thermal design (i.e. reduced possibility of convection losses)[38]. In order to reduce this 'surface spread area', 3D stainless steel metal posts were used to constitute the PCR chamber during the PDMS replica molding process. Cylindrical metal posts (0.75 mm radius x 1mm height) were cleaned by a brief immersion in hot Piranha, rinsed, dried and placed upon the master mold at the locations of the PCR chambers (Figure 4-5, step 5). Thus in the final PDMS mold, the PCR chamber will have a volume equal to the volume of the metal posts plus the volume of the photoresist underneath it (i.e. a total of ~ 1.75 µl). It was observed that when the PDMS was molded with these posts the PDMS did not adhere to them. Any seepage was easily removed in the later stage of the fabrication process.

The PDMS fabrication was a three-layer structure in which the top and bottom layer was composed of PDMS while the middle layer was a PE implant embedded in the PDMS. To fabricate the PDMS with the mold of the photoresist features patterned on the metalized glass and with the PE layer implanted within, either the chemical or the physical implant method described below was used, represented as step 5 in Figure 4-5.

Chemical implant method 1: Polyethylene (PE) resin or film, (Glad Metric Offer, ON, Canada), is soluble in a variety of solvents with affinity to hydrocarbon solvents like toluene and xylene[54]. We chose toluene as a solvent to dissolve PE, (Fair Lawn, NJ, USA), due to its moderate interaction and absorption by the PDMS[51] as this causes an inter-diffusion into the PDMS structure (similar to an interpenetrating polymer network (IPN)[55])and results in an irreversible interfacial adhesion between the PE and PDMS. PE (0.5 grams) and toluene (25 ml) were placed in an Erlenmeyer flask with a magnetic stir bar in it. The Erlenmeyer flask is then mounted on a stirrer-hot plate instrument, (Isotemp, Fisher Scientific, ON, Canada) and stir-heated at 200 rpm and a nominal temperature of 120 °C. Upon 10 mins of stir-heating, the PE was completely dissolved and a homogenous (liquid) mixture was obtained. (**Caution:** Toluene is a carcinogenic, aromatic hydrocarbon and care should be taken for safe handling inside a fume hood. The Erlenmeyer flask should remain uncapped at all times to prevent pressure build-up in the flask). To implant the PE, first a portion of the liquid PDMS (15 grams) was poured into a metallic holder housing the master. Then the homogenous liquid of toluene and PE was poured over the PDMS and let-stand for 15mins to cause a visible partial drying of the toluene. The thickness of the PE implant layer is ~35 μm on the 4.2"x4.2" wafer mould assuming a distinct layer and a 25% handling loss (since some residue was left behind in the flask). To increase the thickness of the PE layer, more dissolved PE could be used or the layering process can be repeated. After the partial drying of the toluene, the remaining portion of the PDMS (5 grams) was poured on the master, making up a total thickness of about 2 mm. The PDMS with the implanted PE is then thermally cured at 90 °C for 1.5 hours in an oven.

Physical implant method : In this implant method, a pre-cast PE film of 12 μm thickness, (Glad Metric Offer, ON, Canada), was used. The process is similar to method 1 in that 15 grams of the PDMS was poured in a metallic holder housing the master. Then the PE film is introduced on the surface of the PDMS before the remaining PDMS (5 grams) was poured on the master thus creating an implant of the PE film. The PDMS with the implanted PE is then thermally cured in an oven at 90 °C for 1.5 hours and then

the temperature is ramped to 135 °C (approximately at 1 °C/sec) for 10 minutes. This final temperature ramping was performed to thermally treat and soften the PE implant near its melting point (137 °C) to cause an irreversible interfacial adhesion between the PDMS and the PE. However, in the chemical implant method, this final temperature ramping was not required, as the irreversible adhesion is possibly achieved due to the inter-diffusion of the dissolved PE in the PDMS.

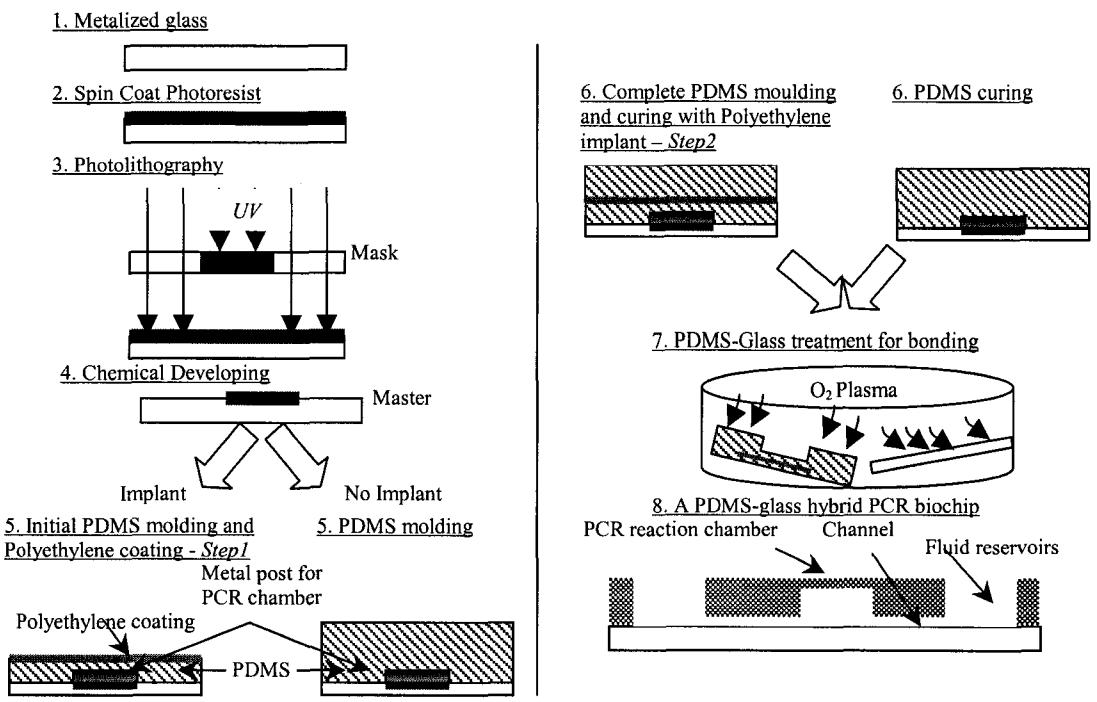

Figure 4-5. PDMS biochip fabrication procedure

4.3.3 Integrated Thin Film Heater Processing for PCR-CE Chips

For the PCR-CE chips, the lower glass substrate was processed for patterning metal heaters as described below prior to bonding the PDMS to the lower substrate. The microfabrication process steps involved in this process is shown in Figure 4-6.

The design of the metal heater was drawn in L-Edit v8.0, (MEMS Pro, MEMS CAP, CA, USA) and then transferred to a chrome mask wafer using a pattern generator, (DWL 200, Heidelberg Instruments, CA, USA). A 4"x4" borofloat glass substrate, (Silicon Valley Microelectronics, CA, USA), was cleaned in a hot Piranha solution (1:3

by volume of hydrogen peroxide and sulphuric acid, T > 80 °C) and spin-rinse dried (ST-206D, Semitcot) with de-ionized water and nitrogen to clean the surface of any organic contaminants. The glass substrate is then sputtered with a layer of chrome (Cr) metal to a thickness of about 20 nm and then with a layer of gold metal (Au) to a thickness of 200 nm (chamber pressure in argon gas: 7 mTorr and power: 300 Watts) in a sputtering system, (KJLC-CMS-18HV, Kurt J Lesker, Clariton, USA). The thickness of the metal layer is estimated based on the known vapor deposition rate. Although only the Au metal was required as a heating element, an underlying chrome layer was necessary since gold does not readily adhere to the glass. Alternatively, Cr adheres to the glass as well as gold and hence can be used as an interface layer between them. The metalized Cr-Au glass substrate is then spin coated with 10 ml of HRP 504 positive photoresist (Shipley Microelectronics, MA, USA) at a spread speed of 500 rpm for 10 sec and a spin speed of 4000 rpm for 40 sec (model # 5110-CD, Solitec Spinner, CA, USA). Then the substrate is soft-baked in an oven at 115 °C for 30 min and then cooled to room temperature under ambient conditions (T ≈20 °C) for 30 min. UV exposure (4 seconds, 356 nm, intensity of 19.2 mW/cm^2) on the spin-coated substrate is performed through the chrome mask using a mask aligner system, (ABM Inc., CA, USA). The substrate is then chemically developed in developer 354 (Shipley Microelectronics, MA, USA) for 25 sec and rinsed in de-ionized water and dried in nitrogen. The wet chemical etch process to remove the metal from regions of the substrate where it is not desired is performed in two steps – first for the upper Au layer and then the bottom Cr layer. The Au etch is performed with a Au etchant (prepared with 100 gm potassium iodide and 25 gm iodine dissolved in 1 liter of de-ionized water) for typical about 1 min – end point determined by visual appearance of the underlying Cr layer. The substrate is then rinsed with de-ionized water and dried in nitrogen. This is followed by a Cr etch with a Cr etchant (Arch Microelectronic materials, MA, USA) for about 15 sec, with the end time determined by the appearance of the glass substrate below the Cr layer – the Cr metal turns blackish in color before it disappears. The substrate is then rinsed with de-ionized water and dried in nitrogen and inspected

under an optical microscope. If any residual metal in the form of Au or Cr is observed in areas not protected by the photoresist, the process of metal etch is repeated as required.

The etch times for either of the metals described above (i.e. ~ 1 min for Au and ~ 15 sec for Cr) has been experimentally determined by the thickness of the deposited metal. Care should be taken to avoid over-etching especially for the Cr as it forms the binding layer for the Au without which the Au film is expected to peel-off. Finally, the photoresist is stripped from the upper Au metal by washing with acetone, isoproponal (IPA), and spin-rinse-dried with de-ionized water and nitrogen.

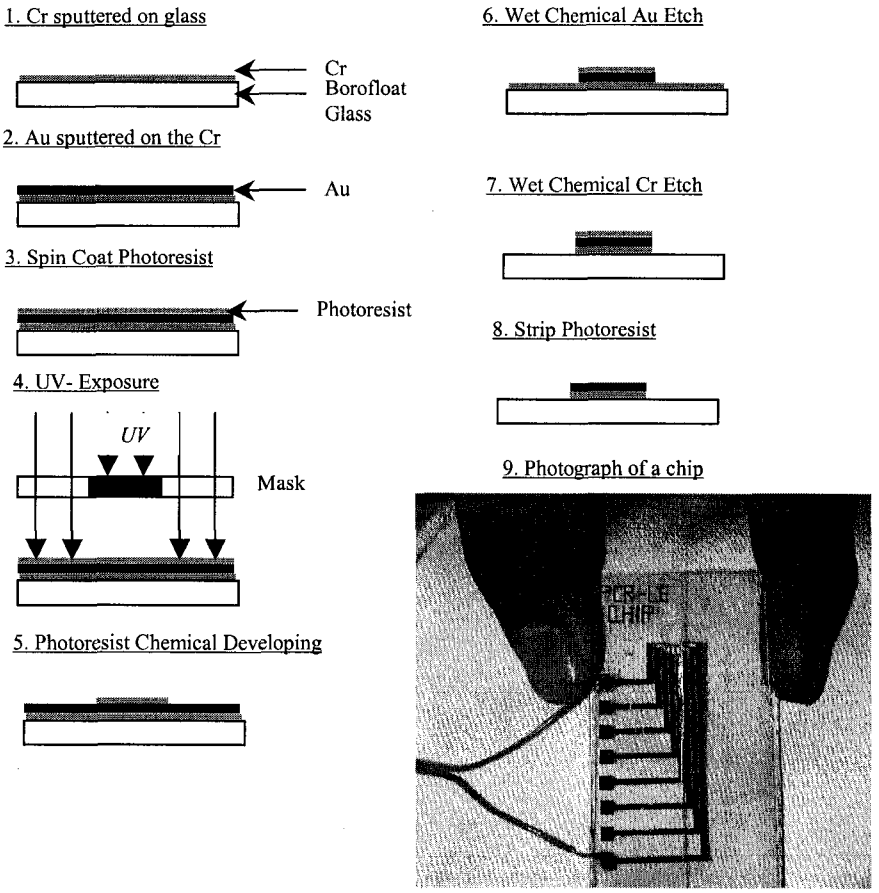

Figure 4-6. Microfabrication steps for patterning metal heaters on glass

For these PCR-CE chips with integrated metal heaters, the glass substrate with the patterned metal heater is flipped-over such that the metal is on the bottom surface of the

chip and the unpatterned glass side is the surface that is bonded to the PDMS. In this approach, the metal is separated from the fluidic circuit in the chip and hence does not make contact with the reagents. Contact of any metal with the PCR reagents (especially Cr) is avoided as metals are known to strongly inhibit the PCR genetic amplification process[56].

4.3.4 Device Packaging

Once the PDMS is peeled from the master it is open- roofed and has to be bonded to a lower substrate to produce enclosed channels and chambers. PDMS can be reversibly bonded by conformal contact (via the van der Waals forces) or irreversibly bonded to itself or Si-based materials[16] (e.g. glass). For PCR applications a completely irreversible bond (one in which the PDMS is fused to the glass and the layers cannot be separated without tearing) was critical to

1. Prevent any form of vapor loss from the PCR chamber at the interface layer (i.e. between the PDMS and the glass) during the PCR thermal cycling, and
2. Enable the fluid plumbing and valving, the uses of high pressure.

For the above reasons achieving a completely irreversible bond on the entire surface of the chip, one in which the PDMS is completely fused to the glass, was a critical requirement in this application. Irreversible bonding is also otherwise desired, as it prevents possibly introducing contaminants during chip handling that could potentially inhibit the PCR[57]. Two protocols to irreversibly bond the PDMS to the glass were developed and are described below.

The cured PDMS (with or without the implanted PE) was peeled-off from the master and diced along chip boundaries with a razor knife. Plain glass substrates for the PCR chips or integrated heater glass substrates in the case of PCR-CE chips are also diced in a dicing saw (DAD 321, Disco Hi-Tec America, USA) to the dimensions of the chips. For the PCR chips, Pirahna cleaning of the glass substrate is performed prior to bonding. In the case of the PCR-CE chips, Pirahna cleaning at this stage is not required as it was performed prior to patterning the metal heaters on the glass. The PDMS is then bonded to the glass using either the O_2 plasma technique[16] described below or the corona

discharge[58, 59] technique of which the O_2 plasma technique offers faster batch processing times.

4.3.4.1 Oxygen Plasma Bonding Technique

A Reactive Ion Etch (RIE) system (Plasmalab, Plasma Technology) equipped with O_2 plasma gas and a hot plate were used in this protocol to achieve a fully irreversible bond (one in which the PDMS is completely fused to the glass). It is believed that a combination of surface oxidation and UV treatment from the RIE is possibly the cause for the irreversible bond[9, 14].

The mating surfaces of the PDMS and the glass are placed face-up in the RIE with 80% O_2 gas flow at a pressure of 0.15 torr, a power of 37 watts and treated for 70 seconds. Venting of the RIE takes approximately takes 2 min after which the mating surfaces were brought in contact immediately (within 1 minute) and mild pressure was applied before thermal treatment on a hot plate for 5 min at a nominal temperature of 100 °C. The chip is again placed in the RIE with the glass surface of the chip on the floor of the RIE chamber and treated with the same condition as before to complete the PDMS bonding protocol. It was found that the second RIE treatment always resulted in a fusion type bond (i.e. the PDMS was irreversibly fused to the PDMS). While a single RIE treatment also resulted in an irreversible bond in some locations, the entire surface of the PDMS was not always completely fused to the glass. Care was taken to prevent contact of any material on the mating surfaces of the PDMS or the glass prior to bonding as it prevented irreversible bonding of the surfaces in those areas.

Pre-treatment of the RIE was required for the following reason. First, the conditions for O_2 plasma treatment are specific to the plasma system used and hence literature parameters cannot be generalized. Second, in the literature[48] this bonding process has been reported to cause inhibition of the PCR. It is possible that this is because the RIE system is commonly used for other processes such as etching of metals, photoresist, Si. Contaminants like metals and Si migrating to the surface of the chip during the RIE bonding process can potentially inhibit PCR[4, 11]. To prevent such ill effects, a manual cleaning of the floor of the RIE chamber with a clean room wipe

moistened with isopropanol (IPA) was done and this was followed by a 'dummy run' of the RIE system for 30 min with the same parameters as the bonding protocol. With such a cleaning and pre-treatment protocol it is hoped that the inhibition of the PCR will be minimized (if not prevented).

4.3.5 Mass Production

In the final stage, reservoir holes to access the channels are punched with a custom-made hand punch with 2 mm diameter. Alternatively, posts higher than the thickness of the PDMS mould can be used when molding and removed upon curing to form access holes[60]. With the photolithographic processing of a single 4"x 4" master substrate with patterned channels and wells, the master was reused for up to typically 5 replica moldings of PDMS devices. It was found that the photoresist patterns tend to peel-off along with the PDMS when more the master is used than typically more than 5 times. As many as 30 PCR biochips (Figure 4-7) were fabricated in each such replica molding process which highlights the cheap prototyping advantage of PDMS devices.

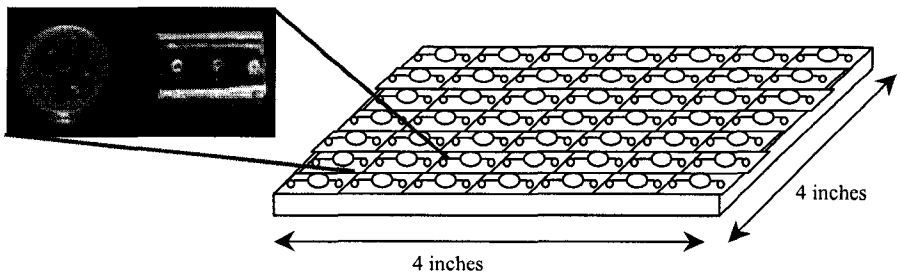

Figure 4-7. Cost efficient mass production of PDMS devices

4.4 Discussion on the PDMS Bonding Protocol

Generally, silicone rubber PDMS is a non-adhering surface[52] (i.e. it does not adhere to other materials or itself) and hence it is also commercially promoted by the manufacturer (Dow Corning, USA) as a release-agent coating for packaging adhesive tapes (e.g. the commercially available adhesive tape Tesa® 7454 uses silicon rubber as a release coating). On the other hand, recently due to the extensive application of PDMS in

microfluidics application irreversible sealing of PDMS devices have come to be explored[9, 37], such as with the protocol described above.

Although the theory behind the chemical reaction that establishes this irreversible bond has not been completely understood in the literature, a few mechanisms have been suggested. In one, the Si-CH_3 (methyl group) is destroyed during the O_2 treatment and silanol (Si-OH) groups are introduced[14], which results in the irreversible bonding of PDMS structures[58, 59] probably due to the bridging of siloxane bonds (Si-O-Si) through condensation reactions between the silanols on the two opposite plates (PDMS-PDMS or PDMS-glass) [9, 58]. Experimentally it was also found that if the bonding surfaces are to be aligned after the first surface oxidation, they should be aligned without the physical contact of the surfaces. Contacting and releasing the bonding surfaces during the alignment always leads to a very weak and unreliable bond.

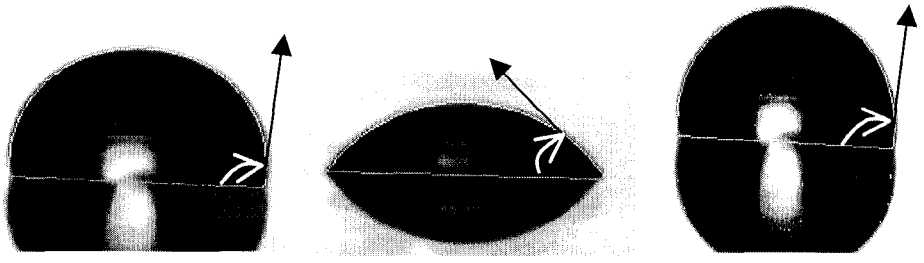

Virgin PDMS – hydrophobic - angle = 98 °

Oxidized PDMS – hydrophilic - 10 mins after treatment, angle = 41 °

Complete hydrophobic recovery - about 48 hrs, angle = 102 °

This O_2 or corona treatment also causes the PDMS surface to change its characteristic from hydrophobic to hydrophilic[9]. Figure 4-8 is a photograph of a de-ionized water droplet on the PDMS before and after O_2 treatment, processed using a contact angle measurement device (FTA135, Contact Angle Analyzer). As shown in the sequence of pictures, the hydrophobic PDMS turns hydrophilic after the O_2 treatment but gradually recovers back to its hydrophobic condition over a period of about 48 hrs.

Figure 4-8. Hydrophobic and hydrophilic properties of PDMS measured with de-ionized water droplet using a contact-angle analyzer

Although PDMS retains its hydrophilic property for (typically) a few hours, the mating surface should be brought in contact within a minute. It was also found that both

the mating surfaces (i.e. the PDMS and the glass) should be O_2 plasma or corona discharge treated to obtain reliable bonding of the PDMS structures, although the surface chemistry is not fully understood in this regard[51]. Optical surface studies have shown that when corona discharge is applied to PDMS, extensive cracking occurs on the surface of the PDMS and a thin (glassy) Si like layer of about 10 to 12 nm thick is formed on the PDMS surface[52, 59]. The RIE O_2 plasma bonding protocol parameters were developed over a year ago (by the author) and only recently has Lee *et al.* [51] reported a similar protocol.

The irreversible bonding attained using this O_2 treatment technique can withstand a pressure as high as 100 PSI[61], which is well above the maximum vapor pressure (~12 PSI[62, 63]) in the PCR chamber during the PCR thermal cycling. However, bonding achieved using high strength epoxies can only withstand a pressure of at most 10 PSI[61] before leakage occurs and hence not recommended in applications such as PCR. Although these pressure values are geometry specific, they were determined in typical microfluidic structures.

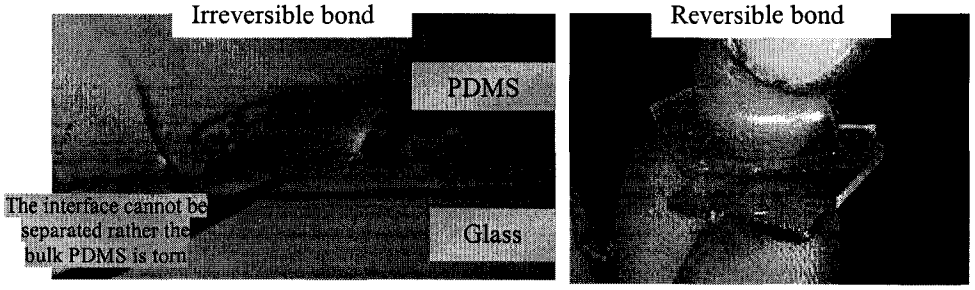

Figure 4-9. Left: An irreversibly bonded chip in which the PDMS could not be separated nondestructively from the glass. Right: Changing the parameters in the bonding protocol resulted in the undesirable reversible bond

Figure 4-9 shows the difference between an irreversibly bonded PDMS-glass structure and a reversibly bonded structure; the reversible bonding was a result of altering the protocol in terms of varying parameters such as time, oxygen flow rate in the RIE, or RIE chamber pressure. The bonding protocol parameters presented here is not a standardized literature protocol and was developed upon numerous experimental trials.

The O_2 plasma and the corona discharge[58, 59] techniques have now come to be established as the most prevalent methods for bonding PDMS devices. One other PDMS bonding method developed by the Quake's group[37] relies on heat and variation in curing agent mixing ratio during the PDMS fabrication.

4.5 Conclusion

In this chapter, the microfabrication processing of PDMS-glass hybrid biochips was described. Two chips were fabricated in this work, a PDMS-glass hybrid chip for performing the PCR and a PDMS-glass hybrid chip with integrated thin film heaters for performing the PCR and subsequent CE detection. The heater in the PCR-CE chip was anticipated to serve as an integrated on-chip heater for enabling PCR thermal cycling.

In addition, the PDMS microfabrication processes presented here (which involved implanting a material in the PDMS) was a first-of-a-kind fabrication technique not only in the fabrication facility at the University of Alberta, Canada, but also among the research community in this field (Prakash *et al.* submitted [49]). Ongoing and upcoming PDMS based projects in our laboratory have adopted this protocol to fabricate microfluidic devices. PDMS is a relatively new material in MEMS processing and at the time of fabricating these chips, no standardized protocols or dedicated equipment were available at the fabrication facility. Much difficulty was encountered during the initial stage of processing. For example, a mold to hold the master firmly against the floor of the mold (i.e. in a petri dish) to prevent the PDMS from seeping underneath was not available. Second, since the PDMS is a liquid polymer, the oven in which it is cured should be accurately leveled (to prevent the movement of the PDMS on the master). Because of many such shortcomings, it was difficult to fabricated PDMS with consistent thickness. Only recently have most shortcoming been addressed (by machining dedicated molds, handling equipment, leveled ovens) and now more consistent fabrication is achievable.

The protocols developed (by the author) to (1) irreversibly bond PDMS and (2) fabricated PDMS devices with implants are the only methods and a first-of-a-kind

approach at the fabrication facility at the University of Alberta. This method has also become a standardized protocol and to-date such skills remain within our laboratory.

4.6 References

[1] J. H. Daniel, S. Iqbal, R. B. Millington, D. F. Moore, C. R. Lowe, D. L. Leslie, M. A. Lee, M. J. Pearce, *Silicon microchambers for DNA amplification,* Sensors and Actuators a-Physical, 1998, *71*, 81.

[2] D. S. Yoon, Y. S. Lee, Y. Lee, H. J. Cho, S. W. Sung, K. W. Oh, J. Cha, G. Lim, *Precise temperature control and rapid thermal cycling in a micromachined DNA polymerase chain reaction chip,* Journal of Micromechanics and Microengineering, 2002, *12*, 813.

[3] Z. Zhao, Z. Cui, D. Cui, S. Xia, *Monolithically integrated PCR biochip for DNA amplification,* Sensors and Actuators A: Physical, 2003, *108*, 162.

[4] A. M. Chaudhari, T. M. Woudenberg, M. Albin, K. E. Goodson, *Transient liquid crystal thermometry of microfabricated PCR vessel arrays,* Journal of Microelectromechanical Systems, 1998, *7*, 345.

[5] Y. C. Lin, M. Y. Huang, K. C. Young, T. T. Chang, C. Y. Wu, *A rapid micro-polymerase chain reaction system for hepatitis C virus amplification,* Sensors and Actuators B-Chemical, 2000, *71*, 2.

[6] I. Erill, S. Campoy, N. Erill, J. Barbe, J. Aguilo, *Biochemical analysis and optimization of inhibition and adsorption phenomena in glass-silicon PCR-chips,* Sensors and Actuators B-Chemical, 2003, *96*, 685.

[7] B. C. Giordano, J. Ferrance, S. Swedberg, A. F. R. Huhmer, J. P. Landers, *Polymerase chain reaction in polymeric microchips: DNA amplification in less than 240 seconds,* Analytical Biochemistry, 2001, *291*, 124.

[8] J. N. Yang, Y. J. Liu, C. B. Rauch, R. L. Stevens, R. H. Liu, R. Lenigk, P. Grodzinski, *High sensitivity PCR assay in plastic micro reactors,* Lab on a Chip, 2002, *2*, 179.

[9] J. C. McDonald, G. M. Whitesides, *Poly(dimethylsiloxane) as a material for fabricating microfluidic devices,* Accounts of Chemical Research, 2002, *35*, 491.

[10] B. Ziaie, A. Baldi, M. Lei, Y. D. Gu, R. A. Siegel, *Hard and soft micromachining for BioMEMS: review of techniques and examples of applications in microfluidics and drug delivery,* Advanced Drug Delivery Reviews, 2004, *56*, 145.

[11] A. F. R. Huhmer, J. P. Landers, *Noncontact infrared-mediated thermocycling for effective polymerase chain reaction amplification of DNA in nanoliter volumes,* Analytical Chemistry, 2000, *72*, 5507.

[12] P. Sethu, C. H. Mastrangelo, *Cast epoxy-based microfluidic systems and their application in biotechnology,* Sensors and Actuators B: Chemical, 2004, *98*, 337.

[13] K. W. Ro, W. J. Chan, H. Kim, Y. M. Koo, J. H. Hahn, *Capillary electrochromatography and preconcentration of neutral compounds on poly(dimethylsiloxane) microchips,* Electrophoresis, 2003, *24*, 3253.

[14] J. M. K. Ng, I. Gitlin, A. D. Stroock, G. M. Whitesides, *Components for integrated poly(dimethylsiloxane) microfluidic systems,* Electrophoresis, 2002, *23*, 3461.

[15] B. D. Gates, G. M. Whitesides, *Replication of vertical features smaller than 2 nm by soft lithography,* Journal of the American Chemical Society, 2003, *125*, 14986.

[16] S. K. Sia, G. M. Whitesides, *Microfluidic devices fabricated in poly(dimethylsiloxane) for biological studies,* Electrophoresis, 2003, *24*, 3563.

[17] J. H. Park, K. B. Lee, I. C. Kwon, Y. H. Bae, *PDMS-based polyurethanes with MPEG grafts: Mechanical properties, bacterial repellency, and release behavior of rifampicin,* Journal of Biomaterials Science-Polymer Edition, 2001, *12*, 629.

[18] F. Abbasi, H. Mirzadeh, *Properties of poly(dimethylsiloxane)/hydrogel multicomponent systems,* Journal of Polymer Science Part B-Polymer Physics, 2003, *41*, 2145.

[19] F. Abbasi, H. Mirzadeh, A. A. Katbab, *Bulk and surface modification of silicone rubber for biomedical applications,* Polymer International, 2002, *51*, 882.

[20] Q. G. He, H. Chen, Z. C. Liu, P. F. Xiao, N. Y. He, Z. H. Lu, *Hydrophilic modification on PDMS surface by microwave plasma-induced grafting,* Rare Metal Materials and Engineering, 2001, *30*, 415.

[21] S. W. Hu, X. Q. Ren, M. Bachman, C. E. Sims, G. P. Li, N. Allbritton, *Surface modification of poly(dimethylsiloxane) microfluidic devices by ultraviolet polymer grafting,* Analytical Chemistry, 2002, *74*, 4117.

[22] M. T. Khorasani, H. Mirzadeh, P. G. Sammes, *Laser surface modification of polymers to improve biocompatibility: HEMA grafted PDMS, in vitro assay - III,* Radiation Physics and Chemistry, 1999, *55*, 685.

[23] A. Papra, A. Bernard, D. Juncker, N. B. Larsen, B. Michel, E. Delamarche, *Microfluidic networks made of poly(dimethylsiloxane), Si, and Au coated with polyethylene glycol for patterning proteins onto surfaces,* Langmuir, 2001, *17*, 4090.

[24] H. J. Crabtree, E. C. S. Cheong, D. A. Tilroe, C. J. Backhouse, *Microchip injection and separation anomalies due to pressure effects,* Analytical Chemistry, 2001, *73*, 4079.

[25] C. J. Backhouse, H. J. Crabtree, D. M. Glerum, *Frontal analysis on a microchip,* Analyst, 2002, *127*, 1169.

[26] A. Bernard, B. Michel, E. Delamarche, *Micromosaic immunoassays,* Analytical Chemistry, 2001, *73*, 8.

[27] J. C. McDonald, S. J. Metallo, G. M. Whitesides, *Fabrication of a configurable, single-use microfluidic device,* Analytical Chemistry, 2001, *73*, 5645.

[28] E. Eteshola, D. Leckband, *Development and characterization of an ELISA assay in PDMS microfluidic channels,* Sensors and Actuators B-Chemical, 2001, *72*, 129.

[29] A. Y. Fu, C. Spence, A. Scherer, F. H. Arnold, S. R. Quake, *A microfabricated fluorescence-activated cell sorter,* Nature Biotechnology, 1999, *17*, 1109.

[30] L. L. Sohn, O. A. Saleh, G. R. Facer, A. J. Beavis, R. S. Allan, D. A. Notterman, *Capacitance cytometry: Measuring biological cells one by one,* Proceedings of the National Academy of Sciences of the United States of America, 2000, *97*, 10687.

[31] D. C. Duffy, J. C. McDonald, O. J. A. Schueller, G. M. Whitesides, *Rapid prototyping of microfluidic systems in poly(dimethylsiloxane),* Analytical Chemistry, 1998, *70*, 4974.

[32] C. S. Effenhauser, G. J. M. Bruin, A. Paulus, M. Ehrat, *Integrated capillary electrophoresis on flexible silicone microdevices: Analysis of DNA restriction fragments and detection of single DNA molecules on microchips,* Analytical Chemistry, 1997, *69*, 3451.

[33] W. J. Chang, D. Akin, M. Sedlak, M. R. Ladisch, R. Bashir, *Poly(dimethylsiloxane) (PDMS) and silicon hybrid biochip for bacterial culture,* Biomedical Microdevices, 2003, *5*, 281.

[34] A. Folch, A. Ayon, O. Hurtado, M. A. Schmidt, M. Toner, *Molding of deep polydimethylsiloxane microstructures for microfluidics and biological applications,* Journal of Biomechanical Engineering-Transactions of the Asme, 1999, *121*, 28.

[35] N. L. Jeon, D. T. Chiu, C. J. Wargo, H. K. Wu, I. S. Choi, J. R. Anderson, G. M. Whitesides, *Design and fabrication of integrated passive valves and pumps for flexible polymer 3-dimensional microfluidic systems,* Biomedical Microdevices, 2002, *4*, 117.

[36] S. R. Quake, A. Scherer, *From Micro- to Nanofabrication with Soft Materials,* Science, 2000, *290*, 1536.

[37] M. A. Unger, H.-P. Chou, T. Thorsen, A. Scherer, S. R. Quake, *Monolithic Microfabricated Valves and Pumps by Multilayer Soft Lithography,* Science, 2000, *288*, 113.

[38] J. Liu, M. Enzelberger, S. Quake, *A nanoliter rotary device for polymerase chain reaction,* Electrophoresis, 2002, *23*, 1531.

[39] J. Liu, C. Hansen, S. R. Quake, *Solving the "world-to-chip" interface problem with a microfluidic matrix,* Analytical Chemistry, 2003, *75*, 4718.

[40] J. W. Hong, S. R. Quake, *Integrated nanoliter systems,* Nature Biotechnology, 2003, *21*, 1179.

[41] P. G. Vahey, S. H. Park, B. J. Marquardt, Y. N. Xia, L. W. Burgess, R. E. Synovec, *Development of a positive pressure driven micro-fabricated liquid chromatographic analyzer through rapid-prototyping with poly(dimethylsiloxane) - Optimizing chromatographic efficiency with sub-nanoliter injections,* Talanta, 2000, *51*, 1205.

[42] J. S. Kim, D. R. Knapp, *Microfabricated PDMS multichannel emitter for electrospray ionization mass spectrometry,* Journal of the American Society for Mass Spectrometry, 2001, *12*, 463.

[43] J. Gao, J. D. Xu, L. E. Locascio, C. S. Lee, *Integrated microfluidic system enabling protein digestion, peptide separation, and protein identification,* Analytical Chemistry, 2001, *73*, 2648.

[44] T. Kanagasabathi, C. J. Backhouse, K. Kaler, in *Nanotech 2004*, Boston, MA, 2004.

[45] O. J. A. Schueller, X. M. Zhao, G. M. Whitesides, S. P. Smith, M. Prentiss, *Fabrication of liquid-core waveguides by soft lithography,* Advanced Materials, 1999, *11*, 37.

[46] P. J. A. Kenis, R. F. Ismagilov, G. M. Whitesides, *Microfabrication inside capillaries using multiphase laminar flow patterning,* Science, 1999, *285*, 83.

[47] E. Delamarche, A. Bernard, H. Schmid, A. Bietsch, B. Michel, H. Biebuyck, *Microfluidic networks for chemical patterning of substrate: Design and application to bioassays,* Journal of the American Chemical Society, 1998, *120*, 500.

[48] Y. S. Shin, K. Cho, S. H. Lim, S. Chung, S. J. Park, C. Chung, D. C. Han, J. K. Chang, *PDMS-based micro PCR chip with parylene coating,* Journal of Micromechanics and Microengineering, 2003, *13*, 768.

[49] A. R. Prakash, S. Adamia, V. Sieben, P. Pilarski, L. M. Pilarski, C. J. Backhouse, *Small Volume PCR in PDMS Biochips with Integrated Fluid Control and Vapour Barrier,* Sensors and Actuators B-Chemical, 2004, *submitted on July 30, 2004.*

[50] C. K. Yeom, S. H. Lee, H. Y. Song, J. M. Lee, *Vapor permeations of a series of VOCs/N-2 mixtures through PDMS membrane,* Journal of Membrane Science, 2002, *198*, 129.

[51] J. N. Lee, C. Park, G. M. Whitesides, *Solvent compatibility of poly(dimethylsiloxane)-based microfluidic devices,* Analytical Chemistry, 2003, *75*, 6544.

[52] J. Kim, M. K. Chaudhury, M. J. Owen, *Hydrophobicity loss and recovery of silicone HV insulation,* IEEE Transactions on Dielectrics and Electrical Insulation, 1999, *6*, 695.

[53] H. Hillborg, U. W. Gedde, *Hydrophobicity changes in silicone rubbers,* Ieee Transactions on Dielectrics and Electrical Insulation, 1999, *6*, 703.

[54] T. W. deLoos, L. J. deGraaf, J. D. Arons, *Liquid-liquid phase separation in linear low density polyethylene-solvent systems,* Fluid Phase Equilibria, 1996, *117*, 40.

[55] J. S. Turner, Y. L. Cheng, *Preparation of PDMS-PMAA interpenetrating polymer network membranes using the monomer immersion method,* Macromolecules, 2000, *33*, 3714.

[56] T. B. Taylor, S. E. Harvey, M. Albin, L. Lebak, Y. Ning, I. Mowat, T. Schuerlein, E. Principe, *Process Control for Optimal PCR Performance in Glass Microstructures,* Biomedical Microdevices, 1998, *1*, 65.

[57] J. B. Findlay, S. M. Atwood, L. Bergmeyer, J. Chemelli, K. Christy, T. Cummins, W. Donish, T. Ekeze, J. Falvo, D. Patterson, J. Puskas, J. Quenin, J. Shah, D. Sharkey, J. W. H. Sutherland, R. Sutton, H. Warren, J. Wellman, *Automated Closed-Vessel System for in-Vitro Diagnostics Based on Polymerase Chain-Reaction,* Clinical Chemistry, 1993, *39*, 1927.

[58] K. W. Ro, K. Lim, H. Kim, J. H. Hahn, *Poly(dimethylsiloxane) microchip for precolumn reaction and micellar electrokinetic chromatography of biogenic amines,* Electrophoresis, 2002, *23*, 1129.

[59] B. Wang, Z. Abdulali-Kanji, E. Dodwell, J. H. Horton, R. D. Oleschuk, *Surface characterization using chemical force microscopy and the flow performance of modified polydimethylsiloxane for microfluidic device applications,* Electrophoresis, 2003, *24*, 1442.

[60] P. Krulevitch, W. Bennett, J. Hamilton, M. Maghribi, K. Rose, *Polymer-based packaging platform for hybrid microfluidic systems,* Biomedical Microdevices, 2002, *4*, 301.

[61] S. F. Li, S. C. Chen, *Polydimethylsioxane fluidic interconnects for microfluidic systems,* Ieee Transactions on Advanced Packaging, 2003, *26*, 242.

[62] R. Weast, *Handbook of Chemistry and Physics*, 54th Edition ed., CRC Press, Ohio, 1973-1974.

[63] Y. J. Liu, C. B. Rauch, R. L. Stevens, R. Lenigk, J. N. Yang, D. B. Rhine, P. Grodzinski, *DNA amplification and hybridization assays in integrated plastic monolithic devices,* Analytical Chemistry, 2002, *74*, 3063.

Chapter – 5

Thermal Instrumentation and Control

Investigations to design, build and implement a control system suitable for performing PCR genetic amplification are presented in this chapter. A novel controller in the form of a non-linear PD-PI controller was developed to enable fast temperature transitions between the PCR setpoints, as well as to maintain accurate temperature at each of the denaturation, annealing and extension temperatures. Since the system was a nonlinear system, gain scheduling was incorporated to implement the controller. With these, a critically damped system response was achieved. Finally, thermal calibration issues pertaining to the material properties of the chip and the thermal module are estimated, experimentally verified, and appropriate compensations incorporated.

5.1 Introduction

For the success of the PCR, one of the key requirements is a thermal control module capable of rapid thermal cycling between the denaturation (94 °C) and the annealing (~ 50 °C) temperatures. The controller must maintain an accurate temperature at each of the denaturation, annealing, and extension temperatures. To perform PCR in microfabricated chips (design as discussed in Chapter 4) an automated thermal module that meets the PCR requirements was built. The goal of this portion of the research project was to build an inexpensive thermal module and to design and implement a tailor-made controller for this system. This was accomplished by constructing a thermal device with thermoelectric elements (Peltier), in-house electronics, and a customized digital P/I/D controller. While the temperature ramp rate is a function of both the thermal mass and the control algorithm used, the temperature accuracy at a given setpoint is essentially dictated only by the control algorithm[1].

In the PCR genetic amplification application, there has been relatively little work in implementing system-specific in-house controllers and a thermal system. A vast majority of the demonstrations have used commercial thermal cycling devices and/or control modules[2-5]. Although this simplifies the tasks of the research project, these systems are invariably expensive and do not provide a means for prototyping novel biochip designs or a cost-efficient device for potential commercialization. Even among those that implemented in-house thermal devices and controllers (e.g. in the form of a PID), the temperature accuracy in the system has been an area of concern with typical overshoots > 4 °C [6-13] and setpoint accuracy up to ± 0. 5 °C [1, 6-11, 14-16]. Overshooting in particular should be avoided[10, 17, 18] because it can cause boiling of the sample and potentially destroy the DNA and enzymes in the PCR mix. In one PCR control scheme, to enable fast temperature transition, a method was used in which maximum power was output to the heating system until (nearly) reaching the setpoint whereupon a controller was invoked to control the setpoint temperatures[7, 15]. However, here too temperature overshoots were not fully preventable[15]. Moreover, this is not an optimal algorithm because the system was operated in an uncontrolled manner during temperature transition.

As it will be shown in this chapter, the inefficient controllers in PCR systems could be attributed to the lack of conceptual understanding for the implementing the PID controller for this application. Only recently has it been suggested in the literature that a split control algorithm[19] and a non-linear implementation[20] of the P/I/D controllers will be capable of overcoming the observed flaws in the thermal profile of PCR systems.

In this work, a 'dual digital non-linear PD-PI controller' is presented. The digital controller implemented here has three key features: (1) a split PD-PI process control (2) non-linear implementation by gain scheduling and (3) a dual action control.

As will be shown in section 5.3, the heating and cooling rates within the PCR temperature range are non-linear (i.e. the Peltier heats and cools ranging up to 4.5 °C/sec) which implies that the time constants are different at any given instance within the boundary temperature. Hence a non-linear controller was required to ensure accurate control of the temperature at each of the setpoints (i.e. denaturation, annealing and extension temperatures).

Second, for this bioMEMS application a conventional PID controller was split into a PD and a PI part to ensure optimal controller performance. This was particularly required because the PCR process involves two opposing requirements – one that requires fast transition between setpoints and another that requires stable operation at setpoints. It is well known [21] that in a system with negligible dead-time, the use of the D part at setpoints can cause heavy oscillation; hence only a PI controller was used for accurate setpoint control. On the other hand, if a PI controller was used during temperature transition between setpoints, the absence of the D part is expected to result in slow heating/cooling, also the presence of an I part can cause high overshoots[20]. Hence during the temperature cycling for fast temperature transition without overshooting, a non-linear PD controller was used. It will be shown that the combination of these two controllers with non-linear implementation gives a system response that is representative of an ideal critically damped system.

Finally, the third aspect of the control system is that it encompasses a dual action control (i.e. parallel processing of two systems). This was required because a two stacked-thermoelectric device (Peltier) arrangement was found necessary to enable the system to heat to temperatures as high as 94 °C - this aspect is discussed in section 5.3. To control this second Peltier, another PI controller (termed as PI_2) was used, which at the background of the PD-PI controller controls the temperature of the second Peltier at 60 °C.

This form of split control and non-linear implementation was developed well before these issues were discussed in the PCR literature. However, recently (in the later part of 2003 and in 2004) both these issues have been addressed in the literature[20, 22]. For the first time Sung *et al.*[20] characterized a PCR system as one that is nonlinear and implemented a nonlinear PI algorithm. Lao *et al.*[18] implemented the gain scheduling procedure to ensure that a consistent accuracy at each of the setpoints in the non-linear PCR system is achieved. Erill *et al.*[22] (in a yet to be published paper) have stressed the need to split the control algorithm to ensure both fast heating/cooling as well as maintain accurate temperature at setpoints.

The control system design presented here encompasses all the above discussed features in a digital format and hence the name 'dual non-linear PD-PI controller'[23],

with the performance much like a 'parallel processing control system' with zonal tuning and gain scheduling for non-linear implementation[24-26].

Finally, thermal calibration issues pertaining to the material properties of the chip and the thermal module are estimated, experimentally verified, and appropriate compensations executed. This calibration was an important because the temperature is monitored on the assembly housing the chip and not from the fluid sample inside the chip. The calibration ensured that the biosample inside the chip actually reached the setpoint temperatures.

5.2 Thermal Hardware

Single stage thermoelectric elements, Peltiers (TZ11055-01, Ferrotec, NH, USA)[27], were used in this system. The Peltier is a device that works in accordance with the Peltier effect, which effectively cools on one side of its surface and heats on the opposite side. This heating/cooling results from the passage of a DC current through a semiconductor junctions (typically Bi_2 Te_3) assembled between and bonded to two layers of ceramic plates. Heat is "pumped" from the hot side to the cold side or vice versa, depending on the electrical connection. The cold side and the hot sides of the Peltier are determined by the direction of the current flow. The heat on the hot side can be theoretically determined using the relationship[27]

$$T_{hot} = T_{amb} + R_T\left(Q + P_{in}\right) \tag{5.1}$$

where, T_{hot} = Temperature of the hot side, T_{amb} = Temperature of the surrounding, R_T = Thermal resistance of a heat exchanger, Q_c = Amount of heat absorbed from the cold side, and P_{in} = Input power given to the Peltier.

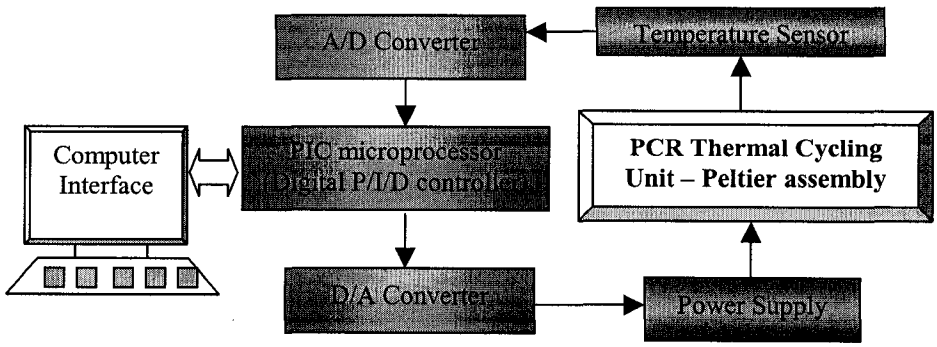

Figure 5-1. Block diagram of the thermal module

Evidently with all the parameters in Eq. 5.1 being a constant in a stable system, the input power to the Peltier (P_{in}) determines the heat generated by the Peltier. The specification of the Peltier used in the PCR system was a ±12 V (DC) and 2.5 A (max) rated device. Thus a dedicated power supply along with supporting electronic modules such an analog to digital (A/D) converter, microprocessor (PIC microcontroller), digital to analog (D/A) converter, and a temperature sensor, were specifically built for this system; the block diagram of which is shown in Figure 5-1.

The modules in Figure 5-1 are briefly discussed in the subsequent sections and a circuit diagram of the same can be found in the appendix.

5.2.1 PIC microcontroller

The PIC microprocessor (16f877, 8bit, 40 PIN, CMOS chip, Microchip Technology Inc., CA, USA) is a highly versatile 5 port Peripheral Interface Controller and forms the essential central unit in the circuitry. Software written in C language (i.e. the non-linear PD-PI controller and other hardware initializations) is compiled (CCS C compiler, CCS Inc., WI, USA) and written into the EPROM of the PIC to perform the following important functions: (1) data acquisition from the temperature sensor through the A/D, (2) data processing based on the P/I/D controller code written in the software and, (3) data-out through the D/A converter that limits the power supplied to the Peltiers.

The Master Synchronous Serial Port (MSSP) module in the PIC is used as the channel to communicate to the A/D and D/A converters. The Master Synchronous Serial Port (MSSP) module can be operated in the Serial Peripheral Interface (SPI) mode. The SPI mode allows only 8 bits of data transfer at a time but the A/D and D/A were 12 bit converters; hence necessary modification was included in the software to send or receive only 8 bits of data at-a-time. The PIC is interfaced to a computer through the RS232 serial port.

5.2.2 Temperature Sensor and A/D Converter

The temperature sensors used in the circuit are the LM50 (National Semiconductors, USA). The LM 50 has an acquisition temperature in the range of – 40 to +125 °C, which is well above the PCR requirements (i.e. 25 °C to 95 °C). The output

voltage of the sensor is linearly proportional to the temperature in Celsius (+10mV/ °C) and has an offset of +500 mV. Thus the output voltage (V_{out}) at any given temperature is calculated using Eq. 5.2.

$$V_{out} = (10 \text{ mV per degree Celsius} \times \text{Temperature in degrees Celsius}) + 500 \text{ mV} \quad (5.2)$$

The offset of 500 mV also allows for reading negative temperature without the requirement for a negative supply. The ideal output voltage of the LM50 ranges from +100 mV to 1.75 V for a – 40 °C to +125 °C temperature range. Calibration of the device involved verification of temperature reading based on the output voltage and comparison of this reading with other calibrated temperature sensing devices. When a temperature lead or a lag occurred, the appropriate lead/lags compensations were included in Eq 5.2.

The temperature sensor is connected to the A/D converter (TLC2543, Texas Instruments) with a 12-bit resolution and can multiplex up to 11 channels. In our application, only 3 temperature sensors were required to monitor the temperature of the thermoelectric element. This appears to be a device-to-device manufacturing variation.

5.2.3 D/A Converter

The LTC 1590 dual serial 12 bit multiplexing D/A converter (Texas Instruments, USA) was used in the circuitry. The dual functionality in the application essentially means that it is capable of handling both positive and negative voltages. The 'digital input binary number'(DIB) of this device for the dual operation range was 0 to 4095, where 0 corresponds to maximum negative voltage and 4095 corresponds to maximum positive voltage, -12 V and +12 V, respectively. As per this specification this implies that 0 V will correspond to a DIB of 2047.5 but practically it was observed to be 1856 in the circuitry. The discrepancies in the value were found to differ from device to another and were measured with a high impedance meter at the DAC output. However, no explanation for this discrepancy is found in the literature.

5.3 Thermoelectric Housing Thermal Management

The heating scheme chosen for the system was the 'bottom-up planar heating approach'[28], which is among the most popular heating methods for PCR applications. In this scheme the heating elements are on the lower surface of the biochip and hence easy access to the chip features (e.g. wells, channels) is attainable from the top surface of the

chip for purposes such as pumping[29], valving and DNA detection [30, 31]. The housing module of the device is briefly explained below.

Heat from the Peltier device was made uniform by placing a good thermal conducting plate above it in the form of a copper plate – 'a heat pacifier'. The heat pacifier consisted of three copper plates – a lower copper plate in contact with the Peltier, a middle copper plate with a hole drilled through its center to accommodate a temperature sensor and an upper copper plate (~ 8 mm thick). This three-plate sandwich arrangement was required primarily to house the temperature sensor in the path of the heat flow (i.e. from the Peltier to the chip), as this will facilitate a feedback temperature loop to control the temperature of this copper plate on which the biochip would be placed. The temperature sensors (LM50) were pasted to the device using a thermal glue (product no.: A8A0502, Wakefield Engineering Inc., USA).

As described earlier, Peltiers function much like a heat pump and hence the lower surface of the Peliter is attached to a large heat sink (– a thick copper block of dimensions 5″ x 5″ x 1″) to facilitate heat to be pumped from the top surface to the heat sink during thermal cycling (cooling phase). Intimate thermal contact between either of the plates and the Peltier (above and below) was achieved by applying a layer of organic thermal compound (Silicon heat transfer compound, MG Chemicals, Canada). Four nylon screws at the four corners of the copper plates then held the assembly together. In the first prototype, this thermal housing module was as shown in Figure 5-2.a.

Unfortunately, due to the large thermal mass of the three-plate copper assembly above the Peltier, the temperature of the top assembly would not heat beyond ~ 85 °C (within a 1 hour observation time) and the heating and cooling rates (i.e. the thermal ramp rates) were as low as 0.2 °C / sec. The denaturation temperature (94 °C) for performing PCR is well above the maximum temperature that the system would heat and the thermal ramp rates were too low to perform reliable genetic amplification[16]. In this work the device was operated well within the Peltier device specifications.

However, it was experimentally noted that the Peltier itself was able to heat at a rate of up to 6 °C / sec and well beyond 85 °C. This experimental confirmation led to a remodeling of the thermal housing assembly to one with reduced thermal mass, as shown in Figure 5-2.b. In this restructured assembly, a thin copper plate (~ 0.5 mm thick),

replaced the three-plate arrangement and the temperature sensor was pasted on the top surface of this plate at a corner, as shown in the Figure 5-2.b. This resulted in a much higher heating rate than the earlier prototype but the thermal ramp rates reduced as the temperature increased (although these rates were much lower than the earlier prototype). This was attributed to the working conditions of the Peltier – the cold side of the Peltier (lower heat sink) was at around room temperature (~ 25 °C), and as the Peltier heated on the top side (upper copper plate), the ΔT (hot side - cold side) increased quickly approaching the maximum ΔT value of ~70 °C for this model of Peltier[27]; hence the slope of the heating curve reduced as ΔT increased. To alleviate this problem, the ΔT value should be kept to a minimum[27] and experimentally it was found that within a ΔT range of ~ 40 °C the ramp rates can be expected to be fairly uniform (with roughly a 30% variation) over the entire PCR temperature range.

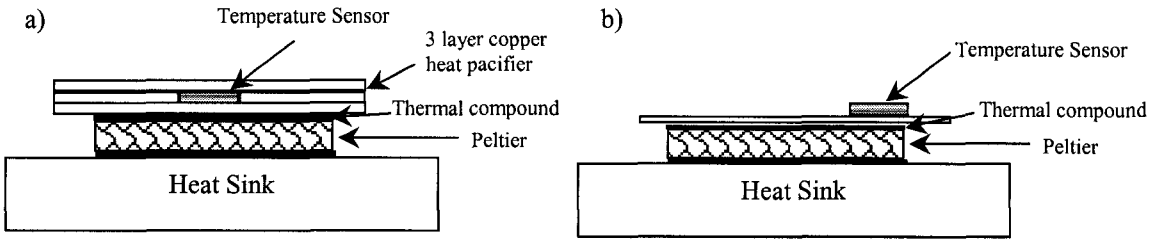

Figure 5-2. (Left) The three layer copper assembly above the Peltier. (Right) Altered single layer copper plate (reduced thermal mass) above the Peltier.

Therefore, in the next prototype version, the thermal assembly was modified to a two-stacked Peltier arrangement as shown in Figure 5-3. In this arrangement, the lower side of Peltier 1 was placed on the lower copper plate (LCP), which in turn is seated on a second Peltier (labeled Peltier 2 in the figure). Peltier 2 effectively acts as a secondary thermal pump and maintains the temperature of the LCP at 60 °C. Hence the maximum ΔT for Peltier 1 during the PCR thermal cycling would be (60 °C – denaturation temperature (94 °C) =) 34 °C, which is only half the maximum ΔT value for the model of Peltier used in the setup. Thus with this setup, a steady ramp rate of 3 to 4 °C/sec (heating or cooling) was achievable and easy cycling of the temperature within the PCR thermal cycling range (50 to 94 °C) was possible.

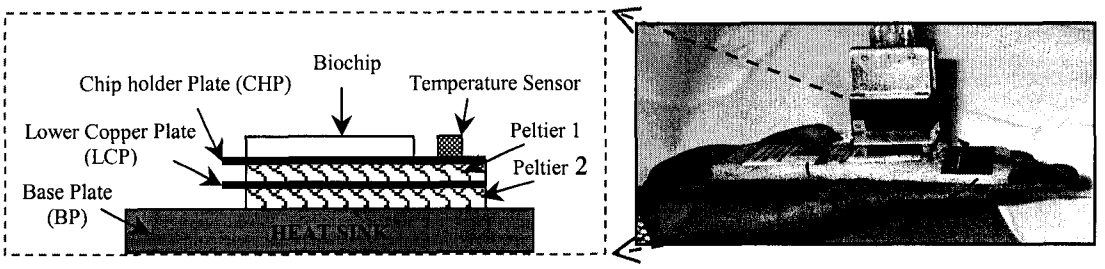

Figure 5-3. (Left) The final prototype of the thermal housing assembly (Right) Picture of the thermal assembly with an integrated prototype microfluidic plumbing system attached on the top

Effectively, the operation of Peltier 2 is like a complementary heat pump to Peltier 1 as described below. When Peltier 1 is in the heating mode, Peltier 2 is also in the heating mode supplying heat to LCP which in turn is drawn-up by Peltier 1 to heat the CHP. On the other hand, when Peltier 1 is in the cooling mode, Peltier 2 is also in the cooling mode removing heat that is pumped by Peltier 1 from the CHP to the LCP. And finally when Peltier 1 is at a given setpoint (e.g. denaturation, annealing or extension temperature) Peltier 2 is also maintained constant at 60 °C. Thus the overall efficiency and thermal ramp rates were greatly improved from earlier prototypes.

The stacked-Peltier arrangement was a highly efficient and compact design as compared to heating the biochip from both the top and the bottom side as demonstrated by some[10, 12, 14] with about the same or lower heating efficiency.

5.4 P/I/D Controls

5.4.1 Introduction

For many decades now, Proportional Integral and Derivative (PID) controllers have been the most widely used tools for industrial automation. They have many favorable characteristics such as low cost of maintenance, robust performance to the plant variations, both theoretical and experimentally oriented tunings, user-friendly manipulations, and widely available commercial products. More recently, there seems to be a renewed interest in PID controllers especially due to the extensive efforts for automation in almost all forms of engineering[32], even in biotechnology applications as in this demonstration. The number of publications in the last ten years on PID based controllers is far more than the number published prior 1990[33]. In process control, nearly

95% of the control loops are based on PID controllers but sometimes with some variations in the algorithm to meet user specific requirements[34]. PID controls are also often combined with logic, sequential functions and selectors to build custom-made control modules for target specific applications[34].

Since their implementation in the process control industry in the early 1940's, PID controls have survived many changes in technology, from mechanical and pneumatics to microprocessors. A recent survey[34] revealed that practically all PID controllers commercially made or custom-built are based on microprocessors, i.e. digital PID controllers, which provides a high level of automation for parallel processing of multiple control loops using the same control module.

The PID controller, as the name suggests, has three independent modes, the Proportional (P) mode, the Integral (I) mode (also called reset mode) and the Derivative (D) mode (also called differential mode). All three modes operate on an error signal generated in a feedback system, where the error signal is the difference between the desired process value and the existing process value[35]. The P mode causes a corrective control actuation proportional to the error, the I mode gives a correction proportional to the integral of the error[32] and the D mode gives a predictive capability yielding a control action proportional to the 'rate of change of the error'[35]. The I mode has the positive feature of ultimately ensuring that sufficient control effort is applied to reduce the error signal to zero[35]. The goal of the PID controller is to drive the error to nil and maintain nil error for as long as the controller is active. This goal is primarily achieved by the capacity of the PID controller to eliminate steady-state error (because of the I action) and the ability to anticipate output changes and quickly ramp to satisfy setpoint changes (when D action is employed)[33].

There are some basic terminologies associated with control system design, which are briefly introduced here to familiarize the reader, as these terms will often be used during the course of this chapter. Figure 5-4 graphically represents these terms.

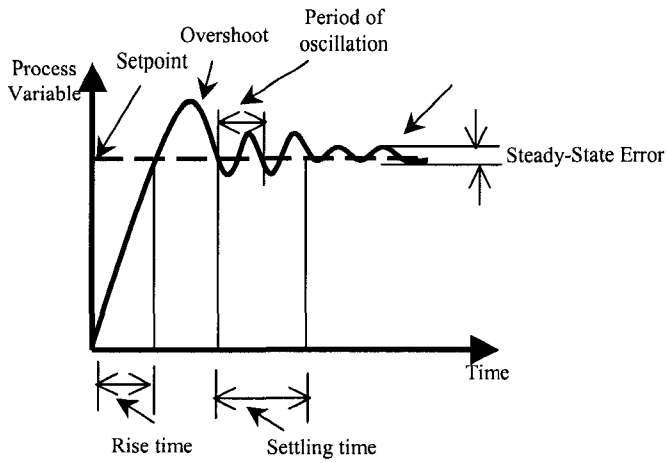

Figure 5-4. Representation of control system design terminology

Overshoot: the amount the process variable exceeds the setpoint when coming up to the setpoint.

Rise time: the time required for the output to rise from 10% to 90% of the setpoint, as it responds to a step change in the input.

Period of oscillation: the time taken for one complete oscillatory cycle of the system response.

Steady-state error: the consistent difference between the process variable and the setpoint after the system has reached steady-state (or after the settling time).

Settling time: the time required for the system to settle to within a finite error.

Tuning: the adjustment of control parameter values to produce a desired control effect in a system, which causes the system to respond at optimal performance within a user-defined tolerance limit.

5.4.2 Split PD-PI Controllers

A conventional (linear) PID controller may be the most popular method for controlling automated processes. However, it many may not always be suited for all applications.

For PCR applications there are certain desirable design criteria; they are – minimal steady state error (preferably zero), short settling time, short rise time and minimal overshoot. It is fairly uncommon to find an application where all of the design criteria stated earlier are critical, as was the case in the PCR genetic amplification application. Unfortunately, using a conventional PID control law all the above design

criteria can not be satisfied as it is well known that helping the function of one of the above design criteria defeats the others[21]; and that the gains of P, I and D should be a best compromise[21]. Depending on the application, one of the design criteria may be more desirable than the others[33] and this is depicted in Figure 5-5 (from Dummermuth[21]). A faster rise time may be chosen over high percentage overshoot, often the case in chemical processes[33], or a low percentage overshoot may be chosen over very slow rise time, as in the case of plastic glove manufacturing[33].

The three curves in Figure 5-5 representing a PID control system with various gain settings can be easily interpreted as follows: The gains of the P part are common to any of the curves. Curve 1 is a system response with very high D gain and fairly low I gain, which causes the system to respond quickly but with the compromise of a large overshoot and long settling time. Curve 3 is a system response with comparatively smaller D gain but with an I gain that builds-up as the system rises to the setpoint; this results in a nil-to-negligible overshoot and nil-to-negligible settling time but at the expense of a slow rise time. Curve 2 is a PID gain setting that is intermediate to that for curve 1 and curve 3. As stated earlier[21], clearly the use of a single PID controller results in a trade-off between rise time, overshoot, settling time. Often depending upon the knowledge and understanding of control system designs, the designer may opt for a best compromise of the design criteria.

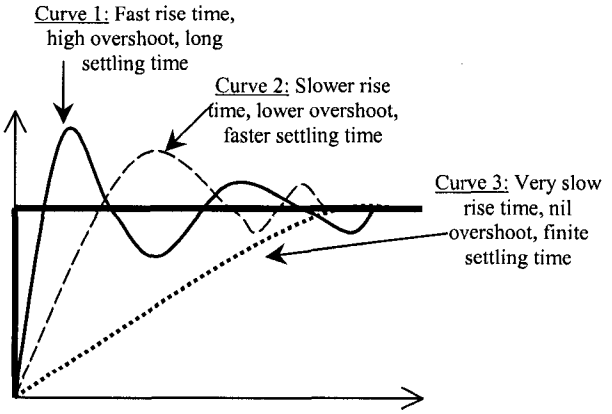

Figure 5-5. Response of a single PID system for various gain settings

In PCR applications, the consequence of overriding any of the design criteria can be disastrous especially when working with highly sensitive human DNA samples. The

steps in PCR are temperature critical processes[16] and since the amplification is an exponential process, an unsuccessful step even in a single thermal cycle is expected to exponentially affect the quantity of the end DNA product[36]. The potential reasons for an unsuccessful PCR genetic amplification due to non-fulfillment of the design criteria are briefly outlined below, of these the focus is on problems related to the denaturation and annealing temperatures as they are the most critical setpoint temperatures in the PCR genetic amplification process[36, 37].

1. Overshooting at the denaturation temperature (94 °C) can cause the destruction of the DNA and enzymes due to boiling[10, 17, 18].
2. Large oscillation at the denaturation temperature can result in improper DNA strand separation. Each time the DNA strand is improperly separated, the effective DNA amplification during the following thermal cycle is zero.
3. Undershooting (or negative overshoot when the system is cooled from the denaturation to the annealing temperature) at the annealing temperature (60 °C) can cause the primer to bind at incorrect sites in the template DNA, potentially resulting in amplification of an untargeted gene or failure of amplification.
4. Large oscillation at the annealing temperature can cause similar effects such as the undershoot at this temperature (– as described above).
5. Fast thermal cycling, meaning minimal time for temperature transition especially during the cooling in a thermal cycle, is desired to ensure the efficiency of the *Taq* DNA polymerase[1]. Slow cycling may result in lowering the efficiency of the *Taq* as the cycle number progresses.
6. From the materials point of view, high thermal ramp rates are desirable as this minimizes the time for the overall PCR thermal cycling and hence reduces 'volumetric loss' in the PDMS (– as described in Chapter 7, section 7.3.4).

PCR thermal cycling process can be split into two processes – one that requires increasing/decreasing the temperature from one setpoint to another (i.e. from denaturation to annealing to extension to denaturation) and another that requires an accurate setpoint control (i.e. at each of the denaturation, annealing and extension). In a control system design these two are considered to be two opposing effects and it seems impossible to satisfy these design criteria using a single PID controller. Hence a different approach may

need to be sought, one in which two independent controllers are used for each of these processes (i.e. the use of split controllers).

Split controllers (e.g. PD-PI, PD-PID, P-PI) are now becoming increasingly common in industrial process control applications and are coming to be referred to by a variety of terms (e.g. hybrid[38], coupled[39], two-term[40], two-step[19]). Kodagoda *et al.*[39, 41] have studied the use of such a PD-PI controller for autonomous guided vehicles (AGV) in which the vehicle speed control, steering wheel control and breaking control are independent of each other using either of the two control components; experimentally they also show that this form of controller outperforms a conventional PID controller particularly in terms of steady state error. Ryu *et al.*[38] have studied the performance of a PD/PI controller for robotic finger object grabbing application; it was highlighted that such a controller was able to increase the rise time and decrease the steady state error which otherwise seemed difficult with PID controllers. Many other robotic applications[42, 43] (one of the most extensive targets of modern control systems) have also explored the advantages and practical implementation of the altered forms of the PID controllers.

For this (PCR) application the split PD-PI controller was implemented. The PD part of the controller can guarantee a fast rise time and 'minimal to nil' overshoot [44] (because of the characteristics of the D part) and is used for fast transition between setpoints. The PI part of the controller ensure minimal steady state error and a finite settling time [18, 44] (because of the characteristics of the I part) and is used when a stable system response is desired (i.e. at setpoints). By using the PD without the I term during temperature transition, the inherent problem of 'integral overshoot' can be completely eliminated [19, 33]. Also, since the thermal system had a very small deadtime (<1 sec), the differential term (D) in the PI was removed; here again it is well known that in fast response systems the differential term in a PID can unsettle the setpoint operation[19, 33], i.e. it results in unpredictably high steady state error[19, 33]. On the other hand if a system had a very large deadtime, it would be advisable to alter the split algorithm as a 'non-linear PD-PID controller' as suggested by Erill *et al.*[19].

The split control algorithm avoids having to compromise the design criteria and it is possible to satisfy the design requirements for PCR application.

Alternatively, for fast-responding systems (e.g. thin film heaters that exhibit ramp rates > 50 °C[17]) the PD part of the controller may not be required[1] if the non-linearity is small. However, in the system used in this work, Peltier devices were used which have slow heating rates (typically up to 5 °C) as compared to thin film heaters. For these reasons the PD part was required in the control system to ensure that the controller has sufficient power to drive comparatively low responding systems like Peltier heaters and glass chips.

5.4.3 Non-linear Controls

Since the 1960's automated control system designs have progressed in many ways (e.g. model based tuning[45], error based feedback tuning[46], adaptive PID controllers to cope with noise and system dynamics, self-tuning or auto-tuning algorithm proposals[47-49], predictive controllers[50, 51], and non-linear controls). Of these, non-linear controls have become an independent branch of study in control systems. More recently, new control algorithms are being proposed to meet specific system requirements[52] such as those in non-linear systems. Examples of non-linear systems are turbulent flow systems, pressure and temperature in chemical reactors[50], elastic based flexible manipulators[44]. In PCR applications however, the implementation of a non-linear control has not been extensively explored. Only recently did Sung *et al.*[20] present a detailed description of a non-linear controller for this application.

This work is not aimed at exploring or proposing mathematical modeling of the non-linear thermal system used in PCR applications; rather a practical approach to implementing the PD-PI controller in a non-linear format is sought. The following subsections outline three key issues – (1) the requirement for a non-linear controller in PCR applications, (2) a gain scheduling approach to implement the non-linear controller and (3) possible future enhancements in the form of a more robust non-linear implementation.

5.4.3.1 Need for a Non-linear Control Operation

In the PCR thermal cycling range, convection heat losses and the internal resistance of the Peltier are non-linear over the entire range. Theoretically, convection losses and heater resistances (i.e. based on the temperature coefficient of resistance of

any resistive heating device as discussed in Chapter 8, section 8.3) are expected to vary even for even small changes in the temperature although the variation is largely dependent on the thermal mass of the system[1]. The PCR thermal system is more complex than a non-linear system, in the sense that genetic amplification involves both heating and cooling between the annealing (50 °C) and denaturation (94 °C) temperatures and this results in one non-linear heat loss during the heating phase and a completely different non-linear heat loss during cooling phase. These non-linear losses arise from the convection heat loss from the system to the ambient (room) and typically (and naturally) as the temperature difference between the ambient and the system increases the convection losses are higher, leading to a steeper non-linear heat loss curves[18]. Hence for the thermal controller independent non-linear tuning was necessary for each of the algorithms (i.e. PD and PI) within temperature zones of their operation and this implementation is described below.

5.4.3.2 Non-linear Control Implementation by Gain Scheduling

To implement non-linear controls, many research groups have proposed heuristics, which are primarily control laws and tuning algorithms developed based on the expertise of human operators and designers[53-57]. However these heuristics cannot be generalized for all systems and are often not well supported with theory. Therefore it is best to be selective in adopting a proposed method, as their drawbacks may be unforeseen until encountered. The primary drawback with most standard control laws is that the gain constant tuning methods do not offer non-linear adaptability of the control law itself[58]. This drawback is the reason for extensive research in the field of control systems for proposal of control laws and heuristics for non-linear implementation, that are more often than not, specific to the system under investigation[59-61]. Due to such uncertainties, in this work a more simple approach was adopted to implement a non-linear control by a method known as 'gain scheduling'[18, 62, 63], as described below.

Within the PCR genetic amplification temperature operating range (i.e. 50 °C to 94 °C), the setpoints are generally predefined at 94 °C for denaturation of the DNA, between 50 °C and 60 °C for annealing of primers to the DNA, and 72 °C for complete DNA strand bonding. This predefinition of the temperature to some extent simplifies the non-linear tuning implementation[18]. For the setpoint control algorithm (i.e. the PI), the

system can be tuned independently at the denaturation (94 °C), annealing (50 to 60 °C), and extension temperatures(72 °C) to obtain the gain constants for the proportional and integral terms[18, 64]. For the temperature transition control algorithm (i.e. the PD) the system can be tuned independently for about 90 % of each of the setpoint value, since switching between PD/PI occurs at this value (- as described in section 5.6.1).

This process of temperature tuning is known as a zonal approach[18]. Since the PD-PI controller is implemented digitally, the gain constants can be stored in a memory array in the software and selectively chosen based on the operation performed – this is referred to as 'gain scheduling for non-linear implementation'[18]. (Note: the term gain constants or tuning parameters are one and the same.) Details on the various tuning parameters involved in this non-linear zonal tuning are discussed later in this chapter.

5.4.3.3 Robust Non-linear Implementation

Evidently, in the gain scheduling method the non-linearity is not generalized but is predefined with temperature setpoints within the operating temperature boundary. Alternatively, if the setpoints were unknown, then a slight change in the algorithm may be required, one that is non-linear within the annealing (50°C) and denaturation (95 °C) temperatures. The intricacies involved in developing such a non-linear algorithm requires a mathematical modeling of the system that characterizes the non-linear temperature behavior over the operating temperature boundary conditions[60]. Once an understanding and characterization of such a non-linear behavior has been established, the gain constants can be manipulated in an automated manner[65].

The effective combination of the PD-PI controller with non-linear implementation presents a smart control algorithm with many advantages as outlined earlier and summarized below: (1) prevents integral overshoot (when approaching setpoints) since the integral term is only used at setpoints and not during transition (2) provides fast transition between setpoints since the D part is used during temperature transitions (i.e. the PD controller) (3) non-linear gain constant tuning accounts for convection heat losses from the system since the operating temperature range is fairly wide (i.e. from 50 to 94 °C) (4) with accurate tuning methods, the settling time and steady state error were kept to a minimum (typically under ±0.1 °C).

5.5 Theory of P/I/D Controls

The aim of this section of this research project was to practically implement a control system that would be suited for PCR thermal cycling applications and one that is adaptable to the Peltier based device. In the following section, only a basic overview of the theoretical aspect of implementing the P/I/D control system is provided which provides sufficient understanding to implement the control system as designed earlier.

The PCR thermal module setup used in this application is a single input single output (SISO) first order system[54] and can be represented as shown in Figure 5-6.

As shown, a single input signal (*i*) is feed in the form of a setpoint value. This is then summed with a feedback signal (f) taken from the output (o) of the system and fed as the error signal (e) to the P/I/D control module. After the necessary processing, the control module outputs a control signal (u) into the thermal module to control the process variable (pv) (i.e. temperature). The feedback control process is repeated within predefined time intervals for as long as required – in this case for the entire PCR experiment.

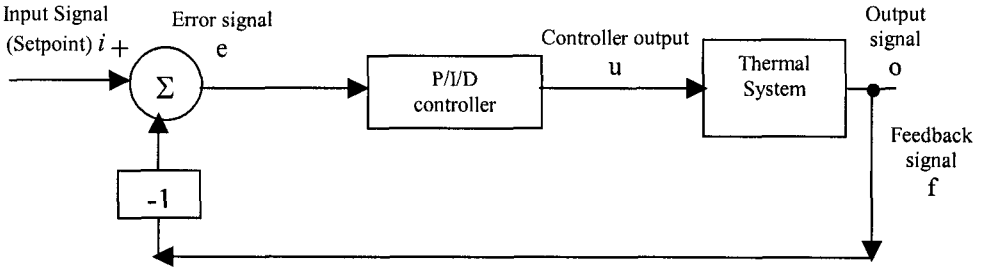

Figure 5-6. Representation of thermal module as a first-order single input, single output system

In the following section, the basics of the Proportional, Integral and Derivative modules that constitute a P/I/D controller are reviewed to provide a working understanding of the control system for the PCR thermal module.

The mathematical representation of a P mode is given as[32]

$$\left[\frac{u(s)}{e(s)}\right] = K_p \quad \text{(Laplace domain) or} \qquad \text{- (5.3)}$$

$$u(t) = K_p \cdot e(t) \quad \text{(Time domain)}$$

where u(t) is the controller output at the time t, K_p is defined as the proportional gain and e is the error signal at the same time instance as u. The error, e, is the difference between the setpoint (sp) and the process variable (pv). The larger the value of K_p, the more the controller output will change for a given error. For instance, with unity gain (K_p=1) and an error of 10% of the measuring scale, the controller output will change by 10% of the measuring scale. A simple proportional controller alone will not be capable of eliminating the error but rather reduce it, i.e. an offset between the setpoint and the process variable will normally exist[34].

The addition of an integral term to the proportional term will automatically correct the offset (or error) over a finite time[34]. The integral controller output is proportional to not just the error but the accumulated error over the entire past operating time for which the I controller was active. Mathematically the I controller is defined by Eq 5.4 [32].

$$\left[\frac{u(s)}{e(s)}\right] = K_p\left(\frac{1}{T_i\, s}\right) \quad \text{(Laplace domain) or} \qquad \text{- (5.4)}$$

$$u(t) = K_p\left[\frac{1}{T_i}\int e(t)\, dt\right] \quad \text{(Time domain)}$$

where Ti is the integral time (other terms have similar definition as before). Evidently, the integral term determines the oscillation fade-off and the steady state error[34] but is a slow process as it acts on accumulated error.

At a given setpoint a PI controller will ensure nil or negligible error in finite time and as described in Eq 5.4. The integral term is expected to have the best response in near-static systems (defined as a system with small error signals). This is clear evidence to eliminate the use of I term in the PCR thermal system during temperature transition where the error signal is large and dynamically changing, but to include the I part for setpoint control where the error signal is only changing by a small quantity (i.e. a near static system). Therefore for the PCR thermal system PI controller designed will have a summation of Eq 5.3 and Eq 5.4 (in the time domains) to give Eq 5.5 [32].

$$u(t) = K_p\, e(t) + K_p\left[\frac{1}{T_i}\int_0^t e(t)\, dt\right] \qquad \text{- (5.5)}$$

Unlike the P or the I mode, the D mode is solely dependent on the slope of the error signal, i.e. dynamic changes in the operating conditions[34]. The derivative (or differential) mode is mathematically represented as[32]

$$\left[\frac{u(s)}{e(s)}\right] = K_P\, T_D\, s \text{ (Laplace domain) or} \qquad \text{- (5.6)}$$

$$u(t) = K_p\left[T_D\frac{de(t)}{dt}\right] \text{ (Time domain)}$$

where T_D is the differential time (other terms have similar definition as before). The working of a derivative action is such that it anticipates where the process is heading by observing the time rate of change of its derivative (i.e. the derivative of the error). Hence the derivative mode is both theoretically and practically ideally suited for dynamic systems[34]. Thus in PCR applications it is a justifiable candidate for inclusion during temperature transitions between setpoints, where the system is highly dynamic with steep temperature slopes, typically nearly 50 °C change in temperature (50 °C – 94 °C) is required. The PD controller equation for temperature transition during PCR is described in Eq 5.7 [32].

$$u(t) = K_P\, e(t) + K_p\left[T_D\frac{de(t)}{dt}\right] \qquad \text{- (5.7)}$$

Astrom[34] has suggested that "*.....the use of D mode is highly discouraged in noisy systems or near-stable systems because even a small error signal will have derivative action, which will cause a high offset (or error) at the setpoint for a period equal to the time required for oscillation fade-off in the system*"[34]. This is further justification in the attempt to eliminate the D mode for controlling the setpoint temperatures (denaturation, annealing and extension) since in the PCR thermal system the thermal mass (i.e. the of the CHP in the thermal module) is fairly low and even a small derivative action is expected to unsettle the system and cause large oscillations.

5.5.1 Discretization of the P/I/D Control

The implementation of the controller for this application was chosen to be in digital form because in an experimental environment the devices are constantly evolving. In such cases, digital controls are preferred as they do not require change in the electronics each time a new prototype is tested or if the system requires retuning. Apart

from the numerous other advantages, digital controls offer this advantage of versatility and robustness.

In order to implement a digital P/I/D control algorithm, it is necessary to approximate the integral (I) and the derivative (D) term from the continuous-time model to a discrete-time model[34, 66].

Error and Proportional term

The error signal at a sampling instance t_k is given by

$$e(t_k) = sp - pv(t_k) \quad \text{- (5.8)}$$

where $e(t_k)$ is the error, sp is defined as the setpoint (temperature) and $pv(t_k)$ is defined as the process variable (i.e. the feedback temperature) at the sampling instance t_k.

The Proportional term at the sampling instance t_k would be

$$P(t_k) = K_p \cdot e(t_k) \quad \text{- (5.9)}$$

where K_p is defined as the proportional gain.

Integral term

For the Integral term, from Eq 5.4 it follows that

$$\left[\frac{dI}{dt}\right] = e(t) \cdot \left(\frac{K_p}{T_i}\right) \quad \text{- (5.10)}$$

The derivative of the above for a sampling instance t_k is approximated by a forward difference to give[34],

$$\frac{I(t_{k+1}) - I(t_k)}{h} = Kp \cdot e(t_k) \quad \text{- (5.11)}$$

where I (t_k) is the integral term at the sampling instance t_k and h is the sampling time interval (other terms as defined earlier).

The simplification of the above leads to a forward recursive equation for the I term as[34]

$$I(t_{k+1}) = I(tk) + \left[\frac{K_p \cdot e(t_k) \cdot h}{T_i}\right] \quad \text{- (5.12)}$$

The value of $(K_p/T_i)$is referred to as the Integral gain (K_i).

Derivative Term

The continuous-time derivative term (D) given by Eq 5.6 can be approximated to a discrete-time in the same manner as the integral term but by a backward difference, which yields[34],

$$D(t_k) = K_p \cdot T_D \left[\frac{e(t_k) - e(t_{k-1})}{h}\right] \quad \text{- (5.13)}$$

The value of $(K_p \cdot T_D)$ is defined as the derivative gain (K_D).

Thus the PI controller output (u_{PI}) is defined as the summation of Eq 5.9 and Eq 5.12 to give Eq 5.14.

$$u_{PI}(t_k) = P(t_k) + I(t_{k+1}) \quad \text{- (5.14)}$$

and the PD controller output (u_{PD}) is defined as the summation of Eq 5.9 and Eq 5.13 to give Eq. 3.15.

$$u_{PD}(t_k) = P(t_k) + D(t_k) \quad \text{- (5.15)}$$

5.6 Performance Enhancement

The performance of a control system is specific to many parameters discussed earlier but the use of the Integral term in P/I/D controllers gives rise to certain inherent problems, specifically 'transient effects'[34, 67] and 'integral windup'[68]. The other problem in the PCR thermal system was a small amount of disturbance in the feedback that required correction. In this subsection these issues are discussed and suitable solutions are provided.

5.6.1 Bumpless Transfer

Any control system is dynamic and hence a change in the controller parameters is expected to automatically result in a change in its output[69]. When there are changes in controller modes or controller parameters, such as the operation of PD and a PI controller, non-linear parameter settings and/or manual and automatic modes, 'transient effects' are a common problem[34, 67]. These effects arise because, when the control system is switching modes (or gain parameters) due to non-linear operation, the control algorithms produces a control signal at the sampling instance (t_k) that may be drastically different from the control signal output at the previous sampling instance (t_{k-1}). Hence it is necessary to ensure that the transient effects are avoided by operating the controller in what is called a 'bumpless transfer'[67, 68] during the switching phase.

In specific reference to the PCR system and the controller designed for it, the PD controller is used during temperature transition and the value of D approaches zero as setpoint is neared. Now when the controller is switched to a PI controller (i.e. at about

90% of the setpoint value), a large input signal in the form of the integral gain (K_I) and error (at setpoint) is introduced to the controller. This could potentially result in transient effects. Hence at the switching phase (from PD to PI), the integral part is modified as in Eq 5.16[34, 68]

$$I(t_{k+1})_{transition} = I(t_k) + \frac{1}{T_i}\left[\left(K_p(t_{k-1}) \cdot e(t_{k-1}) \cdot h\right) - \left(K_p(t_k) \cdot e(t_k) \cdot h\right)\right] \qquad (5.16)$$

The above equation is taken from Astrom[34] and is a slight variation to the earlier Eq 5.12. First at the switching phase, the Integral part $I(t_{k+1})$ takes the difference between the Proportional gain of the PD controller ($K_p(t_{k-1})$) and the Proportional gain ($K_p(t_k)$) of the PI controller. And secondly, the same is also done with the error signal ($e(t_{k-1})$ - $e(t_k)$). With this altered equation, the value of the Integral part ($I(t_{k+1})_{transition}$) will be an intermediate value between zero and the actual Integral output at the next sampling instance ($e(t_{k+1})$), because the Integral output ($I(t_{k-1})$)at the previous sampling instance was missing in the PD controller. Therefore large change in the controller output at the switching phase can be eliminated.

With simple alterations to the Integral equation (as shown above) at the switching phase, it is possible to eliminate large bumps in the controller output. Literature recommendations have also suggested that if the difference in gain constant values (i.e. K_p for PD and K_p, K_i for PI) and the steady state error are very large, then $I(t_{k+1})_{transition}$ should be performed for a very long phase (i.e. from $I(t_{k+1})_{transition}$ to $I(t_{k+X})_{transition}$) in order to provide a smooth transition[34, 68]. The value of X will depend on the characteristics of the system and will have to be experimentally determined[34, 68].

The bumpless transfer can also be implemented by performing the switching (between the PD-PI mode) at about 85-95% of the setpoint value. This way the integral term will build over the error value between the instance of switching and the instance of reaching the setpoint. In this method of implementation the (initial tuned) integral gain value will have to be slightly lowered (quantity specific to the system) from the tuned parameter value since the integral gain accumulates as a function of the error prior to setpoint. There are many others ways of implementing the bumpless transfer feature and this comprises another interesting control system design challenge.

5.6.2 Anti-Integral Windup

When an integral term is used in the controller, there exists a possibility of "integral windup"[34]. The following scenario explains the integral windup. When the error signals are generated for a significantly large period of time the integral term in the controller will increase (since it is the integration of the error itself) by a rate governed by the integral time (T_i). This will eventually cause the controller output ($u(t_{k+n})$) to reach 100 % (or 0%) of the measuring scale, i.e. maximum or minimum limits, causing the system to behave haphazardly[34, 68]. There are a number of scenarios that can cause the integral windup, examples are when cascade controllers[70] are used, or when constant steady state error exists, or during prolonged controller operation, or constant noise and disturbance inputs, unknown system non-linearity [68, 70].

In the PI controller used here, this integral windup scenario was not particularly observed and the reasons for this could be:

1. Because this is a time bound system in which the PI controller is invoked for not more than 60 sec at each setpoint temperature before the PD controller is invoked for temperature transition. And during this operation, no unknown disturbances affect the system.
2. The algorithm is defined to reset the integral value (or sum of integral) to zero each time the controller is switched from a PD to a PI or vice versa. This ensures that there is no carry over integral values from the previous setpoint.

Although the integral windup in the PI controller was not observed, an anti-windup equation was devised[32, 34, 66, 68] for the control system and is given by a conditional statement as shown below.

If ([$P(t_k)$ > minimum permissible controller output] && [$P(t_k)$ < maximum permissible controller output])

{

$I(t_{k+1}) = I(t_k) + [(K_p \cdot e(t_k) \cdot h)/ T_i]$

output $u_{PI}(t_k) = P(t_k) + I(t_{k+1})$

}

Else

output $u_{PI}(t_k) = P(t_k) + I(t_k)$

In the above conditional statement[34], the integral term $I(t_{k+1})$ is executed (i.e. with the integral manipulation of all the past errors) only if the value of the Proportional

term, $P(t_k)$, is within the maximum and minimum possible output limits – in this application, the maximum and minimum current that is required to maintain the setpoint temperatures (i.e. < ±0.5 Amps above the setpoint sustenance current (defined as the amount of current required to maintain the temperature at a given setpoint), which was determined experimentally from one of the prototypes). Else the integral part of the output is a frozen value prior to exceeding output limits. There are numerous other ways to implement the anti-windup (e.g. using error or integral values instead of $P(t_k)$) and forms an interesting part of the control system design.

On the other hand for the PI_2 controller, which controls the temperature of the lower Peltier, an anti-integral windup was required. This is because this controller is continuously operated (linearly but with non-linear disturbances as outlined below) during the entire PCR thermal cycling experiment, typically for over 90, 000 sampling instances (i.e. 2.5 hrs). Moreover, during the cooling phase of the top Peltier a large amount of heat is sunk into this PI_2 controller (i.e. to the LCP) and hence causes nonlinear disturbances in the operating conditions for the PI_2 controller. Upon implementation of an anti-windup loop, the performance of this controller remained stable for any extended period of time.

5.6.3 Feedback Disturbance Correction

The P/I/D controller solely performs based on the error (or feedback) signal from the system[32]. Hence any disturbances in the feedback path can lead to an unpredictable controller performance. In the PCR thermal module it was noted that some disturbances in the feedback path, meaning the feedback temperature value from the thermal housing unit, seemed inconsistent even when the operating conditions were kept unchanged (i.e. under nil variables – defined as a condition where the system output is not influenced by any variable). This is illustrated by the experimental data shown in Figure 5-7. In the experiment, the Peltier device did not influence the temperature of the thermal housing (i.e. the Peltier was disconnected) and the ambient (room) temperature remained almost constant (23 °C). In spite of the constant operating conditions (i.e. nil temperature variables), the feedback temperature was fluctuating between 22.7 °C and 23.3 °C. This is attributed to a combination of quantization error and pick-up noise. However, future systems did not have such high noise.

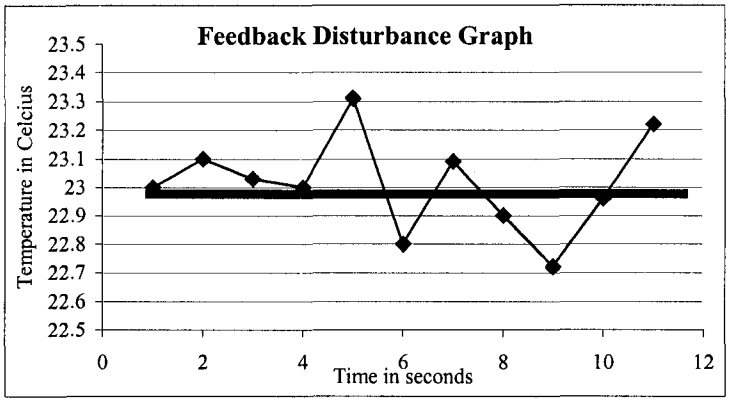

Figure 5-7 . Feedback disturbances in our thermal system – expected temperature value = 23 °C but the observed value fluctuates between 22.7 and 23.3 °C.

To circumvent this problem, at the setpoint temperatures the software included a conditional command in which the error signal was modified as

$$\text{If } ([e(t_k) - e(t_{k-1})] > 0.28\ ^{\circ}C)$$
$$e(t_k) = e(t_k) \cdot 75\% + e(t_{k-1}) \cdot 25\%$$

This form of modification is referred to by a variety of terms in the literature (e.g. error weighting, error weightage)[34]. Effectively, at the setpoint temperature the above command checks if the feedback temperature value at the sampling instance t_k is over 0.28 °C (value devised based on numerous experimental observations) of the setpoint temperature and if it was, then a feedback disturbance signal is suspected. In such a case only 75% of the error at the sampling instance $e(t_k)$ is taken along with 25% of the error at the previous sampling instance $e(t_{k-1})$. This way the influence of the suspected feedback disturbance at that sampling instance ($e(t_k)$) is lowered. The percentage of influence is not a static value for all systems and can be varied based on a careful study of the problems pertaining to a system. Other forms of implementing this feature would be by using a 'time-average weighted error calculation' approach (similar to that found in literature[34]).

5.6.4 Sampling Time

In a digital control system implementation the performance of the control system is also dependent on the sampling interval – defined as the time between two consecutive feedback signals[34, 66, 71]. In most cases this sampling interval is determined by the limitations of the electronics; for example the combined clock speeds of the different

electronic chips associated with the system. Based on a rough estimation of the clock speeds (ADC, D/A, PIC) and the limitation of the analog performance of the temperature sensor (LM50), an estimated sampling interval more than 10 m-sec was deemed ideal in the PCR thermal system. However, in the practical implementation, a sampling time of ten times higher, i.e. 100 m-sec, was chosen.

Therefore, if an analog (temperature) input is read at a sampling time of h, then the average delay of the measurement system is $(h/2)$[34]. Although the computation time of the PIC microprocessor is in the order of a few μ-sec (- from data sheets), in practice the floating point operations combined with all the control manipulations take many m-sec. This implies that the total delay between control signals is still $(h/2)$. With a 100 m-sec sampling interval, a control action delay of 50 m-sec can be expected. A h of 100 ms provided sufficient time for calculation while being rapid enough to control the system temperature accurately.

In the PCR thermal system the 100 m-sec sampling interval seemed sufficient as the system performance remained unchanged even when the sampling interval was reduced by a factor of four (i.e. to 25 m-sec). However, increasing the sampling time by a factor of four (400 m-sec) severely affected the steady-state error, i.e. it resulted in large error values at the setpoints (typically $>\pm 0.25$ °C).

It should be noted that the sampling interval is customized based on a study of the system under investigation (e.g. a system response to a step change in the input as discussed in section 5.7). For a system with small deadtime (i.e. low thermal mass systems) a high sampling rate (i.e. short sampling intervals) is desired, on the other hand for a system with large deadtime (i.e. high thermal mass systems) a high sampling rate may not be required.

5.6.5 Gain Scheduling

As described earlier, due to the non-linear controller operation between a predefined range and at predefined setpoints, the system was 'zonal tuned' for the PD and the PI controller. This indicates that at the precise controller operating temperature (either for the PD or the PI), the tuning parameters are to be selected appropriately. In the software developed for the PCR system, the control algorithm checks the operating range

to select the corresponding tuning parameters for that particular setpoint / operating range. This process of selecting the tuning parameters is referred to as gain scheduling[18].

5.7 Tuning the Controller

Tuning a PID controller is a challenging skill. Tuning of a controller refers to determining the gain constants specific to the system in which the controller is implemented[72]. Second only to the control algorithm, the tuning is the most important aspect of implementing an accurate control system[32, 72]. The tuning process is the final and most critical aspect in the 'design and implementation' of a P/I/D controller[32]. There are several methods to tune a P/I/D controller – the majority of which are based on empirical rules derived from measurements made from the system on which the controller is implemented. These tuning methods can be classified into either closed loop tuning or open loop tuning, and some of the popular methods are discussed below.

Over the years there have been many well established tuning methods – 1. the Ziegler-Nichols closed loop and open loop (or step response) method[46, 73], 2. the Cohen Coon method[74], 3. the Internal mode control (IMC)[75, 76], 4. Integral time-weighted absolute error optimum for setpoint change and disturbance response (ITAE)[65], 5. Integral squared error optimum for setpoint change (ISE)[65], and many others. Among these methods, the Ziegler-Nichols and the Cohen Coon method have been in existence for many decades. However, the Cohen Coon method is not suitable for tuning systems with zero or virtually no time delay (i.e. low deadtime)[74] and invariably most systems exhibit some deadtime even if the values are in the order of milliseconds. Hence the most historical and popular of the above approaches has been the Ziegler-Nichols method – named after the two inventors Ziegler and Nichols[46, 73]. The primary reason for the popularity of the method is because it avoids the need for a mathematical model of the system; and hence no prior knowledge of the system is required to implement the P/I/D controller. In the following subsection the open loop Ziegler-Nichols tuning method and its application to the PCR thermal control system are discussed. The Ziegler-Nichols closed loop tuning method is also widely used (and preferred) but due to limitations such as a lack of a graphical user interface (GUI), it could not be implemented in this system since it requires online control parameter adjustments[34].

5.7.1 Ziegler-Nichols Open Loop Tuning

The open loop Ziegler-Nichols tuning method takes into account the inherent system parameters for obtaining the controller constants. To perform this tuning, a step change in the input is supplied to the system. In the PCR thermal system this refers to sourcing a current value to the Peltier device and monitoring the temperature value. The system response to step change is then graphically plotted (offline); Figure 5-8 shows a schematic of such a graphical representation.

The important system response parameters that are derived from the graphical representation are: (1) The dead time (d_T), defined as the time taken for the system to respond to an applied input signal. In the PCR system this is the time taken for an observational change in the temperature value for an applied current sourced to the Peltier. (2) The time constant of the system (T_C), defined (from the graph) as the time interval after the dead time and until the point of intersection of the tangent to the expected value of process variable. (3) The process gain (P_g), defined as the ratio of the expected process variable (DOP) to the observed process value (DPV).

With the values of d_T, T_C and P_g, the controller constants are obtained using the formulation[33] given in the table below. Table 5-I lists the formulation for obtaining controller constants for either PI, PD or a PID controller.

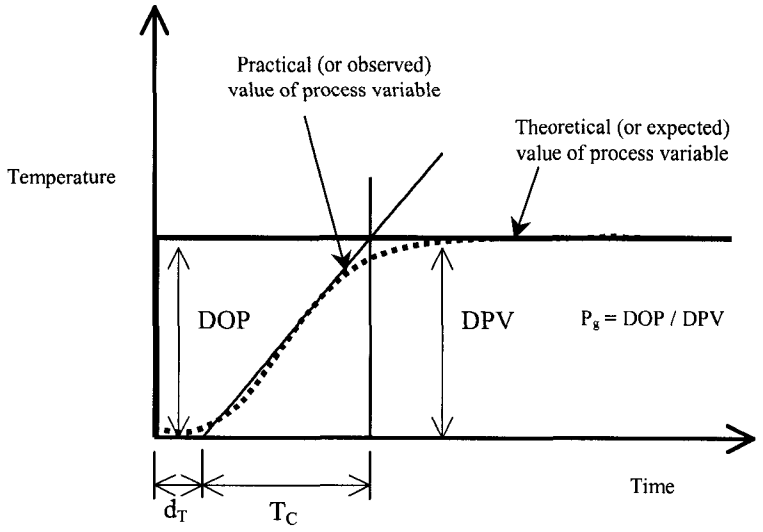

Figure 5-8. Representation of the system response to a step change in input for performing the open loop Ziegler-Nichols tuning

Table 5-I. Formulation for deriving gain for a P/I/D controller

Controller	K	K_p	T_i	K_i	T_D	K_D
PI	$\frac{T_c}{P_g \bullet d_T}$	0.9 * K	3 * d_T	$\frac{K_p}{T_i}$	-	-
PD	$\frac{T_c}{P_g \bullet d_T}$	1.2 * K	-	-	0.5 * d_T	K_p * T_D
PID	$\frac{T_c}{P_g \bullet d_T}$	1.2 * K	2 * d_T	$\frac{K_p}{T_i}$	0.5 * d_T	K_p * T_D

Based on tuning numerous prototypes of this system (due to the evolving design of this system), as a 'rule of thumb' it was found that the values of the times d_T and T_C range between 8-10 % and 85-90%, respectively, of the time required to reach the setpoint for the given step change in input.

The Ziegler-Nichols open loop tuning procedure can be summarised in four steps.

1. Graphically obtain the system's step response.
2. Draw the steepest straight-line tangent to the response.
3. Obtain the measure of d_T, T_C and P_g
4. Set the parameters of K_p, K_i, and K_D according to Table 5-I.

As described earlier, the PCR system required a non-linear controller and hence tuning over many temperature zones (i.e. linearized tuning at each setpoint) was required. The PD-PI controller tuning can be broken down into:

PD controller	PI controller
Tune for temperature transition between room temperature and denaturation temperature (~ 94 °C) – to be used during the first PCR cycle	Tune for denaturation temperature range (94 to 96 °C)
Tune for temperature transition between denaturation and annealing; the annealing temperature ranges between 50 to 60 °C.	Tune for annealing temperature range (50 to 60 °C)
Tune for temperature transition between annealing and extension (72 °C) temperature.	Tune for extension temperature range (72 °C)
Tune for temperature transition between extension and denaturation temperature.	

Finally, the PI_2 controller is also tuned at 60°C for the lower Peltier operation. Completing all the above tuning procedural steps completes the implementation of the control system.

5.7.2 Fine Tuning

Traditionally, since the invention of the PID controller, tuning is performed by trial and error experimentation [58]. The Ziegler-Nichols tuning method was devised based on extensive simulation with a design criteria of 'quarter amplitude decay ratio'[34, 46, 73], meaning the amplitude of an oscillation should be reduced by a factor of four over a whole period of oscillation. Thus the damping ratio (ζ) would be about $\zeta = 0.2$, which is representative of an underdamped system[32, 34] ($\zeta > 1$ for overdampled systems), when an ideal system is actually critically damped ($\zeta = 1$). In addition, the tuning parameters are derived from only a few system dynamics (e.g. d_T, T_C), although it has been suggested that this is insufficient data[34] to characterize a system. In spite of the drawbacks, this tuning method has been very popular. "*.....practically all manufactures of controllers have used the (Ziegler-Nichols tuning) rules...*"[34], primarily because of its ease of implementation and hierarchy of invention (i.e. one of the oldest tuning method). Hence, the values of gain constants obtained using the Ziegler-Nichols tuning methods provide a good starting point to fine-tune a system[34]. When tuning a P/I/D controller, generally the aim is to match some preconceived 'ideal' response profile for the closed loop system. There are three possible forms of system response – one that represents an overdamped system, an underdamped system or a critically sampled system, of which as described earlier, a near-critically damped system response is desired for temperature critical PCR experiments.

Since the PD-PI control algorithm prevents large overshoots, the only parameters of concern at setpoint temperature are the settling time and the steady state error, of which the settling time will be fairly quick because large overshoot is prevented[32]. Table 5-III provides a quick 'rule of thumb' to adjust the gain constants to minimize (or possibly eliminate) steady state error, settling time and small overshoots in either the PD or the PI control algorithm.

As highlighted by Badreddine *et al.*[60], the only intricacies involved in tuning a controller are the requirements for manual intervention during the tuning process and

proper judgment in adjusting the gain constants[60]. More so in the PCR system as noted earlier, since online graphical representation was not readily feasible, fine-tuning the gain constants was a tedious process. With experience and a good visual understanding of the controller operation, the process of tuning and fine-tuning a controller is less time consuming and tedious.

Table 5-III. A quick rule of thumb reference to fine tuning a system

Requirement	K_p	K_i	K_D
Reduce settling time	↓	↑	-
Reduce steady state error	↓	↓	-
Reduce any observed (small) overshoot	↑	-	↓

Legend: ↓ indicates decrease and ↑ indicates increase

Although only the Ziegler-Nichols tuning method is described here and the PCR system was tuned using this method, other methods stated earlier have also been demonstrated as efficient ways to accurately tune a control system[1, 20].

5.7.3 Controller Performance Degradation

In any control system that is designed on the basis of a simulation or if system parameters vary over time, the controller performance is bound to deteriorate[60]. For this PCR system, the controller was tuned with an actual working model of the thermal module and hence rapid performance deterioration due to this factor was not observed. However, a reasonable performance deterioration occurred over a prolonged operation, i.e. the steady-state error at the setpoint temperature increased by manifolds (i.e. up to ± 0.6 °C and sometimes much greater) from the original average value of < ± 0.1 °C (typically within ± 0.05 °C) and the overshoot/undershoot was as high as 1 °C (and sometimes higher). This has been analyzed to be due to the one of the following,

1. The degradation/drying of the thermal compound between the Peltier and the copper plates. The thermal compound is used to make intimate thermal contact between two heat transfer masses (i.e. the Peltier heat source and the copper plates) and was necessary for proper functioning of the Peltier device[27].
2. The degradation/drying of the thermal glue that was used to paste the temperature sensors onto the copper plates.

3. The deterioration of the particular model of Peltier used in constructing this system. However, this problem could be overcome in future prototypes by using a Peltier suited for this application.

The immediate remedy to this deterioration process was to fine-tune the system as-and-when required. Practically the thermal system was fine-tuned at an average of once every few weeks.

This performance degradation effect of the controller could be substantially eliminated by a better mechanical design of a thermal module with minimal use of organic materials such as the thermal compound and glue, and using a more reliable Peltier device (as discussed in the conclusion).

5.8 The Complete Thermal Controller

The main features associated with the design of the control system were discussed thus far. Figure 5-9 shows a classical representation of the control system designed and implemented for the PCR thermal module with all of the components described in the earlier sections of this chapter.

The output of the thermal system ($o(t_k)$) provides the feedback signal ($f(t_k)$) which is processed for 'feedback disturbance correction' (when the setpoint temperature is controlled) and the negative of that signal is fed to a summation module. The summation module computes the sum of the input signal ($I(t_k)$) and the negative feedback signal to produce the error signal ($e(t_k)$). The error signal is then supplied to either one of the switches (A or B) depending on the state of the thermal system. If the setpoint temperature is to be controlled then the switch is in position A. In either of the paths (i.e. switch A or B) the appropriate gain constants for the particular setpoint/transition-temperature are selected from a predefined array in the software.

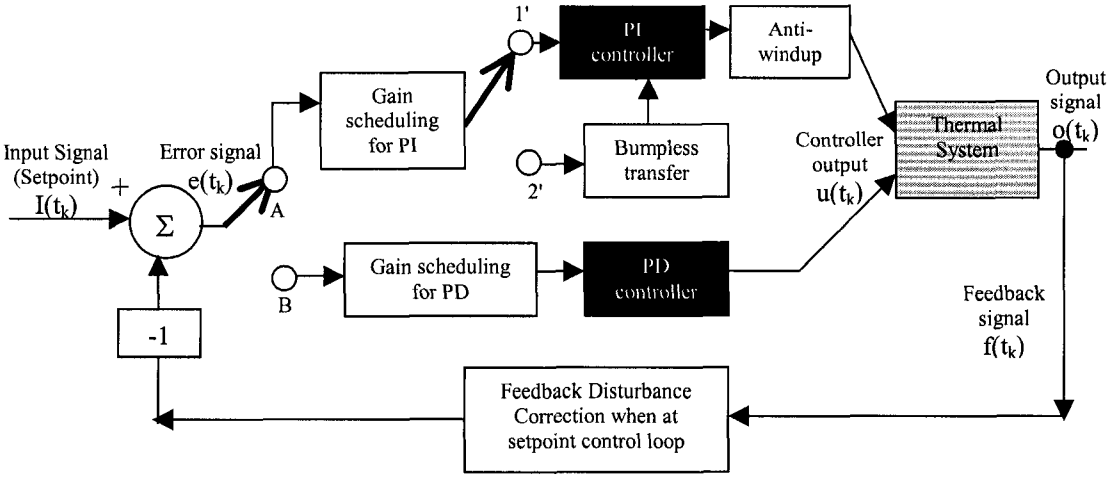

Figure 5-9. Schematic representation of the control system for the PCR application thermal module

In path A operation, if the error signal ($e(t_k)$) is sourced for the first time, then it indicates a transition between PD to PI and hence the signal would be sourced through the sub-switch 2' during the switching phase to enable the bumpless transfer mode.

Alternatively, if the temperature transition between the setpoint temperatures is taking place during the PCR thermal cycling, the error signal is feed to the PD control block through switch B. Switching between the modules (switch A, B, 1' or 2') is selectively performed in the software as required. The output of either of these paths produces the control signal ($u(t_k)$) to the thermal system.

The above control scheme is for controlling the temperature of the chip holder plate (CHP, Figure 5-3) on which the biochip is placed to perform PCR genetic amplification. However, simultaneously, another PI controller (which was termed as PI_2) controls the temperature of the lower copper plate (i.e. the second Peltier LCP, Figure 5-3) between the Peltier 1 and Peltier 2 at about 60 °C for optimal system performance as described earlier. However, this controller does not involve temperature cycling and the intricacies involved with split controller performance or non-linear operation are not encountered.

The control system described here is operated in a dual mode (i.e. PD or PI from Peltier 1 and PI_2 for Peltier 2) much like a "parallel processing control system" [24, 25] for multi-loop control[77], one in which two temperature processes (chip holder plate (CHP) and the lower copper plate (LCP)) are simultaneously controlled.

Features such as gain-scheduling, feedback disturbance correction, anti-integral windup, timers that determine the dwell times at each setpoint, safety loops that check for malfunctioning of the device, temperature cycle counters, ADC/sensor compensation calibration, DAC calibration were all implemented in the software code.

5.8.1 Performance Comparison

The graph in Figure 5-10 shows the thermal cycling performed with the PCR thermal system– one that was implemented with a 'digital non-linear PD-PI controller', tuned using the Ziegler-Nichols open loop method and elaborately fine-tuned.

The critically damped system performance (magnified inset in Figure 5-10) is attributed to the split PD-PI control law, the use of the dual PI_2 controller and the all other additional features as described earlier. The thermal ramp rates (heating and cooling) were as high as 4 °C and the setpoint accuracy for all the prototypes was tuned to be in the order of $< \pm 0.1$ °C with an average steady-state error (i.e. the average accuracy at setpoints) within ± 0.05 °C.

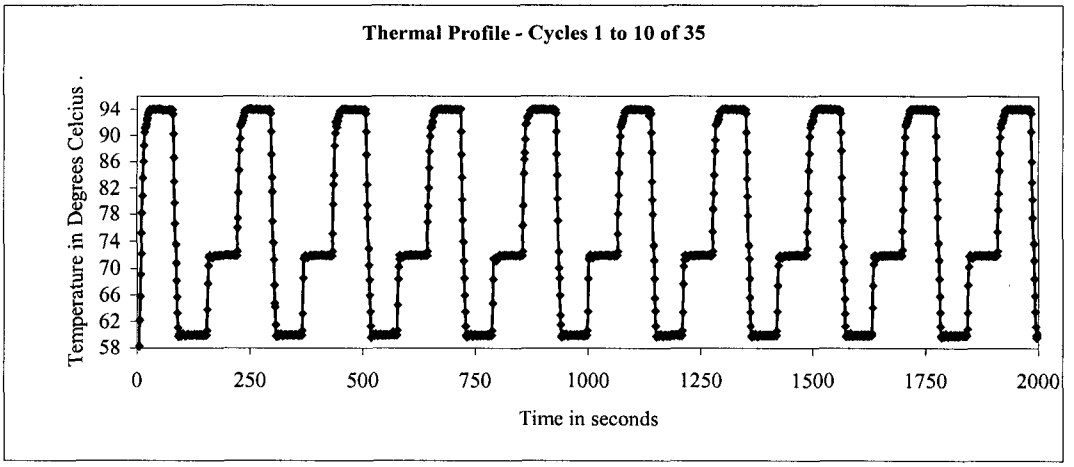

Figure 5-10. Thermal cycling graph of the thermal module used in this work

In the PCR related literature, although scarce, even among those that demonstrated in-house thermal modules and controllers, a critically damped system response is not always observed. A depiction of few example graph traces from literature is shown in Figure 5-11. A P/I/D controller[10] (possibly tuned for fast response) (Figure 5-11.a) gives a overshoot up to 2 °C and an steady state error of about ± 2 °C. An optimized PID response[7, 8] (possibly with linear tuning) (Figure 5-11.b)gives varying

overshoots with steady state error that varies up to 0.6 °C depending on the setpoint temperature. It is worth noting that the only recent demonstration of a non-linear PI controller for the PCR application by Yoon *et al.*[1] yielded a good system response (Figure 5-11.c) and is comparable with the system response obtained in this work (Figure 5-11.d). A vast majority of other demonstrations in PCR application show inconsistent performance where typically overshoots > 4 °C [6-13] and setpoint accuracy (i.e. steady state error) up to ± 0. 5 °C [1, 6-11, 14-16] are observed. Evidently, the control system implemented in this work outperforms those that are commonly found in the PCR literature. The exceptions[78] to our knowledge are those that used commercial thermal cycling systems.

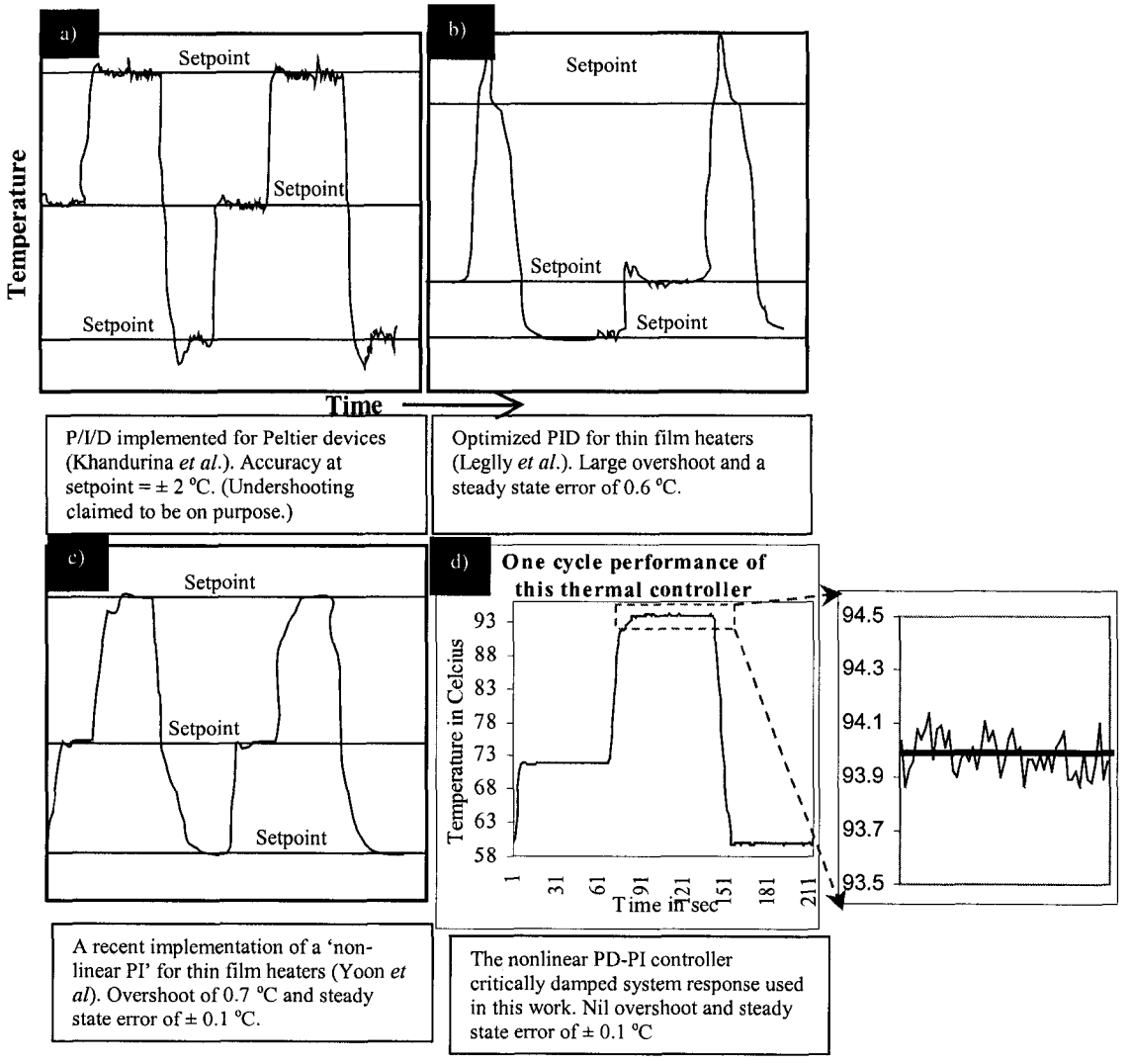

Figure 5-11. Several representative traces and comparison of the thermal profiles from literature (a-c) on the implementation of P/I/D controllers and that of this work (d).

5.9 Thermal Calibration

Temperature calibration of thermal devices is perhaps as important as constructing the device itself and usually forms the final capping exercise before the system can be tested with a DNA based PCR experiment. Calibration issues arise because of the inherent thermal properties of the materials used in the system, e.g. specific heat capacitance, thermal conductivity and thermal resistance[28].

There are essentially two calibrations that were required in the PCR thermal system presented in this work– time and temperature calibration which are outlined as follows. First is the 'thermal time delay' calculation to estimate the time delay for uniform heat distribution to the entire PCR sample in the chip. And second, the thermal capacitance/ resistance calibration (because of the poor thermal conductivity property of the glass material that was used to structure the chip) to compensate for the heat stored/discharged in the glass substrate of the chip before it is transferred to the PCR sample.

Both these calibrations are critical to the success of a DNA amplification experiment because PCR genetic amplification is both a time and a temperature critical process, and hence a detailed discussion is provided below.

5.9.1 Thermal Delay

In thermal systems where heat is transferred from one material to another, thermal delay (t_d) is a phenomenon of interest in understanding the nature of the heat transfer between the materials. Thermal delay property can be illustrated as shown in Figure 5-12.

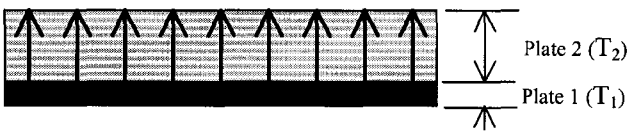

Figure 5-12. Illustration of thermal delay across two plates

In the above figure, say the temperature of plate 1 has been set to an elevated temperature T_1 as compared to the temperature of plate 2, which is at a lower temperature T_2. The time period for the top surface of plate 2 to reach T_1 is defined as the thermal time delay (t_d) or the thermal diffusion time. This thermal time delay of a material is a function of its specific heat capacitance and thermal conductivity[28].

The value of t_d can be derived from the thermal diffusion theory of a one-dimensional heat flow as (Eq 5.17)[28, 79]:

$$\left(\frac{T}{t_d}\right) = D_T\left(\frac{T}{L^2}\right) \qquad \text{- (5.17)}$$

where T is the temperature, L is the thickness through which the thermal diffusion has to take place and D_T is the thermal diffusion coefficient. The value of D_T is derived from the equation below (Eq 5.18).[28]

$$D_T = \frac{\lambda}{\rho c} \qquad \text{- (5.18)}$$

where λ is the thermal conductivity of the material (W/ m K), ρ is the thermal density (commonly represented in units of W-sec/ m^3, cal/cm^2, kg/m^3) and c is the specific heat capacity of the material (J/ kg K).

The earlier diffusion theory for one-dimension (Eq 5.17) is simplified as[7, 28]

$$t_d \cong \frac{L^2}{D_T} \qquad \text{- (5.19)}$$

The relevance of thermal delay in the PCR system is critical because, the feedback from the thermal module is taken from the copper chip holder plate (CHP) and not from the PCR sample. Thus depending on the material properties of the chip, the rate at which the heat is transferred to the PCR sample may be significantly different from that of the CHP. The PCR thermal system developed in this work can be modeled as shown in Figure 5-13.

First it is assumed that the temperature of the copper plate is of uniform temperature due to the excellent thermal conductivity of copper. Second, the thermal delay from the Peltier to the copper plate (CHP) is not a concern because the feedback (i.e. the system temperature) is obtained from this plate, which implies that the CHP is now the heat source. Thus there are primarily only two other thermal time delay concerns in the above model that need attention for the success of a PCR genetic amplification experiment. They are:

1. The thermal time delay involved in the heat transfer across the thickness of the glass substrate to the PCR sample ($t_{d\text{-glass}}$) and
2. The thermal time delay for the uniform distribution of heat to the entire volume of the PCR chamber ($t_{d\text{-fluid}}$) (assuming that the chamber is fully filled).

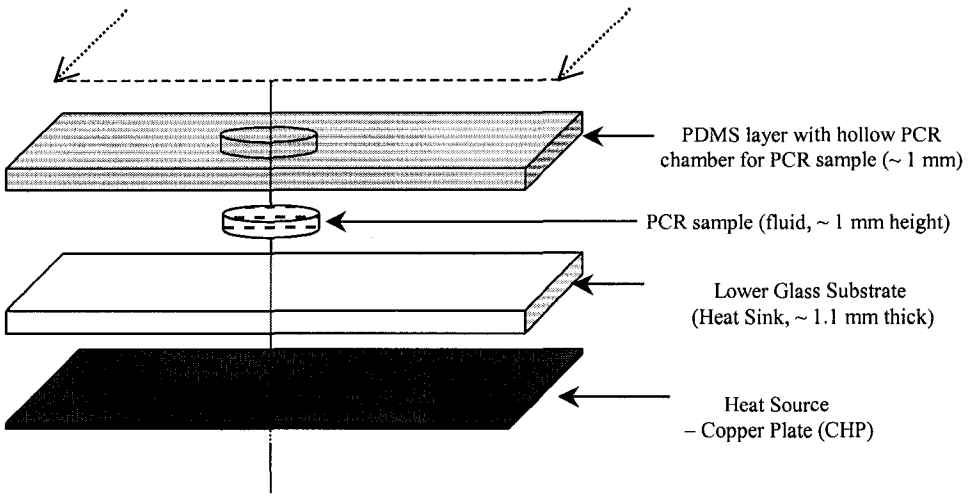

Figure 5-13. Thermal Diffusion layered model of our system

In order to estimate these thermal delays, a few important thermal parameters of the associated materials that structure the chip (and also that of Si) are summarized in Table 5-IV [14, 28, 80-82].

Table 5-IV. Thermal parameters of materials of interest to building our biochip

Material	λ(W/ m K)	ρ (kg/m^3)	c (J/ kg K)	D_T (m^2/sec)
Glass	1.05	2500	NA	4.7×10^{-7}
PDMS	0.17	NA	NA	NA
PCR sample (water)	0.643	1.0	4.2×10^3	1.5×10^{-7}
Silicon	150	2.33×10^3	0.7×10^3	920×10^{-7}
NOTE: Slight variation in most of these values exists from different sources.				

Using the parameters from the above table in Eq 5.19, the value of $t_{d\text{-glass}}$ through the 1.1 mm (L_1) thick glass substrate of the chip is estimated as follows.

$$t_{d-glass} \cong \frac{L^2_1}{D_T} \Rightarrow \frac{\left(1.1x10^{-3}\right)^2}{\left(4.7x10^{-7}\right)} \cong 2.57 \text{ sec}$$

Similarly, the value of t_{d2} through the ~ 1 mm (L_2) (height) PCR sample is estimated as

$$t_{d-fluid} \cong \frac{L^2_2}{D_T} \Rightarrow \frac{\left(1x10^{-3}\right)^2}{\left(1.5x10^{-7}\right)} \cong 6.66 \text{ sec}$$

Thus the total thermal delay ($t_{d\ total}$) for a uniform temperature distribution to the PCR sample is estimated to be

$$t_{d\ total} \cong t_{d\text{-}glass} + t_{d\text{-}fluid} \Rightarrow 9.23 \text{ sec}$$

This implies that at each setpoint (denaturation, annealing and extension temperatures), apart from the user defined dwell times (usually between 30 and 60 sec at each temperature) an added 9.23 sec is the recommend time value to compensate for thermal time delays within the chip structure. Considering a 25% uncertainty error in the thermal delay estimation because of the variation in the literature values for the constants given in Table 5-IV, the value of $t_{d\ total}$ can be approximated to be 12 sec and this is the time-compensation that was added to the user-defined dwell times for the denaturation, annealing and extension setpoint temperatures for the PCR performed in biochips.

5.9.2 Thermal Conductivity

Metals are very strong inhibitors of the PCR reaction[83, 84] and most reusable temperature sensing devices (e.g. RTD, thermocouples) are composed of metal components; thus it is not advisable to insert them into the PCR chamber for feedback temperature measurements. Temperature measurement in PCR systems is usually taken from the near vicinity of the chamber. Since such temperature measurements do not represent the temperature of the PCR (fluid) sample itself or the actual temperature inside the PCR chamber, temperature calibration is an important step in the success of PCR reaction. Unlike PCR performed in tubes, after proper temperature calibration any remaining small temperature spatial variations, will tend to be damped-out[85] because of the small (height of the) sample volume in a fully filled fluid chamber.

Although simulation analysis using finite element modeling can provide a good estimation of the temperature lag, this may not be very useful because of the following reasons. Firstly, if the lower glass substrate of the chip is not firmly held against the heat source (i.e. the CHP) then air will be introduced between the two surfaces and can cause temperature lags of many ^{o}C[1]. In this PCR experimental setup this issue was not a great concern since the valving actuators (rods as described in Chapter 6) firmly press the chip (from above) against the heat source beneath. Secondly, if the surface of the heat source (i.e. the copper plate, CHP) is uneven due to construction/machining conditions, the entire surface of the glass substrate of the chip is not expected to make good thermal contact and hence air might be introduced between the surfaces; which again might cause large temperature lags in the chip[85]. In both of the above stated cases, using organic

thermal compound can be a potential solution but is usually very 'messy'. If good thermal contact is made between the chip and the heat source, then the software simulation methods might be meaningful. However, experimental verification is critical.

There are many methods to execute the temperature calibration process. Temporal and spatial temperature uniformities within PCR chambers in biochips have been experimentally observed by some groups by suspended liquid crystals in the chamber and monitoring the hue (color intensity) change[78, 85]. These crystals have very distinct color change especially above 90 °C, which is in the range of the PCR denaturation temperature, and is a useful way to observe the actual temperature inside the PCR chamber. Nanocrystals [86], melting organic salts [17] and dyes [87] have all been adopted as reliable techniques for temperature measurement and calibration of biochip based thermal devices. In another approach, a metallic temperature sensor was inserted into a reference chamber adjacent to the PCR chamber and this was filled with a fluid sample similar to the PCR sample and feedback temperature was taken from this chamber. However, this approach may be a bit complicated for integrated systems because of the need for additional microfluidic valves for this reference chamber.

Alternatively such temperature calibration measurements can also be performed using (what is now termed as) a 'cross-referencing method'. This method is done once, as a final calibration exercise prior to using the system for PCR experimentation. In this method, an external temperature-measuring device is inserted into the PCR chamber and the temperature reading of this external device is mapped to the system's temperature reading and analyzed for non-uniformities.

Prior to such analysis, the system temperature sensor and the external temperature sensing device were calibrated. The calibration exercise for the external temperature sensing device involved another cross-referencing experiment with a mercury thermometer. In this method, the thermometer and the sensing device were immersed in a heated water bath and were verified for accuracy. It was found that the temperature reading of the two devices closely followed each other (with a variation of less than 0.2 °C). The system temperature sensor was then calibrated based on Eq 5.2 with necessary compensations.

Finally, to perform the cross-referencing calibration, an experimental setup as shown in the block diagram in Figure 5-14 was setup.

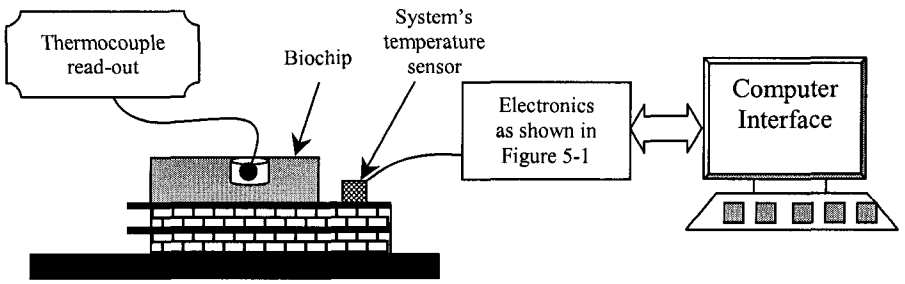

Figure 5-14. Cross-referencing temperature calibration setup

A small insertion was made in the PDMS chip above the PCR chamber and filled with the organic thermal paste (Thermal compound, Wakefield Engineering Inc., USA). Then the probe of an external thermocouple (K type, Fluke 179, Fluke Inc., USA) was inserted into the chamber. This digital external thermocouple meter is manufacturer calibrated and the uncertainties with the device are under ± 2 % of the temperature reading (in ^{o}C) and the predictable accuracy of the device was verified by cross-referencing its performance with a mercury thermometer in a heated water bath. In this setup, air draft influences and insulation of the chamber with a cover-slip were not a concern because the chamber was filled with the thermal compound and hence airflow is not expected to affect the inserted probe temperature. The thermally conductive paste should suppress temperature shifts due to heat conduction from the thermocouple waire. Moreover, this setup is indicative of an actual PCR experimental setup and hence is descriptive of the application. The system was thermally cycled for the PCR specification and the temperature readings of both the thermocouple and the system's sensor were noted. Upon completion, the two independent temperature values were plotted on the same scales (temperature vs. time). The graph in Figure 5-15 (left) shows this experimental data. (Note: The x-axis time scale is approximate for the external thermocouple reading because it had to be manually noted as it did not have data accusation capabilities).

Quite evidently, due to the poor thermal conductivity and heat capacitance[28] of the glass substrate, the temperature in the PCR chamber varied (above or below) by up to

2.5 °C from the temperature of the system (i.e. the heat source, CHP). At the denaturation temperature (94 °C), the temperature in the PCR chamber (i.e. the thermocouple reading) was about 2 °C below the temperature reading on the CHP. At the annealing temperature (60 °C) however, the temperature was about 2 °C warmer than the CHP and at the extension temperature (72 °C) the temperature was below by about 2 °C. The warmer temperature inside the PCR chamber at the annealing temperature is believed to be because the heat capacitance of the glass that stores thermal energy when cooling from the denaturation temperature to the annealing temperature[28]. On the other hand, the cooler temperatures in the PCR chamber at the denaturation and extension temperature is believed to be due to the poor thermal conductivity of the glass substrate[6, 8]. This lead/lag effect is also noted in the literature[7]. Thermal simulation and experimental evidence by Lagally *et al.*[7] revealed that lead/lags of as much as ~10 °C are observed in glass structured chips (used with thin film heaters). Necessary compensation[7] of higher heating/cooling was necessary to compensate for the poor thermal conductivity of the glass.

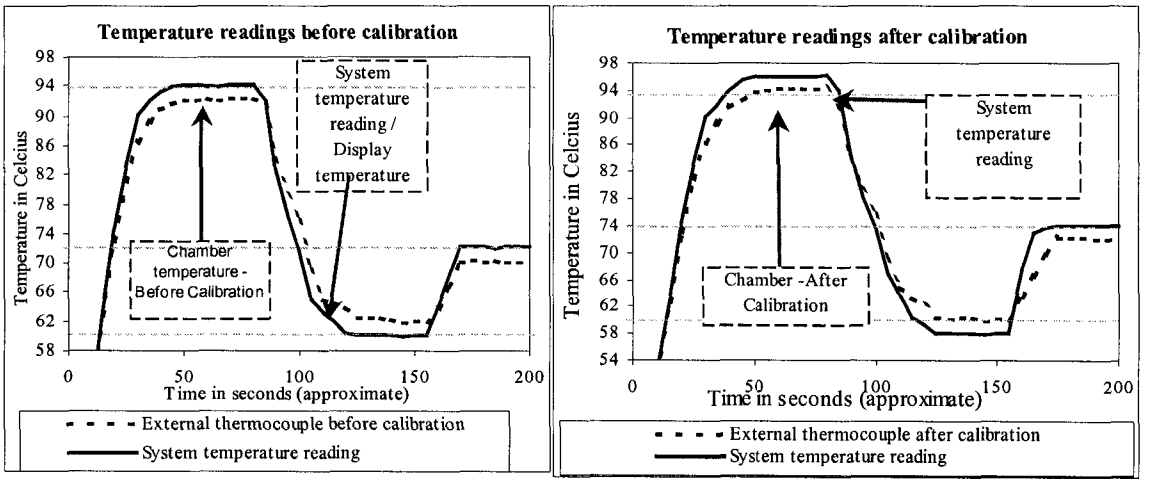

Figure 5-15. Graph of the temperature vs. time response of the system temperature and the PCR chamber temperature. Left: before cross-referencing calibration. Right: after cross-referencing calibration

The temperature lead/lags (observed in the biochips used in this work) were confirmed to be the influence of the glass and not the temperature sensor and this was verified by: (1) Calibrating the system's sensors at room temperature prior to working with the system. This involved the addition/subtraction of a marginal temperature value

(in °C) to Eq 5.2 in the software. (2) Cross-verifying that this calibrated value matches that of an external thermometer at room temperature and at an elevated temperature by heating the Peltier device and placing the thermocouple in a thermal compound substance on the copper plate (CHP). It was found to only have a difference of 0.25 °C. (3) At one instance placing the thermocouple probe on the CHP rather than inside the PCR chamber and ensuring that the temperature reading matched that of the system's temperature sensor. This confirmed that the sensor and the external thermocouple were calibrated and had identical temperature characteristics. (4) Performing the same experiment with just a glass slide without the PDMS yielded the same results.

Having confirmed that the material properties of the glass were the cause of the temperature lead/lags inside the PCR chamber, necessary compensations for these calibrations were included in the software, as described below. At the denaturation temperature, the system was actually set to heat to 96 °C rather than 94 °C, at the annealing temperature the system was cooling (from 94 °C) to 58 °C rather than 60 °C and at the extension temperature the system was heating (from 58 °C) to 74 °C rather than 72 °C. By performing such adjustments, the actual temperatures in the PCR chamber matched the user defined PCR thermal cycling temperatures. The graph in Figure 5-15 (Right) shows a calibrated thermal response from the system – system temperature and the PCR chamber temperature.

With this calibration, the necessary compensation for the poor thermal properties of the lower glass substrate of the chip were accounted-for which allowed for successful PCR experimentation with DNA samples as discussed in Chapter 7.

5.10 Summary and Conclusion

The efforts in implementing a thermal instrument and a suitable control system capable of performing the PCR genetic amplification in biochips was successfully implemented in this part of the research project. Peltier devices housed in a copper arrangement with minimal thermal mass were designed and tailor-made to accommodate the PCR biochip. The heating scheme used in this demonstration was the bottom-up planar heating method[28].

The set-up was then supported with suitable in-house electronics in the form of a PIC microprocessor, an ADC, a DAC, temperature sensors, a ±12 V power supply, and computer interface with a software module. A novel control system in the form of a 'digital non-linear PD-PI controller' with dual action was designed and implemented. A non-linear implementation was required since the operating temperature boundary for PCR was broad in the range of about 50 °C (i.e. annealing temperature – the denaturation temperature) and the convection losses added to the change in the resistance of the heating device resulted in a highly nonlinear system response over the wide temperature range[1, 20]. The non-linear controller was implemented by accurate zonal tuning using the Ziegler-Nichols open loop method and by appropriate gain scheduling during the control system operation.

The split algorithm (i.e. the PD-PI) was found necessary to ensure a 'ideal critically damped system response' with a fast rise time, minimal-to-nil overshoot, and finite-to-nil settling time. This was implemented well before such a method was described in the PCR literature.

Furthermore, a dual action controller was implemented (i.e. a second PI controller that performs on the background of the non-linear PD-PI) since a two-stacked Peltier arrangement was required to enable the temperature of the PCR system to heat to high temperatures (i.e. the denaturation temperature of 94 °C) during the PCR. This added feature makes the control system performance much like a 'parallel processing control system'.

Features such as anti-integral wind-up, bumpless transfer, feedback disturbance correction, temperature loop cycling, ADC and DAC calibration. were designed and implemented to enhance (and/or compensate for the electronics constraints) and these are believed to have further optimized the control system performance. Also, as per the PCR protocol for DNA samples, added times (typically 2 to 7 min) for denaturation at the first cycle and added times for extension at the last cycle were required and this too was implemented within the software.

Finally, appropriate thermal estimations and calibration were performed to ensure that the PCR fluid sample in the biochip actually reached the setpoint temperatures and not just the Peltier copper assembly in which the chip was housed. This calibration was

particularly required because of the poor thermal conductivity of the glass substrate of the biochip.

This thermal system had good performance but over the years of usage it was found that the particular Peltier model (TZ11055-01) used in this system was not suited for temperature cycling although it meet operating specifications.Typically, it failed at an average of about 10 PCR experiments. This required the frequent and the laborious process of re-tuning and thermal calibration. In the next prototype version a different Peltier model (TZ39038-01) suitable for temperature cycling will be used which is hoped to increase the durability of the system.

Evidently, one of the major components for the success of a PCR from an engineering perspective is the thermal control system. The developed novel control system presented here has now become a standardized module in our laboratory in implementing prototypes capable of the PCR. Currently a new prototype device capable of PCR and CE is being implemented with similar electronics and design. To increase the durability of the Peltiers, a different model (TZ39038-01) is being used which required a change in the power-supply (i.e. from the old ± 12V, 2.5 Amps, to a ± 12V, 6 Amps). With systematic and accurate tuning of this controller in the new system, the performance of that system should also exhibit identical characteristics as described here. Furthermore, the controller designed in this work can be used in future work as well (e.g. those using thin film heaters) and will considerably shorten the start-to-finish time of those projects.

5.11 References

[1] D. S. Yoon, Y. S. Lee, Y. Lee, H. J. Cho, S. W. Sung, K. W. Oh, J. Cha, G. Lim, *Precise temperature control and rapid thermal cycling in a micromachined DNA polymerase chain reaction chip,* Journal of Micromechanics and Microengineering, 2002, *12*, 813.

[2] J. Liu, C. Hansen, S. R. Quake, *Solving the "world-to-chip" interface problem with a microfluidic matrix,* Analytical Chemistry, 2003, *75*, 4718.

[3] X. M. Yu, D. C. Zhang, T. Li, L. Hao, X. H. Li, *3-D microarrays biochip for DNA amplification in polydimethylsiloxane (PDMS) elastomer,* Sensors and Actuators a-Physical, 2003, *108*, 103.

[4] P. J. Obeid, T. K. Christopoulos, H. J. Crabtree, C. J. Backhouse, *Microfabricated device for DNA and RNA amplification by continuous-flow polymerase chain reaction and*

reverse transcription-polymerase chain reaction with cycle number selection, Analytical Chemistry, 2003, *75*, 288.

[5] S. Shandrick, Z. Ronai, A. Guttman, *Rapid microwell polymerase chain reaction with subsequent ultrathin-layer gel electrophoresis of DNA,* Electrophoresis, 2002, *23*, 591.

[6] A. T. Woolley, D. Hadley, P. Landre, A. J. deMello, R. A. Mathies, M. A. Northrup, *Functional integration of PCR amplification and capillary electrophoresis in a microfabricated DNA analysis device,* Analytical Chemistry, 1996, *68*, 4081.

[7] E. T. Lagally, P. C. Simpson, R. A. Mathies, *Monolithic integrated microfluidic DNA amplification and capillary electrophoresis analysis system,* Sensors and Actuators B-Chemical, 2000, *63*, 138.

[8] E. T. Lagally, C. A. Emrich, R. A. Mathies, *Fully integrated PCR-capillary electrophoresis microsystem for DNA analysis,* Lab on a Chip, 2001, *1*, 102.

[9] Y. J. Liu, C. B. Rauch, R. L. Stevens, R. Lenigk, J. N. Yang, D. B. Rhine, P. Grodzinski, *DNA amplification and hybridization assays in integrated plastic monolithic devices,* Analytical Chemistry, 2002, *74*, 3063.

[10] J. Khandurina, T. E. McKnight, S. C. Jacobson, L. C. Waters, R. S. Foote, J. M. Ramsey, *Integrated system for rapid PCR-based DNA analysis in microfluidic devices,* Analytical Chemistry, 2000, *72*, 2995.

[11] C. G. Koh, W. Tan, M. Q. Zhao, A. J. Ricco, Z. H. Fan, *Integrating polymerase chain reaction, valving, and electrophoresis in a plastic device for bacterial detection,* Analytical Chemistry, 2003, *75*, 4591.

[12] J. N. Yang, Y. J. Liu, C. B. Rauch, R. L. Stevens, R. H. Liu, R. Lenigk, P. Grodzinski, *High sensitivity PCR assay in plastic micro reactors,* Lab on a Chip, 2002, *2*, 179.

[13] B. C. Giordano, J. Ferrance, S. Swedberg, A. F. R. Huhmer, J. P. Landers, *Polymerase chain reaction in polymeric microchips: DNA amplification in less than 240 seconds,* Analytical Biochemistry, 2001, *291*, 124.

[14] Y. S. Shin, K. Cho, S. H. Lim, S. Chung, S. J. Park, C. Chung, D. C. Han, J. K. Chang, *PDMS-based micro PCR chip with parylene coating,* Journal of Micromechanics and Microengineering, 2003, *13*, 768.

[15] J. W. Hong, T. Fujii, M. Seki, T. Yamamoto, I. Endo, *Integration of gene amplification and capillary gel electrophoresis on a polydimethylsiloxane-glass hybrid microchip,* Electrophoresis, 2001, *22*, 328.

[16] D. J. Sadler, R. Changrani, P. Roberts, C.-F. Chou, F. Zenhausern, *Thermal management of BioMEMS: temperature control for ceramic-based PCR and DNA detection devices,*

Components and Packaging Technologies, IEEE Transactions on [see also Components, Packaging and Manufacturing Technology, Part A: Packaging Technologies, IEEE Transactions on], 2003, *26*, 309.

[17] J. H. Daniel, S. Iqbal, R. B. Millington, D. F. Moore, C. R. Lowe, D. L. Leslie, M. A. Lee, M. J. Pearce, *Silicon microchambers for DNA amplification,* Sensors and Actuators a-Physical, 1998, *71*, 81.

[18] A. I. K. Lao, T. M. H. Lee, I. M. Hsing, N. Y. Ip, *Precise temperature control of microfluidic chamber for gas and liquid phase reactions,* Sensors and Actuators a-Physical, 2000, *84*, 11.

[19] I. Erill, S. Campoy, N. Erill, J. Barbe, J. Aguilo, *Biochemical analysis and optimization of inhibition and adsorption phenomena in glass-silicon PCR-chips,* Sensors and Actuators B-Chemical, 2003, *96*, 685.

[20] S. W. Sung, S. W. Park, D. S. Yoon, Y. S. Lee, G. B. Lim, *Modeling and control of a microthermal cycler for DNA polymerase chain reaction,* Industrial & Engineering Chemistry Research, 2003, *42*, 6104.

[21] E. Dummermuth, in *Soft Computing in Industrial Applications, 2001. SMCia/01. Proceedings of the 2001 IEEE Mountain Workshop on*, 2001, pp. 105.

[22] I. Erill, S. Campoy, J. Rus, L. Fonseca, A. Ivorra, Z. Navarro, J. A. Plaza, J. Aguiló, J. Barbé, *Development of a CMOS-compatible PCR chip: comparison of design and system strategies,* Journal of Micromechanics and Microengineering, 2004, *14*, 1558.

[23] A. R. Prakash, S. Adamia, V. Sieben, P. Pilarski, L. M. Pilarski, C. J. Backhouse, *Small Volume PCR in PDMS Biochips with Integrated Fluid Control and Vapour Barrier,* Sensors and Actuators B-Chemical, 2004, *submitted on July 30, 2004.*

[24] H. Seraji, in *Robotics and Automation, 1988. Proceedings., 1988 IEEE International Conference on*, 1988, pp. 854.

[25] in *Computer-Aided Control System Design, 1994. Proceedings., IEEE/IFAC Joint Symposium on*, 1994.

[26] A. M. N. Lima, G. S. Deep, L. A. L. de Almeida, H. Neff, M. Fontana, in *Instrumentation and Measurement Technology Conference, 2001. IMTC 2001. Proceedings of the 18th IEEE, Vol. 2*, 2001, pp. 919.

[27] I. Ferrotec, Ferrotec Inc, USA, Nashua, NH, 2000.

[28] Q. B. Zou, Y. B. Miao, Y. Chen, U. Sridhar, C. S. Chong, T. C. Chai, Y. Tie, C. H. L. Teh, T. M. Lim, C. Heng, *Micro-assembled multi-chamber thermal cycler for low-cost reaction chip thermal multiplexing,* Sensors and Actuators a-Physical, 2002, *102*, 114.

[29] N. L. Jeon, D. T. Chiu, C. J. Wargo, H. K. Wu, I. S. Choi, J. R. Anderson, G. M. Whitesides, *Design and fabrication of integrated passive valves and pumps for flexible polymer 3-dimensional microfluidic systems,* Biomedical Microdevices, 2002, *4*, 117.

[30] W. H. Grover, A. M. Skelley, C. N. Liu, E. T. Lagally, R. A. Mathies, *Monolithic membrane valves and diaphragm pumps for practical large-scale integration into glass microfluidic devices,* Sensors and Actuators B-Chemical, 2003, *89*, 315.

[31] T. M. H. Lee, M. C. Carles, I. M. Hsing, *Microfabricated PCR-electrochemical device for simultaneous DNA amplification and detection,* Lab on a Chip, 2003, *3*, 100.

[32] G. C. Goodwin, S. F. Graebe, M. E. Salgado, *Control System Design*, Prentice Hall PTR, 2001.

[33] J. C. Basilio, S. R. Matos, *Design of PI and PID controllers with transient performance specification,* Education, IEEE Transactions on, 2002, *45*, 364.

[34] K. J. Astrom, *Control System Design*, 2002.

[35] P. H. Lewis, C. Yang, *Basic Control Systems Engineering*, Prentice Hall, 1997.

[36] C. H. Mastrangelo, M. A. Burns, D. T. Burke, *Microfabricated devices for genetic diagnostics,* Proceedings of the IEEE, 1998, *86*, 1769.

[37] P. R. Selvaganapathy, E. T. Carlen, C. H. Mastrangelo, *Recent progress in microfluidic devices for nucleic acid and antibody assays,* Proceedings of the Ieee, 2003, *91*, 954.

[38] J. C. Ryu, C. K. Park, in *SICE Annual, 1999. 38th Annual Conference Proceedings of the*, 1999, pp. 1233.

[39] K. R. S. Kodagoda, W. S. Wijesoma, E. K. Teoh, *Fuzzy speed and steering control of an AGV,* Control Systems Technology, IEEE Transactions on, 2002, *10*, 112.

[40] J. Lever, in *Two Decades of Fuzzy Control - Part 2, IEE Colloquium on*, 1993, pp. 11/1.

[41] W. S. Wijesoma, K. R. S. Kodagoda, E. K. Teoh, in *Intelligent Transportation Systems, 1999. Proceedings. 1999 IEEE/IEEJ/JSAI International Conference on*, 1999, pp. 142.

[42] K. Liu, F. L. Lewis, in *Decision and Control, 1993., Proceedings of the 32nd IEEE Conference on*, 1993, pp. 1743.

[43] P. J. S. Goncalves, J. R. C. Pinto, in *Emerging Technologies and Factory Automation, 2003. Proceedings. ETFA '03. IEEE Conference, Vol. 2*, 2003, pp. 377.

[44] M. N. H. Siddique, M. O. Tokhi, in *Control Applications, 2002. Proceedings of the 2002 International Conference on, Vol. 1*, 2002, pp. 471.

[45] D. E. Rivera, M. Morari, S. Skogestad, *Internal Model Control .4. Pid Controller-Design,* Industrial & Engineering Chemistry Process Design and Development, 1986, *25*, 252.

[46] J. G. Ziegler, N. B. Nichols, *Industrial Process Control,* Chemical Engineering Progress, 1947, *43*, 309.

[47] K. J. Astrom, Wittenma.B, *Self Tuning Regulators,* Automatica, 1973, *9*, 185.

[48] K. J. Astrom, B. Wittenmark, *Self-Tuning Controllers Based on Pole-Zero Placement,* Iee Proceedings-D Control Theory and Applications, 1980, *127*, 120.

[49] B. Kristiansson, B. Lennartson, in *American Control Conference, 1998. Proceedings of the 1998, Vol. 5*, 1998, pp. 3131.

[50] E. Katende, A. Jutan, *Experimental evaluation of predictive temperature control for a batch reactor system,* Control Systems Technology, IEEE Transactions on, 2000, *8*, 2.

[51] M. R. Katebi, M. H. Moradi, *Predictive PID controllers,* Control Theory and Applications, IEE Proceedings-, 2001, *148*, 478.

[52] S. Daley, *Developing controllers through a process of natural evolution,* Computing & Control Engineering Journal, 1999, *10*, 42.

[53] C. C. Hang, K. J. Astrom, W. K. Ho, *Refinements of the Ziegler-Nichols tuning formula,* Control Theory and Applications, IEE Proceedings D, 1991, *138*, 111

[54] R. A. Wright, N. Kazantzis, C. Kravaris, in *American Control Conference, 1998. Proceedings of the 1998, Vol. 1*, 1998, pp. 328.

[55] D. Karaboga, A. Kalinli, in *Systems, Man, and Cybernetics, 1996., IEEE International Conference on, Vol. 1*, 1996, pp. 134.

[56] R.-C. Hwang, H.-C. Huang, W.-S. Chi, in *Systems, Man, and Cybernetics, 2000 IEEE International Conference on, Vol. 5*, 2000, pp. 3629.

[57] J.-C. Shen, in *Control Applications, 2001. (CCA '01). Proceedings of the 2001 IEEE International Conference on*, 2001, pp. 459.

[58] Q. M. Zhu, in *Learning Systems for Control (Ref. No. 2000/069), IEE Seminar*, 2000, pp. 11/1.

[59] L. J. Brown, J. S. Schwaber, in *American Control Conference, 1999. Proceedings of the 1999, Vol. 1*, 1999, pp. 139.

[60] B. M. Badreddine, F. Lin, in *Control Applications, 2001. (CCA '01). Proceedings of the 2001 IEEE International Conference on*, 2001, pp. 1031.

[61] T. Iwasa, N. Morizumi, S. Omatu, in *Neural Networks,1997., International Conference on, Vol. 4*, 1997, pp. 2430.

[62] R. F. Harrison, in *Optimisation in Control: Methods and Applications (Ref. No. 1998/521), IEE Colloquium on*, 1998, pp. 9/1.

[63] J. E. A. Filho, S. A. Sandri, E. E. N. Macau, in *Fuzzy Information Processing Society, 2000. NAFIPS. 19th International Conference of the North American*, 2000, pp. 461.

[64] T. F. Cheung, W. L. Luyben, *Non-Linear and Non-Coventional Liquid-Level Controllers,* Industrial & Engineering Chemistry Fundamentals, 1980, *19*, 93.

[65] A. Kaya, O. Akron, T. J. Scheib, *Tuning of PID controls of different structures,* Control Engineering, 1988, 62.

[66] L.-S. Su, in *Instrumentation and Measurement Technology Conference, 1994. IMTC/94. Conference Proceedings. 10th Anniversary. Advanced Technologies in I & M., 1994 IEEE*, 1994, pp. 841.

[67] A. H. Lee, J. Bentsman, C. W. Taft, in *Decision and Control, 2002, Proceedings of the 41st IEEE Conference on, Vol. 2*, 2002, pp. 1307.

[68] Y. Peng, D. Vrancic, R. Hanus, *Anti-windup, bumpless, and conditioned transfer techniques for PID controllers,* Control Systems Magazine, IEEE, 1996, *16*, 48.

[69] M. A. Henson, B. A. Ogunnaike, J. S. Schwaber, *Habituating Control Strategies for Process-Control,* Aiche Journal, 1995, *41*, 604.

[70] C. Maffezzoni, N. Schiavoni, G. Ferretti, *Robust design of cascade control,* Control Systems Magazine, IEEE, 1990, *10*, 21.

[71] P. H. Meckl, G. T.-C. Chiu, P. Davies, in *American Control Conference, 1999. Proceedings of the 1999, Vol. 1*, 1999, pp. 475.

[72] W. K. Ho, O. P. Gan, E. B. Tay, E. L. Ang, *Performance and gain and phase margins of well-known PID tuning formulas,* Control Systems Technology, IEEE Transactions on, 1996, *4*, 473.

[73] J. G. Ziegler, N. B. Nichols, *Dynamic Accuracy in Temperature Measurement,* Science, 1949, *110*, 361.

[74] G. H. Cohen, G. A. Coon, *Theoritical consideration of retarded control,* Trans. Amer. Soc. Mech. Eng., 1953, *75*, 827.

[75] I.-L. Chien, P. S. Fruehauf, *Consider IMC tuning to improve controller performance,* Chemical Engineering Progress, 1990, *86*, 33.

[76] J. Dong, C. B. Brosilow, in *Proceedings of the American Control Conference*, IEEE, Philadelphia, Pennsylvania, 1998, pp. 323.

[77] L. Samet, N. Masmoudi, M. W. Kharrat, L. Kamoun, in *Electronics, Circuits and Systems, 1998 IEEE International Conference on, Vol. 1*, 1998, pp. 291.

[78] J. Liu, M. Enzelberger, S. Quake, *A nanoliter rotary device for polymerase chain reaction,* Electrophoresis, 2002, *23*, 1531.

[79] K. G. Harstad, J. Bellan, *Mixing rules for multicomponent mixture mass diffusion coefficients and thermal diffusion factors,* Journal of Chemical Physics, 2004, *120*, 5664.

[80] B. D. Ferney, M. R. DeVary, K. J. Hsia, A. Needleman, *Oscillatory crack growth in glass,* Scripta Materialia, 1999, *41*, 275.

[81] D. W. van Krevelen, P. Hoftyzer, Amsterdam: Elsevier, 1976.

[82] D. W. Van Krevelen, *Properties of Polymers*, Elsevier Science B.V, Amsterdam, 1997.

[83] A. F. R. Huhmer, J. P. Landers, *Noncontact infrared-mediated thermocycling for effective polymerase chain reaction amplification of DNA in nanoliter volumes,* Analytical Chemistry, 2000, *72*, 5507.

[84] T. B. Taylor, S. E. Harvey, M. Albin, L. Lebak, Y. Ning, I. Mowat, T. Schuerlein, E. Principe, *Process Control for Optimal PCR Performance in Glass Microstructures,* Biomedical Microdevices, 1998, *1*, 65.

[85] A. M. Chaudhari, T. M. Woudenberg, M. Albin, K. E. Goodson, *Transient liquid crystal thermometry of microfabricated PCR vessel arrays,* Journal of Microelectromechanical Systems, 1998, *7*, 345.

[86] H. B. Mao, T. L. Yang, P. S. Cremer, *A microfluidic device with a linear temperature gradient for parallel and combinatorial measurements,* Journal of the American Chemical Society, 2002, *124*, 4432.

Chapter – 6

Microfluidic Valves and Pumps

In this demonstration, a diaphragm pump and pinch-off valves were designed in a macroscopic system that was then adapted to the biochip. This enabled automated processing of fluid sample loading, channel sealing and sample unloading within enclosed chambers and channels in the biochips. It is hoped that this will enable higher levels of on-chip automation in the future prototypes.

6.1 Introduction

As the complexity and feasibility of performing multiple bioassays on microfluidic platforms increases, the requirement for integrating fluid control in the form of valves and pumps becomes increasingly important[1]. This is similar to the electrical miniaturization drive of the mid 1950's (i.e. the IC technology) that was necessary to facilitate complex electrical circuit integration on a single platform[1] (known as a IC). We are witnessing similar requirements in microfluidics as researchers seek to integrate bioprocesses on the same microfluidic platform that require fluid control within designated areas in the biochip.

Microfluidic valving and pumping is often application specific. In the case of the valving of fluidic channels, an air-tight seal may be required if the application involves preventing water vapor or fluid movement due to high temperature or pressure influence, as in the case with PCR genetic amplification[2]. On the other hand, for relatively simple applications such as transporting fluid in a unidirectional manner, a check-valve that acts as a barrier to low-pressure fluid flow can be used[3]. If transportation of fluid is the primary requirement of the plumbing system, electrosmotic flow (EOF) is often preferred[4, 5]. However, EOF suffers from limitations arising from ionic strength, pH,

ionic composition, diffusion, the presence of charged macromolecules in the fluid and low flow rate[3]. Movable mechanical parts made of metal have long been demonstrated as reliable valves in silicon and glass structured chips[6]; however, wear, fatigue and friction are inevitable problems[7]. Many other microfluidic plumbing systems have adopted a vertical multilayer hybrid approach that is very disadvantageous in terms of fabrication complexity and yield of the biochip[3, 8-14]. Vertical hybrid stacked chip structures of up to 13 layers[4] have been demonstrated as successful microfluidic plumbing techniques but have often not been demonstrated as integrated systems in lab-on-a-chip devices due to the complexity in operating the device and the incompatibility with biological substances like DNA and cells[12]. The other disadvantage of complex hybrid structures is that they hinder serviceability and the ability to thoroughly test individual parts before assembly and this leads to unreliability issues with the end products – the assembled chips[12].

In PCR applications there are some essential requirements for a plumbing system. In brief they are: thermal robustness, non-metallic[15-17], non-chemical actuation[18, 19], water vapor and water impermeable[2, 20, 21], and high pressure resistance (i.e. in excess of 15 psi)[22]. Due to these complexities in designing a plumbing system for the PCR application, most demonstrations to date have chosen to evade the topic and opted to sealing chambers with cover slips[2, 21, 23, 24], tape[19, 24] or both with a few demonstrations as exceptions[22, 25-27]. However, valveless and pumpless devices do not facilitate integration of the PCR technique with other genetic techniques (e.g. CE) on a unified structure since they will be incapable of fluid control.

To meet the specific requirements of the PCR application and maintain the goals of developing a fieldable commercial genetic diagnostic system in the near future, integrated fluid control in the form of the diaphragm pump[3] and the pinch-off valves [1, 28] were incorporated in this work. These valves and pump are capable of automated functionality that was facilitated by servomotor actuators to provide a fully reusable microfluidic valving and pumping system. This is considered as an important step in the ongoing development of highly integrated microfluidic systems.

The following section provides a description of the diaphragm pumping technique and the importance of integrating valves to such a pump to facilitate fluid flow in channels in a selective manner. This is followed by a description of the integration of the diaphragm pump and the pinch-off valves in the system constructed to enable performing the PCR in the PDMS-glass in this work.

6.2 Principle of the Diaphragm Pump

The diaphragm based pumping mechanism has been extensively investigated in recent years[3, 7, 10, 29]. Stemme and coworkers were the first to demonstrate the concept of the diaphragm pump in MEMS[29]. This pumping method is a 'diaphragm based diffuser capillary action' mechanism[3, 7, 10, 29]. The design feature of the pump is to create a suction (supply mode) – expulsion (pump mode) mechanism upon deformation of a diaphragm that causes a change in the chamber volume. This is called a 'self-priming' mechanism and can be achieved if the pump has both gas and liquid pumping capabilities[7, 29]. The schematic in Figure 6-1 depicts this supply and expulsion mechanism of the diaphragm pump. The visible drawback of the demonstration was the inability of the device to selectively choose the channel through which the supply or expulsion (of fluid or gas) was to be directed, i.e. the concept of valves to selectively seal channels was not incorporated.

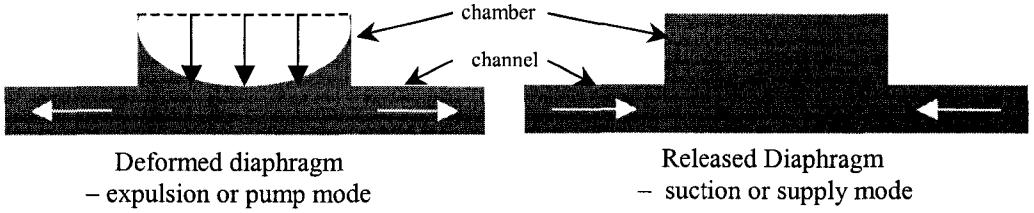

Figure 6-1. Working principle of the diaphragm pump

The diaphragm pump devices demonstrated by Stemme and coworkers were initially fabricated of polycarbonate structures but upon further improvement, Si-glass MEMS fabrication procedures were used to structure a chip with this diaphragm pump [7].

Polycarbonate, Si and glass are rigid materials (i.e. high Young's modulus) and hence they do not offer good flexibility of the diaphragm. PDMS on the other hand is a soft polymer with very high flexibility (shear modulus (G) = up to 3 MPa) with small variation in G even at +100 °C (1.1 kPa / °C) [30, 31]. This had encouraged the Whitesides's group (the introducers of PDMS to bioMEMS) to explore PDMS as a potential material to fabricate the diaphragm pump in microfluidics[3]. A check-valve arrangement made with a 25 to100 μm thick PDMS membranes for unidirectional fluid flow was integrated to a PDMS based diaphragm pump[3]. With a human finger-driven pressure on the diaphragm, fluid flow into and out of the chamber was realized. Selective flow in the channels connecting the diaphragm pump was possible because of the check-valves. A similar check-valve mechanism was also demonstrated by Grover *et al.*[10].

However, these check-valves with flexible PDMS membrane were incapable of air/gas/vapor flow in a controlled and/or an air-tight manner and hence were not demonstrated in high temperature/pressure applications[10] (e.g. the PCR).

6.3 Integration of the Diaphragm Pump and Pinch-off Valves

Using the concept of the diaphragm pump[3] and the principle of the NanoFlex™ valves[1, 26] (i.e. a pinch-off valving mechanism) in PDMS, this work has integrated the diaphragm pump and pinch-off valves[13] to a PDM-glass hybrid chip. In the chip design, the enclosed PCR chamber with a 1 mm thick PDMS roof structure also serves as the diaphragm pump. This simplifies the chip design, increases the device density and reduces the fluid dead volume in the chip. A robotic arm above the surface of the diaphragm pump provides the necessary pump actuation. Pinch-off valving[13] by thrusting the PDMS above the channel onto the lower glass substrate, again using robotic fingers, enables sealing of the channel during the PCR thermal cycling, thus preventing fluid or vapor leakage from the PCR chamber.

Figure 6-2.i) is photograph of the system and the schematic of the diaphragm pump and pinch-off valve is shown in Figure 6-2. ii). The sequential process of fluid

sampling loading, unloading, and sealing of the channels is achieved by upward and downward movements of the servomotor actuated rods.

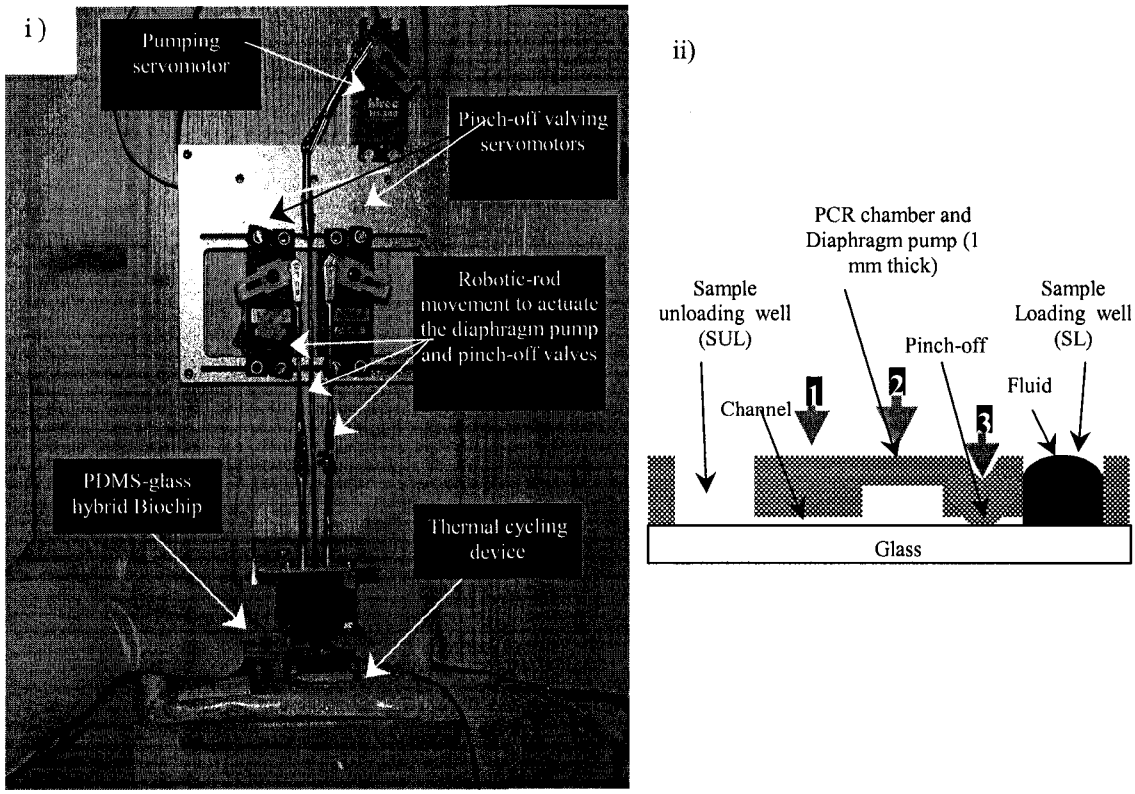

Figure 6-2. i) a photograph of the pumping and valving system. ii) a schematic of the pumping and valving process.

The actuating metallic rods (14 cm length) from the servomotors (HS3000, Hitech, USA) were connected to the servomotor arm at an angle of 45 °. At an unactuated position the rods were positioned 2 mm above the 2.9 mm thick PDMS-glass chip. The servomotors were controlled by pulse width modulation (PWM) using a 16f873 microcontroller. The PWM operation enables stepwise control for the upward and downward motion of the actuating rods. The software (servo.c) can be found in the supplementary CD provided with this thesis.

Since the pump and valve actuating rods are isolated from the PCR sample, i.e. they are not in direct contact with the fluid sample, inhibition and cross-contamination issues do not arise. This remarkably simple yet efficient diaphragm pump and pinch-off

valves offers a fully reusable, thermally robust and effective fluid control system suitable for the PCR genetic amplification and a wide variety of other microfluidics applications.

6.3.1 Prototyping Concerns

There were three major concerns during the prototyping of this device, which are outlined below.

The tip of the rods that actuate the pump and the valve had to be 'capped' with a low thermal conductivity material to prevent heat transfer from the surface of the PDMS chip during the PCR thermal cycling. Initial choice of materials included poor thermal conductors such as polycarbonate and acrylics but due to the force applied by the servomotor on these tips (which was required to completely seal the channels), deformation of the tips was a problem. Unpredictable deformation or flattening of the tips occurred at high temperatures (e.g. the extension and denaturing temperatures) and this caused an improper seal due to force applied on the bulk PDMS, (which has a much lower compression ratio), rather than the channel, thus resulting in the fluid loss from the PCR chamber. After numerous trials with many materials to fabricate these tips, a high temperature resistance plastic material called vespel (available from e.g. Dupont, USA) was selected. Tips made of this material were found to be stable and did not deform even after numerous PCR runs.

A comparison of some of the tips that were tried is shown in Figure 6-3; as shown in the pictures, the tips fabricated with vespel did not deform even after 25 PCR experiments.

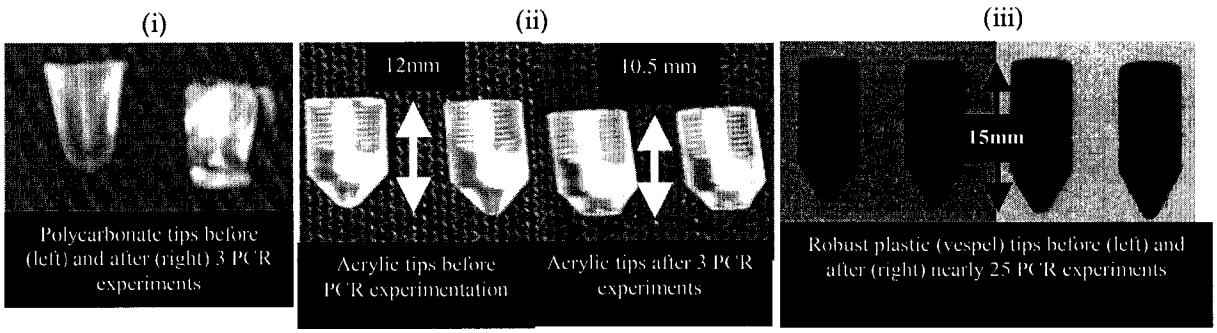

Figure 6-3. Performance evaluation of valving finger capping tips (i) Polycarbonate valving tips (ii) acrylic valving tips (iii) vespel valving tips. The polycarbonate and acrylic tips degraded over time causing improper sealing.

The other issue of concern with the functionality of the device was that with the alignment of the microfluidic channels in the chip to that of the tip of the actuating (valving) rods. The width of the channel was 50 μm and that of the tip was about 0.5 mm. Since this prototype device-setup could not accommodate a microscope arrangement, alignment of the tips to the channel was a challenging issue. Initial tests of the device with colored water (food coloring dye) as the fluid sample provided a fairly reliable alignment by observation due to the colored fluid filled channels in the PDMS chip. However, with the PCR samples (colorless like water) misalignment was a problem. Figure 6-4.i. shows two pictures one that shows an indent directly above the channel which corresponds to a sealed channel and the other that has an indent away from the channel which indicates an unsealed channel. The circular patters are from the indent presumably due to the high force applied by the rods. This difficulty was overcome by tracing the microfluidic channel onto the top surface of the PDMS (i.e. mimicking the colored water tests). Aligning this trace to the tip of the actuating (valving) rods was reliable (i.e. the channels were sealed in every of the over 25 PCR runs which resulted in a good quantity of retrieved fluid). Earlier consideration of the alignment issue involved possibly using 'alignment marks' on the PDMS during the fabrication process; however, this required a new chrome mask for the lithography process and hence was not executed. In another approach, an indent above the PDMS channel was tried. This was done by placing styrofoam balls (2 to 3mm dia) in the liquid (pre-cured) PDMS at the two

designated spots where the valving rods would press-down to seal the channel. Upon curing the PDMS, the balls were removed and an indent was created on the PDMS above the channel. However, this method was not consistently reproducible since it involved manual positioning of the balls and any movement of the pre-cured PDMS caused a dislocation of the indent.

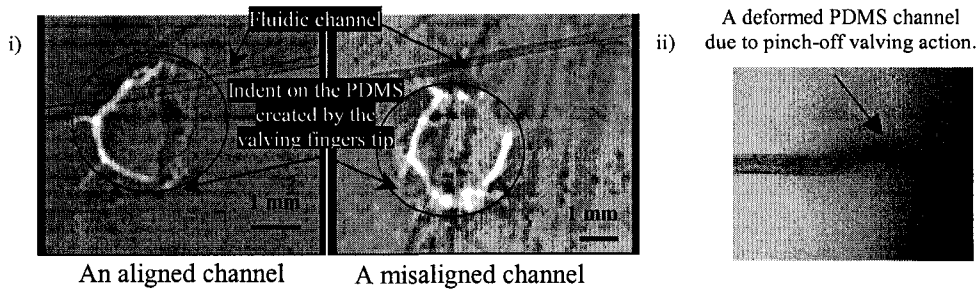

Figure 6-4. Microscope picture of the indent created by the valving fingers on the PDMS surface of the chip i)channel alignment picture ii) A deformed PDMS channel as a result of the valving action after a single PCR thermal cycling run

In addition to the above problems, the deformation of the PDMS channels due to the valving action limits the reuse of the PDMS chips. This is believed to be due to the large force exerted by the servomotor rods required to seal the channels in addition to the material properties of the PDMS (i.e. change in the flexibility of the PDMS as a function of temperature). The change in the flexibility of the PDMS at high temperatures combined with the force required to completely seal the channels is believed to have caused a remolding of the PDMS microfluidic channel (as shown in Figure 6-4.ii). This remolding caused the PDMS to deform in shape and caused discontinuities in the channel, limiting the use of the chips to a single PCR run. In future, improved methods to monitor the current drawn by the servomotor would provide a correlation between the force applied by the rods and the sealing of the channels. This might enable better control of the force exerted by the rods and prevent deformation of the channels. It is beyond the scope of this thesis to describe enhancements to this valving mechanism.

6.4 Conclusion

This chapter presented a microfluidic valving and pumping system based on the integration of the diaphragm pumping and pinch-off valving techniques. In integrated systems (e.g. PCR-CE) the incorporation of a fluid control becomes increasingly important because the fluidic circuits (e.g. channels and wells) in the chip may need to be isolated from each other during the bioanalysis. In future prototypes it is hoped that a sequential process of performing single-cell PCR[32] would be possible and this would represent a high throughput lab-on-a-chip device. In such chip designs sequential control of fluid flow during the analysis becomes an integral part of the integrated system. The valving and pumping system described is hoped to be readily adaptable with such systems.

Although the system exhibited satisfactory operation, performance issues (as discussed earlier) and the compatibility of using a macroscopic system with a biochip with microscopic features has been a major limitation. Alternative valving techniques that are enclosed within the biochip itself (e.g. the Nanoflex valves, gel valves) are being explored as enhanced alternatives to this valving system.

6.5 References

[1] M. A. Unger, H.-P. Chou, T. Thorsen, A. Scherer, S. R. Quake, *Monolithic Microfabricated Valves and Pumps by Multilayer Soft Lithography,* Science, 2000, *288*, 113.

[2] Z. Zhao, Z. Cui, D. Cui, S. Xia, *Monolithically integrated PCR biochip for DNA amplification,* Sensors and Actuators A: Physical, 2003, *108*, 162.

[3] N. L. Jeon, D. T. Chiu, C. J. Wargo, H. K. Wu, I. S. Choi, J. R. Anderson, G. M. Whitesides, *Design and fabrication of integrated passive valves and pumps for flexible polymer 3-dimensional microfluidic systems,* Biomedical Microdevices, 2002, *4*, 117.

[4] B. H. v. d. S. Elisabeth M J Verpoortets, Sylvain, A. M. Jeanneretf, H M Widmert and Nico F de Rooijt, *Three-dimensional micro flow 1, manifolds for miniaturized chemical analysis systems,* J. Micromech. Microeng., 1994, *4*, 246.

[5] S. H. Yao, D. E. Hertzog, S. L. Zeng, J. C. Mikkelsen, J. G. Santiago, *Porous glass electroosmotic pumps: design and experiments,* Journal of Colloid and Interface Science, 2003, *268*, 143.

[6] M. Kohl, K. D. Skrobanek, S. Miyazaki, *Development of stress-optimised shape memory microvalves,* Sensors and Actuators a-Physical, 1999, *72*, 243.

[7] H. Andersson, W. van der Wijngaart, P. Nilsson, P. Enoksson, G. Stemme, *A valve-less diffuser micropump for microfluidic analytical systems,* Sensors and Actuators B-Chemical, 2001, *72*, 259.

[8] T. Gerlach, *Microdiffusers as dynamic passive valves for micropump applications,* Sensors and Actuators a-Physical, 1998, *69*, 181.

[9] T. Gerlach, M. Schuenemann, H. Wurmus, *A New Micropump Principle of the Reciprocating Type Using Pyramidic Micro Flowchannels as Passive Valves,* Journal of Micromechanics and Microengineering, 1995, *5*, 199.

[10] W. H. Grover, A. M. Skelley, C. N. Liu, E. T. Lagally, R. A. Mathies, *Monolithic membrane valves and diaphragm pumps for practical large-scale integration into glass microfluidic devices,* Sensors and Actuators B-Chemical, 2003, *89*, 315.

[11] C. R. Neagu, J. G. E. Gardeniers, M. Elwenspoek, J. J. Kelly, *An electrochemical microactuator: Principle and first results,* Journal of Microelectromechanical Systems, 1996, *5*, 2.

[12] H. Suzuki, R. Yoneyama, *Integrated microfluidic system with electrochemically actuated on-chip pumps and valves,* Sensors and Actuators B-Chemical, 2003, *96*, 38.

[13] C. R. Tamanaha, L. J. Whitman, R. J. Colton, *Hybrid macro-micro fluidics system for a chip-based biosensor,* Journal of Micromechanics and Microengineering, 2002, *12*, N7.

[14] R. Zengerle, J. Ulrich, S. Kluge, M. Richter, A. Richter, *A bidirectional silicon micropump,* Sensors and Actuators a-Physical, 1995, *50*, 81.

[15] A. F. R. Huhmer, J. P. Landers, *Noncontact infrared-mediated thermocycling for effective polymerase chain reaction amplification of DNA in nanoliter volumes,* Analytical Chemistry, 2000, *72*, 5507.

[16] E. T. Lagally, P. C. Simpson, R. A. Mathies, *Monolithic integrated microfluidic DNA amplification and capillary electrophoresis analysis system,* Sensors and Actuators B-Chemical, 2000, *63*, 138.

[17] T. B. Taylor, S. E. Harvey, M. Albin, L. Lebak, Y. Ning, I. Mowat, T. Schuerlein, E. Principe, *Process Control for Optimal PCR Performance in Glass Microstructures,* Biomedical Microdevices, 1998, *1*, 65.

[18] J. Khandurina, T. E. McKnight, S. C. Jacobson, L. C. Waters, R. S. Foote, J. M. Ramsey, *Integrated system for rapid PCR-based DNA analysis in microfluidic devices,* Analytical Chemistry, 2000, *72*, 2995.

[19] I. Erill, S. Campoy, N. Erill, J. Barbe, J. Aguilo, *Biochemical analysis and optimization of inhibition and adsorption phenomena in glass-silicon PCR-chips,* Sensors and Actuators B-Chemical, 2003, *96*, 685.

[20] Y. S. Shin, K. Cho, S. H. Lim, S. Chung, S. J. Park, C. Chung, D. C. Han, J. K. Chang, *PDMS-based micro PCR chip with parylene coating,* Journal of Micromechanics and Microengineering, 2003, *13*, 768.

[21] S. Shandrick, Z. Ronai, A. Guttman, *Rapid microwell polymerase chain reaction with subsequent ultrathin-layer gel electrophoresis of DNA,* Electrophoresis, 2002, *23*, 591.

[22] C. G. Koh, W. Tan, M. Q. Zhao, A. J. Ricco, Z. H. Fan, *Integrating polymerase chain reaction, valving, and electrophoresis in a plastic device for bacterial detection,* Analytical Chemistry, 2003, *75*, 4591.

[23] J. H. Daniel, S. Iqbal, R. B. Millington, D. F. Moore, C. R. Lowe, D. L. Leslie, M. A. Lee, M. J. Pearce, *Silicon microchambers for DNA amplification,* Sensors and Actuators a-Physical, 1998, *71*, 81.

[24] P. Sethu, C. H. Mastrangelo, *Cast epoxy-based microfluidic systems and their application in biotechnology,* Sensors and Actuators B: Chemical, 2004, *98*, 337.

[25] E. T. Lagally, C. A. Emrich, R. A. Mathies, *Fully integrated PCR-capillary electrophoresis microsystem for DNA analysis,* Lab on a Chip, 2001, *1*, 102.

[26] J. Liu, C. Hansen, S. R. Quake, *Solving the "world-to-chip" interface problem with a microfluidic matrix,* Analytical Chemistry, 2003, *75*, 4718.

[27] J. Liu, M. Enzelberger, S. Quake, *A nanoliter rotary device for polymerase chain reaction,* Electrophoresis, 2002, *23*, 1531.

[28] P. Krulevitch, W. Bennett, J. Hamilton, M. Maghribi, K. Rose, *Polymer-based packaging platform for hybrid microfluidic systems,* Biomedical Microdevices, 2002, *4*, 301.

[29] A. Olsson, O. Larsson, J. Holm, L. Lundbladh, O. Ohman, G. Stemme, *Valve-less diffuser micropumps fabricated using thermoplastic replication,* Sensors and Actuators a-Physical, 1998, *64*, 63.

[30] J. C. Lotters, W. Olthuis, P. H. Veltink, P. Bergveld, *The mechanical properties of the rubber elastic polymer polydimethylsiloxane for sensor applications,* Journal of Micromechanics and Microengineering, 1997, *7*, 145.

[31] J. Kim, M. K. Chaudhury, M. J. Owen, *Hydrophobicity loss and recovery of silicone HV insulation,* IEEE Transactions on Dielectrics and Electrical Insulation, 1999, *6*, 695.

[32] D. V. Volgin, J. Swan, L. Kubin, *Single-cell RT-PCR gene expression profiling of acutely dissociated and immunocytochemically identified central neurons,* Journal of Neuroscience Methods, 2004, *136*, 229.

Chapter – 7

Polymerase Chain Reaction in PDMS biochips

PDMS microfluidic devices suffer from liquid/vapor loss due to the permeability properties of the PDMS. In the past, the vapour and liquid diffusion properties of the PDMS material have impaired the performance of microfluidic devices, especially the PCR. In this work, PDMS devices were fabricated with an enhanced soft-lithography technique in which a novel implant material in the PDMS prevented vapor diffusion from such devices. With this method, the overall fluid loss was almost eliminated and the reliability of the PCR (even with low copy number samples) was greatly increased. An experimental quantification and theoretical verification of the loss, and its impact on the PCR, are presented in this chapter. Experimental results of a demonstration of the PCR performed with DNA samples obtained from myloma and Waldenstrom's macroglobulinemia patients is also presented in this work. The contents of this chapter is based on a recently submitted manuscript[1].

7.1 Introduction

Biochip PCR gives low reagent consumption and faster processing while allowing the production of highly integrated devices for high-throughput multiplexed diagnostic applications[2]. Glass and Si have been extensively used in the microfabrication of these devices[2] and the PCR has been successfully demonstrated in these materials with nano[3] and even picoliter volumes[4]. But as discussed in Chapter 4, PDMS, an inexpensive elastomeric polymer (silicon rubber), has emerged as a promising material for bioMEMS applications[5]. Among the silicone rubber polymers, PDMS exhibits the highest flexibility[6] (Table 7-I) which is essentially a result of its low glass transition

temperature, high free volume and porosity[7, 8]. The high flexibility of PDMS is advantageous in that it facilitates easy replica molding of PDMS devices and enables simple PDMS based valving and pumping techniques [9-11] in microfluidics devices as described in Chapter 6. However, the property of PDMS that gives it the flexibility (e.g. high free volume and porosity) is also responsible for diffusion properties such as vapor permeation[12, 13], and liquid absorption[8, 14]. While these diffusion properties of PDMS have been advantageously used in membrane applications for the vapor separation of volatile gases[12], they are undesirable in many microfluidic devices as they can result in the rapid loss of reagents through vapor loss (especially loss during the thermal cycling used in the PCR process)[15]. The resulting vapor loss (sometimes to the extent of complete drying-out)[15] changes the concentrations of the PCR reagents and this is often the cause of an unsuccessful[15] genetic amplification.

Table 7-I. List of a few useful physical/chemical properties of PDMS[5-7, 14-17]

PDMS Property	Value
Chemical structure (repeating groups)	$O\text{-}Si(CH_3)_2$
Density	920 kg/m^3
Shear Modulus (high elasticity)	up to 3 Mpa
Optical UV detection (good visibility)	240 to 1100 nm
Surface tension of wetting	24 mN/m
Water contact angle (virgin – hydrophobic)	> 100 °
Glass transition temperature (low)	-125 °C
Thermal conductivity (low)	0.17 W/ m K
Permeability to water (high for polymers)	80.5 $x10^{-11}$ g · cm / cm^2 · sec · cmHg
Diffusion coefficient of water at 25 °C	~ 2 x 10^{-9} m^2/sec
Water uptake capacity (high for polymers)	0.38 % (w/w)
Activation energy for water diffusion	14 kJ/mol
Dielectric strength (high)	~14 V/μm
Electrical resistance	10^{13} Ωm

Unfortunately, the fluid loss problem in PDMS has been scarcely addressed in the literature[14] and there have been relatively few reports of PCR genetic amplification performed in PDMS devices[15, 18-21] and each of them have developed means of coping with the liquid loss, sometimes through the simple means of using very large sample volumes. The initial demonstration of the PCR in PDMS biochips by Fujii and

coworkers[18] used sample volumes as high as 30 µl to 50 µl. This was an important step in developing PDMS based on-chip PCR devices but such large volumes are comparable to those of conventional methods, thereby losing many of the advantages of miniaturization. Although Liu *et al.*[21] and Yu *et al.*[19] subsequently showed successful results with arrays of small-volume PCR wells, their success can be attributed to either the use of a fluid filled hydraulic (flow control) channels layered above the PCR chambers or the high density of wells within a particular chip geometry. However, such high-density chip designs are not readily compatible with bioassays (e.g incorporating CE).

More recently, Shin *et al.*[15] performed small volume PCR in PDMS devices and explicitly addressed the sample loss problem by surface coating the PDMS with a low permeability material called Parylene C. The irreversible bonding of PDMS layers (i.e. the layers are fused together and cannot be separated non-destructively) is often required in biochips for pumping[9] and valving[11], and is desirable for routine handling. Although cured PDMS is difficult to bond to, procedures have been developed to irreversibly bond PDMS to glass, silicon, silicon nitride, polystyrene, and PDMS[22]. It is unclear whether Shin *et al.*[15] were able to irreversibly bond their Parylene-coated PDMS chips. However, the Parylene coating may impede irreversible PDMS bonding as the replacement of the methyl group (Si-CH_3) with silanol group (Si-OH) in the PDMS, (which turns the surface hydrophilic and causes the irreversible bond [22]) may be hindered by the coating. To the best of the author's knowledge, there have been no reports of bonding Parylene in a MEMS device and in fact, Parylene is used as a 'release agent' in MEMS processing[23]. The Parylene surface coating demonstrated by Shin *et al.*[15] was applied by a chemical vapor deposition method that used a dedicated off-site deposition system in another facility. Such a method can significantly increase fabrication costs and hinders the use of PDMS as a rapid prototyping material.

The diffusion properties of PDMS have been a concern in other microfluidic applications as well. Chang *et al.* [8] recently reported on the fluid loss in PDMS-Si biochips due to the liquid absorption property of PDMS during bacterial culture (T < 50

°C). To retard this fluid loss, the PDMS was fabricated with increased ratio of curing agent to pre-polymer PDMS (up to 1 : 2.5), much higher than the manufacturer's recommended ratio of 1 : 10. However, increasing the proportion of the curing agent results in a more rigid PDMS structure[8]and is expected to greatly affect PDMS based pumping[9] and valving[11, 24] techniques. In fact for the PDMS based pumping[9] and valving[11, 24] methods, a mixing ratio of as high as 1:20 is recommended[11, 20, 21] but such high proportions of PDMS pre-polymer are expected to result in an increased water uptake by more than six times[8] – highly undesired in most microfluidic application, especially with the small volume PCR. As it will be discussed later, since this work has incorporated PDMS based pumping and valving techniques in the system, fabricating rigid PDMS structures by decreasing the proportion of the pre-polymer to impair the water uptake capability of the PDMS was not a viable option. Moreover, as it will be shown experimentally in this chapter, it was found that the vapor loss from the PCR chamber in the PDMS chip to the atmosphere was the largest contributor (~ 75%) to the fluid loss problem during the PCR thermal cycling. Therefore altering the flexibility of the PDMS to retard the water uptake does not fully resolve the fluid loss problem.

An easily implemented solution to the vapor diffusion problem was recently demonstrated[1] as a consequence of this work. This was accomplished by implanting a vapor/moisture barrier in the form of a polyethylene (PE) implant in the PDMS. It will be experimentally shown that the vapor loss can lead to the failure of the PCR and it was experimentally found that the vapor diffusion from PDMS microfluidic devices during thermal cycling can be reduced several-fold by implanting the vapor barrier in the PDMS. Furthermore, with this implanted vapor barrier technique, PCR compatibility[25] issues are not a concern, since the implant material does not make any contact with the PCR sample. The PE implantation was implemented by a first-of-a-kind enhanced soft-lithography fabrication technique and a protocol to obtain irreversible interfacial adhesion between the implant and PDMS was developed. The microfabrication processes involved in this implant technique was described earlier in Chapter 4.

Sylgard 184 PDMS (Dow Corning) has been demonstrated to be an effective material for fabricating microfluidic devices. However, no diffusion studies in this PDMS have been reported in the literature[8]. Here two diffusion-based mechanisms have been investigated for the loss of liquid from PDMS devices – vapor loss from an enclosed (PCR) chamber to the atmosphere and absorption of the liquid by the PDMS bulk. Experimental results indicate that the vapor loss is the dominant factor.

Next in this chapter the PCR genetic amplification is successfully demonstrated in the PDMS biochips with yeast and cDNA samples from Myeloma and Waldenstrom's macroglobulinemia patients (kindly provided by the Pilarski group, Cross Cancer Institute). Comparisons of conventional clinical processing to those on the biochips appear to be on-par with each other. Such demonstrations are hoped to revolutionize the future of clinical testing at the molecular level.

7.2 PDMS Experimentation and Discussion

7.2.1 Need for Minimizing Sample Loss During the PCR

Among the many Si polymers, PDMS exhibits the highest flexibility[6], very high gas/vapor permeability[12] (Table 7-IV [26]) and moderate liquid absorption properties (around 700 ppm by mass[14] or 0.38% (w/w)[16, 17]). The high permeability and porosity of the material has encouraged many research groups to use PDMS as a permeable membrane for vapor purification[12, 13], aeration membrane in gas sensors [27], and similar applications.

The PCR amplification of genetic material is a temperature cycling experiment in which vaporization of fluid occurs at the denaturation temperature (94 °C) and in a PDMS biochip without a vapor barrier this results in a very large loss of fluid sample[15]. This loss of sample often results in the unsuccessful amplification of DNA[15].

Empirically, it was found that samples that lost more than about 50% of their volume during the PCR stage were generally unsuccessfully amplified and this is attributed to some combination of temperature non-uniformity caused by the partially

filled well (partially filled chambers are known to cause a temperature drop of up to 5°C at the denaturation temperature[28]) and the change in the reagent concentrations. In this context, based on the quantification of fluid loss experimentation (as described later) it is believed that the PCR may only be successful if the PCR is started with a sufficiently large number of sample DNA (template) molecules (i.e. a high 'copy number') so as to obtain a detectable PCR product after about 20 cycles. This was corroborated by (1) performing on-chip PCR successfully with a high copy number sample (e.g. yeast genome) that in conventional processing gave a strong signal within 20 cycles[29] and (2) by unsuccessfully amplifying a low copy number sample (e.g. human DNA samples)[30] that in conventional processing required at least 35 cycles to obtain a detectable signal[31] (data not shown).

In a PDMS chip without a vapor barrier, the typical retrievals after 35 thermal cycles were well under 1 μl (i.e. > 50% loss). Such high loss may not present itself as a useful method for performing small volume PCR especially with low copy number samples. Investigations in this regard involved performing a series of PCR experiments in an unimplanted PDMS chip with both high and low copy number samples. While the success rates with high copy number samples (i.e. with yeast genome 4730 DNA samples. PCR procedure can be found in prior work[29, 32]) in a PDMS chip without a vapor barrier were about 60%, the success rate with low copy number samples (i.e. cDNA samples with PCR primers specific to the HAS gene was nil (0%) (Table 7-II). These PCR procedures can be found in Adamia *et al.* [30, 33]). Although the success rate with high copy number samples is typically over 90% in conventional testing in our lab, the 60% success rate is considered acceptable at this stage of prototyping.

Table 7-II. A summary of PCR success rates with high and low copy number samples in PDMS chips WITHOUT a vapor barrier

PCR Sample	No. of experiments	Date of experiment	No. of successful PCR	Success rate
Yeast DNA (4730)	7	Nov 18th – 25th 03	4	~ 60%
Patient DNA (HAS primers)	8	Aug –Nov 03	0	0%

The failure of a PCR experiment is attributed to either due to the sample loss (as addressed below) or due to surface adsorption effects (as discussed in section 7.5.1), both of which are discussed in this chapter.

It was apparent that to perform reliable small volume PCR with low copy number samples in PDMS devices a means of minimizing the loss was required. In the following section it will be shown that the novel microfabrication technique of implanting a PE vapor barrier in the PDMS rendered itself as a useful method of preventing large sample loss during the PCR thermal cycling and hence enabled performing successful PCR even with low copy number samples.

7.2.2 PDMS Diffusion Experimentation and Discussion

To quantify the sample loss resulting from the diffusion properties of the PDMS during the PCR thermal cycling, experiments were performed in which PDMS chips were loaded with double distilled water (DDW) sample and subjected to thermal cycling (94 °C, 60 °C and 72°C for 30 sec each). After a predefined number of thermal cycles, the sample from the chip was unloaded and quantified in a micropipette (Pipetman, Gilson, WI, USA). (**Note:** Quantification of such small quantities of fluid can be an error prone process as a result of handling and evaporation losses. Hence a technique was adopted in which the quantification was performed within a micropipette.) The micropipette quantification was done by first setting the micropipette to 2.25 µl (25% above maximum) and then with the micropipette depressed (expulsion mode), the micropipette tip was immersed into the liquid. This was followed by collecting the liquid into the micropipette tip (suction mode) and since the micropipette was set to a quantity slightly more than was initially loaded, the liquid was completely collected and was followed by about 0.5 µl of air. By adjusting the setting on the micropipette until the air is again expelled, the amount of remaining liquid can be determined. This method avoids some handling and evaporation losses since the quantification is done in a single step within the micropipette tip itself and the uncertainties in this process was found to be about ±5%.

Measurements were made after 0, 5, 10, 20, and 35 cycles. The graphical representation of this fluid quantification is termed as a *'Diffusion curve'*. Four such diffusion curves were obtained from separate experiments. The first diffusion curve experiment was performed in a PDMS chip without a vapor barrier implant. The second was performed in a PDMS chip with a smooth, flat glass piece (or capping, 3 mm (*l*) x 3 mm (*w*) x 1 mm (*t*)) pressed against the PCR chamber. The glass capping was held firmly against the PDMS surface by rod 2 of our pumping system (as described in Chapter 6) and was seen to make intimate contact (i.e. no air gap) with the flat top surface of the PDMS. The third and the fourth diffusion curve experiments were performed in PDMS chips that were fabricated with a PE vapor barrier implant using each of the implantation methods described earlier (i.e. chemical and physical implant). In all the experiments the sample volume loaded in the PCR chamber was about 1.75 μl.

Figure 7-1 shows four 'diffusion curves' obtained from the four separate diffusion loss experiments. Figure 7-1.a is a diffusion curve from a PDMS chip without an implant and shows a fluid sample loss of nearly 1.25 μl after 35 thermal cycles (about a 75% loss of sample). Figure 7-1.b is a diffusion curve from a PDMS chip without an implant but with the glass capping; this shows a fluid loss of about 0.4 μl, i.e. only a 23% fluid loss. Figures 7-1.c and 7-1.d are diffusion curves from PDMS chips that were fabricated with a PE vapor barrier implanted in the PDMS using the chemical and physical implant methods respectively. These show a loss of about 0.4 μl, again corresponding to a 23% sample loss.

It was apparent that this loss of liquid from PDMS impairs reliable operation with microlitre volumes and it was also clear that there was a need for a method to minimize this loss lest it preclude operation with smaller volumes. While a glass capping above the PCR chamber in an unimplanted biochip was a potential solution to prevent the vapor loss, it presents an additional thermal mass on the chip that could cause temperature gradients in the chamber. The rigidity of the glass also hinders the automated operation of the pumping and valving processes (as described in Chapter 6). But clearly, the novel PE implant technique rendered itself as an efficient approach in minimizing the loss.

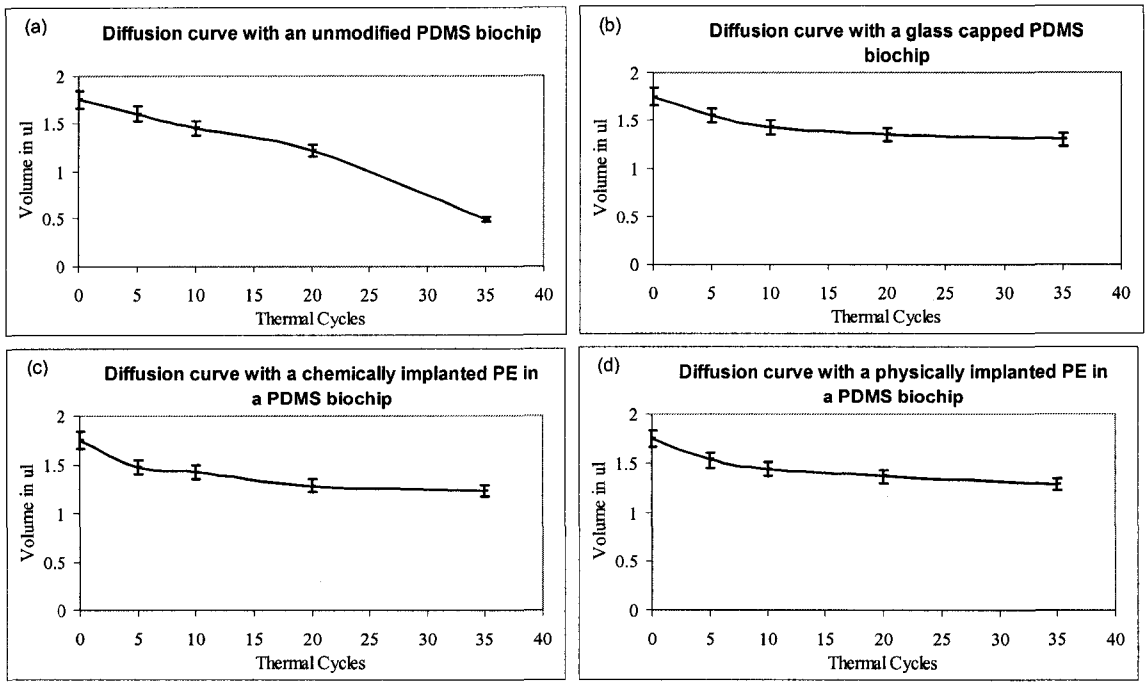

Figure 7-1. Quantifying fluid sample loss resulting from PCR thermal cycling. (a) PDMS biochip without a vapor barrier (b) PDMS biochip with external glass capping (c) PDMS biochip with a physically implanted vapor barrier (d) PDMS biochip with a chemically implanted vapor barrier

7.2.3 Implant in the Context of the PDMS Biochip

Implantation in this context refers to embedding a material in the PDMS. To the best of the author's knowledge, there has been no report of an implanting method in PDMS based MEMS processing.

To choose an implant material there were a few requirements and/or desirable properties from the PCR application point of view, which are briefly outlined below and are listed in order of their priority.

1. Unlike PDMS the implant material should have very low water/vapor permeability
2. The implant material should have elasticity that is comparable with PDMS as this is critical in the compatibility of the diaphragm pumping and pinch-off valving technique. One of the sole reasons for using PDMS in this work is due to its

elastic property (i.e. high flexibility)[6] that enabled the incorporation of the microfluidics pumping and valving techniques[9, 11].

3. The implanted material should adhere (or bond) to the PDMS to function reliably as a vapor barrier.
4. The implant material should not exhibit performance degradation as a function of temperature since the PCR involves high temperature operating (i.e. > 90 °C)
5. And if possible, it should have good optical clarity comparable with that of PDMS, although this was not a critical requirement since the lower substrate of the chip was (clear) glass and optical inspection of the channels and wells in the chip can always be done from the lower surface.

Polyethylene (PE) has very low permeation to water, water vapor (Table 7-IV, approximately 100 less than that of PDMS)[26] and gases, hence exhibits a very good barrier to vapor diffusion. Due to its excellent water/vapor barrier property, PE is commonly used in the food industry as a wrapping material for moisture preservation[34-36]. PE also has a high melting point (137 °C), which is well above the denaturation temperature (94 °C) in a PCR thermal cycling experiment. PE also has high elasticity (G ~ 18 MPa, elongation of 900% at break[35]) and was not expected to hinder the microfluidic plumbing process. With such favorable properties, PE was an obvious choice as an implant material.

Achieving a good adhesion between the implant and the PDMS was critical. If not the effect of the implant will be lost (described in section 7.4). In order to obtain an implantation protocol that results in a good adhesion of the implanted material to the PDMS, a basic understanding of the possible bonding/adhering mechanism is required. Below the three most prevalent adhesion mechanisms are described.

Mechanical interlocking bonds surfaces together by allowing the adhesive or sealant to take advantage of the microscopic roughness of the substrates to lock them together as shown in the figure below (Figure 7-2). The mechanical interlock bonding mechanism in polymers is similar to the interpenetrating polymer network (IPN)[37] mechanism.

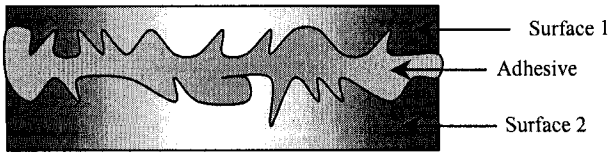

Figure 7-2. Mechanical Interlock bonding between two surfaces using an adhesive

Electrostatic attraction uses the ability of polar groups in the adhesive to be attracted to those in the substrate (Figure 7-3 below). Substrates such as PDMS and PE do not have polar groups, so usually no molecular attraction occurs; hence could result in a poor adhesion.

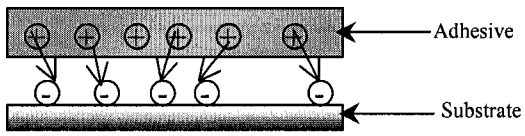

Figure 7-3. Electrostatic attraction bonding mechanism

Covalent chemical bonding uses mutually reactive chemical groups on the substrate and adhesive to form the strongest, most durable bond. This is among the most reliable method used to bond most materials.

Since PDMS is a non-polar chemical compound[38] and a non-adhering material[7], either electrostatic or mechanical interlock adhesion mechanisms alone is expected to result in a poor adhesion. The PDMS polymer matrix is loosely packed and has high free volume (in other words - porous)[7, 8]. A combination of the mechanical interlock adhesion in the porous PDMS combined with covalent chemical adhesion is expected to result in an enhanced adhesion of the bonded materials.

Two implantation fabrication protocols were developed (as described earlier in Chapter 4) to implant the PE in the PDMS – i.e. the chemical and physical implant methods. The adhesion mechanism in the chemical implant method is based on the mechanical interlock adhesion initiated by a chemical absorption of the dissolved PE. As described in the protocol (Chapter 4, section 4.3.2), toluene was chosen as the solvent to dissolve PE because of its moderate interaction and absorption by the PDMS[38] and this is expected to cause a partial inter-diffusion of the PE into the PDMS thus causing an

(mechanical interlock) entanglement of PE in the PDMS polymer matrix. In the case of the physical implant method where a pre-cast PE films was implanted in the PDMS, the curing of the PDMS was a critical step in achieving a good adhesion. In the curing protocol, after the PDMS was cured at 90 °C for 1.5 hours, the temperature in the oven was ramped to 135 °C to cause the PE to partially melt and mould to the PDMS – again a mechanism similar to the mechanical interlock adhesion. Both these implant methods gave a very reliable adhesion between the PDMS and the PE and this is discussed in section 7.4.

Diffusion curves obtained from PDMS chips with an implanted PE vapor barrier (Figure 7-1.c and 7-1.d) show much reduced fluid loss (by about a factor of 3) as compared to a PDMS chip without a vapor barrier (Figure 7-1.a). After 35 thermal cycles the fluid loss in an unimplanted PDMS chip was about 1.25 μl whereas that in a PDMS chip with a PE implant it was only 0.4 μl.

7.2.4 Impact of a Modified Chip on the PCR

The earlier PCR experiments in an unmodified chip (i.e. no capping or implanted layer) suggested that the PDMS chip was incapable of successfully amplifying samples having a small number of template molecules (i.e. low copy number samples)[30]. However, experimentation with a modified chip showed promising results, in that it was now able to successfully amplify similar low copy number PCR samples with much improved success rates – typically about 50%(from the earlier 0%). Three sets of experiments were performed with low copy number[33] samples (i.e. cDNA samples with PCR primer specific to the HAS gene (section 7.5.2.2) – prepared by S. Adamia, Pilarski group, Cross Cancer Institute) and each set yielded successful PCR amplification.

Table 7-III. A summary of PCR success rates with high and low copy number samples in modified PDMS chips (i.e. with a vapor barrier)

PCR Sample	No. of PCR experiments	Date of experiment	No. of successful PCR experiments	Success rate
Patient DNA (HAS primers)	10-12 (3 sets)	Jan –Mar 04	5	~50%

Evidently, a good improvement in the success of the PCR for the targeted application (i.e. analysis of cancer patient samples) was seen upon preventing large sample loss in PDMS chips resulting from thermal cycling. Further improvement is possible in the form of preventing the loss completely or by investigating other issues such as surface adsorption (as discussed in section 7.5.1) but it is believed that this particular PCR experiment (which seeks to amplify a portion of the HAS gene) is challenging even with conventional clinical laboratory processing. Hence the obtained success rate with the on-chip approach for this gene is deemed satisfactory at this stage of development.

The following section presents a theoretical analysis of the PMDS diffusion loss and it is hoped to provide a fundamental understanding of the water/vapor diffusion properties of the PDMS material and the influence of an implant.

7.3 Estimation of Fluid Loss in PDMS

Although many groups have experimented and estimated the diffusion parameters of the PDMS for volatile gases[12, 13, 39, 40], large discrepancies are apparent in the reported data. It has been suggested that the differences in the literature data is due to the uncharacterized behavior of the PDMS polymer[8]. However, recently Yoem *et al.*[13] and Watson *et al.*[14] developed more accurate industrial instruments to characterize PDMS. Typically, these diffusion studies are performed in a large industrial setting[12, 13, 41] with a complex instrumentation setup to accurately monitoring various parameters (e.g. pressure, rate of gas / vapor flow, vapor measurement within the absorbing medium, temperature, etc.) during the experiment. But even such exhaustive instrumentation sometimes fail to explain the unpredictable behavior of the PDMS polymer [14].

Experimental studies on the transport of water molecules in a few brands of PDMS (e.g. RTV 615 and PS 342.5) have been reported in the literature but again large variations are apparent among these as well, clearly suggesting the unknown characteristics of the material[14, 42]. There have also been controversies over the

mechanisms of water movement in the PDMS, but more recent measurements suggest that the diffusion coefficient of liquids and vapors are a constant[14, 42].

Watson *et al.*[14] have experimentally determined the value of the constant diffusion coefficient of water to be approximately 2 x 10^{-9} m^2/sec and found reasonably good agreement with theory - this value has been widely used in literature and was verified (with a small % error) in a later independent study[42]. But unfortunately even these studies have not taken into account the influence of elevated temperature and pressure[8]. PDMS microfludic devices used in genetic testing applications (e.g. the PCR or cell culturing[8, 27]) are subjected to high temperature and pressure influences. Furthermore, diffusion parameters are known to significantly vary with different sources of PDMS[8] and hence it would be important to conduct such studies in the commonly used brands of PMDS, such as Sylgard 184. However, no diffusion data are available[8] for Sylgard 184. In the following, theoretical models of the diffusion-based losses are applied and it is found that these are consistent with the experimental data (i.e. the diffusion curve data) obtained earlier.

In a diffusion process, the diffusion length d (m) is the distance a diffusing molecule can travel in a given time as given by an expression (from Einstein's law of diffusion) based on diffusion in an isotropic three dimensional geometry[43],

$$d = \sqrt{2Dt} \qquad \text{- (7.1)}$$

(d will be $\sqrt{2}$ larger for two dimensional diffusion[44]), where D is the diffusion coefficient of water in PDMS (m^2/sec) and t is the time duration (sec) over which the diffusion occurs. If the diffusion length and chamber size are small relative to the PDMS thickness then the diffusion process is best described by the isotropic three-dimensional case (Eq. 7.1). On the other hand, in the limit of a diffusion length much larger than the PDMS thickness and chamber size, the diffusion process is best described by the two dimensional case. Since these two cases differ by only about 40%, Eq. 7.1 is used for the estimates. The diffusion coefficient is expected to exponentially vary with temperature and is described by the following Arrhenius relationship[45]

$$D = D_0\left(e^{-\left(\frac{E_D}{RT}\right)}\right) \quad \text{- (7.2)}$$

where D_0 is the pre-exponential factor of diffusion coefficient, E_D is the activation energy (found to be 14 kJ/mol)[14], R is the gas constant (8.3 J/mol· K)[46] and T is the temperature in Kelvin. Within the PCR thermal cycling temperature range, the ratio of D at the maximum (94 °C) and minimum (60 °C) PCR temperatures differ by less than a factor of 2, as shown below.

Given the large variation (by orders of magnitude[8, 14, 42]) in the literature of estimates of the diffusion coefficient of water in PDMS , the estimated factor of 1.75 variation within the PCR temperature range is negligible. Hence in the calculations the value of D for water (i.e. 2 x 10^{-9} m^2/sec) is taken to be a constant throughout the PCR temperature range and the total time of the experiment as being the time for which the diffusion process occurs. Therefore from Eq. 7.1, the diffusion length *d* for a 35 cycle PCR experiment lasting ~7000 sec is estimated to be 5.5 mm.

In a simplified model of the chip without an implant, the loss mechanisms is considered to be a combination of 'vapor loss to the atmosphere' and 'volumetric loss' (i.e. absorption) by the PDMS bulk, as depicted in Figure 7-4. The shortest distance the water molecules have to travel before vapor loss to the atmosphere occurs is across the 1 mm thick PDMS chamber roof. Since this distance is much less that any other distance, the 'vertical' loss is expected to be dominant in the unmodified chip. By implanting a low permeability PE layer, the overall sample loss was reduced by a factor of 3 (Figure 7-1.a and 7-1.c) and this is attributed to a reduction in the vertical vapor loss. The loss still observed in the implanted chip may be due to volumetric loss as analyzed below.

7.3.1 Volumetric Loss

The dimensions of the bulk PDMS below the implant are 19 mm (length) x 8 mm (width) x ~1 mm (thickness). The scale of the diffusion length *d* (5.5 mm as calculated above) is comparable to that of the chip and the water molecules are expected to diffuse throughout a volume of approximately $\pi R^2 H$ from the PCR chamber i.e. ~ 96 mm^3 where

R is 5.5 mm and H is 1 mm. If it is assumed that Sylgard 184 will absorb the same quantity of water as RTV615 PDMS (given as 0.38% (w/w) by Blume *et al.* [16, 17]), the volumetric loss by the bulk PDMS below the implant for the above estimated diffusion length would be ~0.37 µl. In the experiment in a chip with a PE vapor barrier implant, the water loss was about 0.4 µl, which is consistent with the theoretical estimation of the volumetric loss. Also, the equal losses from the implanted and glass capped chips suggests that the vertical vapor loss has been eliminated and the agreement between the theoretical and experimental data suggest that the loss in unmodified PDMS chips was predominantly volumetric loss.

7.3.2 Vertical Vapor Loss

Flux is defined as the rate at which a gas or a fluid flows across the polymer (usually expressed as flow per unit area per unit time having the units of L/sec· m^2, g/ sec· m^2, or mol/ sec· m^2). The relationship between the flux F and the diffusion coefficient D is given by

$$F = D\left(\frac{C}{d}\right) \qquad \text{- (7.3)}$$

where C is the concentration of water in the PDMS (L/m^3) and *d* is the membrane thickness across which the diffusion occurs (m). The PCR well is approximated to be consisting of a 1mm membrane with a surface area of 3.14 mm^2 (i.e. the PCR chamber roof). Assuming a 0.38% (w/w) sorption value for water in Sylgard 184, C would be 3.8 lit/ m^3. Thus, with the reported diffusion coefficient value (Table 7-I), the flux from Eq. 7.3 would be 8.36 µl/sec· m^2. This implies that over a thermal cycling time of 7000 sec, the vapor loss would be 0.18 µl. Although this value is about 4 times less than the experimentally observed vapor loss of ~ 0.85 µl, (i.e. difference in loss between a chip with and without implant), this constitutes a good agreement given the uncertainty of the diffusion constant as reported in the literature and the fact that the diffusion from the sidewalls of the PCR chamber were neglected. It is estimated that the effect of the sidewalls would double the effective area of the membrane. Using Eq. 7.2 to estimate the value of D at 77 °C (the middle of the PCR temperature range), one would obtain a value

2.3 times larger than the value at 25 °C (4.6 x 10^{-9} m^2/sec). Together these could explain the factor of 4, however, all of these parameters have high uncertainties.

7.3.3 Effect of an Implant on the Permeability

Permeability is defined as the ability of a polymer to transmit gas and/or fluid through its pores. As calculated below, an alteration in the permeability of the structure is expected by implanting a PE vapor barrier in the PDMS. The relationship between flux and permeability in a polymer membrane is defined by [26]

$$\frac{P}{d} = \frac{F}{A \cdot \Delta p} \qquad \text{- (7.4)}$$

where P is the permeability coefficient (g · cm / cm^2 · sec · cm Hg), d is the thickness of the membrane (cm), F is the vapor flux (g / cm^2 · sec), A is the membrane surface area (cm^2), and Δp is the pressure difference across the membrane(cm Hg).

The resistance of a material to the permeation of a vapor or liquid is defined as the 'permeance resistance' (R_p)[47, 48] where higher permeance resistance indicates lower diffusion loss. The permeance of a material (P/*d*) is inversely proportional to the permeance resistance, R_p [47], and from Eq. 4 it is defined as,

$$R_p = \frac{A \cdot \Delta p}{F} = \frac{d}{P} \qquad (2.5)$$

As Figure 7-4 depicts, the effective permeance resistance of a set of layers of material is the sum of their individual permeance resistances[47] (analogous to adding electrical resistances that are in series) with the high permeance resistance of the thin PE layer added to the permeance resistance of the thicker PDMS (– the permeability values are summarized in Table 7-IV). For simplicity the permeance resistance of the two PDMS layers (above and below the implant in the roof of the chip) have been combined to one thicker layer.

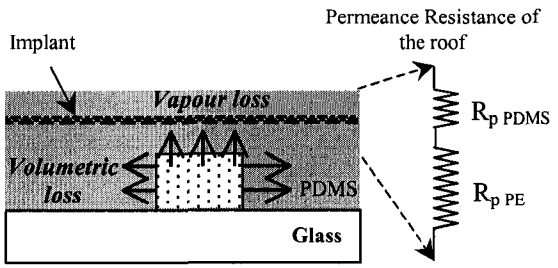

Figure 7-4. *Left:* A cross-section depiction of the PDMS-glass chip with a PE implant. *Right:* Permeance resistance modeling of the 1 mm roof of the PDMS chip with a PE implant.

Thus the permeance resistance of the PDMS roof structure with an implant, $R_{p\ implant+\ PDMS}$ can be expressed as[47]

$$R_{p\ implant\ +\ PDMS} = \frac{d_1}{P_{\ PDMS}} + \frac{d_2}{P_{\ PE}} \qquad \text{- (7.6)}$$

where d_1 is the total thickness of the membrane PDMS material above the chamber (965 μm), P_{PDMS} is the permeability of the PDMS (80.5 x 10^{-11} g · cm / cm^2 · sec · cm Hg), d_2 is the thickness of the PE implant (35 μm), and P_{PE} is the permeability of the PE(0.83 x 10^{-11} g · cm / cm^2 · sec · cm Hg). The permeance resistance $R_{p\ implant\ +\ PDMS}$ from the above equation is calculated to be 5.3 x 10^8 cm^2· sec· cm Hg /g.

Similarly the permeance resistance of the PDMS material without an implant, $R_{p\ PDMS}$, is expressed as[47]

$$R_{p\ PDMS} = \frac{d}{P_{\ PDMS}} \qquad (2.7)$$

where d is the thickness of the PDMS (1000 μm) and P_{PDMS} is the permeability of the PDMS. From Eq. 2.7 the permeance resistance $R_{p\ PDMS}$ is calculated to be 1.2 x 10^8 cm^2· sec· cm Hg /g; which is about 4 times less than the permeance resistance of a PDMS structure with a thin layer of PE implant. Hence in an implanted chip, the vapor loss is expected to be reduced by a factor of 4. The fact that the implanted chips gave similar results to that of the glass-capped chip suggests that the vapor loss was in fact reduced to a negligible level, i.e. the remaining loss is primarily volumetric and vapor loss from the roof of the chamber has been eliminated. This suggests that the vapor barrier has been even more effective that calculated. This might be explained by the formation of a PDMS

IPN[37] wherein the intermixing of polymers effectively results in a pore filling effect and a further reduction in the vapor loss.

7.3.4 Reducing Volumetric Loss

In the future, apart from preventing the vapor loss from the PDMS chip with the novel implant method, a reduction in the volumetric loss needs to be sought. Increasing the proportion of the curing agent to the pre-polymer PDMS, has been shown to drastically reduce such volumetric loss[8]. However, this method results in a trade-off between volumetric loss and flexibility of the PDMS. Although many fabrication methods were tried (as part of this work) in regards to fabricating the PDMS in multi-layers (with each layer made of varying hardness) to try and retard the volumetric loss, it invariably made the chip incompatible with the valving and pumping system. Two other potential solutions are provided below and should be considered in future prototypes of similar PDMS devices.

Quake and coworkers[21] fabricated PDMS chips containing an array of PCR chambers with many fluid-filled hydraulic channels layered above them, but sample loss from the PCR chamber was not reported (or measured). This could be attributed to the fluid within the hydraulic channels saturating the pores in the PDMS so that no loss occurred from the underlying PCR chambers. Even for the relatively low temperatures ($T < 37\ ^{\circ}C$) of a bacterial culture application, a similar humidified environment was deemed necessary to show successful biological experimentation in PDMS microfluidic chips as fluid loss occurred even at such low temperatures[27].

It is suggested that in PDMS microfluidic devices used in experiments at elevated temperatures (apart from preventing the vapor loss by the techniques demonstrated here) saturation be considered as an additional means of greatly minimizing fluid sample loss. For example, assuming that the vertical vapor loss has been suppressed with an implant, this saturation mechanism could be implemented by a 'guard channel' (analogous to a guard line in electronics) that saturates the PDMS with water along the perimeter of the chip to prevent losses.

In another approach, fabricating the biochips with the PCR chamber in the lower glass substrate by etching techniques[25] will minimize the contact area of the water with the PDMS (i.e. along the side walls of the PCR chamber) and consequently volumetric loss. However, this might hinder the rapid prototyping advantage of fabricating PDMS devices as the glass etching process is usually far more time consuming than the PDMS replica molding process.

7.3.5 Discussion on this Diffusion Study

Although this work had presented a substantial study on the PDMS diffusion properties, it will be critical to undertake a more in-depth study on the PDMS properties that are associated with many microfluidic applications (e.g. high vapor pressure, elevated temperature, protein/ enzyme affinity, etc.) and factors that are known to affect the PDMS vapor/liquid diffusion phenomena. These factors include, polymer fillers[14], degree of cross-linking[13, 45], plasticization[12], degree of pore saturation[8, 14], and the influence of high/fluctuating temperature and pressure[8, 13, 14, 41, 45]. Further, even among the different commercially available brands of PDMS, some are composed of additional 'polymer fillers'[14] that are known to significantly affect the PDMS properties[14] (e.g. elasticity, vapor/liquid diffusion). But unfortunately no concrete studies have been undertaken in this regard, although it is believed[8] that such studies will be crucial to the universal acceptance of PDMS in microfluidic applications.

7.4 Implant Merits

PDMS biochips with the implanted PE are handled no differently from non-implanted biochips. Special consideration was not required for the PCR. No signs of separation of the fully processed PDMS devices were found after Scotch-tape tests (- a method in which a Scotch tape is pasted to the PDMS and peeled off). However the physically implanted chips without the high temperature curing step (as discussed earlier) failed these tests and this delamination of the PE was also experimentally observed during a thermal cycling experiment as discussed below.

Figure 7-5 shows a microscope picture of a PDMS biochip with a physically implanted vapor barrier fabricated prior to optimizing the final high temperature curing during chip fabrication (i.e. ramping the final curing temperature to 135 °C, slightly below the PE melting point of 137 °C). When such a chip was subjected to a thermal cycling experiment, it was noted that the water vapor from the PCR chamber permeated through the PDMS and condensed on the lower surface of the PE film. But such a loss or delamination was not observed after the bonding of the physical implant was made irreversible by optimizing the curing procedure as described in the fabrication protocol (Chapter 4). On the other hand, increasing this final ramping temperature very high (> 175 °C) caused the PE film to shrink (dark lines in the photograph) as shown in Figure 7-5(ii).

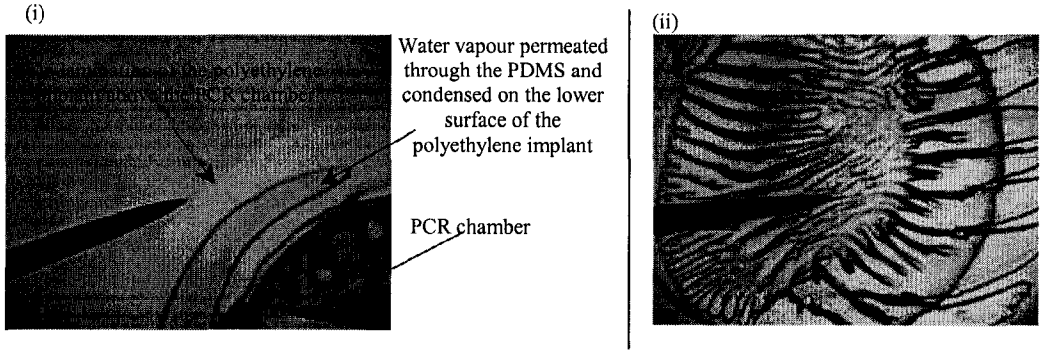

Figure 7-5. (i) De-lamination and condensation of the water vapor below an improperly bonded PE implant (ii) Shrinking (dark lines) of the PE implant due to high temperature treatment (> 175 °C)

These PE implantation methods offer numerous advantages - first, surface-coating methods with sealants, paints or epoxies are difficult to apply. Experiments with EpoTek301-2FL (Epoxy Tech., MA, USA), NOA60 (Norland, NJ, USA), acrylics dissolved in acetone (Anachemia Science, Edmonton, Canada), paints, were found to be futile as these materials were either non-adherent to the PDMS or created a rigid surface on the PDMS that cracked rather than flexed when used with the pumping and valving system. With the present implant method the flexibility of the PDMS was unchanged and hence the pumping and valving remained unaffected.

Second, the irreversible bonding of the PDMS to a glass substrate using the O_2 plasma technique in which the methyl group (Si-CH_3) is replaced with silanol group (Si-OH) [22, 38] in the PDMS, was not affected because the exterior surface chemistry of the PDMS remained unchanged with this layered implantation fabrication technique. Unlike surface coating methods (e.g. Parylene coating)[15] that might impede the chemical activity on the surface of the PDMS during the bonding process, either of the lateral PDMS surfaces can be irreversibly bonded to a variety of other surfaces[22].

Third, since the implanted layer is not in direct contact with the PCR sample, inhibition of the PCR genetic amplification by the implant material was not a concern. Thus, this novel implant method provides a simple, inexpensive and straightforward method that was readily adopted within the soft-lithography process without the requirement of special equipments. The cost of a 100 meters PE film was under $5 and the cost of a liter of toluene was less than $20. Typically, many hundreds of implants on PDMS chips can be performed with such low cost materials. Further, this method also lends itself to multi-layer implantations.

7.4.1 Examining the PDMS Porosity

Among the first of the experimentations to find a solution to the sample loss problem, experiments with food-coloring (dye) fluid samples were performed. A PDMS chip without a vapor barrier was loaded with a green food-coloring sample that had very high density of dye molecules. The chip was thermally cycled for 35 cycles and the final volumes retrieved were comparable with those performed with de-ionized water in glass capped or implanted PDMS chips. This is believed to be because of the clogging of the pores in the PDMS by the dye molecules which effectively prevented water / water vapor diffusion.

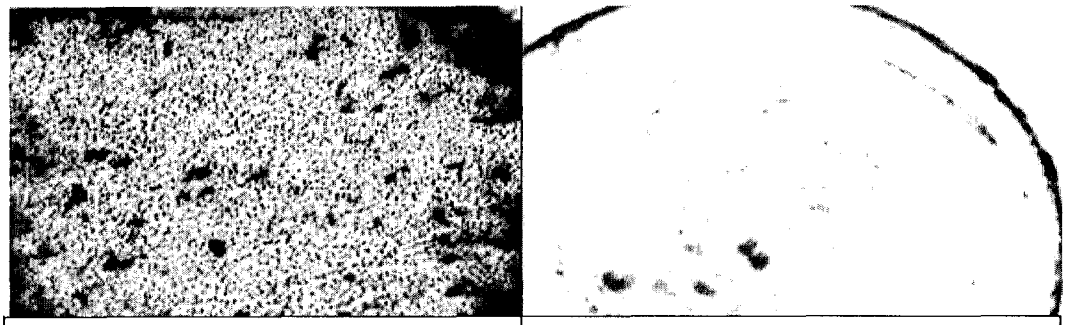

The pores in the PDMS have been clogged (dark green grains in the picture) by the dye in the food coloring. Picture was taken within 15 min of sample retrieval.	The pores in the PDMS seem clean after thermal cycling a water sample.
Note: the larger dark dots and lines in the pictures are due to the refraction of light under the microscope. These (black) refraction marks can be easily differentiated from the tiny (green) food coloring molecules in a color picture.	

Figure 7-6. (Left) Microscope picture of the PDMS PCR chamber after a thermal run with food coloring. (Right) similar picture in a separate chip with de-ionized water sample.

The microscope pictures in Figure 7-6 are those of a PDMS PCR chamber from two separate chips – one that was thermally cycled with food coloring and the other with de-ionized water. The picture on the left shows the dense (dark green) dye molecules clogging the pores in the PDMS when the food coloring sample was used while the picture on the right does not indicate any such clogging evidence since the de-ionized water sample did not have large suspended particles like the dye molecules in the food coloring. As stated earlier, the relative volumes were comparable with an implanted chip and an unimplanted chip, respectively.

By visual inspection it was apparent that the pores in the PDMS[15] were clogged by green dye molecules. The clogging of the PDMS pores seemed to have taken place well inside the PDMS structure and not just on the surface and this is justified by the fact the dye molecules did not wash-away along with the residual retrieved sample after the thermal cycling nor by a simple single flushing of the chamber with de-ionized water. The penetration of the dye molecules could possibly be due to the high vapor pressure (> 12 PSI at the denaturation temperature[49]) inside the chamber that might have driven the dye molecules into the pores in the near surface of the PDMS.

The microscope picture above is a clear evidence of the highly porous nature of the PDMS which may not be ideally suited for applications such as PCR, especially with

low copy number samples as this may result in the DNA molecules easily adhering to the PDMS walls. Such a phenomena could result in the DNA not participating in the enzymatic reaction and consequently greatly affecting the yield of the end product (i.e. amplified genes).

7.4.2 Alternative Materials for Implant

In this work diffusion data from PE implanted PDMS biochips were presented, although fluoropolymer (Dyneon THV220, kindly provided by 3M Inc., ON, Canada) and poly(vinylidene chloride) (Saran®) implants also showed good vapor diffusion barrier properties and the final fluid volumes retrieved were similar to those with PE (data not shown). However, the high rigidity of the fluoropolymer (flexural modulus = 80 MPa) made the biochip incompatible with the pumping and valving system. Table 7-IV lists polymers with low water vapor permeability that could be used as implants or copolymer fillers in the PDMS to counteract the water/vapor diffusion. Suggested solvents for the polymers[38] with their experimental swelling ratios (defined as the ratio of the length of the PDMS polymer in the solvent to the length of the dry PDMS polymer) are also summarized in the table.

Table 7-IV. A list of low water permeability polymers as potential implant materials in PDMS to prevent vapor diffusion

Material	Water / water vapor Permeability[26] x 10^{-11} g · cm / cm^2 · sec · cmHg	Suggested solvent# [50]	Swelling ratio (S) of solvent in PDMS*[38]
PDMS	80.5	-	-
Poly(vinylidene chloride)	~0.052	Cyclohexane	1.33
Polypropylene	0.42	Trichloroethylene	1.34
Polyethylene (LDPE)	0.83	Toluene	1.31
Polyacrylonitrile	2.45	Dimethylformamide	1.02
Poly(vinyl chloride)	2.5	Xylene	1.41
Fluoropolymers (3M, Canada)	N/A	Acetone	1.06

Heat may be required for dissolution.
* S = D / Do, where D is the length of the PDMS in the solvent and Do is the length of the dry PDMS. S values are based on the experimental data on a cured PDMS sample (Lee *et al.*[38])

In the chemical implant fabrication protocol, it was observed that the PE turned 'hazy' when dissolved in toluene; to avoid this, an alternative solvent can be explored. Choosing a solvent that is only partially absorbed by the PDMS is also critical in successfully performing this implantation protocol in a controlled manner as highly absorbing solvents may cause extensive swelling and deformation of the chip features in the PDMS[38]. It is further suggested that for a better control of the inter-diffusion of the implant material, partial curing of each layer (PDMS-implant-PDMS) be done before one layer is introduced on top of the other. This implantation method also renders itself to multiplayer polymer fabrication.

7.5 DNA PCR Demonstration

This section first discusses the adsorption effect of DNA and enzymes that are known to occur in biochips PCR. Adsorption effects are critical issues that need to be addressed as they can result in an unsuccessful PCR[2]. This discussion is followed by a presentation of the PCR experimental data.

7.5.1 Biochip Conditioning

PCR performed in biochips is prone to protein/enzyme adsorption at chip walls due to an increased surface–to-volume ratio and this has been repeatedly mentioned in the literature[2]. Typically, the surface-to-volume ratio for PCR performed in tubes to that in chips increases by about a factor of over 10[51-53] (in this case for about a 12 μl chamber volume in a chip). This manifold increase in the surface-to-volume ratio is cited as one of the primary reason for unsuccessful PCR when performed in chips as it causes adsorption of *Taq* polymerase, DNA, and primers[28] at the walls. If all the DNA and/or primers are not adsorbed at the chamber walls, then a genetic amplification might occur but with greatly reduced efficiency with the end quantity of DNA product too low in concentration for detection[28].

There have been a number of theories suggesting the mechanism for the DNA and the *Taq* adsorption that result in either unsuccessful or low PCR efficiency[52, 53]. One

theory suggests that, although clean materials of glass and Si are negatively charged, they have a positive charge at the exterior surface as a result of an electrical double layer[4]. Since DNA have a negative charge (at a pH of ≈7.0) they are easily attracted to the positively charged chamber walls and this causes the DNA to adhere to the walls preventing their involvement in the PCR replication process[4]. Another suggests[4, 15] that the hydrophilic surface properties of glass and Si is the primary reason for attraction of the DNA and *Taq* to the chamber walls. Although no in-depth studies have been undertaken in this regard, it is believed that a combination of all the above factors may be responsible for adsorption effects, which at times is very problematic in successfully performing the PCR. The absorption problem is a greater concern if the PCR is performed with low copy number samples[33] as in the case with the target application of this project (i.e. for cancer gene detections). Hence in the following, ways to prevent such enzyme absorption phenomena within the PCR chamber have been explored – by an altered PCR reaction mixture and/or surface treatment procedures.

Initial demonstrations of biochip PCR used an increased proportion (up to as many as 5 times) [54] of *Taq* DNA Polymerase so as to provide sufficient enzymes for the amplification process even if the walls of the reaction chamber absorbed a large amount of the enzyme. But the *Taq* Polymerase is the most expensive component in the PCR reaction mix and it may not be always advisable to increase the *Taq* concentration for cost-efficient genetic testing, unless the PCR reaction mix is prepared in sub-microliter volumes. More recently, Bovine Serum Albumin (BSA) and Polyethylene Glycol (PEG) have been explored as cheap alternatives[2, 4, 49, 55-61] to increasing the *Taq* concentration for the purpose of counteracting the adsorption effect. BSA, a protein derived from the blood of animals possesses a negative charge (similar to DNA) at pH $\approx$ 7.0[4] and is commercially available in powder or liquid form (e.g. from Fisher, USA). This heavy molecular weight enzyme lends itself as a sacrificial adsorption enzyme, thus preventing exhaustive *Taq* or DNA adsorption.

If a glass surface is used in the PCR biochips, apart from the recommended addition of BSA or PEG to the PCR reaction mixture, surface passivation by chemical or

physical coating has also been proposed in the literature as an added precautionary measure. For glass substrates, the Hjerten coating method[3, 54, 62, 63] (first proposed by Hjerten in 1985) has been demonstrated as an additional passivation technique. Alternatively, another group has proposed the epoxy (poly)dimethylacrylamide (EPDMA) as a robust coating technique to prevent the adsorption phenomena and to passivate glass surfaces [54].

Shin *et al.*[15] coated PDMS surfaces (channels and wells) with a low permeable Parylene material to prevent diffusion of fluid in the PDMS and since Parylene was also a hydrophobic material, it has been suggested that the adsorption of *Taq* and DNA might have been retarded. Similarly, it has been suggested that the hydrophobic PDMS also prevents cellular materials from strongly adhering to it[22]. However, here again, as with many other PDMS properties, there are contradicting theories. More recently, Lin *et al.*[64] suggest that hydrophobic PDMS exhibits a high affinity to cellular materials. This is probably a more substantiated theory considering the fact that the adsorption property of hydrophobic PDMS has vastly promoted its use as a material for immobilizing proteins, enzymes and DNA[64, 65]. More recently, Fukuba *et al.*[66] have coated the internal surfaces of their PDMS chips with 2-methacryloyloxyethyl phosphorylcholine (MPC) based polymer to retard the surface adhesion property of the PDMS. It has been reported that the yield of the PCR in non-treated PDMS surface was nil but greatly improved after the MPC treatment. Ishihara and coworkers[67] have extensively researched the properties of this MPC polymer for decades and found it to be non-attractive to cellular rich substances (e.g. blood, cells, proteins) and DNA.

On the other hand, non-hydrophobic (i.e. hydrophilic) surfaces in the chip are also known to influence the adsorption of proteins[15]. As discussed in Chapter 4, the surfaces of the PDMS are hydrophilic after the O_2 plasma treatment (performed for bonding the PDMS to the glass) but hydrophobic recovery occurs within few hours if the PDMS is exposed to air[22]. Hence, typically by the time the chip is used for a PCR experiments the surfaces are expected to be hydrophobic and therefore hydrophilicity effects may not be a concern.

Evidently there are many contradicting theories when it comes to discussing the nature of this relatively new polymer. Lack of a substantial understanding of the nature of this material is proving to be a stumbling block in implementing standardized protocols for use in genetic testing. This is unfortunate because tasks that could have been relatively simple with glass or Si have been far more time consuming and uncertain because of the uncharacterized nature of this material.

In the PCR biochip used in this work, the floor of the PCR chamber is made of glass while the walls and the roof are made of PDMS. Hence in this hybrid structure careful consideration of both of the surfaces is required to account for the absorption phenomena. To minimize the adsorption of bioreagents (i.e. DNA, enzymes) at the PDMS chip walls, the PDMS chips were treated by a protocol as described below.

The internal surfaces of the chip (channels and chamber) were pre-treated by a developed protocol in which a set of PCR compatible reagents were repeatedly filled (at least 3 times) into the PCR chamber with the following reagents: 'DNA away' in original concentration (Molecular BioProducts, USA) (- a solution that destroys DNAs and RNAs), 1M of NaOH, water (Sigma Chemicals, USA), and Phosphate-Buffered Saline (PBS) that is free of magnesium and chloride. Later, the PCR chamber and the channels were filled with 10 mg/ml of BSA and left undisturbed for 30 min prior to loading the chip with the PCR mix. In some of the most recent PCR genetic amplification experiments, preconditioning with many of the reagents were omitted but the 30 min of BSA surface conditioning was adopted as a standardized approach. In future, optimally optimizing the concentration of the BSA and the *Taq* in the PCR reaction mixture itself and exploring other potential alternatives would be sought to minimize or possibly eliminate the prolonged surface treatment.

In the low copy number experiments performed in implanted chips, a success rate of about 50% was noted and this was considered satisfactory because of the nature of the experiment (i.e. the difficulty in identifying the HAS gene and almost similar results seen with conventional processing). However, if the observed success rates were indeed due to the surface adsorption effects, then it could be considerably improved by exploring a

better retardation technique (e.g. using the MPC to prevent adsorption). Although the 30 min BSA pretreatment performed prior to the PCR experiments is expected to retard the cellular adsorption at the chamber walls, the MPC polymer coating[66] on the internal walls may provide a more robust technique (as claimed by Fukuba *et al.*[66]).

7.5.2 DNA PCR Experimentation and Analysis

In this section, experimental results of PCR genetic amplification performed in the PDMS biochips using devices built in-house (i.e. thermal cycling system and microfluidic plumbing system), is presented. Although numerous on-chip PCR experiments were performed with both yeast and cDNA samples, only two such demonstrations are presented below.

In a majority of the PCR experiments, a control experiment was also performed in Eppendorf tubes on a commercial thermocycler (PTE-200, MJ Research, MA, USA). Analysis of the biochip PCR and control experiment offers an easy means of quantifying the efficiency of the PDMS chip based approach for performing genetic amplification. In most experiments, it was noted that the quantity of amplified product, which is determined by the intensity of the fluorescence peak by CE, was about the same as that of the on-chip PCR experiments, confirming the efficiency of the prototype devices.

Upon completion of PCR thermal cycling, the PCR product was retrieved from the chip (or from the PCR tube in case of the control experiment), and stored in a refrigerator at –20 ^{o}C until the CE processing time. It is believed that the shelf-life of the amplified DNA can easily exceed many months when stored under such freezing conditions as this retards enzyme activity. In PCR experiments, the DNA analysis by CE using the uTK (as described in Chapter 3) was typically performed the same day or within a week of performing the PCR.

Although for each DNA fragment analysis of the PCR product at least three injection-separation runs were performed and the graphs were identical. However, only one of each of those graphical representations is presented here.

7.5.2.1 Yeast Genomic PCR

In some of the initial PCR experiments, genomic amplification with the yeast DNA[29] was performed and one such experiment is presented below.

The PCR product was amplified from yeast genomic DNA template with 24 bp primers specific to the SCO1 gene. The primer sequences were 5'-GACTGCTAGGAATTCAGCAATGGC-3' (SCO1-9) and 5'-ATATAATCGGCATGCGAAACGTATG-3' (SCO1-8). The primers were purchased from Synthetic Genetics (San Diego, CA, USA) and both were labeled with the fluorophore sulfoindocyanine succinimidyle ester (Cy5) at the 5' end. A PCR reaction master mix of 25 μl was prepared of which ~ 1.75 μl was loaded in a biochip and the remaining was used for a control run on a commercial thermocycler. The recipe for the PCR reaction master mix was as follows, 2 μl of SCO1-8 (1 p mol / μl), 2 μl of SCO1-9 (1 p mol / μl), 1.6 μl of nDNA (150 ng) derived from yeast genome (4730), 2 μl of dNTPs (2.5 mM), 2.5 μl of 10 x PCR buffer (Tris HCl 200 mM (pH 8.5), KCl 500 mM), 2.5 μl of BSA diluted in double distilled water (10 mg / ml), 0.75 μl of $MgCl_2$ (1.5 mM), 0.5 μl of *Taq* Polymerase, and 11.1 μl of double distilled autoclaved water. The molecular weight of 1 bp DNA is about 660 g/mol and the length of the yeast genome being 10, 00, 000 bp. This implies that the template concentration at the start of the PCR in this experiment (i.e. with 150 ng of nDNA) would be about 10^{12} copies. This is considered[3] to be a fairly high copy number for PCR experiments.

The thermal cycling parameters (for both the control experiment and the chip PCR) were, initial denaturation temperature (94°C) for 2 min followed by 35 cycles of denaturation (94°C), annealing (55°C) and extension (72°C) temperatures for 30 sec each and a final extension temperature (72°C) for 10 min. Upon completion, the PCR product was retrieved and analyzed using the CE technique as described in Chapter 3.

The channels in the CE chip were loaded with a sieving medium, (GeneScan polymer, PE Biosystems, CA, USA), by syringe and the sample waste, buffer, and buffer waste wells were filled with 3 μl of 1x TBE running buffer. The on-chip PCR product was diluted in 0.1 x TBE to constitute a total volume of 3 μl and loaded in the sample

well. In the case of the control experiment product analysis, only 0.3 μl of the PCR product was used which was diluted in 2.7 μl of 0.1 x TBE and loaded in the sample well. An injection voltage of 0.4 kV was applied for 60 sec between the sample and sample waste well to move PCR product from the sample well to the channel intersection. This was followed by a separation voltage of 6 kV applied between the buffer and buffer waste well, which resulted in the separation of the primer from the product and these were laser induced fluorescence (LIF) detected at a distance of 76 mm from the channel intersection.

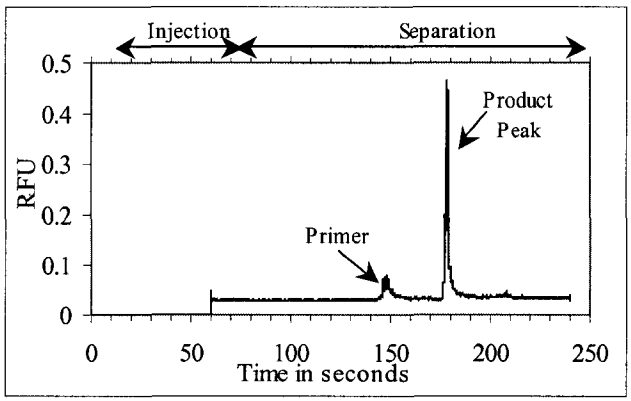

Figure 7-7. Yeast DNA PCR product analysis performed in a biochip

Figure 7-7 shows the electropherogram (Relative Fluorescence Intensity (RFI) vs. time in sec) of the on-chip PCR. The weak primer peak was seen at ~ 148 sec and a strong product peak was seen at ~ 178 sec. In this experiment size standards were not used but the size of the resulting product (322 base pairs) was verified by comparison with a λ*Hin*dIII-ϕX174*Hae*III size standard, as separated on a 1% agarose gel with ethidium bromide[29, 32] (data not shown). Both the experiments (i.e. the on-chip and the conventional process) had identical primer and product peaks (322 base pairs), confirming the comparable performance of the chip-based approach.

7.5.2.2. Cell Line Sample

In this experiment, a cell line (CCL 110) sample from a human cancer patient was used. The cDNA for the PCR was obtained from the reverse transcriptase (RT) of mRNA

(courtesy of S. Adamia, Cross Cancer Institute) and amplified by a forward and a reverse primer set. The number of DNA molecules is comparable to the number of RNA molecules and it is thought to be small (i.e. low copy number samples)[33].

The goal of the PCR was to amplifies a fragment of hyaluronan synthase (HAS) 1 transcripts, the presence of which is characteristic of Myeloma and Waldenstrom's macroglobulinemia patients[33]. Further details on similar experiments can be found in the work of Adamia *et al.*[33].

From the primer sets, the 5' primers (Applied Biosystems, USA) were labeled at their 5 ends. The on-chip PCR reaction was performed under the following condition: 5 μl cDNA was added to 24 μl of PCR mix containing 2.5 μl of 10X PCR buffer, 1 μl of 50 mM $MgCl_2$, 1 μl of 10 mM dNTPs, 1 μl each of 10 μM primers and 0.6 μl of 5 U/μl HiFi platinum *Taq* (GIBCO/BRL). The PCR cycling parameters were the following: primary denaturation at 94 °C for 5 min at the first cycle, followed by denaturation at 94 °C for 30 secs, annealing at 60 °C for 30 sec, extension at 72 °C for 30 secs repeated for 35 cycles and a final extension at 72 °C for 7 min.

The PCR product analysis for this experiment was analyzed (courtesy of S. Adamia, Cross Cancer Institute, Edmonton, Canada) on a 3100 DNA genetic analyzer[33] (Applied Biosystems, USA). The retrieved PCR product was mixed with a loading buffer, 12 μl of formamide and 1 μl of internal size standard GeneScan 500 (Applied Biosystems, USA). Next, the PCR product was denatured for 4 min at 96 °C and after a spin on a centrifuge, the sample was immediately transferred to ice for 15 min. The sample was then separated on the capillary (3100 DNA genetic analyzer) filled with POP4 polymer (Applied Biosystems, USA). The electrophoresis conditions were as follows: a run voltage and injection voltage 15000 V, injection duration 6-10 sec, a temperature 60 °C, and a laser power of 9 mW.

The electropherogram is shown in Figure 7-8. The two PCR product peaks were seen at 86 bp and 221 bp with a fairly high intensity (RFU ~ 400). The primer peaks are not seen in the graph. The result indicated that the amplification of not only the HAS1 was possible but also other novel variants of HAS1, HAS1Va. This expression appears to

be characteristics of malignant circulating B cells obtained from Myeloma and Waldenstrom's macroglobulinemia patients[68, 69]. Many on-chip PCR experiments (5 successful runs from 3 independent patients and 1 successful run with β_2 primers from another patient) were performed with cDNA patient samples and a manuscript (Adamia *et al.*) on this topic is in preparation.

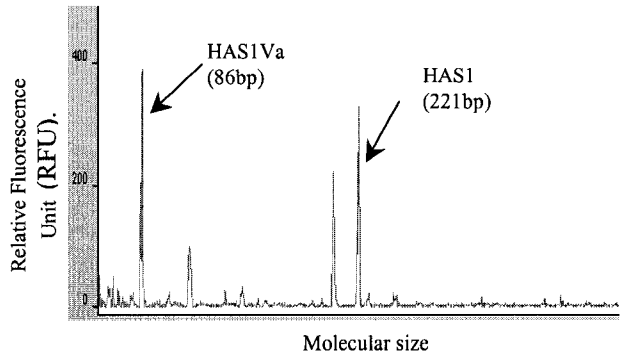

Figure 7-8. Cell line sample analysis. 86 and 221 bp are PCR products

In this experiment, two additional peaks (116 bp and 206 bp) were also observed between the two product peaks. This is speculated to be either a nonspecific genetic amplification[3] (defined as an untargeted amplification) or a contaminant.

Nonspecific genetic amplification is an issue of concern in biochip PCR especially when using the poor thermal conductive material glass (of 1.1 mm thickness) to structure the chip (as in this demonstration). Although glass was desired since it readily facilitates the integration of CE in future prototypes, it is known to cause thermal non-uniformities[3]. In one such glass chip demonstration found in the literature[3], the PCR chamber was etched in the lower glass substrate to ensure (a thinner substrate and hence a) better thermal uniformity within the PCR chamber. However, even with this alteration a nonspecific genetic amplification was observed[3] and this could possibly be attributed to the poor thermal properties of the glass substrate. Glass may not be ideally suited for the PCR as it also exhibits high thermal capacitance and this was experimentally discussed in Chapter 5, section 5.9.2.

Although nonspecific genetic amplifications did not occur in all the PCR experiments, it occasionally occurred with cDNA (human sample) PCR and this can potentially be attributed to the poor thermal properties of the glass substrate. Recommendations in this regard would be to use better thermally conductive materials (e.g. Si) and the optimization of the PCR reaction mixture. However, this may impede the integration of CE in the same chip substrate as Si is not optically comparable with glass.

Although at this level of experimentation, the verification of the experimental data for either non-specific amplification or contaminants have not been done with conventional laboratory procedures. It is hoped that in the future such verification will be possible.

7.6 Conclusion

This chapter presented two critical issues concerning small volume PCR in biochips – (1) an enhanced soft-lithography technique to microfabricate PDMS microfluidic devices that reduces vapor loss from such devices, and (2) the demonstration of small volume (~ 1.75 μl) PCR genetic amplification in PDMS-glass hybrid biochip with both small and large DNA template concentrations.

7.6.1 Enhanced PDMS Fabrication Technique

Water loss in PDMS microfluidic devices has limited their use in applications with small volumes at elevated temperatures. To the author's knowledge, the only reports of PDMS-based sub-microlitre PCR are from work that has been performed with high-density arrays of PCR wells and these compact geometries may have enabled their success[19, 21]. However, with higher levels of integration (e.g. incorporating CE) this density may be lost, possibly preventing the operation of small scale PCR in integrated devices. Clearly, a means of a better control of this vapor loss was required. In this work the loss mechanisms and their control were explored. Investigations revealed that the loss during the PCR thermal cycling was primarily due to vapor loss from the chip to the atmosphere due to the significantly large diffusion properties of PDMS. A first-of-a-kind new method for microfabricating PDMS devices with an implanted PE vapor barrier was

presented here. This method is an inexpensive and straightforward approach that is accomplished without the requirement for unusual equipment.

The experimental observations indicated that the vapor loss from the roof of the chip was prevented by the implanted layer. In an implanted chip, the observed small fluid loss is attributed to volumetric loss (i.e. loss through the sidewalls) and this was consistent with a theoretical estimate. However, the volumetric loss can be reduced by limiting the volume of PDMS that is available for absorbing water or by using 'guard channels' (as described in section 7.3.4). This finding is hoped to enable smaller volume PCR in future PDMS developments.

An interesting concept that is understood with the PDMS experimentation is that, materials that are easily adaptable for fabricating biochips for certain bioprocesses are not always suited for other bioprocesses. For example, PDMS has long been demonstrated as an excellent material for fabricating microfluidic devices for applications such as CE[5, 22, 70-72], DEP[73], mass spectroscopy[74, 75], etc. without any 'material property difficulties' but the same could not be applied for the heated PCR application.

7.6.2 PCR Experimentation

The PCR genetic amplification was successfully demonstrated in the PDMS-glass biochips presented in this work. Prior to modifying the PDMS (i.e. with a glass capping or an implant), the PCR could only be reproducibly performed with high copy number samples and experiments with the more difficult human DNA samples yielded a 0% success rate. However, upon demonstrating a better control of the fluid loss in a modified chip, the PCR success rate with the human cancer patient samples (i.e. low copy number samples) (with primers specific to the HAS gene) increased from 0% to nearly 50%. Unfortunately due to time and man-power limitations, titration experimentation (specifically the *Taq*, BSA, and primer concentrations) to optimize the biochemical aspect of the PCR (i.e. to counteract the adsorption phenomena) could not be undertaken as part of this work. It is hope that in the future, investigations will be made in this regard as well.

PCR experiments such as the ones presented in this chapter have been used by other groups for a variety of other applications including, detecting hereditary disorders[19], environmental studies[66], hepatitis C virus detection[76], malaria detection[77], and pathogen/infectious disease detection[78]. This device is readily adaptable for such applications as well and these molecular diagnostic experiments can be carried out without any perceivable changes to the system.

7.6.3 Concluding Remarks

It was not the initial intended goals of this research to investigate the material properties (i.e. liquid/vapor diffusion) of PDMS. However, it was deemed necessary since small volume PCR could not be reliably demonstrated for the targeted application (i.e. low concentration human DNA samples) in unmodified PDMS devices. The study of material property came to dominate the research project. This work has been submitted[1] for publication to a respected MEMS journal. The novel implant technique and other protocols presented here have now been incorporated in ongoing work.

In this work, the PCR and the CE were demonstrated in separate chips and the success with these individual techniques has paved the way for the integration of the two on a single unified chip (discussed in Chapter 8 of this thesis).

7.7 References

[1] A. R. Prakash, S. Adamia, V. Sieben, P. Pilarski, L. M. Pilarski, C. J. Backhouse, *Small Volume PCR in PDMS Biochips with Integrated Fluid Control and Vapour Barrier,* Sensors and Actuators B-Chemical, 2004, *submitted on July 30, 2004.*

[2] L. J. Kricka, P. Wilding, *Microchip PCR,* Analytical and Bioanalytical Chemistry, 2003, *377*, 820.

[3] E. T. Lagally, P. C. Simpson, R. A. Mathies, *Monolithic integrated microfluidic DNA amplification and capillary electrophoresis analysis system,* Sensors and Actuators B-Chemical, 2000, *63*, 138.

[4] H. Nagai, Y. Murakami, Y. Morita, K. Yokoyama, E. Tamiya, *Development of a microchamber array for picoliter PCR,* Analytical Chemistry, 2001, *73*, 1043.

[5] J. C. McDonald, G. M. Whitesides, *Poly(dimethylsiloxane) as a material for fabricating microfluidic devices,* Accounts of Chemical Research, 2002, *35*, 491.

[6] J. C. Lotters, W. Olthuis, P. H. Veltink, P. Bergveld, *The mechanical properties of the rubber elastic polymer polydimethylsiloxane for sensor applications,* Journal of Micromechanics and Microengineering, 1997, *7*, 145.

[7] J. Kim, M. K. Chaudhury, M. J. Owen, *Hydrophobicity loss and recovery of silicone HV insulation,* IEEE Transactions on Dielectrics and Electrical Insulation, 1999, *6*, 695.

[8] W. J. Chang, D. Akin, M. Sedlak, M. R. Ladisch, R. Bashir, *Poly(dimethylsiloxane) (PDMS) and silicon hybrid biochip for bacterial culture,* Biomedical Microdevices, 2003, *5*, 281.

[9] N. L. Jeon, D. T. Chiu, C. J. Wargo, H. K. Wu, I. S. Choi, J. R. Anderson, G. M. Whitesides, *Design and fabrication of integrated passive valves and pumps for flexible polymer 3-dimensional microfluidic systems,* Biomedical Microdevices, 2002, *4*, 117.

[10] W. H. Grover, A. M. Skelley, C. N. Liu, E. T. Lagally, R. A. Mathies, *Monolithic membrane valves and diaphragm pumps for practical large-scale integration into glass microfluidic devices,* Sensors and Actuators B-Chemical, 2003, *89*, 315.

[11] M. A. Unger, H.-P. Chou, T. Thorsen, A. Scherer, S. R. Quake, *Monolithic Microfabricated Valves and Pumps by Multilayer Soft Lithography,* Science, 2000, *288*, 113.

[12] T. C. Merkel, V. I. Bondar, K. Nagai, B. D. Freeman, I. Pinnau, *Gas sorption, diffusion, and permeation in poly(dimethylsiloxane),* Journal of Polymer Science Part B-Polymer Physics, 2000, *38*, 415.

[13] C. K. Yeom, S. H. Lee, H. Y. Song, J. M. Lee, *Vapor permeations of a series of VOCs/N-2 mixtures through PDMS membrane,* Journal of Membrane Science, 2002, *198*, 129.

[14] J. M. Watson, M. G. Baron, *The behaviour of water in poly(dimethylsiloxane),* Journal of Membrane Science, 1996, *110*, 47.

[15] Y. S. Shin, K. Cho, S. H. Lim, S. Chung, S. J. Park, C. Chung, D. C. Han, J. K. Chang, *PDMS-based micro PCR chip with parylene coating,* Journal of Micromechanics and Microengineering, 2003, *13*, 768.

[16] I. Blume, E. Smit, M. Wessling, C. A. Smolders, *Diffusion through Rubbery and Glassy Polymer Membranes,* Makromolekulare Chemie-Macromolecular Symposia, 1991, *45*, 237.

[17] I. Blume, P. J. F. Schwering, M. H. V. Mulder, C. A. Smolders, *Vapor Sorption and Permeation Properties of Poly(Dimethylsiloxane) Films,* Journal of Membrane Science, 1991, *61*, 85.

[18] J. W. Hong, T. Fujii, M. Seki, T. Yamamoto, I. Endo, *Integration of gene amplification and capillary gel electrophoresis on a polydimethylsiloxane-glass hybrid microchip,* Electrophoresis, 2001, *22*, 328.

[19] X. M. Yu, D. C. Zhang, T. Li, L. Hao, X. H. Li, *3-D microarrays biochip for DNA amplification in polydimethylsiloxane (PDMS) elastomer,* Sensors and Actuators a-Physical, 2003, *108*, 103.

[20] J. Liu, M. Enzelberger, S. Quake, *A nanoliter rotary device for polymerase chain reaction,* Electrophoresis, 2002, *23*, 1531.

[21] J. Liu, C. Hansen, S. R. Quake, *Solving the "world-to-chip" interface problem with a microfluidic matrix,* Analytical Chemistry, 2003, *75*, 4718.

[22] J. M. K. Ng, I. Gitlin, A. D. Stroock, G. M. Whitesides, *Components for integrated poly(dimethylsiloxane) microfluidic systems,* Electrophoresis, 2002, *23*, 3461.

[23] P. Sethu, C. H. Mastrangelo, *Cast epoxy-based microfluidic systems and their application in biotechnology,* Sensors and Actuators B: Chemical, 2004, *98*, 337.

[24] C. R. Tamanaha, L. J. Whitman, R. J. Colton, *Hybrid macro-micro fluidics system for a chip-based biosensor,* Journal of Micromechanics and Microengineering, 2002, *12*, N7.

[25] I. Erill, S. Campoy, N. Erill, J. Barbe, J. Aguilo, *Biochemical analysis and optimization of inhibition and adsorption phenomena in glass-silicon PCR-chips,* Sensors and Actuators B-Chemical, 2003, *96*, 685.

[26] J. R. Fried, *Polymer Science and Technology*, Second ed., Prentice Hall Professional Technical Reference, New Jersey, 2003.

[27] A. Zanzotto, N. Szita, P. Boccazzi, P. Lessard, A. J. Sinskey, K. F. Jensen, *Membrane-aerated microbioreactor for high-throughput bioprocessing,* Biotechnology and Bioengineering, 2004, *87*, 243.

[28] D. S. Yoon, Y. S. Lee, Y. Lee, H. J. Cho, S. W. Sung, K. W. Oh, J. Cha, G. Lim, *Precise temperature control and rapid thermal cycling in a micromachined DNA polymerase chain reaction chip,* Journal of Micromechanics and Microengineering, 2002, *12*, 813.

[29] C. J. Backhouse, H. J. Crabtree, D. M. Glerum, *Frontal analysis on a microchip,* Analyst, 2002, *127*, 1169.

[30] S. Adamia, T. Reiman, M. Crainie, A. R. Belch, L. M. Pilarski, *Aberrant splicing of hyaluronan synthase 1 (HAS1) gene in multiple myeloma (MM): HAS1 and novel HAS1 splice variants in MM B cells have an adverse impact on patient survival,* Blood, 2003, *102*, 371B.

[31] S. Adamia, M. Crainie, J. Kriangkum, M. J. Mant, A. R. Belch, L. M. Pilarski, *Abnormal expression of hyaluronan synthases in patients with Waldenstrom's macroglobulimenia,* Seminars in Oncology, 2003, *30*, 165.

[32] D. M. Glerum, I. Muroff, C. Jin, A. Tzagoloff, *COX15 codes for a mitochondrial protein essential for the assembly of yeast cytochrome oxidase,* Journal of Biological Chemistry, 1997, *272*, 19088.

[33] S. Adamia , M. Crainie , J. Kriangkum , M. Mant , A. Belch , L. Pilarski, *Abnormal expression of hyaluronan synthases in patients with Waldenstrom's macroglobulimenia,* Seminars in Oncology, 2003, 165.

[34] S. N. Dirim, H. O. Ozden, A. Bayindirli, A. Esin, *Modification of water vapour transfer rate of low density polyethylene films for food packaging,* Journal of Food Engineering, 2004, *63*, 9.

[35] A. E. Goulas, K. A. Riganakos, A. Badeka, M. G. Kontominas, *Effect of ionizing radiation on the physicochemical and mechanical properties of commercial monolayer flexible plastics packaging materials,* Food Additives and Contaminants, 2002, *19*, 1190.

[36] K. A. Riganakos, W. D. Koller, D. A. E. Ehlermann, B. Bauer, M. G. Kontominas, *Effects of ionizing radiation on properties of monolayer and multilayer flexible food packaging materials,* Radiation Physics and Chemistry, 1999, *54*, 527.

[37] J. S. Turner, Y. L. Cheng, *Preparation of PDMS-PMAA interpenetrating polymer network membranes using the monomer immersion method,* Macromolecules, 2000, *33*, 3714.

[38] J. N. Lee, C. Park, G. M. Whitesides, *Solvent compatibility of poly(dimethylsiloxane)-based microfluidic devices,* Analytical Chemistry, 2003, *75*, 6544.

[39] E. F. Castro, E. E. Gonzo, J. C. Gottifredi, *The analysis of sorption data of organic vapors in polymeric membranes through novel theories,* Journal of Membrane Science, 1996, *113*, 57.

[40] E. Favre, P. Schaetzel, Q. T. Nguygen, R. Clement, J. Neel, *Sorption, Diffusion and Vapor Permeation of Various Penetrants through Dense Poly(Dimethylsiloxane) Membranes - a Transport Analysis,* Journal of Membrane Science, 1994, *92*, 169.

[41] J. M. L. C.K. Yeom, Y.T. Hong, K.Y. Choi, S.C. Kim, *Analysis of permeation transients of pure gases through dense polymeric membranes measure by a new permeation apparatus,* J. Membr. Sci., 2000, *166*, 71–83.

[42] M. E. Rezac, T. John, P. H. Pfromm, *Effect of copolymer composition on the solubility and diffusivity of water and methanol in a series of polyether amides,* Journal of Applied Polymer Science, 1997, *65*, 1983.

[43] K. Pappaert, J. Vanderhoeven, P. Van Hummelen, B. Dutta, D. Clicq, G. V. Baron, G. Desmet, *Enhancement of DNA micro-array analysis using a shear-driven micro-channel flow system,* Journal of Chromatography A, 2003, *1014*, 1.

[44] K. S. McCain, D. C. Hanley, J. M. Harris, *Single-molecule fluorescence trajectories for investigating molecular transport in thin silica sol-gel films,* Analytical Chemistry, 2003, *75*, 4351.

[45] S. C. George, S. Thomas, *Transport phenomena through polymeric systems,* Progress in Polymer Science, 2001, *26*, 985.

[46] R. Weast, *Handbook of Chemistry and Physics*, 54th Edition ed., CRC Press, Ohio, 1973-1974.

[47] F. Peng, J. Liu, J. Li, *Analysis of the gas transport performance through PDMS/PS composite membranes using the resistances-in-series model,* Journal of Membrane Science, 2003, *222*, 225.

[48] J. M. S. Henis, M. K. Tripodi, *Composite Hollow Fiber Membranes for Gas Separation - the Resistance Model Approach,* Journal of Membrane Science, 1981, *8*, 233.

[49] C. G. Koh, W. Tan, M. Q. Zhao, A. J. Ricco, Z. H. Fan, *Integrating polymerase chain reaction, valving, and electrophoresis in a plastic device for bacterial detection,* Analytical Chemistry, 2003, *75*, 4591.

[50] J. Brandrup, E. Immergut, *Polymer Handbook*, Third ed., Wiley Interscience, New York, 1989.

[51] P. R. Selvaganapathy, E. T. Carlen, C. H. Mastrangelo, *Recent progress in microfluidic devices for nucleic acid and antibody assays,* Proceedings of the Ieee, 2003, *91*, 954.

[52] M. A. Shoffner, J. Cheng, G. E. Hvichia, L. J. Kricka, P. Wilding, *Chip PCR .1. Surface passivation of microfabricated silicon-glass chips for PCR,* Nucleic Acids Research, 1996, *24*, 375.

[53] J. Cheng, M. A. Shoffner, G. E. Hvichia, L. J. Kricka, P. Wilding, *Chip PCR .2. Investigation of different PCR amplification systems in microfabricated silicon-glass chips,* Nucleic Acids Research, 1996, *24*, 380.

[54] B. C. Giordano, E. R. Copeland, J. P. Landers, *Towards dynamic coating of glass microchip chambers for amplifying DNA via the polymerase chain reaction,* Electrophoresis, 2001, *22*, 334.

[55] J. N. Yang, Y. J. Liu, C. B. Rauch, R. L. Stevens, R. H. Liu, R. Lenigk, P. Grodzinski, *High sensitivity PCR assay in plastic micro reactors,* Lab on a Chip, 2002, *2*, 179.

[56] B. C. Giordano, J. Ferrance, S. Swedberg, A. F. R. Huhmer, J. P. Landers, *Polymerase chain reaction in polymeric microchips: DNA amplification in less than 240 seconds,* Analytical Biochemistry, 2001, *291*, 124.

[57] T. Fujii, *PDMS-based microfluidic devices for biomedical applications,* Microelectronic Engineering, 2002, *61-2*, 907.

[58] Y. J. Liu, C. B. Rauch, R. L. Stevens, R. Lenigk, J. N. Yang, D. B. Rhine, P. Grodzinski, *DNA amplification and hybridization assays in integrated plastic monolithic devices,* Analytical Chemistry, 2002, *74*, 3063.

[59] J. Khandurina, T. E. McKnight, S. C. Jacobson, L. C. Waters, R. S. Foote, J. M. Ramsey, *Integrated system for rapid PCR-based DNA analysis in microfluidic devices,* Analytical Chemistry, 2000, *72*, 2995.

[60] J. Khandurina, T. E. McKnight, S. C. Jacobson, L. C. Waters, R. S. Foote, J. M. Ramsey, *Integrated system for rapid PCR amplification and electrophoretic analysis in microfluidic devices,* Abstracts of Papers of the American Chemical Society, 2000, *219*, U95.

[61] L. C. Waters, S. C. Jacobson, N. Kroutchinina, J. Khandurina, R. S. Foote, J. M. Ramsey, *Microchip device for cell lysis, multiplex PCR amplification, and electrophoretic sizing,* Analytical Chemistry, 1998, *70*, 158.

[62] A. T. Woolley, D. Hadley, P. Landre, A. J. deMello, R. A. Mathies, M. A. Northrup, *Functional integration of PCR amplification and capillary electrophoresis in a microfabricated DNA analysis device,* Analytical Chemistry, 1996, *68*, 4081.

[63] A. T. Woolley, M. A. Northrup, R. A. Mathies, *Microfabricated integrated DNA analysis systems,* Abstracts of Papers of the American Chemical Society, 1996, *212*, 155.

[64] F. Y. H. Lin, P. M. Sherman, D. Q. Li, *Development of a novel hand-held immunoassay for the detection of enterohemorrhagic Escherichia coli O157 : H7,* Biomedical Microdevices, 2004, *6*, 125.

[65] D. J. Liu, R. K. Perdue, L. Sun, R. M. Crooks, *Immobilization of DNA onto poly(dimethylsiloxane) surfaces and application to a microelectrochemical enzyme-amplified DNA hybridization assay,* Langmuir, 2004, *20*, 5905.

[66] T. Fukuba, T. Yamamoto, T. Naganuma, T. Fujii, *Microfabricated flow-through device for DNA amplification - towards in situ gene analysis,* Chemical Engineering Journal, 2004, *101*, 151.

[67] K. Ishihara, T. Hasegawa, J. Watanabe, Y. Iwasaki, *Protein adsorption-resistant hollow fibers for blood purification,* Artificial Organs, 2002, *26*, 1014.

[68] S. Adamia, P. M. Pilarski, R. Prakash, J. Lauzon, C. J. Backhouse, L. M. Pilarski, *Microsystems and cancer: Improved detection of disease related genes in myeloma patients using microfluidics platforms,* Blood, 2003, *102*, 682A.

[69] C. M. Adamia S, Kriangkum J, Mant MJ, Belch AR, Pilarski LM, *Abnormal expression of hyaluronan synthases in patients with Waldenstrom's macroglobulimenia,* Semin Oncol., 2003, 165.

[70] G. Ocvirk, M. Munroe, T. Tang, R. Oleschuk, K. Westra, D. J. Harrison, *Electrokinetic control of fluid flow in native poly(dimethylsiloxane) capillary electrophoresis devices,* Electrophoresis, 2000, *21*, 107.

[71] D. Erickson, D. Sinton, D. Q. Li, *Joule heating and heat transfer in poly(dimethylsiloxane) microfluidic systems,* Lab on a Chip, 2003, *3*, 141.

[72] S. K. Sia, G. M. Whitesides, *Microfluidic devices fabricated in poly(dimethylsiloxane) for biological studies,* Electrophoresis, 2003, *24*, 3563.

[73] T. Kanagasabathi, C. J. Backhouse, K. Kaler, in *Nanotech 2004*, Boston, MA, 2004.

[74] J. S. Kim, D. R. Knapp, *Microfabricated PDMS multichannel emitter for electrospray ionization mass spectrometry,* Journal of the American Society for Mass Spectrometry, 2001, *12*, 463.

[75] J. Gao, J. D. Xu, L. E. Locascio, C. S. Lee, *Integrated microfluidic system enabling protein digestion, peptide separation, and protein identification,* Analytical Chemistry, 2001, *73*, 2648.

[76] K. W. Lai, K. C. Young, P. N. Cheng, S. H. Chen, T. T. Chang, *Interspousal transmission of hepatitis C virus: Application of comparing the variability of HVR1 nucleotide region,* Hepato-Gastroenterology, 2004, *51*, 791.

[77] P. Gascoyne, J. Satayavivad, M. Ruchirawat, *Microfluidic approaches to malaria detection,* Acta Tropica, 2004, *89*, 357.

[78] E. T. Lagally, J. R. Scherer, R. G. Blazej, N. M. Toriello, B. A. Diep, M. Ramchandani, G. F. Sensabaugh, L. W. Riley, R. A. Mathies, *Integrated portable genetic analysis microsystem for pathogen/infectious disease detection,* Analytical Chemistry, 2004, *76*, 3162.

Chapter – 8

Towards Integration of the Polymerase Chain Reaction and Capillary Electrophoresis

This chapter describes the integration of PCR and CE in a unified chip with the added feature of on-chip thin film gold (Au) heaters to enable the PCR thermal cycling. A performance evaluation of the chip suggested that the Au metal is not suitable for the high temperature PCR application and alternate metals such as platinum are needed. A detailed experimental study undertaken to characterize the gold heaters is presented followed by suggestions for future work.

8.1 Introduction

The PCR in PDMS biochips was demonstrated in chapter 7. PCR product retrieved from the PCR chip had to be analyzed in a different chip using the CE process (i.e. a CE chip compatible with the μTk). However, it is possible to integrate these two bioprocess (i.e. the PCR and the CE) in the same chip. Towards this goal, higher levels of integration were attained in this part of the project. This involved the integration of on-chip thin film heaters.

In MEMS processing many novel techniques that enable higher levels of on-chip integration have been explored in recent years. One such has been the integration of metal heaters in the biochips. Integrated thin film heaters offer numerous advantages such as compact design thus eliminating the need for the bulky Peltiers, and gives faster thermal ramp rates due to the reduced thermal mass of the heater/chip (up to 90 °C/sec

has been demonstrated)[1]. These advantages are particularly critical in integrated biochips that seek to minimize components while increasing the device-density.

The primary intent of this chapter is to demonstrate the feasibility of integrating thin film resistive heaters to enable PCR thermal cycling. Thin film heaters are more efficient (in terms of thermal ramp rates and power consumption) than the traditional Peltier heaters. In addition, with thin film heaters it is also possible to sense the temperature through a temperature coefficient of resistance (TCR) measurement, thus eliminating the need for an external temperature sensor such as the ones required for Peltier devices.

A wide range of metals have been deposited by physical vapor deposition in a manner compatible with MEMS processing[1-6]. Most of these approaches (including the PCR application) used platinum (Pt) [1-6] (with titanium (Ti) as the lower adhesion layer) as the resistive metal for the heater with one exception in which polysilicon[7] heaters were used. However, patterning gold (Au) with chrome (Cr) as an adhesion layer has been demonstrated as an efficient method for fabricating electrodes[8] and resistive heaters[9]. Au-Cr heaters metals (with metal thicknesses similar to that used in this work) has been demonstrated as effective thin film heaters for temperature ranging upto 50 °C. Moreover, since Au has a high melting point (above 1000 °C) it was expected to show good characteristics as a resistive heater in heating applications[9]. Au-Cr patterning is less time consuming than Pt-Ti patterning as it can be easily accomplished using the wet-etching process. In this work, the Au-Cr metals were used as resistive heaters that were patterned on a glass substrate with a PDMS microfluidic device bonded to the glass to constitute the PCR-CE chip (as described in chapter 4).

The following section reviews the literature work on the topic of integrated PCR-CE demonstrations in biochips followed by an experimental discussion of the performance of the thin film Au resistive heaters.

8.2 History of PCR-CE

In this section some recent demonstrations of PCR and CE in integrated devices are reviewed and summarized. Fluid sample volumes for performing these genetic amplification and analysis techniques (i.e. PCR and CE) in integrated biochips have ranged from the high microliter[10] to the low sub microliter[4] volumes. Mathies and coworkers[11, 12] were among the first to demonstrate the feasibility of performing both the PCR and the CE in a integrated chip. A four port glass structured CE chip was used in which a small plastic (polyproplene) tube was inserted in the sample wells of the CE chip to form the PCR chamber. The polyproplene insert was surrounded by polysilicon heaters microfabricated using processes such as wet etching and chemical vapour deposition. The polysilicon heater was then vertically glued to the sample well in the glass CE chip with epoxy and the hollow polyproplene tube was inserted into this structure forming a PCR well with a volume of 20 μl. To prevent evaporation during PCR thermal cycling, the open PCR well was simply capped and held firmly against the chip.

In a later demonstration of the PCR-CE in biochips, Mathies and coworkers had improved the functionality of such the device by performing PCR with even smaller volumes (about 0.28 μl) in glass and Si structured chips[4, 5]. The highlight of this work was the functional integration of valves that enabled performing the PCR in an enclosed chamber within the chip. More recently, the CE detection system and the PCR instrumentation were assembled in the same setup and was used for on-site pathogen and infection detections[6].

Ramsey and coworkers have also demonstrated PCR and CE in glass structures[13-15]. The sample well in a 4-port CE chip were used as the PCR reaction chamber. The channels in the rest of the CE chip were filled with a highly viscous solution (polyacrylamide) and all the four wells including the PCR chamber were topped with mineral oil to prevent evaporation during the PCR thermal cycling. The entire chip was thermocycled in a commercial thermocycler (MJ Research Inc., MA, USA) to perform the PCR genetic amplification. In a subsequent demonstration[14], in-house assembled thermoelectric devices (Peltiers) were used as heating and cooling elements. Two Peltier

devices, one above the PCR chamber and one below the PCR chamber were used to achieve heating and cooling of the reaction mix at the rate of ~2 °C and 3-4 °C, respectively, with an accuracy of ± 0.5 °C at setpoints.

The above discussion was on demonstrations in biochips that were structured with glass and Si materials. Microfabrication processing with these materials is time consuming and expensive[16]. This has led to researchers exploring alternative polymer materials that facilitate easier fabrication. Liu *et al.* [17] used polycarbonate material to fabricate PCR-hybridization biochips using CO_2 laser to etch and cut though a black polycarbonate sheet. The laser cutting process was also used to pattern channels and wells by drilling through the polycarbonate sheet. This cut sheet was then thermally bonded to two other transparent polycarbonate sheets on the top and bottom surface to produce a biochip with an enclosed fluid circuit. A serpentine channel design constituted the PCR chamber of 38 μl volume. In this demonstration of the PCR-hybridization biochip, for the first time a thermal liquid cured gel (Pluronic crystals) was used in PCR application to form valves that seal channels and prevent evaporation during the PCR thermal cycling. The Pluronic gel was prepared by dissolving Pluronic powder in cold buffer solution and then inserted into the channel to form the valve.

In a demonstration of PCR and CE using a similar valving approach as above, Koh *et al* [18] used a poly(cyclic olefin) material to fabricated PCR-CE chips and used UV-cured gel valves to seal channels connecting a 29 to 84 nl PCR chamber. The novelty of this work was the screen printing (silver/ graphite ink) of metal (100 μm thick) on the poly(cyclic olefin) to form heaters for the PCR thermal cycling and electrodes for CE detection.

Fujii and co-workers demonstrated PCR and subsequent CE in a unified PDMS-glass hybrid biochip[10, 19, 20]. Channels and wells were structured in the PDMS and this was then sealed to a glass substrate to produce a biochip. Unlike some of the earlier demonstrations by other groups that integrated valves, in this work PCR was performed with 30 μl to 50 μl in an open well, which was then capped with an adhesive tape to

prevent evaporation during the PCR thermal cycling. Thermoelectric elements were used to perform the PCR genetic amplification thermal cycling.

8.3 Thin Film Heater Experimentation

Au heaters with Cr as the adhesion metal layer (200 nm Au and 10 nm Cr similar to the fabricated PCR-CE chip) has been demonstrated[9] as an effective thin film heater. It was hoped that for PCR applications this combination of metal heater (i.e. Cr-Au bilayer) would be effective. However, the experimental work shown below indicates that for high temperature applications (i.e. > 50 °C), the resistance of the Au metal was unstable, unlike the characteristics of a good metal heater (e.g. Pt). Recent studies[21] have suggested that this is possibly due to the diffusion of Cr atoms into the (above) Au layer that occurs at elevated temperature, and that this is responsible for an increase in the resistance of the thin film.

In the chip design, the patterned Au-Cr thin film on the glass serves two purposes – as a resistive heater and as a feedback path for temperature measurement based on the temperature coefficient of resistance (TCR)[5]. This technique of heating and sensing by the same element eliminates the need for a temperatures sensor like those required in Peltier device setups (described in chapter 5). For the purpose of supplying heat as well as to measure the temperature based on the TCR, a Keithley Source Measuring Unit (SMU-232, Keithley Instruments, USA) was used. When connected to a resistor, the instrument was capable of sourcing a constant voltage of up to 110 Volts or a constant current of up to 100 m A. The advantage of using this particular unit was that it is possible to source a constant current and measure the voltage across the same resistor. Thus any change in the voltage across the resistor is indicative of a change in the temperature of the metal and the corresponding temperature value can be calculated using the TCR.

The TCR equation that translates a given resistance value into temperature is given by[22]

$$\left[\frac{(R-R_o)}{R_o}\right] = \alpha[T-T_o] \qquad \text{- (8.1)}$$

where, R_o is the initial resistance of the resistive metal (gold), T_o is the temperature value at R_o, R is the resistance of the metal at an elevated temperature T, and α is a constant defined as the coefficient of resistance (– for Au α = 0.0034 / K measured at 20 °C)[22].

The inherent properties of most metals are such that the resistance of the metal will increase as a function of the temperature (i.e. positive TCR). Hence if a constant current (I) was sourced to the resistive heater then the resistance (R) of the metal is expected to increase. By monitoring the voltage across this resistor, the value of R at any given value of V can be found using Ohms law:

$$R = \left(\frac{V}{I}\right) \qquad \text{- (8.2)}$$

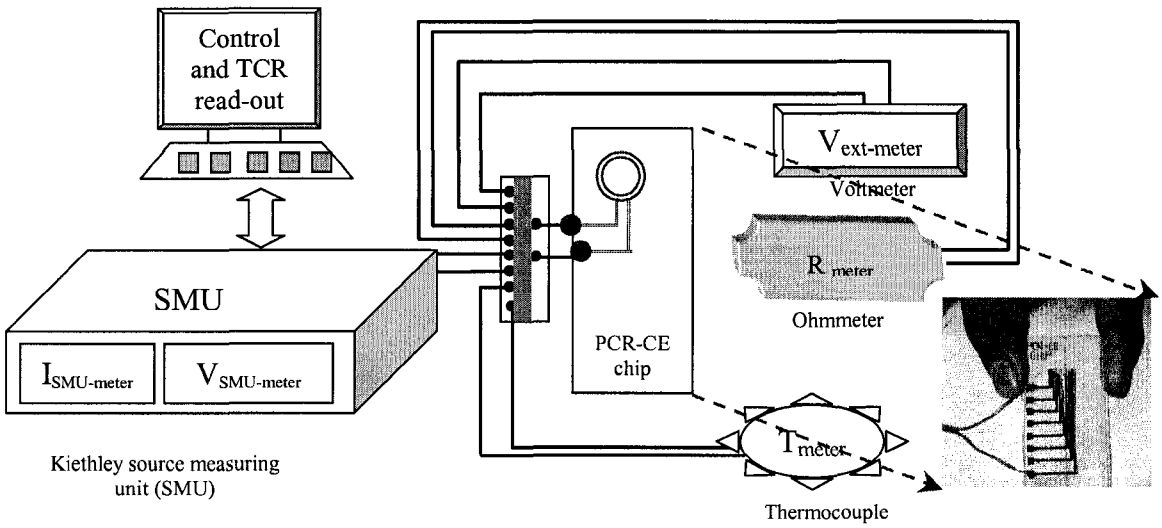

Figure 8-1. Setup for the Temperature coefficient of resistance measurement

To demonstrate the performance of such a resistance-temperature measuring technique for the PCR-CE chip, an experiment was setup as shown in Figure 8-1. The wire connections were made using alligator clips and connector pins. A chip with a patterned Au resistive heater was connected to the SMU ($I_{SMU-meter}$ and $V_{SMU-meter}$) along with an additional voltmeter ($V_{ext-meter}$), Ohmmeter (R_{meter}) and a thermocouple

temperature sensor (T_{meter}) (similar to that described in Chapter 5, section 5.9.2). The $V_{ext\text{-}meter}$, R_{meter} and T_{meter} were connected as cross-referencing meters to the SMU device measurements and to verify the calculated temperature based on the TCR.

8.3.1 Low Temperature Experimentation

Initially, the experiment was setup for low temperature applications, i.e. the maximum heat output was kept under 50 °C. The current sourced ($I_{SMU\text{-}meter}$) from the SMU was kept constant at 15 mA, the initial resistance (R_o) of the gold film was 1140 Ω and the initial room temperature (T_o) was 24.1 °C. The SMU was controlled from a computer using a GPIB interface. Immediately upon sourcing the current, the parameters on all of the meters were noted and necessary calculations (i.e. the $R_{ohm\text{-}law}$ and the T_{TCR} from Eq 8.1 and 8.2) were performed; the values are summarized in Table 8-I.

Table 8-I. TCR data from low temperature experiments with on-chip resistive heaters

$I_{SMU\text{-}meter}$ (mA)	$V_{SMU\text{-}meter}$ (V)	$V_{ext\text{-}meter}$ (V)	$R_{ohm\text{-}law}$ (Ω)	R_{meter} (Ω)	T_{TCR} °C	T_{meter} °C
15	**18.35**	18.32	**1220.00**	1220.00	**44.74**	44.80
15	**12.44**	12.44	**1229.33**	1230.00	**47.15**	47.30
15	**18.49**	18.5	**1232.67**	1235.50	**48.01**	48.00
15	**18.55**	18.52	**1236.67**	1236.80	**49.04**	49.00
15	**18.60**	18.61	**1240.00**	1240.00	**49.90**	49.90
15	**18.63**	18.63	**1242.00**	1241.90	**50.42**	50.50

From the table, the calculated temperature value and the measured temperature value were almost equal (error < ± 1%), and as shown in the graph in Figure 8-2, linearity between Resistance ($R_{ohm\text{-}law}$) and temperature (T_{TCR}) showed a reasonably good linear function suggesting a fairly stable TCR (α) for the Au resistive heater (i.e. α uncertainty was ± 1% which included the above measurement uncertainty of ± 1%). The experimental data was reproducible within the same batch of fabricated chips. However, the experimental range in this experiment was kept between room temperature (~ 25 °C) and 50 °C. Similar heater characteristics were not observed for high temperature experiment as discussed below.

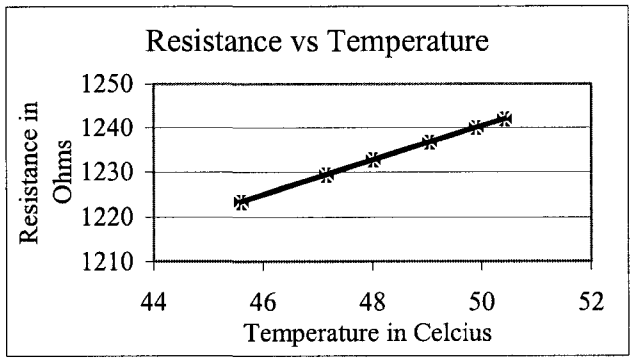

Figure 8-2. Plot of $R_{ohm\text{-}law}$ vs T_{TCR}

8.3.2 High Temperature Experimentation

In this experiment, current (I) supplied to the resistor was increased to 25 mA to cause an increase in the output heat. Similar to the previous set of experiments, external meters were connected to monitor the voltage ($V_{ext\text{-}meter}$), resistance (R_{meter}) and temperature (T_{meter}). Table 8-II summarizes the values with $R_{ohm\text{-}law}$ and T_{TCR} calculated as earlier.

Table 8-II. TCR data from high temperature experiments with on-chip resistive heaters

$I_{SMU\text{-}meter}$ (mA)	$V_{SMU\text{-}meter}$ (V)	$V_{ext\text{-}meter}$ (V)	$R_{ohm\text{-}law}$ (Ω)	R_{meter} (Ω)	T_{TCR} °C	T_{meter} °C
25	**30.00**	30.08	**1200.10**	1203.00	**39.61**	**41.50**
25	**37.26**	37.15	**1490.45**	1485.90	**114.52**	**47.30**
25	**38.75**	38.76	**1550.10**	1550.50	**129.90**	**48.00**
25	**55.56**	55.46	**2222.33**	2218.23	**303.34**	**49.00**
25	**87.52**	87.27	**3500.88**	3490.90	**633.20**	**60.00**
25	**160.51**	160.64	**6420.50**	6425.50	**1386.46**	**82.50**

There are many obvious discrepancies with the obtained experimental data, which are discussed below.

The T_{TCR} (i.e. the temperature calculation based on the TCR) calculated from Eq 8.1 and the $R_{ohms\text{-}law}$ values from the above table shows an unrealistically large temperature value. Although the T_{meter} reading from the external thermocouple is believed to read the actual temperature of the device, this greatly differs from the T_{TCR} temperature

value. This is believed to be because the value of α and R_o are not constant during the course of the experiment. The initial resistance R_o was 1140 Ω at the start of the experiment and increased by nearly a factor of 3 (to 3360 Ω) by the end of the experiment. Recent studies suggest that this increase in the resistance is due to the unpredictable diffusion of Cr into the Au[21, 22] due to the repositioning of the grain boundaries of the Au atoms[21]. In these PCR-CE chips, this is visualized by the color of the Au film which turns pale upon completion of experiments[5] (- since Cr is much like the color of silver and Au is dark yellow, a pale yellow was observed) since prolonged annealing (as described below) was not performed prior to testing this chip.

Annealing metals upon fabrication is a common approach in resistive heating applications[2, 4, 5]. However, these annealing techniques were not helpful[21] for such an unstable Cr diffusion. This phenomena has recently been studied in the literature[21] and was experimentally verified by placing a newly fabricated chip with patterned Au-Cr heaters in an oven at 250 °C for time varying over a period of 1 to 7 hr. Periodica removal of the chip from the oven and followed by cooling to room temperature (about 22 °C) gave the resistance measurements that indicated an increase in the R_o value at each data point (as shown in Figure 8-4). The initial resistance (R_o) increased from ~1140 Ω to over 7250 Ω by the end of this 7 hr annealing experiment. When this annealed resistive heater was used for a TCR experiment, the R_o gain increased by about another 150 Ω.

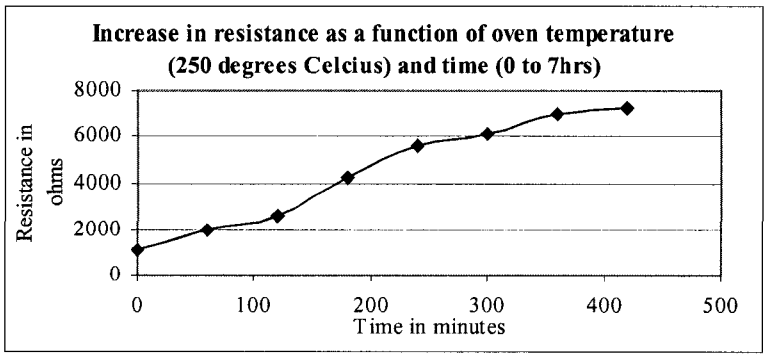

Figure 8-4. An experimental graph indicating the increase in resistance of the thin film heater as a function temperature and time

Although it is believed that at some stage of annealing[21], the Au-Cr diffusion will stabilize leading to a stable R_o, this will result in an inconsistency between batches of fabricated chips making it very difficult to stably control the temperature based on a standardized control algorithms (e.g. the PD-PI described in chapter 5). For instance, if the P/I/D control algorithm was tuned for accurately maintaining temperature for a given chip with a specific R_o value, the same controller may not perform with the same temperature accuracy if a different chip is used, because the time constants (i.e. based on the R_o) may be different for this new chip. In applications such as PCR where the temperature accuracy is highly critical, it seemed virtually impossible to incorporate such Au integrated heaters.

Furthermore, unlike Pt heaters that show stable TCR over a wide range of high temperatures[1, 2, 5], the TCR of Au even for low temperature applications seem to vary by at least a factor of 3 among reported data in literature[23] (operating temperatures <50 °C). Hence, it was concluded that for high temperature applications (e.g. PCR), Au-Cr resistive heaters are not suitable because of the initial resistance (R_o) of the Au-Cr thin film increases[21] at temperatures over 50 °C and does return to the original value upon cooling.

8.4 Future work

In future prototypes, it is recommended that Pt with Ti as the adhesion layer be used as thin film heaters as they have shown to be a stable metal combination even for the PCR application[2, 5]. The microfabrication procedure involved in this system is described below. In addition, an enhancement in chip layout is also proposed.

8.4.1 Choice of Metal for Resistive Thin Film Heaters

In future prototypes it is strongly recommended that platinum (Pt) heater with Ti[2, 5] or TiN[24] as an adhesion layer be used as thin film resistive heaters for fabricating the PCR-CE chips. However, patterning Pt on glass or Si substrates cannot be easily accomplished by a process similar to the Au-Cr patterning (i.e. the wet chemical etch) because Pt metal does not easily dissolve in chemical solvents. Aqua Regia (3:1,

$HCl:HNO_3$ hot) is a suggested etching solvent but is a hazardous chemical and not commonly used or recommended for patterning Pt films as it does not easily etch away the metal. Alternatively, a process called 'lift-off' has been adopted for pattering Pt thin films[2, 4, 5, 25-27]. In the 'lift-off' process, as shown in Figure 8-5, a glass substrate is first spin-coated with a photoresist. This is followed by a negative mask photolithographic UV exposure and developing. Then a layer of Titanium (Ti) is sputtered on the wafer followed by sputtering of the Pt metal on the Ti. The Ti metal is required as it provides a beneath adhesion layer for the Pt – similar to the beneath Cr layer required for patterning Au on a glass wafers. Finally, the photoresist is stripped from the wafer and the Ti and Pt metals that were sputtered on the photoresist are also removed with it. This leaves the glass substrate with the Pt patterned as desired with a Ti adhesion layer. Such Pt-Ti structures have been widely used as thin film heaters for high temperature applications including the PCR[5].

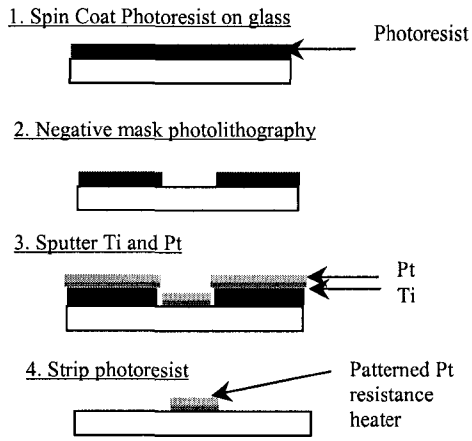

Figure 8-5. Lift-off process for patterning Pt resistive metal heaters

8.4.2 Enhanced Chip Layout

In chapter 7, section 7.3.4, it was suggested that the volumetric loss in PDMS could be reduced by the use of a sacrificial water channel in the near vicinity of the PCR chamber. In this regard, an enhanced PCR-CE is proposed below that incorporates an enclosed fluid channel around the PCR chamber for this purpose. Apart from this

recommended change, the chip layout has been modified to accommodate the PCR chamber in a lower arm connecting the sample well in a standard sample-cross[28] CE chip. The layout of the proposed chip is shown in Figure 8-6.

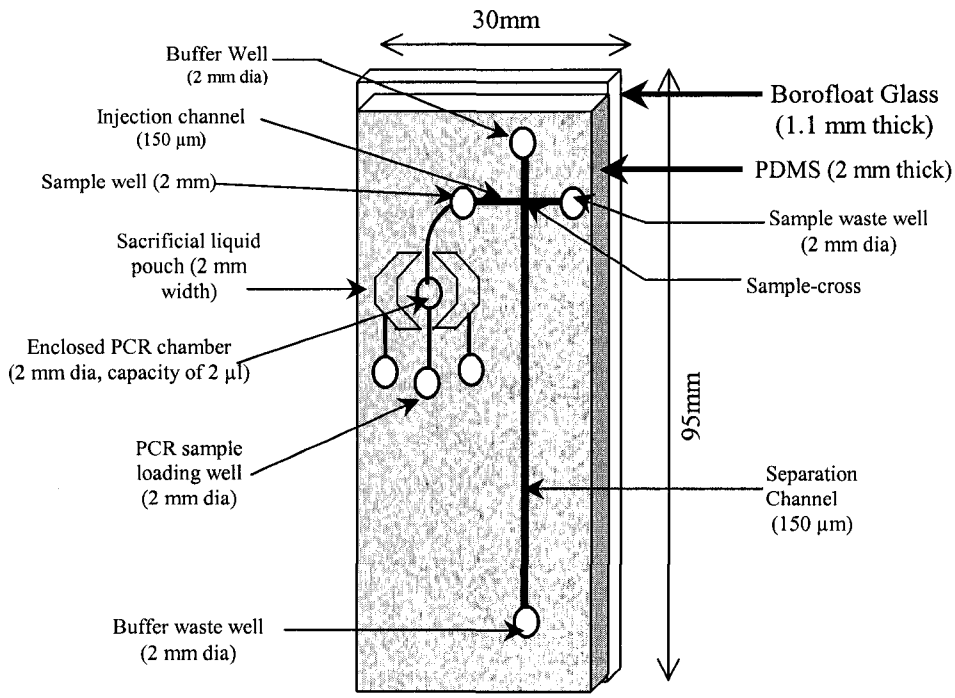

Figure 8-6. The enhanced layout of the PCR-CE chip

8.5 Conclusion

Although the Au thin film heater could not be used for a PCR and CE experiment, the feasibility and electronic setup for such a thin film heater setup was successfully demonstrated in this work. In future prototypes of this system, the Peltiers can be eliminated and Pt thin film heaters used in a similar manner presented here and this will enable the PCR thermal cycling. It is hoped that the experiments presented here will facilitate future prototypes of on-chip integrated heaters. Implementing the recommendations presented in this chapter forms a basis for future work that has been

split into two components – first, the fabrication of the PCR-CE chip without thin film heaters but with the enhanced fluidic layout (using the standardized PDMS protocol presented in chapter 4), and second, the fabrication of the PCR-CE chip similar to the above description along with the incorporation of Pt heaters using the recommended (section 8.4.1) fabrication protocol.

Again (as in chapter 7 with the PDMS diffusion intricacies), an important concept that is, materials and processes that are well adapted for one bioprocess may not be readily adaptable with another bioprocess. For example, Cr-Au metal patterns on similar chip structures are incorporated for dielectrophoresis[29-31] biochips and low temperature heating device[9], however it could not be used for the high temperature PCR application.

8.6 References

[1] J. H. Daniel, S. Iqbal, R. B. Millington, D. F. Moore, C. R. Lowe, D. L. Leslie, M. A. Lee, M. J. Pearce, *Silicon microchambers for DNA amplification,* Sensors and Actuators a-Physical, 1998, *71*, 81.

[2] D. S. Yoon, Y. S. Lee, Y. Lee, H. J. Cho, S. W. Sung, K. W. Oh, J. Cha, G. Lim, *Precise temperature control and rapid thermal cycling in a micromachined DNA polymerase chain reaction chip,* Journal of Micromechanics and Microengineering, 2002, *12*, 813.

[3] T. B. Taylor, S. E. Harvey, M. Albin, L. Lebak, Y. Ning, I. Mowat, T. Schuerlein, E. Principe, *Process Control for Optimal PCR Performance in Glass Microstructures,* Biomedical Microdevices, 1998, *1*, 65.

[4] E. T. Lagally, P. C. Simpson, R. A. Mathies, *Monolithic integrated microfluidic DNA amplification and capillary electrophoresis analysis system,* Sensors and Actuators B-Chemical, 2000, *63*, 138.

[5] E. T. Lagally, C. A. Emrich, R. A. Mathies, *Fully integrated PCR-capillary electrophoresis microsystem for DNA analysis,* Lab on a Chip, 2001, *1*, 102.

[6] E. T. Lagally, J. R. Scherer, R. G. Blazej, N. M. Toriello, B. A. Diep, M. Ramchandani, G. F. Sensabaugh, L. W. Riley, R. A. Mathies, *Integrated portable genetic analysis microsystem for pathogen/infectious disease detection,* Analytical Chemistry, 2004, *76*, 3162.

[7] I. Erill, S. Campoy, N. Erill, J. Barbe, J. Aguilo, *Biochemical analysis and optimization of inhibition and adsorption phenomena in glass-silicon PCR-chips,* Sensors and Actuators B-Chemical, 2003, *96*, 685.

[8] J. L. Yan, Y. Du, J. F. Liu, W. D. Cao, S. H. Sun, W. H. Zhou, X. R. Yang, E. K. Wang, *Fabrication of integrated microelectrodes for electrochemical detection on electrophoresis microchip by electroless deposition and micromolding in capillary technique,* Analytical Chemistry, 2003, *75*, 5406.

[9] B. Yang, J. L. Liu, K. L. Wang, G. Chen, *Simultaneous measurements of Seebeck coefficient and thermal conductivity across superlattice,* Applied Physics Letters, 2002, *80*, 1758.

[10] J. W. Hong, T. Fujii, M. Seki, T. Yamamoto, I. Endo, *Integration of gene amplification and capillary gel electrophoresis on a polydimethylsiloxane-glass hybrid microchip,* Electrophoresis, 2001, *22*, 328.

[11] A. T. Woolley, M. A. Northrup, R. A. Mathies, *Microfabricated integrated DNA analysis systems,* Abstracts of Papers of the American Chemical Society, 1996, *212*, 155.

[12] A. T. Woolley, D. Hadley, P. Landre, A. J. deMello, R. A. Mathies, M. A. Northrup, *Functional integration of PCR amplification and capillary electrophoresis in a microfabricated DNA analysis device,* Analytical Chemistry, 1996, *68*, 4081.

[13] J. Khandurina, T. E. McKnight, S. C. Jacobson, L. C. Waters, R. S. Foote, J. M. Ramsey, *Integrated system for rapid PCR amplification and electrophoretic analysis in microfluidic devices,* Abstracts of Papers of the American Chemical Society, 2000, *219*, U95.

[14] J. Khandurina, T. E. McKnight, S. C. Jacobson, L. C. Waters, R. S. Foote, J. M. Ramsey, *Integrated system for rapid PCR-based DNA analysis in microfluidic devices,* Analytical Chemistry, 2000, *72*, 2995.

[15] L. C. Waters, S. C. Jacobson, N. Kroutchinina, J. Khandurina, R. S. Foote, J. M. Ramsey, *Microchip device for cell lysis, multiplex PCR amplification, and electrophoretic sizing,* Analytical Chemistry, 1998, *70*, 158.

[16] J. C. McDonald, S. J. Metallo, G. M. Whitesides, *Fabrication of a configurable, single-use microfluidic device,* Analytical Chemistry, 2001, *73*, 5645.

[17] Y. J. Liu, C. B. Rauch, R. L. Stevens, R. Lenigk, J. N. Yang, D. B. Rhine, P. Grodzinski, *DNA amplification and hybridization assays in integrated plastic monolithic devices,* Analytical Chemistry, 2002, *74*, 3063.

[18] C. G. Koh, W. Tan, M. Q. Zhao, A. J. Ricco, Z. H. Fan, *Integrating polymerase chain reaction, valving, and electrophoresis in a plastic device for bacterial detection,* Analytical Chemistry, 2003, *75*, 4591.

[19] T. Fujii, *PDMS-based microfluidic devices for biomedical applications,* Microelectronic Engineering, 2002, *61-2*, 907.

[20] T. Fujii, *Microchip-based biochemical analysis devices for 'Bioarchitect' Research,* RIKEN Review, 2001, *No. 41*, 98.

[21] Y. Huang, H. Qiu, F. P. Wang, L. Q. Pan, Y. Tian, P. Wu, *Effect of annealing on the characteristics of Au/Cr bilayer films grown on glass,* Vacuum, 2003, *71*, 523.

[22] P. R. N. Childs, J. R. Greenwood, C. A. Long, *Review of temperature measurement,* Review of Scientific Instruments, 2000, *71*, 2959.

[23] Z. F. Fan, J. M. Engel, J. Chen, C. Liu, *Parylene surface-micromachined membranes for sensor applications,* Journal of Microelectromechanical Systems, 2004, *13*, 484.

[24] G. Faglia, E. Comini, A. Cristalli, G. Sberveglieri, L. Dori, *Very low power consumption micromachined CO sensors,* Sensors and Actuators B-Chemical, 1999, *55*, 140.

[25] R. S. Keynton, J. Roussel, T. J., M. M. Crain, D. J. Jackson, D. B. Franco, J. F. Naber, K. M. Walsh, R. P. Baldwin, *Design and development of microfabricated capillary electrophoresis devices with electrochemical detection,* Analytica Chimica Acta, 2004, *507*, 95.

[26] A. I. K. Lao, T. M. H. Lee, I. M. Hsing, N. Y. Ip, *Precise temperature control of microfluidic chamber for gas and liquid phase reactions,* Sensors and Actuators a-Physical, 2000, *84*, 11.

[27] S. W. Sung, S. W. Park, D. S. Yoon, Y. S. Lee, G. B. Lim, *Modeling and control of a microthermal cycler for DNA polymerase chain reaction,* Industrial & Engineering Chemistry Research, 2003, *42*, 6104.

[28] C. J. Backhouse, H. J. Crabtree, D. M. Glerum, *Frontal analysis on a microchip,* Analyst, 2002, *127*, 1169.

[29] T. Kanagasabathi, C. J. Backhouse, K. Kaler, in *Nanotech 2004*, Boston, MA, 2004.

[30] Y. Huang, J. M. Yang, P. J. Hopkins, S. Kassegne, M. Tirado, A. H. Forster, H. Reese, *Separation of simulants of biological warfare agents from blood by a miniaturized dielectrophoresis device,* Biomedical Microdevices, 2003, *5*, 217.

Chapter – 9

An Integrated Biochip and Future work

Thermophoresis and heated capillary electrophoresis have emerged as two recent topics of interest in molecular diagnosis. This chapter discuss these topics followed by an description of an integrated biochip with capabilities for performing thermophoresis for DNA diffusion based concentration, heated capillary electrophoresis for point-mutation detection, and conventional capillary electrophoresis (CE). In addition, this chip also uses integrated on-chip thin film heaters perform these genetic assays without the requirement of external heating devices. The integration of on-chip platinum heaters presented in this chapter is based on the earlier work with Au heaters discussed in Chapter 8.

9.1 Introduction

Although little-explored, both theoretical studies with mathematical modeling and experimental studies on enhancing DNA based genetic analysis can be found in the literature. Two such techniques are discussed, both of which benefit from heated environments coupled with Capillary Electrophoresis (CE); they are 'thermophoresis for DNA concentration'[1] and 'heated CE DNA separation for point-mutation detection'[2]. This chapter provides a literature review on these topics and a description of an integrated microfluidic chip design able to incorporate these techniques. In Chapter 8 the on-chip resistive heater was explored and a method was developed to heat and measure the temperature using the temperature coefficient of resistance (TCR) characteristics.

For the integrated chip designed and fabricated in this work, platinum metal heaters were used to enable both the thermophoresis and the mutation detection.

9.2 Review and Discussion

9.2.1 Thermophoresis

In 1856 Ludwig and in 1879 Soret reported on the migration of particles as a result of a temperature gradient, typically from a hot region to a colder region[1, 3]. This heat induced migration effect has come to be referred to by a variety of terms including, thermal diffusion, thermodiffusion, the Ludwig-Soret phenomena, and thermophoresis. The thermophoresis principle is similar to the earlier discovery of the Brownian motion[4] (discovered by the biologist Robert Brown in 1827). The Brownian movement[4] of particles occurs when the particles are suspended in a liquid. The thermal activation for this movement is provided by the thermal vibrations in the liquid. Because the particles are in a fluid, they are constantly moving in more or less random directions.

The thermophoresis effect differs from Brownian movement in two ways. (1) The Brownian motion of a particle usually occurs in liquids while thermophoresis is known to occur in other media as well (e.g. air, polymers)[1] and (2) The thermophoresis of particles in liquids differs from the Brownian motion in that the movement is no longer random. Rather it is biased by a temperature gradient. The thermal vibrations[4] of the particles are higher in the hot region than in the colder region. This causes the particle to move from the high velocity (hot) region to the lower velocity (cold) region causing the effective of particle concentration in the colder region.

The thermophoretic effect plays a role in some of the theories on the prebiotic evolution of organisms[1, 5]. However, for nearly a century since its discovery, the mechanism and understanding of this thermophoresis phenomenon remained unclear because of limited investigation on the topic. The thermophoretic effect has been studied for only some particles (e.g. aerosols and dust particles in air)[1] because the thermophoresis is a complex function[6] of many parameters including the individual species, their mass and size, and their interaction forces. More recently, a renewed interest on research in this field has occurred[3]. In the mid 1970's Giglio *et al.*[7, 8] studied the thermophoretic movement of particles (a mixture of aniline and cyclohexane) by a laser beam deflection. Two decades later in the late 1990's this was followed by the work

of Tabiryan *et al.*[6, 9] who performed a similar study with the enhancement of heating the liquid (for the thermophoretic effect) with the same laser source as used for the measurement. Recently, a similar study on the movement of DNA under the thermophoretic effect was undertaken by Braun and coworkers[1, 10] using much the same heating principle as described by Tabiryan *et al.*[6] but with better imaging techniques (using CCD cameras) to study the migration of the DNA molecules. In recent years, the thermophoresis principle has been applied to a wide range of applications and has been extensively used for the separation of low molecular weight polymers[3, 11-13], particle separation in gases[14] (particularly air), and similar applications. However, in this work the focus is on the application of the thermophoresis principle for genetic analysis.

Methods such as dielectrophoresis[15-18], optical tweezers[19], capillary electrophoresis[20-23], and more recently magnetic labeling[24] are now deemed mature methods to sort, move and transport cells and/or DNA molecules. Unfortunately, many of these methods are difficult[1] to miniaturize and require large samples or sophisticated instrumentation with complex microfluidic structures[1]. On the other hand, thermophoresis may be a simple yet elegant approach to purify and analyze biological particles[1]. Since the primary requirement for this technique is heat, it can be easily incorporated into the genetic analysis process. Moreover, this technique is proven to perform even with very low sample concentrations[1].

The thermophoretic effect of DNA is similar to other molecules (as described earlier) and it suggests[1, 10] that under a given condition of a temperature gradient, DNA molecules are repelled from a high temperature region and move to a stable stagnation point near a colder region[1, 10]. This principle has been demonstrated as a means to trap and concentrate 5 kbp DNA within a cold region due to a 1000-fold depletion in the hot region at a ΔT of 50 K[1]. The temperature within the PDMS chamber in which the thermophoretic effect was studied was monitored by a temperature sensitive dye, and fluorescence imaging monitored the temperature of the buffer and the DNA. Based on some theoretical estimations, Braun *et al.*[1] estimated the thermal diffusion coefficient ($D_{Thermal}$) of DNA sample to be 0.4×10^{-8} cm^2 / sec.K [1]. It is also believed that the value

of $D_{Thermal}$ is independent of the DNA strand length[1]. Below a means of estimating the distance DNA molecules could travel under the influence of the thermophoretic conditions is described.

Diffusion coefficient calculations are described by many equations of 1,2,or 3 dimensions. For example, lateral heat diffusion (1-D) calculation was shown in Chapter 5, section 5.9.1; 2-D water molecule diffusion in polymers was shown in Chapter 7, section 7.3, and below DNA diffusion in fluids is described. However, since thermophoretic diffusion is described by a temperature gradient and not a random diffusion, an alteration to the description of the DNA diffusion in water based on Brownian motion was required as explained below.

A 2-dimensional DNA diffusion migration is described by Eq 9.1[25-27].

$$l = \sqrt{2\,D\,t} \qquad (9.1)$$

where l (m) is the distance to which a DNA will travel, D (m^2/sec) is the constant diffusion coefficient of the DNA sample, and t (sec) is the time for which the diffusion process occurs. However, Eq. 9.1 only describes the distance a DNA molecule will travel without the influence of an external heat gradient (i.e. Brownian motion and not thermophoresis) and usually the value of D corresponds to the Brownian motion. As described earlier for the thermophoretic effect, the thermal diffusion coefficient ($D_{Thermal}$ has units of cm^2 / sec.K unlike D which has units cm^2 / sec) is used and hence Eq. 9.1 was modified by me as given in Eq 9.2.

$$l = \sqrt{2\,D_T \cdot t \cdot \Delta T} \qquad (9.2)$$

where ΔT (Kelvin) is the temperature difference between the hot and the cold region in which the DNA is present and the distance between the two regions is separated by a distance l. With the literature estimate of D_T (0.4×10^{-8} cm^2 / sec.K), it is possible to estimate the distance to which DNA molecules will travel under a given conditions of temperature gradient.

In this work, a microfluidic chip design is described that has integrated Pt thin film resistive heaters to accommodate the thermophoretic behavior of the DNA within a CE design.

9.2.2 Heated Capillary Electrophoresis (SNP detection)

Single-nucleotide polymorphisms (SNP), genetic variations or alterations, occur at a frequency of roughly 1 SNP/1000 bp[28]. Some of the traditional ways to detect SNPs are to perform DNA sequencing or hybridization [2]. However, these methods are laborious and time consuming. For example, one protocol involving hybridization requires a 15 h heated-spin (44 °C, 40 rpm) technique[28] and similar methods[29]. Costs are also a concern in such methods[2]. Clearly better methods and protocols are required to perform SNP analysis.

CE has now become a well established method for applications such as DNA sequencing, mutation detection[30-32]. Detection of SNPs using CE relies on slight changes in conformations in single-stranded DNA (the method is called SSCP)[33] and is applied to cancer genetic studies[34]. Although this method has been applied for such studies, it posses some limitations (as described by Gao *et al.*[2]) in terms of DNA denaturing conditions, optical detection limitations, and fragment size. This has initiated a more novel scheme for conducting the SNP experiments in CE devices using the influence of heat to cause 'partial melting of the DNA strands' specific to the point-mutant[35]. Two such heat based methods have been explored in recent years. The first is a 'constant denaturing temperature CE (CDCE)[2, 36]' and the second is a 'temperature gradient CE (TGCE)[37, 38]' scheme. In the CDCE method, a prior knowledge of the exact denaturing temperature of the point-mutation[39] is required. However, this at times is difficult to apply since reagent and environmental influencing factors (e.g. temperature, inclusion of other reagents) can cause uncertainties in determining the mutation denaturing temperature. However, the TGCE method offers higher versatility in that if a temperature gradient is applied along a CE separation column, denaturing of point-mutations within that temperature range can be expected, without prior knowledge of the specific denaturing temperature for a particular mutation. A wide variety of methods have been explored to apply a temperature gradient to a fluidic column during the CE separation to implement the TGCE technique. In one method a temperature gradient was applied based on Joule heating produced by the voltage ramp over time using the same high voltage

supply used for the CE separation[39]. In another method[35, 40] (by the same group of researchers), in addition to the denaturing temperature gradient a polymer gel was used to improve the sensitivity. More recently, Gao *et al.*[2] have demonstrated the TGCE scheme using techniques similar to the above demonstrations with the enhancement of an array of capillary channels. Heat from a external hot plate above the chip was used to attain a temperature gradient between 55 and 70 °C along the channels with the poly(vinylpyrrolidone) sieving matrix as the gel medium within the channels.

Using point-mutation detection by a temperature gradient effect, a CE chip was designed with integrated Pt resistive heaters to heat the separation channel in the CE. This chip design was combined with the earlier described thermophoresis design, thus encompassing a chip with three features – thermophoresis, temperature gradient CE, and the conventional CE. The design of this integrated biochip is described below.

9.3 An Integrated Biochip

This section discusses the three feature (i.e. the thermophoresis, TGCE and CE) chip design that was fabricated of glass chips with embedded Pt resistive heaters. The design and layout was performed at the University of Alberta as part of the work for this thesis and the chip was fabricated at a MEMS foundry[41].

Until recently, thermophoresis has not been considered in microfluidics[1] and here for the first time the integration of the thermophoresis principle to a CE design is attempted on a microfluidic platform. The chip was designed for a two-layer borofloat glass structure (each 1.1mm thick) in which the lower glass was etched for the fluidic channels (50 μm x 20 μm) and for depositing the platinum (Pt) metals that composed the resistive on-chip heaters. The upper glass had 2 mm diameter holes drilled at designated spots that constitute the wells and give access to the Pt for electrical bonding connection. The outline of the designed chip is shown in Figure 9-1. The design of both the fluidic and the on-chip integrated resistive heaters are briefly discussed below.

Fabrication of the chips was done using glass etching and the 'lift-off' microfabrication techniques (similar to that described in Chapter 8, section 8.4.1). The

fluidic channels in the chip are similar to the 4 port CE chip (as described in Chapter 3) with the exception of a tapered injection channel which is now termed a 'diffusion channel'. Three chip designs of the diffusion channel were fabricated as shown in the insert in Figure 9-1. The first design has a diffusion channel that is 2 mm long, the second 4 mm long and the third 6 mm long and with the separation channel deflected by 2 mm to the right. The diameter of the four open wells (sample, sample waste, buffer, and buffer waste) is 2 mm.

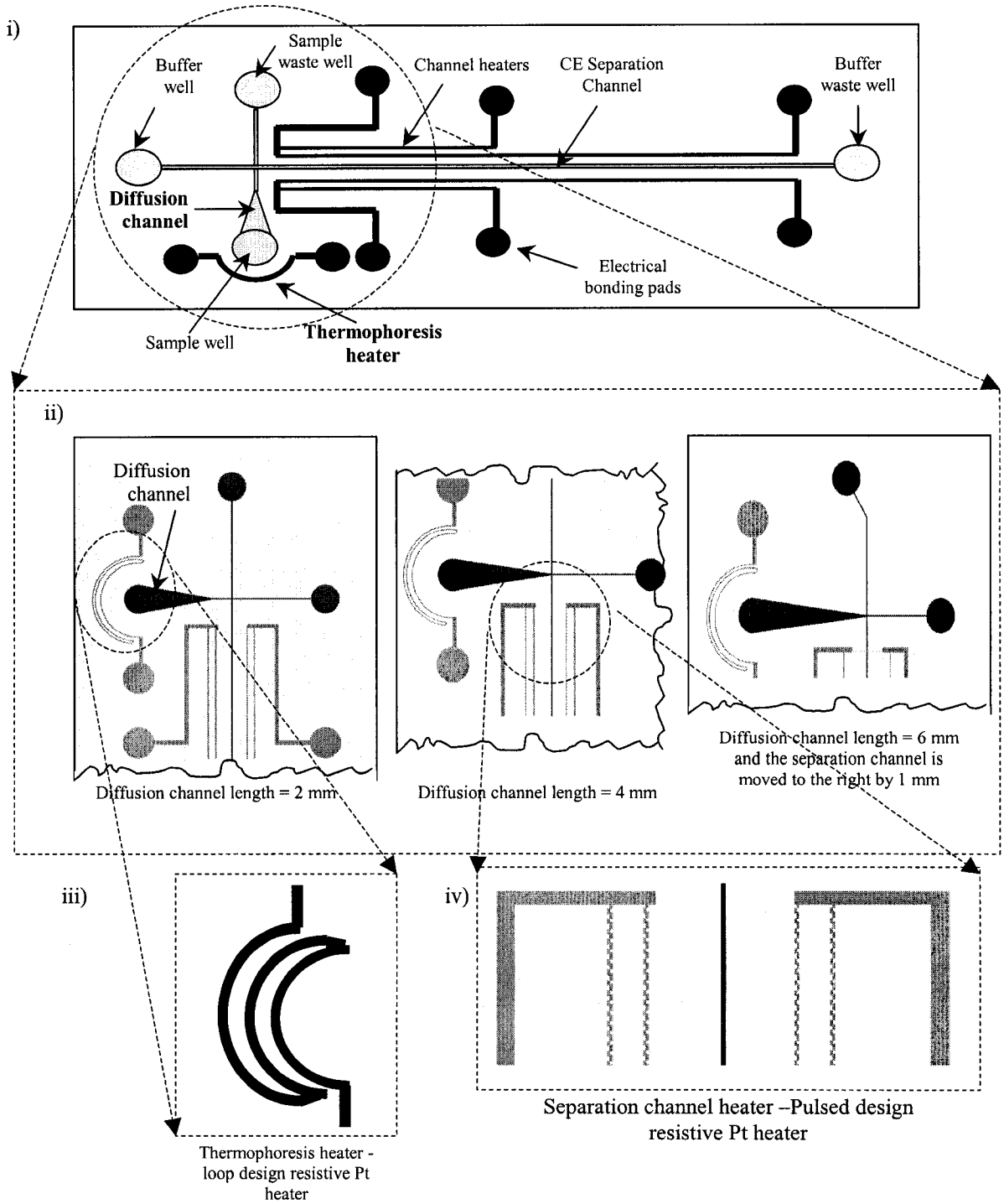

Figure 9-1. An integrated resistive Pt heater chip layout capable of thermophoresis DNA concentration, temperature gradient CE point-mutation detection and conventional CE

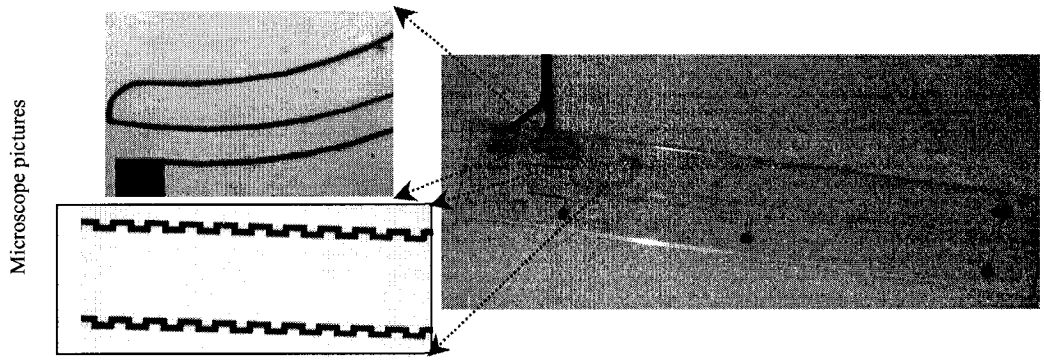

Figure 9-2. A photograph of the integrated biochip

The resistive metal heaters on the chip are designed with the aim of using these chips for performing thermophoresis experiments[1, 10] in the sample well and/or performing SNP based point-mutation detection[2, 35, 40, 42] in a heated CE separation channel. The looped heater design on the periphery of the sample well constitutes the thermophoresis heater, with a parallel square wave (SW) design heater along the separation channel. The separation channel heaters are constituted of two SW design heaters on either sides of the fluidic channel. On either sides of the fluidic channel, one SW heater runs alongside the fluidic channel to about half the length of the fluidic channel while another runs alongside for the entire length of the channel.

An earlier design of a similar chip for the point-mutation detection technique involved an external, height-adjustable copper block heater above the chip. However, the heating method did not yield uniform heat distribution along the length of the separation channel, especially at the front/back ends of the heaters. Details on that work can be found in archived documents[43]. The current design included an addition heater (shorter SW heaters) at the front end of the separation channel to compensate for heat losses that may occur at this end and hence enable achieve a uniform heat distribution along the length.

The pattern and location of the heaters are depicted in the magnified inserts in Figure 9-1 and photographs of the chips are shown in Figure 9-2. The resistance of each of the heaters are as summarized in Table 9-I, although a 25% variation in the resistance was noted between batches of fabricated chips. This is not uncommon with such fabrication technologies.

Table 9-I. Resistance measurements of the on-chip heaters

Thermophoresis heater (loop design) Ω	Short parallel heater left of separation channel (pulsed design) Ω	Long parallel heater right and left of separation channel (pulsed design) Ω	Short parallel heater right of separation channel (pulsed design) Ω
1200	1132	5102	2457

Note: A log of the fabricated chips can be found in the suplimentary CD provided with this thesis *(Titled ThermophoresisChipInspection.doc)*

These integrated biochips were made compatible with the 4-port μTk unit (described in Chapter 3) capable of performing the CE injection-separation. Heating on these chips was performed with the Keithley source-measuring unit (SMU) in a manner similar to that described in Chapter 8, section 8.3. Preliminary heat experimentation with these chips showed good performance characteristics of the Pt thin film heaters. The resistance of the film remained stable even when heated to high temperatures (tested to about 120 ^{o}C by applying a current in excess of 40 mA), unlike the gold (Au) heaters used in the earlier PCR-CE chips (Chapter 8). Upon cooling to room temperature, the resistance of the Pt metal returned to the initial value, which is characteristic of a good thin film heater. Clearly, implementing the suggestion (in Chapter 8, section 8.4.1) on the use of Pt metal proved to be a productive approach. For the separation channel heaters, the heat in the fluidic channel is expected to be the same as that corresponding to the TCR of the heaters (i.e. the SW long heaters) since the channel is heated from either side. However, for the thermophoresis effect, since the looped heater is at one peripheral end of the injection well, a temperature gradient is expected on the other side of the injection well (i.e. close to the channel-intersection which is connected by the diffusion channel).

A room temperature (~ 25 °C) at the channel-intersection may be possible if suitable holes are drilled in the glass chip at the near vicinity of the channel- intersection.

9.4 Experimental Discussion

Experimentation with DNA can be performed in these chips using the thermophoretic principle within the diffusion channel in the chip or the SNP detection using the TGCE in the separation channel. For the thermophoresis experiment, the goal is to achieve a higher fluorescence intensity (as compared to the intensity without the thermophoretic effect) because of the concentration of the DNA samples at the end of the diffusion channel prior to an injection-separation CE run. In a conventional CE injection-separation the DNA sample loaded in the sample well is usually dispersed in the buffer medium in the well. However, using the thermophoretic effect, concentration of the DNA sample to a region (i.e. within the diffusion channel) is possible. This is hoped to enable higher sensitivity in the CE measurement (i.e. even DNA with very low concentration can potentially be detected by thermophoresis concentration followed by injection-separation CE process of the concentrated DNA using a method similar to that described in chapter 3, section 3.3.2).

The thermophoresis experiment can be executed in the following manner. First by filling the sample well in the chip with a buffer and loading the DNA sample in the proportion of 1:10 of buffer solution to DNA concentration (Burn *et al.*[1] had used a buffer with a pH value of 7.8). [Note: It has been (experimentally found and) reported in the literature[1] that the thermophoretic effect in DNA vanishes at elevated salt concentration, typically above 500 mM NaCl and above 20 mM $MgCl_2$. Hence it is recommended that high salt concentrations be avoided[1]]. Then by applying a heat to the looped heater (using the SMU as described in Chapter 8, section 8.3 with a current of between 28 to 30 mA which corresponds to about 80 °C at the looped heater with the chip kept at room temperature conditions) for a time period as estimated below. Since the looped heater is situated to the left of the sample well, the DNA is expected to diffuse away from this region [1, 10]. The DNA would migrate to the end of the diffusion channel

towards the channel-intersection and concentrate in that region. Once the diffusion has occurred, the injection-separation process involved in the conventional CE can be performed (as described in Chapter 3, section 3.3.2). This should result in a high intensity fluorescence peak because the DNA was concentrated prior to separation along the separation channel in the CE chip.

The time taken for the thermophoretic concentration to occur is estimated from Eq 9.2 and using the values of D_T = 0.4 x 10^{-8} cm^2 / sec.K, and ΔT = 50 K[1] (i.e. the difference between room temperature (~298.15 K) and 348.15 K (from literature[1])). Hence from Eq 9.2 the time required for the DNA to concentrate to the end of a 2 mm diffusion column would be 27 hours. Although this thermophoretic diffusion time seems fairly large, given that DNA experiences phase changes at elevated temperatures. In the future, this may be demonstrated successfully using this integrated chip.

In the case of the heated separation CE for mutation detection, the CE injection-separation is performed in a similar manner as described in Chapter 3, section 3.3, along with heat applied by connecting the SW long heater to the SMU as described in Chapter 8, section 8.3.

9.5 Conclusion and Future Work for the Integrated Biochip

In this chapter two relatively new fields in CE-based research have been discussed – the thermophoresis diffusion for DNA concentration and heated CE separation for point-mutation detection. Preliminary heat tests showed good thin film characteristics of the Pt heaters incorporated in these chips. Although insufficient time was available to perform experiments with DNA, the chips have been designed, fabricated and experimental procedures proposed. It is hoped that both the thermophoresis and the point-mutation detection techniques could be readily performed using this integrated biochip. This could enhance many of the conventional genetic analysis processes.

9.6 Concluding Remarks on this Thesis

The research projects undertaken as part of this thesis have yielded good results. The achievements are briefly summarized below.

- A novel nonlinear PD-PI controller with parallel processing capabilities. This control system design exhibited good performance in that it enabled an ideal critically damped system response (i.e. a nil overshoot and a steady state error of less than ± 0.1 °C).
- The development of a first-of-a-kind enhanced soft-lithography technique to fabricate PDMS biochips with implants. These implants reduce vapor loss from such devices and greatly improve the yield of the PCR.
- The integration of on-chip thin-film heaters in a PCR-CE biochip. The fabrication of biochips and instrumentation methods were developed to demonstrate on-chip heating and sensing without the requirement for the bulky Peltiers and additional temperature sensors. Although the Au-Cr metals used in the work showed unstable characteristics at high temperatures, the thin film chip facilitated the prototyping of temperature actuation and sensing using the TCR technique. This TCR technique will facilitate future prototyping of similar chips.
- The development of an integrated biochip with Pt thin film heaters for performing DNA concentration. The thermophoresis principle for DNA concentration was incorporated in an integrated biochip that was designed with CE process and thermophoresis capabilities. Preliminary tests revealed excellent functionality of the Pt heaters (unlike the earlier Au heaters). The Pt heaters were used with the TCR principle.
- The integration of SNP detection in the same chip as that used for thermophoresis. Pt heaters were incorporated on either sides of the CE separation channel to enable heated DNA separation. Here again, preliminary tests showed good functionality of the heaters using the TCR principle.
- The surface adsorption effects during PCR were studied and a chip conditioning method was developed to counteract the phenomenon. Studies indicated that

although PDMS and glass may not be suitable materials for the PCR (especially with low copy number samples), a method to cope with the problem was developed.

Future work based on the research projects is expected to have tremendous potential. Some immediate future goals are encapsulated below. The demonstration of the PCR-CE with the design proposals was presented in Chapter 8, section 8.4.2. The chip would use the same PDMS-glass fabrication protocol presented in Chapter 4 and the identical Peltier heating device with the incorporation of the PD-PI control system designed in Chapter 5. Microfluidic valves and pumps demonstrated in Chapter 6 can be readily included in that work. Upon successful demonstration, the integration of on-chip heaters in the form of Pt-Ti (similar to that demonstrated in Chapter 9 and temperature measurement and control shown in Chapter 8, section 8.3) would provide a high-throughput genetic analysis system. A project is underway to address these goals, which is in essence based on the work presented in this thesis.

9.7 References

[1] D. Braun, A. Libchaber, *Trapping of DNA by thermophoretic depletion and convection,* Physical Review Letters, 2002, *89*.

[2] Q. F. Gao, E. S. Yeung, *High-throughput detection of unknown mutations by using multiplexed capillary electrophoresis with poly(vinylpyrrolidone) solution,* Analytical Chemistry, 2000, *72*, 2499.

[3] S. Semenov, M. Schimpf, *Thermophoresis of dissolved molecules and polymers: Consideration of the temperature-induced macroscopic pressure gradient,* Physical Review E, 2004, *69*.

[4] O. A. Hernandez-Flores, M. Mayorga, *The effect of direct interactions in steady state electrophoresis and thermophoresis of colloids,* Journal of Physics-Condensed Matter, 2004, *16*, S2071.

[5] D. Braun, N. L. Goddard, A. Libchaber, *Exponential DNA replication by laminar convection,* Physical Review Letters, 2003, *91*.

[6] N. V. Tabiryan, W. L. Luo, *Soret feedback in thermal diffusion of suspensions,* Physical Review E, 1998, *57*, 4431.

[7] M. Giglio, A. Vendramini, *Optical Measurements of Gravitationally Induced Concentration Gradients near a Liquid-Liquid Critical-Point,* Physical Review Letters, 1975, *35*, 168.

[8] M. Giglio, A. Vendramini, *Thermal-Diffusion Measurements near a Consolute Critical-Point,* Physical Review Letters, 1975, *34*, 561.

[9] N. V. Tabiryan, C. Umeton, *Thermodiffusive photorefractive phenomena in liquid crystals,* Physical Review E, 1998, *58*, 4619.

[10] D. Braun, N. L. Goddard, A. J. Libchaber, *Thermphoretic trapping of DNA and convective PCR: New physical approaches to the origin of life,* Biophysical Journal, 2003, *84*, 6A.

[11] J. C. Giddings, *Polymer Characterization by Thermal Field-Flow Fractionation and Related Methods,* Abstracts of Papers of the American Chemical Society, 1988, *196*, 1.

[12] M. E. Schimpf, J. C. Giddings, *Characterization of Thermal-Diffusion in Polymer-Solutions by Thermal Field-Flow Fractionation - Dependence on Polymer and Solvent Parameters,* Journal of Polymer Science Part B-Polymer Physics, 1989, *27*, 1317.

[13] J. C. Giddings, V. Kumar, P. S. Williams, M. N. Myers, *Polymer Separation by Thermal Field-Flow Fractionation - High-Speed Power Programming,* Advances in Chemistry Series, 1990, 3.

[14] M. A. Gallis, D. J. Rader, J. R. Torczynski, *Thermophoresis in rarefied gas flows,* Aerosol Science and Technology, 2002, *36*, 1099.

[15] L. F. Hartley, K. Kaler, R. Paul, *Quadrupole levitation of microscopic dielectric particles,* Journal of Electrostatics, 1999, *46*, 233.

[16] Y. L. Li, K. Kaler, *Dielectrophoretic fluidic cell fractionation system,* Analytica Chimica Acta, 2004, *507*, 151.

[17] T. Kanagasabathi, C. J. Backhouse, K. Kaler, in *Nanotech 2004*, Boston, MA, 2004.

[18] E. G. Cen, C. Dalton, Y. Li, S. Adamia, L. M. Pilarski, K. V. I. S. Kaler, *A combined dielectrophoresis, traveling wave dielectrophoresis and electrorotation microchip for the manipulation and characterization of human malignant cells,* Journal of Microbiological Methods, 2004, *58*, 387.

[19] S. Katsura, K. Hirano, Y. Matsuzawa, K. Yoshikawa, A. Mizuno, *Direct laser trapping of single DNA molecules in the globular state,* Nucleic Acids Research, 1998, *26*, 4943.

[20] T. Footz, S. Wunsam, S. Kulak, H. J. Crabtree, D. M. Glerum, C. J. Backhouse, *Sample purification on a microfluidic device,* Electrophoresis, 2001, *22*, 3868.

[21] C. J. Backhouse, H. J. Crabtree, D. M. Glerum, *Frontal analysis on a microchip,* Analyst, 2002, *127*, 1169.

[22] C. J. Backhouse, A. Gajdal, L. M. Pilarski, H. J. Crabtree, *Improved resolution with microchip-based enhanced field inversion electrophoresis,* Electrophoresis, 2003, *24*, 1777.

[23] A. Manz, N. Graber, H. M. Widmer, *Miniaturized Total Chemical-Analysis Systems - a Novel Concept for Chemical Sensing,* Sensors and Actuators B-Chemical, 1990, *1*, 244.

[24] S. Katsura, T. Yasuda, K. Hirano, A. Mizuno, S. Tanaka, *Development of a new detection method for DNA molecules,* Superconductor Science & Technology, 2001, *14*, 1131.

[25] K. Pappaert, P. Van Hummelen, J. Vanderhoeven, G. V. Baron, G. Desmet, *Diffusion-reaction modelling of DNA hybridization kinetics on biochips,* Chemical Engineering Science, 2003, *58*, 4921.

[26] K. Pappaert, J. Vanderhoeven, P. Van Hummelen, B. Dutta, D. Clicq, G. V. Baron, G. Desmet, *Enhancement of DNA micro-array analysis using a shear-driven micro-channel flow system,* Journal of Chromatography A, 2003, *1014*, 1.

[27] K. S. McCain, D. C. Hanley, J. M. Harris, *Single-molecule fluorescence trajectories for investigating molecular transport in thin silica sol-gel films,* Analytical Chemistry, 2003, *75*, 4351.

[28] D. G. Wang, J. B. Fan, C. J. Siao, A. Berno, P. Young, R. Sapolsky, G. Ghandour, N. Perkins, E. Winchester, J. Spencer, L. Kruglyak, L. Stein, L. Hsie, T. Topaloglou, E. Hubbell, E. Robinson, M. Mittmann, M. S. Morris, N. P. Shen, D. Kilburn, J. Rioux, C. Nusbaum, S. Rozen, T. J. Hudson, R. Lipshutz, M. Chee, E. S. Lander, *Large-scale identification, mapping, and genotyping of single-nucleotide polymorphisms in the human genome,* Science, 1998, *280*, 1077.

[29] E. A. Winzeler, D. R. Richards, A. R. Conway, A. L. Goldstein, S. Kalman, M. J. McCullough, J. H. McCusker, D. A. Stevens, L. Wodicka, D. J. Lockhart, R. W. Davis, *Direct allelic variation scanning of the yeast genome,* Science, 1998, *281*, 1194.

[30] T. Footz, M. J. Somerville, R. Tomaszewski, K. A. Sprysak, C. J. Backhouse, *Heteroduplex-based genotyping with microchip electrophoresis and dHPLC,* Genetic Testing, 2003, *7*, 283.

[31] T. Footz, M. J. Somerville, R. Tomaszewski, B. Elyas, C. J. Backhouse, *Integration of combined heteroduplex/restriction fragment length polymorphism analysis on an electrophoresis microchip for the detection of hereditary haemochromatosis,* Analyst, 2004, *129*, 25.

[32] L. Chen, J. C. Ren, *High-throughput DNA analysis by microchip electrophoresis,* Combinatorial Chemistry & High Throughput Screening, 2004, *7*, 29.

[33] M. Orita, H. Iwahana, H. Kanazawa, K. Hayashi, T. Sekiya, *Detection of Polymorphisms of Human DNA by Gel-Electrophoresis as Single-Strand Conformation Polymorphisms,* Proceedings of the National Academy of Sciences of the United States of America, 1989, *86*, 2766.

[34] Y. Suzuki, Y. Murakami, M. Orita, K. Hayashi, T. Sekiya, *Detection of DNA Aberrations in Human Cancers by Single-Strand Conformation Polymorphism Analysis of Polymerase Chain-Reaction Products,* Mutation Research, 1991, *253*, 279.

[35] C. Gelfi, P. G. Righetti, M. Travi, S. Fattore, *Temperature-programmed capillary electrophoresis for the analysis of high-melting point mutants in thalassemias,* Electrophoresis, 1997, *18*, 724.

[36] P. J. Oefner, P. A. Underhill, *Comparative DNA-Sequencing by Denaturing High-Performance Liquid-Chromatography (Dhplc),* American Journal of Human Genetics, 1995, *57*, 1547.

[37] D. Riesner, G. Steger, R. Zimmat, R. A. Owens, M. Wagenhofer, W. Hillen, S. Vollbach, K. Henco, *Temperature-Gradient Gel-Electrophoresis of Nucleic-Acids - Analysis of Conformational Transitions, Sequence Variations, and Protein-Nucleic Acid Interactions,* Electrophoresis, 1989, *10*, 377.

[38] D. Riesner, G. Steger, U. Wiese, M. Wulfert, M. Heibey, K. Henco, *Temperature-Gradient Gel-Electrophoresis for the Detection of Polymorphic DNA and for Quantitative Polymerase Chain-Reaction,* Electrophoresis, 1992, *13*, 632.

[39] C. Gelfi, P. G. Righetti, L. Cremonesi, M. Ferrari, *Detection of Point Mutations by Capillary Electrophoresis in Liquid Polymers in Temporal Thermal-Gradients,* Electrophoresis, 1994, *15*, 1506.

[40] C. Gelfi, A. Vigano, S. De Palma, P. G. Righetti, S. C. Righetti, E. Corna, F. Zunino, *Single-strand conformation polymorphism for p53 mutation by a combination of neutral pH buffer and temperature gradient in capillary electrophoresis,* Electrophoresis, 2002, *23*, 1517.

[41] Micralyne, Edmonton, Canada, 2003.

[42] P. Liu, W. L. Xing, D. Liang, G. L. Huang, Y. X. Zhou, J. Cheng, *Fast screening of single-nucleotide polymorphisms using chip-based temperature gradient capillary electrophoresis,* Analytical Letters, 2003, *36*, 2823.

[43] A. R. Prakash, *Thermal issues in DNA analysis,* Backhouse Lab documents, 2002, 34.

[44] Y. Zheng, T. Footz, D. Manage, C. J. Backhouse, *Controlled and Rapid Self-Assembly of DNA on a Microfluidic Chip,* Journal of Nanobiotechnology, 2004, *submitted July'04.*